

**FOSSUHH  
EZH  
MGR**

**NIPER-710  
(DE94000105)**

**SCREENING OF MIXED SURFACTANT SYSTEMS:  
Phase Behavior Studies and CT Imaging of  
Surfactant-Enhanced Oil Recovery Experiments**

**Topical Report**

**By  
F.M. Llave  
B.L. Gall  
P.B. Lorenz  
I.M. Cook  
L.J. Scott**

**November 1993**

**Performed Under Cooperative Agreement No. DE-FC22-83FE60149**

**IIT Research Institute  
National Institute for Petroleum and Energy Research  
Bartlesville, Oklahoma**



**Bartlesville Project Office  
U. S. DEPARTMENT OF ENERGY  
Bartlesville, Oklahoma**

## **DISCLAIMER**

This report was prepared as an account of work sponsored by an agency of the United States Government. Neither the United States Government nor any agency thereof, nor any of their employees, makes any warranty, express or implied, or assumes any legal liability or responsibility for the accuracy, completeness, or usefulness of any information, apparatus, product, or process disclosed, or represents that its use would not infringe privately owned rights. Reference herein to any specific commercial product, process, or service by trade name, trademark, manufacturer, or otherwise does not necessarily constitute or imply its endorsement, recommendation, or favoring by the United States Government or any agency thereof. The views and opinions of authors expressed herein do not necessarily state or reflect those of the United States Government or any agency thereof.

This report has been reproduced directly from the best available copy.

Available to DOE and DOE contractors from the Office of Scientific and Technical Information, P.O. Box 62, Oak Ridge, TN 37831; prices available from (615)576-8401, FTS 626-8401.

Available to the public from the National Technical Information Service, U.S. Department of Commerce, 5285 Port Royal Rd., Springfield, VA 22161.

SCREENING OF MIXED SURFACTANT SYSTEMS:

Phase Behavior Studies and CT Imaging of  
Surfactant-Enhanced Oil Recovery Experiments

Topical Report

By

F.M. Llave

B.L. Gall

P.B. Lorenz

I.M. Cook

L.J. Scott

November 1993

Work Performed Under Cooperative Agreement No. DE-FC22-83FE60149

Prepared for  
U.S. Department of Energy  
Assistant Secretary for Fossil Energy

Jerry Casteel, Project Manager  
Bartlesville Project Office  
P.O. Box 1398  
Bartlesville, OK 74005

Prepared by  
IIT Research Institute  
National Institute for Petroleum and Energy Research  
P.O. Box 2128  
Bartlesville, OK 74005



## TABLE OF CONTENTS

	<u>Page</u>
ABSTRACT .....	1
INTRODUCTION .....	2
ACKNOWLEDGMENTS.....	6
I. SCREENING OF MIXED SURFACTANT SYSTEMS .....	7
Materials and Experimental Procedures Used .....	7
Materials.....	7
Phase Inversion Temperature Measurements .....	8
Phase Behavior Measurements - Salinity Scans .....	9
Interfacial Tension Measurements.....	9
RESULTS AND DISCUSSION .....	9
Mixed Surfactant Screening .....	9
Screening by Phase Inversion Temperature Method .....	10
Comparison of Methods of Surfactant Systems Screening.....	23
Modeling the Behavior of Mixed Surfactants .....	27
Application of the Models .....	43
Summary and Conclusions of Mixed Surfactant System Studies.....	49
II. CT-IMAGING OF CHEMICAL EOR COREFLOODING EXPERIMENTS .....	53
Materials and Experimental Procedures .....	53
CT-Imaging Techniques.....	53
Materials.....	54
Coreflooding .....	54
RESULTS AND DISCUSSION .....	55
Effect of Surfactant Slug Size on Oil Production .....	55
Oil Production .....	55
Oil Saturation Distribution.....	60
Oil Movement in Core under Shut In Conditions .....	62
CT-Imaging of Oil Production for Different IFT Conditions.....	63
CT-Imaging of Corefloods in Reservoir Rock.....	66
Summary and Conclusions for CT-Monitored Corefloods .....	68
REFERENCES.....	70
APPENDIX A – Summary of results of phase behavior studies .....	72
APPENDIX B – Summary of CT coreflooding operations .....	106
APPENDIX C – Composite CT-images of coreflood experiments .....	107

## TABLES

	<u>Page</u>
1. List of anionic surfactants studied.....	7
2. List of nonionic surfactants studied.....	7
3. List of surfactant systems studied using PIT method.....	8
4. Average difference in results due to temperature effects.....	23
5. Comparison of results from PIT method and salinity scans.....	24
6. Summary for salinity scan results at 40° and 50° C.....	26
7. Method of obtaining model values for intercepts.....	31
8. Values of coefficients in the models.....	36
9. Conformance of the models to the data.....	38
10. Conformance of the models to selected data at 50° C.....	38
11. Numerical values of slopes of <i>EON</i> vs. <i>ACN</i> .....	39
12. Effect of parameters on coefficients.....	43
13. Effect of parameters on ratio (with/without TRS/IBA).....	43
14. Effect of addition of TRS/IBA on temperature coefficients.....	48
15. Commercial chemicals used for CT-monitored corefloods.....	54
16. Oils used in CT-monitored corefloods.....	54
17. Summary of fluid compositions and core permeabilities.....	56
18. Residual oil saturations after waterflood and chemical flood.....	60

## ILLUSTRATIONS

1. Optimal salinity (PIT-method) vs. HLB of nonionic surfactant component using Genapol mixtures at 50° C with different alkanes.....	11
2. Optimal salinity (PIT-method) vs. HLB of nonionic surfactant component using Igepal mixtures at 50° C with different alkanes.....	12
3. Optimal salinity (PIT-method) vs. HLB of nonionic surfactant component using Genapol mixtures with TRS 10-410/IBA [1:1] at 50° C with different alkanes.....	12
4. Optimal salinity (PIT-method) vs. HLB of nonionic surfactant component using Genapol mixtures with TRS 10-410/IBA [1:1] at 50° C with different alkanes.....	13
5. Log of optimal salinity (PIT-method) vs. alkane carbon number of oil with different HLB of nonionic surfactant component using Genapol mixtures at 40° C.....	15
6. Log of optimal salinity (PIT-method) vs. alkane carbon number of oil with different HLB of nonionic surfactant component using Igepal mixtures at 40° C.....	15

## ILLUSTRATIONS–Continued

	<u>Page</u>
7. Log of optimal salinity (PIT-method) vs. HLB of nonionic surfactant component using Genapol mixtures at 50° C with different alkanes. ....	16
8. Log of optimal salinity (PIT-method) vs. HLB of nonionic surfactant component using Igepal mixtures at 50° C with different alkanes. ....	16
9. Log of optimal salinity (PIT-method) vs. HLB of nonionic surfactant component using Genapol mixtures with TRS 10-410/IBA [1:1] at 50° C with different alkanes. . .	17
10. Log of optimal salinity (PIT-method) vs. HLB of nonionic surfactant component using Genapol mixtures with TRS 10-410/IBA [1:1] at 50° C with different alkanes. . .	17
11. Log of optimal salinity (PIT-method) vs. temperature with different HLB of nonionic surfactant component using Genapol mixtures with n-dodecane. ....	18
12. Log of optimal salinity (PIT-method) vs. temperature with different HLB of nonionic surfactant component using Igepal mixtures with n-dodecane. ....	18
13. Log of optimal salinity (PIT-method) vs. temperature with different HLB of nonionic surfactant component using Genapol + TRS/IBA mixtures with n-dodecane. ....	20
14. Log of optimal salinity (PIT-method) vs. temperature with different HLB of nonionic surfactant component using Igepal + TRS/IBA mixtures with n-dodecane. ....	20
15. Solubilization parameter vs. salinity using AOS-1416 + n-pentanol with n-dodecane at 50° C. ....	22
16. Solubilization parameter vs. salinity using AOS-1618 + n-hexanol with n-dodecane at 50° C. ....	22
17. Solubilization parameter at optimal salinity vs. HLB of nonionic component using Genapol with and without TRS/IBA with n-octane at 40° C. ....	26
18. Solubilization parameter at optimal salinity vs. HLB of nonionic component using Igepal with and without TRS/IBA with n-decane at 40° C. ....	27
19. Plot of $\ln S/dT$ vs. alkane carbon number using Genapol . ....	28
20. Plot $\ln S/dT$ vs. alkane carbon number using Genapol + TRS/IBA. ....	29
21. Plot $\ln S/dT$ vs. alkane carbon number using Igepal. ....	29
22. Plot $\ln S/dT$ vs. alkane carbon number using Igepal + TRS/IBA. ....	30
23a. Plot of intercepts of log of salinity at $T=0^\circ\text{C}$ vs. HLB of nonionic component using Genapol. (ACN: 7 and 8). ....	31
23b. Plot of intercepts of log of salinity at $T=0^\circ\text{C}$ vs. HLB of nonionic component using Genapol. (ACN: 10, 12 and 14). ....	32
24. Plot of quadratic parameters vs. alkane carbon number using Genapol. ....	32

## ILLUSTRATIONS–Continued

	<u>Page</u>
25. Plot of intercepts of log of salinity vs. HLB of nonionic component using Genapol + TRS/IBA with different n-alkanes. ....	33
26. Plot of correlation of slope and intercept values vs. alkane carbon number using Genapol + TRS/IBA . ....	33
27. Plot of intercepts of log of salinity at T=0° C vs. HLB of nonionic component using Igepal. ....	34
28. Plot of intercepts of log of salinity at T=0° C vs. HLB of nonionic component using Igepal + TRS/IBA. (ACN: 8 and 10). ....	34
29. Plot of intercepts of log of salinity at T=0° C vs. alkane carbon number using Igepal + TRS/IBA with different HLBs values. ....	35
30. Plot of quadratic parameters vs. alkane carbon number using Igepal + TRS/IBA.....	35
31. Plot of intercepts of log of salinity at T=0° C vs. HLB of nonionic component using Igepal + TRS/IBA with different alkanes.....	36
32. Plot of EON vs. alkane carbon number using Genapol at different salinities and 50° C. ....	40
33. Plot of EON vs. alkane carbon number using Genapol + TRS/IBA at different salinities and 50° C.....	40
34. Plot of EON vs. alkane carbon number using Igepal at different salinities and 50° C. ....	41
35. Plot of EON vs. alkane carbon number using Igepal + TRS/IBA at different salinities and 50° C.....	41
36. Plot of EON vs. alkane carbon number using Genapol at different salinities and 40° C. ....	42
37. Plot of calculated HLB vs. alkane carbon number using Genapol at different salinities and 50° C.....	42
38. Plot $d\ln S/dT$ vs. alkane carbon number using Genapol with and without TRS/IBA.....	44
39. Plot $d\ln S/dT$ vs. alkane carbon number using Igepal with and without TRS/IBA. ....	44
40. Plot of ratio of optimal salinities ( $S^*_{w/ TRS} / S^*_{w/o TRS}$ ) vs. alkane carbon number using Genapol and Igepal with and without TRS/IBA.....	45
41. Plot of $d[\text{optimal salinity ratio}]/d[\text{HLB}]$ vs. alkane carbon number using Genapol and Igepal with and without TRS/IBA at 50° C.....	45
42. Plot of $d\ln(S)/d[\text{ACN}]$ vs. HLB of nonionic component using Genapol with and without TRS/IBA at 50° C. (ACN>7).....	46

## ILLUSTRATIONS–Continued

	<u>Page</u>
43. Plot of $\ln(S)/d[HLB]$ vs. alkane carbon number using Genapol with and without TRS/IBA.....	46
44. Plot of $\ln(S)/d[HLB]$ vs. HLB of nonionic component using Genapol with and without TRS/IBA. (ACN=14).....	47
45. Plot of $\ln(S)/d[HLB]$ vs. alkane carbon number using Igepal with and without TRS/IBA at different HLB values.....	47
46. Composite CT-image of surfactant-enhanced chemical coreflood.....	53
47. Oil recovery, oil cut, and residual oil saturation for CT-CF 1 .....	57
48. Oil recovery, oil cut, and residual oil saturation for CT-CF 7 .....	57
49. Oil recovery, oil cut, and residual oil saturation for CT-CF 8 .....	58
50. Oil recovery, oil cut, and residual oil saturation for CT-CF 3 .....	58
51. Oil recovery, oil cut, and residual oil saturation for CT-CF 9 .....	58
52. CT-image of a slice from CT-CF 9 16.5 cm from the core inlet.....	59
53. Average oil saturations along the length of the core CT-CF 7 .....	61
54. Average oil saturations along the length of the core CT-CF 8.....	61
55. Average oil saturations along the length of the core for CT-CF 9 .....	62
56. Average oil saturation along the core length for CT-CF 5 .....	63
57. Composite CT-images of CT-CF 5 after surfactant injection .....	64
58. Oil cut production of tests CT-CF 4 and CT-CF 10.....	65
59. Average oil saturations after surfactant CT-CF 4 and 10.....	65
60. Average oil saturations after chemical flood for tests CT-CF 4 and 10.....	65
61. CT-composite images of tracer injection in two core samples from North Burbank Reservoir, Osage County, OK.....	66
62. Drawing of core NBU-2 showing discolored areas.....	67
A1. Log of optimal salinity vs. HLB of nonionic surfactant component using Genapol with n-Heptane at different temperatures. ....	72
A2. Log of optimal salinity vs. temperature using Genapol with n-Heptane at different HLB values. ....	73
A3. Phase inversion temperature vs. HLB of nonionic surfactant component using Genapol with n-Heptane at different salinities. ....	73
A4. Log of optimal salinity vs. HLB of nonionic surfactant component using Genapol with n-Octane at different temperatures. ....	74
A5. Log of optimal salinity vs. temperature using Genapol with n-Octane at different HLB values. ....	74

## ILLUSTRATIONS–Continued

	<u>Page</u>
A6. Phase inversion temperature vs. HLB of nonionic surfactant component using Genapol with n-Octane at different salinities. ....	75
A7. Log of optimal salinity vs. HLB of nonionic surfactant component using Genapol with n-Decane at different temperatures. ....	75
A8. Log of optimal salinity vs. temperature using Genapol with n-Decane at different HLB values. ....	76
A9. Phase inversion temperature vs. HLB of nonionic surfactant component using Genapol with n-Decane at different salinities. ....	76
A10. Log of optimal salinity vs. HLB of nonionic surfactant component using Genapol with n-Dodecane at different temperatures. ....	77
A11. Log of optimal salinity vs. temperature using Genapol with n-Dodecane at different HLB values. ....	77
A12. Phase inversion temperature vs. HLB of nonionic surfactant component using Genapol with n-Dodecane at different salinities. ....	78
A13. Log of optimal salinity vs. HLB of nonionic surfactant component using Genapol with n-Tetradecane at different temperatures. ....	78
A14. Log of optimal salinity vs. temperature using Genapol with n-Tetradecane at different HLB values. ....	79
A15. Phase inversion temperature vs. HLB of nonionic surfactant component using Genapol with n-Tetradecane at different salinities. ....	79
A16. Log of optimal salinity vs. HLB of nonionic surfactant component using Igepal with n-Heptane at different temperatures. ....	80
A17. Log of optimal salinity vs. temperature using Igepal with n-Heptane at different HLB values. ....	80
A18. Phase inversion temperature vs. HLB of nonionic surfactant component using Igepal with n-Heptane at different salinities. ....	81
A19. Log of optimal salinity vs. HLB of nonionic surfactant component using Igepal with n-Octane at different temperatures. ....	81
A20. Log of optimal salinity vs. temperature using Igepal with n-Octane at different HLB values. ....	82
A21. Phase inversion temperature vs. HLB of nonionic surfactant component using Igepal with n-Octane at different salinities. ....	82
A22. Log of optimal salinity vs. HLB of nonionic surfactant component using Igepal with n-Decane at different temperatures. ....	83

## ILLUSTRATIONS–Continued

	<u>Page</u>
A23. Log of optimal salinity vs. temperature using Igepal with n-Decane at different HLB values. ....	83
A24. Phase inversion temperature vs. HLB of nonionic surfactant component using Igepal with n-Decane at different salinities. ....	84
A25. Log of optimal salinity vs. HLB of nonionic surfactant component using Igepal with n-Dodecane at different temperatures. ....	84
A26. Log of optimal salinity vs. temperature using Igepal with n-Dodecane at different HLB values. ....	85
A27. Phase inversion temperature vs. HLB of nonionic surfactant component using Igepal with n-Dodecane at different salinities. ....	85
A28. Log of optimal salinity vs. HLB of nonionic surfactant component using Igepal with n-Tetradecane at different temperatures. ....	86
A29. Log of optimal salinity vs. temperature using Igepal with n-Tetradecane at different HLB values. ....	86
A30. Phase inversion temperature vs. HLB of nonionic surfactant component using Igepal with n-Tetradecane at different salinities. ....	87
A31. Log of optimal salinity vs. HLB of nonionic surfactant component using Genapol + TRS/IBA with n-Heptane at different temperatures. ....	87
A32. Log of optimal salinity vs. temperature using Genapol + TRS/IBA with n-Heptane at different HLB values. ....	88
A33. Phase inversion temperature vs. HLB of nonionic surfactant component using Genapol + TRS/IBA with n-Heptane at different salinities. ....	88
A34. Log of optimal salinity vs. HLB of nonionic surfactant component using Genapol + TRS/IBA with n-Octane at different temperatures. ....	89
A35. Log of optimal salinity vs. temperature using Genapol + TRS/IBA with n-Octane at different HLB values. ....	89
A36. Phase inversion temperature vs. HLB of nonionic surfactant component using Genapol + TRS/IBA with n-Octane at different salinities. ....	90
A37. Log of optimal salinity vs. HLB of nonionic surfactant component using Genapol + TRS/IBA with n-Nonane at different temperatures. ....	90
A38. Log of optimal salinity vs. temperature using Genapol + TRS/IBA with n-Nonane at different HLB values. ....	91
A39. Phase inversion temperature vs. HLB of nonionic surfactant component using Genapol + TRS/IBA with n-Nonane at different salinities. ....	91

## ILLUSTRATIONS–Continued

	<u>Page</u>
A40. Log of optimal salinity vs. HLB of nonionic surfactant component using Genapol + TRS/IBA with n-Decane at different temperatures. ....	92
A41. Log of optimal salinity vs. temperature using Genapol + TRS/IBA with n-Decane at different HLB values. ....	92
A42. Phase inversion temperature vs. HLB of nonionic surfactant component using Genapol + TRS/IBA with n-Decane at different salinities. ....	93
A43. Log of optimal salinity vs. HLB of nonionic surfactant component using Genapol + TRS/IBA with n-Dodecane at different temperatures. ....	93
A44. Log of optimal salinity vs. temperature using Genapol + TRS/IBA with n-Dodecane at different HLB values. ....	94
A45. Phase inversion temperature vs. HLB of nonionic surfactant component using Genapol + TRS/IBA with n-Dodecane at different salinities. ....	94
A46. Log of optimal salinity vs. HLB of nonionic surfactant component using Genapol + TRS/IBA with n-Tetradecane at different temperatures. ....	95
A47. Log of optimal salinity vs. temperature using Genapol + TRS/IBA with n-Tetradecane at different HLB values. ....	95
A48. Phase inversion temperature vs. HLB of nonionic surfactant component using Genapol + TRS/IBA with n-Tetradecane at different salinities. ....	96
A49. Log of optimal salinity vs. HLB of nonionic surfactant component using Igepal + TRS/IBA with n-Heptane at different temperatures. ....	96
A50. Log of optimal salinity vs. temperature using Igepal + TRS/IBA with n-Heptane at different HLB values. ....	97
A51. Phase inversion temperature vs. HLB of nonionic surfactant component using Igepal + TRS/IBA with n-Heptane at different salinities. ....	97
A52. Log of optimal salinity vs. HLB of nonionic surfactant component using Igepal + TRS/IBA with n-Octane at different temperatures. ....	98
A53. Log of optimal salinity vs. temperature using Igepal + TRS/IBA with n-Octane at different HLB values. ....	98
A54. Phase inversion temperature vs. HLB of nonionic surfactant component using Igepal + TRS/IBA with n-Octane at different salinities. ....	99
A55. Log of optimal salinity vs. HLB of nonionic surfactant component using Igepal + TRS/IBA with n-Nonane at different temperatures. ....	99
A56. Log of optimal salinity vs. temperature using Igepal + TRS/IBA with n-Nonane at different HLB values. ....	100

## ILLUSTRATIONS–Continued

	<u>Page</u>
A57. Phase inversion temperature vs. HLB of nonionic surfactant component using Igepal + TRS/IBA with n-Nonane at different salinities. ....	100
A58. Log of optimal salinity vs. HLB of nonionic surfactant component using Igepal + TRS/IBA with n-Decane at different temperatures. ....	101
A59. Log of optimal salinity vs. temperature using Igepal + TRS/IBA with n-Decane at different HLB values. ....	101
A60. Phase inversion temperature vs. HLB of nonionic surfactant component using Igepal + TRS/IBA with n-Decane at different salinities. ....	102
A61. Log of optimal salinity vs. HLB of nonionic surfactant component using Igepal + TRS/IBA with n-Dodecane at different temperatures. ....	102
A62. Log of optimal salinity vs. temperature using Igepal + TRS/IBA with n-Dodecane at different HLB values. ....	103
A63. Phase inversion temperature vs. HLB of nonionic surfactant component using Igepal + TRS/IBA with n-Dodecane at different salinities. ....	103
A64. Log of optimal salinity vs. HLB of nonionic surfactant component using Igepal + TRS/IBA with n-Tetradecane at different temperatures. ....	104
A65. Log of optimal salinity vs. temperature using Igepal + TRS/IBA with n-Tetradecane at different HLB values. ....	104
A66. Phase inversion temperature vs. HLB of nonionic surfactant component using Igepal + TRS/IBA with n-Tetradecane at different salinities. ....	105
C1. CT-images of porosity and oil saturation distributions for CT-CF 1.....	107
C2. CT-images of porosity and oil saturation distributions for CT-CF 3.....	108
C3. CT-images of porosity and oil saturation distributions for CT-CF 4.....	109
C4. CT-images of porosity and oil saturation distributions for CT-CF 5.....	110
C5. CT-images of porosity and oil saturation distributions for CT-CF 7.....	111
C6. CT-images of porosity and oil saturation distributions for CT-CF 8.....	112
C7. CT-images of porosity and oil saturation distributions for CT-CF 9.....	113
C8. CT-images of porosity and oil saturation distributions for CT-CF 10.....	114



## SCREENING OF MIXED SURFACTANT SYSTEMS:

### Phase Behavior Studies and CT Imaging of Surfactant-Enhanced Oil Recovery Experiments

by Feliciano M. Llave, Bonnie L. Gall, Philip B. Lorenz, Idell M. Cook, and Larry J. Scott

---

#### ABSTRACT

A systematic chemical screening study was conducted on selected anionic-nonionic and nonionic-nonionic systems. The objective of the study was to evaluate and determine combinations of these surfactants that would exhibit favorable phase behavior and solubilization capacity. The effects of different parameters including (a) salinity, (b) temperature, (c) alkane carbon number, (c) HLB of nonionic component, and (d) type of surfactant on the behavior of the overall chemical system were evaluated. The current work was conducted using a series of ethoxylated nonionic surfactants in combinations of several anionic systems with various hydrocarbons.

Efforts to correlate the behavior of these mixed systems led to the development of several models for the chemical systems tested. The models were used to compare the different systems and provided some guidelines for formulating them to account for variations in salinity, oil hydrocarbon number, and temperature. The models were also evaluated to determine conformance with the results from experimental measurements. The models provided good agreement with experimental results.

The nonionic-nonionic mixtures generally yielded considerably higher optimal salinity levels compared to those of the anionic-nonionic and anionic systems. The anionic-nonionic mixtures also exhibited relatively higher salinity values than those of the anionic system alone. Mixing the nonionic surfactant with the anionic component contributed to a significant improvement in the overall solutions' range of applicable optimal salinities. The effect of the addition of anionic component on reduction in overall solution optimal salinity diminished with increasing alkane carbon number (ACN) and hydrophilic/lipophilic balance (HLB) levels. The salinity reduction was larger and more sensitive to HLB for the linear alkyl alcohol ethoxylates than for the dialkyl phenols. For most systems tested, the sensitivity to HLB was much higher when the anionic component was added. Thus, a nonionic-rich chemical blend was less dependent on accurate adjustments of HLB to be effective than a nonionic-lean blend. However, this difference in dependence decreased with increasing ACN or HLB values.

Temperature had a significant effect on these mixed surfactant systems. The nonionics were observed to be more temperature sensitive than the anionic surfactants. The observed temperature sensitivity was of the order: linear alkyl alcohol ethoxylate > dialkyl phenol > petroleum

sulfonate/alcohol. The sensitivity of the chemical system to type of hydrocarbon present followed the order: petroleum sulfonate/alcohol > linear alkyl alcohol ethoxylate > dialkyl phenol. Based on this hydrocarbon-sensitivity order, chemical systems formulated with linear alkyl alcohol ethoxylates or petroleum sulfonate/alcohol for a particular oil would require more reformulation effort than the dialkyl phenol systems, in order to be optimized for application with another hydrocarbon.

X-ray computed tomography (CT) was used to study fluid distributions during chemical enhanced oil recovery experiments. CT-monitored corefloods were conducted to examine the effect of changing surfactant slug size injection on oil bank formation and propagation. Reducing surfactant slug size resulted in lower total oil production. Oil recovery results, however, did not correlate with slug size for the low-concentration, alkaline, mixed surfactant system used in these tests. The CT measurements showed that polymer mobility control and core features also affected the overall oil recovery results.

Corefloods were also conducted using reservoir core from the North Burbank Unit (NBU), Osage County, Oklahoma, a Class 1 reservoir. Core heterogeneity and wettability had a significant effect on fluid movement through this core. Only about 50% of the core was well swept by the injected fluids.

## INTRODUCTION

For many U.S. oil reservoirs, chemical flooding enhanced oil recovery (EOR) may be the only viable means of extending their "productive lives". Most of the advances in this area resulted from laboratory work, theory, computational procedures, and improved overall engineering methodology. Several recent reviews of the state of the art provide an overview of the direction of the technology.<sup>1-4</sup> The potential of chemical flooding EOR is hindered by the need for a comprehensive research and development program for efficient and economic application at present and projected oil prices. A workshop sponsored by the U.S. Department of Energy (DOE) was also held recently to assemble industry experts on chemical flooding and identify the research direction, potential prospects, and application of chemical flooding EOR technology.<sup>5</sup>

The application of surfactant flooding EOR has been dictated by economics as seen in reports on field projects.<sup>6-7</sup> Six field projects are currently active in the United States.<sup>1</sup> One test was considered successful, four were promising, and one was too early to tell. New field projects planned by ARCO in Newton County, Texas and by Marathon in Pecos County, Texas were scheduled for startup at the end of 1989. The ARCO project was canceled along with three other projects that were recently terminated, including Texaco's promising Salem (Illinois) field project. Most of the domestic field projects on surfactant flooding were performed in deltaic reservoirs. An analysis of 20 field projects conducted in these deltaic reservoirs<sup>8</sup> revealed that channeling,

compartmentalization, directional permeability trends, formation parting, and formation salinity are the conditions commonly encountered in these field tests contributing to the lower than expected oil recovery. Applications of surfactant flooding technology in foreign oil reservoirs include the Bothamsall project in the UK, the Hankensbuettel project in Germany, the Total project in Handil, Indonesia and the Chateaurnard project in France. The tests in France and Germany appeared to be successful in recovering significant oil, while the test in Bothamsall was discouraging. Information about the Total project is limited. A more recent foreign implementation of chemical flooding EOR was planned for the Romashkino field in Tatarstan, of the former Soviet Union, in the summer of 1992.<sup>9</sup> Information regarding the status of this test is currently unavailable.

The major focus of current R&D efforts has been on (1) improving surfactant system effectiveness; (2) maintaining chemical slug integrity; (3) application under limiting reservoir conditions; and (4) improving economics by using low-concentration surfactant formulations. Key research areas under these headings have included the effects of surfactant structure and formulation of surfactant slugs, temperature, and salinity on properties of surfactant formulations such as interfacial tension (IFT), critical micelle concentration (CMC), and phase behavior, as well as surfactant behavior with respect to adsorption, chromatographic separation, precipitation, phase trapping, and oil recovery. Most of the work conducted on surfactant flooding EOR has been focused on sulfonate-type surfactants. Petroleum sulfonates have been widely investigated based on defined criteria of material cost, reservoir compatibility, and supporting results from laboratory experiments. Petroleum sulfonate-based chemical floods have also been implemented in the field with limited success, both technically and economically.<sup>10</sup> Sensitivity to salinity has often been an overriding factor affecting surfactant performance in the field.<sup>11</sup> Traditionally, cosurfactants or cosolvents consisting of short-chain alcohols have been used to increase surfactant salinity tolerance. Unfortunately, mixtures of surfactant and alcohol are subject to preferential partitioning into the oil phase and also to chromatographic separation of slug components by reservoir rock. Other potentially applicable sulfonate-type surfactants, such as alkyl-aryl sulfonates, may be more expensive to manufacture, but their improved performance potential under adverse reservoir conditions oftentimes offsets their higher costs. These latter-type sulfonates are effective and thermally stable over a wide range of temperatures at relatively low salinity levels. One drawback in the use of these surfactants is the formation of condensed phases and persistent emulsions in the absence of relatively high alcohol cosolvent concentrations.

The DOE National Energy Strategy-Advanced Oil Recovery Program (NES-AORP) was developed as a means of improving domestic oil production. The focus of this program is the advancement of the best currently defined EOR technologies and utilization of these methods to improve recovery from targeted reservoirs. In accordance with DOE's strategy, the goal of the NIPER research program is to develop surfactant systems that are both cost-effective and have

improved adaptability to variations in salinity, hardness, temperature, and dilution for recovery of crude oils from selected fluvial-dominated deltaic reservoirs (designated as Class 1 in the NES-AORP). Research under this program has been focused primarily on mixed surfactant systems that have been shown to have potential advantages over conventional chemical flooding systems. These surfactant systems can be designed to achieve improved tolerance to adverse conditions as well as variability in reservoir conditions encountered by injected fluids. These systems can be formulated with surfactant components that jointly have high oil recovery potential (i.e., high oil solubilization and ultra low interfacial tension) and improved adaptability to different ranges of salinity, divalent ion concentrations, and temperature. The existence of a synergistic effect with mixed compositions can be evaluated to develop a surfactant system or systems that will retain relatively low interfacial tension (IFT) values over a range of target reservoir conditions, while maintaining overall chemical effectiveness at an acceptable level. Factors influencing the economic potential of the chemical system(s) have to be considered as well. A balance between cost and oil recovery effectiveness has to be achieved in order to find the best surfactant systems for field application.

The more recent research work conducted under this program has been focused primarily on identifying mixed surfactant systems that can be formulated with chemical components that synergistically yield high oil recovery potential and improved solution behavior and adaptability. Several commercially available surfactants were tested as primary components in the chemical systems and mixtures used in the study.<sup>12-14</sup> These surfactants were formulated with different secondary as well as tertiary components, including other ethoxylated and non-ethoxylated sulfonates and sulfates. Improved salinity and hardness tolerance were achieved for some of these chemical systems. Oil displacement experiments in Berea sandstone cores showed considerable improvement in oil recovery potential of these systems compared to the tests using chemical systems containing individual surfactant components studied in prior work. Some of these displacement experiments were conducted with the aid of advanced imaging techniques such as NIPER's computer-aided tomography (CT) scanner to determine the progression of the flood.<sup>13,15-16</sup> Both the effectiveness of the surfactant formulation and the mobility control system can be monitored using this technique. Studies were also conducted using two cosurfactant systems added to a primary surfactant component. The studies conducted were based on the concept of balancing the effect of the secondary and tertiary surfactant components in maintaining the oil and water affinity of the overall chemical system, similar to an hydrophilic-lipophilic balance (HLB) gradient approach.<sup>13-14</sup> Results from these studies showed favorable IFT values as well as phase behavior at the conditions tested.

Evaluation of the effectiveness of chemical systems to mobilize oil is a complex process. The ability of the surfactant to solubilize oil depends on the chemical nature of the surfactant and

the oil and other experimental parameters such as brine salinity and temperature. Measurements of solution properties such as interfacial tension, solubilization parameters, and phase behavior are used to screen surfactant formulations to determine conditions under which they can effectively solubilize oil. Ultimately, however, the chemical formulation must be injected into rock samples to test its ability to mobilize discontinuously distributed oil droplets, generate an oil bank, and keep the oil bank mobilized to maximize oil production. In the past, oil production during laboratory tests was monitored using pressure measurements along the core length and by collecting fluids exiting from the core. By watching pressure fluctuations as the fluid fronts advance, average advance of an oil bank can be observed. No information, however, can be obtained for nonuniform fluid distributions during recovery experiments using these techniques. CT-imaging, however, allows visualization of fluid movement during various stages of an oil recovery experiment. Observation of nonuniform saturation distributions that result from core heterogeneities (permeability streaks) or from problems in fluid mobilization (poor chemical design) may help improve design or application criteria for chemical EOR technology.

The research for FY93 continues to focus on the use of mixed surfactant systems on a specific range of conditions. An experimental study was conducted on several mixed surfactant systems containing different primary surfactant components with the addition of a series of ethoxylated nonionic surfactants. This study was performed to evaluate and determine the effect of several experimental parameters of the overall surfactant solution behavior of these systems. These experimental parameters include temperature, salinity, hydrocarbon chain length, and the HLB of various proportions of nonionic surfactants. The particularly focus of the study was on anionic-nonionic mixtures that may exhibit much improved phase behavior and solubilization capacities, compared to the primary anionic formulation. One of the primary chemical anionic systems used for this study was the TRS 10-410/IBA system.<sup>17-18</sup> This chemical system has been shown to develop relatively low interfacial tensions (IFT) at low optimal salinity and low concentrations of divalent ions.<sup>17-18</sup> Another primary surfactant system containing an alpha olefin sulfonate (AOS) was also evaluated for this study. Combinations of these anionic-nonionic surfactants were studied to identify the conditions and chemical systems that result or exhibit favorable solution behavior.

At NIPER, significant effort over the past several years has resulted in the development and use of CT imaging techniques to characterize rock structure and fluid distributions within rock pore space. Information concerning the development of techniques and principles of operation of CT imaging can be found elsewhere.<sup>19-22</sup> Initial efforts to use CT imaging techniques to help understand and evaluate fluid movement and oil production during surfactant/polymer enhanced oil recovery experiments were reported previously.<sup>16,23</sup> The conclusions from this initial study included the following observations. Formation and propagation of an oil bank could be observed

using CT-imaging techniques. Oil banks often propagated in a nonuniform manner. Variation in permeability within the core affected the fluid frontal advance rate so that both the effects of injected chemical effectiveness and core heterogeneities could be observed. Use of a poor mobility control agent was very detrimental to oil recovery. Use of a less effective surfactant system with adequate mobility control could produce as much oil as the use of a good surfactant system with inadequate mobility control. Additional studies using CT-imaging to monitor oil production during EOR experiments were recommended.

Two series of experiments were conducted during FY93, including: experiments (1) to determine the effect of changing injected surfactant slug size on oil movement and recovery and (2) to determine the effect of changing surfactant slug salinity conditions on oil recovery. In addition, a surfactant enhanced oil recovery experiment in reservoir rock from the North Burbank Unit, Osage County, Oklahoma was conducted.

This work is part of a DOE sponsored research project, Improvements in Surfactant Flooding Methods (Project BE4A), to improve chemical EOR flooding methods. Overall objectives of this project are (1) to apply advanced EOR technology based on mixed surfactant systems to improve oil recovery from Class 1 reservoirs; (2) to extend the use of surfactant EOR to different salinity and temperature ranges by developing surfactant systems which are more adaptable to changes in chemical composition in selected reservoirs; (3) to develop cost-effective chemical systems for selected field applications that may contain low concentrations of synthetic surfactant and alkaline additives.

This report is organized into two sections. Section I summarizes screening experiments using mixed surfactant systems, and Section II summarizes coreflood experiments using CT-imaging techniques to determine oil saturations during chemical injection. Additional figures for the screening section are found in appendix A. Appendix B contains generalized CT-coreflooding procedures and composite images of the corefloods described in this report.

## **ACKNOWLEDGMENTS**

This work was sponsored by the U.S. Department of Energy under cooperative agreement DE-FC22-83FE60149. The authors wish to thank Dr. Min K. Tham of NIPER for his guidance and advice in conducting the study. The authors also wish to acknowledge Dr. Liviu Tomutsa and Alan Brinkmeyer of the NIPER CT Imaging Group for their expertise, advice, and assistance in conducting the CT experiments.

## I. SCREENING OF MIXED SURFACTANT SYSTEMS

### *Materials and Experimental Procedures*

#### Materials

A listing of the nonionic and anionic surfactants used in the study is presented in Tables 1 and 2. These chemicals were used without further purification, unless otherwise specified. Table 3 is a listing of the different surfactant systems formulated for the study. The system number listed in Table 3 corresponds to the surfactant systems previously studied and reported.<sup>14</sup> These systems were formulated with a series of nonionic surfactants in combination with an anionic surfactant system. These chemical formulations were prepared using reagent grade salts, and the concentrations are reported as weight of surfactant chemical to volume of solution (wt/vol).

TABLE 1 - List of anionic surfactants studied

Name	Code	Type	Alkane Chain
AOS 14-16	AOS 14-16	Alpha olefin sulfonate	14-16
AOS 16-18	AOS 16-18	Alpha olefin sulfonate	16-18
TRS	TRS 10-410	petroleum sulfonate	

TABLE 2 - List of nonionic surfactants studied

Company	Name	Code	Type	Alkane Chain	EO <sup>1</sup>	HLB <sup>2</sup>
Hoechst	Genapol	26L-3	alcohol ethoxylate	12-16	3	8.0
Hoechst	Genapol	26L-5	alcohol ethoxylate	12-16	5	10.6
Hoechst	Genapol	26L-60	alcohol ethoxylate	12-16	7.3	12.4
Rhone-Poulenc	Igepal	DM-430	ethoxylated dialkyl phenol	9	7	9.4
Rhone-Poulenc	Igepal	DM-530	ethoxylated dialkyl phenol	9	9	10.6
Rhone-Poulenc	Igepal	DM-730	ethoxylated dialkyl phenol	9	15	15.1

<sup>1</sup>number of ethylene oxide groups

<sup>2</sup>hydrophilic/lipophilic balance

TABLE 3 - List of surfactant systems studied using PIT method

System No(s).	Components and Concentration of Surfactant Systems	HLB
3	1 wt% DM-530 and 1 wt% TRS 10-410/IBA [50:50]	10.6
44	1 wt% DM-430/DM-530 [50:50] and 1 wt% TRS 10-410/IBA [50:50]	10.0
45(70)	1 wt% DM-530/DM-730 [91:9] and 1 wt% TRS 10-410/IBA [50:50]	11.0
46(72)	1 wt% DM-530/DM-730 [80:20] and 1 wt% TRS 10-410/IBA [50:50]	11.5
47(74)	1 wt% DM-530/DM-730 [69:31] and 1 wt% TRS 10-410/IBA [50:50]	12.0
48	1 wt% DM-530/DM-730 [58:42] and 1 wt% TRS 10-410/IBA [50:50]	12.5
50	1 wt% Genapol 26-L-3/26-L-5 [42:58] and 1 wt% TRS 10-410/IBA [50:50]	9.5
51(69)	1 wt% Genapol 26-L-5/26-L-3 [77:23] and 1 wt% TRS 10-410/IBA [50:50]	10.0
52	1 wt% Genapol 26-L-5 and 1 wt% TRS 10-410/IBA [50:50]	10.6
53(71)	1 wt% Genapol 26-L-5/26-L-60 [78:22] and 1 wt% TRS 10-410/IBA [50:50]	11.0
54	1 wt% Genapol 26-L-5/26-L-60 [47:53] and 1 wt% TRS 10-410/IBA [50:50]	11.55
55(73)	1 wt% Genapol 26-L-5/26-L-60 [22:78] and 1 wt% TRS 10-410/IBA [50:50]	12.0
57(38b)	2 wt% Genapol 26-L-3/26-L-5 [42:58]	9.5
58(40c)	2 wt% DM-430/DM 530 [83:17]	9.6
59(23)	2 wt% Igepal DM-430/DM-530 [50:50]	10.0
60(26)	2 wt% Genapol 26-L-5/26-L-3 [77:23]	10.0
61(22)	2 wt% DM-530/DM-730 [91:9]	11.0
62(39a)	2 wt% Genapol 26-L-5/26-L-60 [78:22]	11.0
63(31)	2 wt% DM-530/DM-730 [69:31]	12.0
64(39c)	2 wt% Genapol 26-L-5/26-L-60 [22:78]	12.0
65(39b)	2 wt% Genapol 26-L-5/26-L-60 [47:53]	11.55
66(30)	2 wt% DM-530/DM-730 [80:20]	11.5
67(24)	2 wt% Genapol 26-L-5	10.6
68(1)	2 wt% DM-530	10.6

### Phase Inversion Temperature Measurements

Much of the surfactant system screening performed for this study was conducted with the aid of a phase inversion temperature (PIT) measurement apparatus. The PITs of these chemical systems studied were measured using a computer-controlled apparatus designed and constructed at NIPER.<sup>24</sup> The PIT is the temperature condition at which a water-in-oil emulsion changes into an oil-in-water emulsion or vice versa. This phase transition can be detected by measuring the electrical conductivity of a well-stirred mixture as a function of the temperature. The PIT

experiment is routinely associated with measurement of the above phase transition for nonionic surfactants, and the technique has been used extensively by other researchers to evaluate surfactant-oil interaction.<sup>25-26</sup> A detailed description of the experimental procedure utilizing this apparatus has been reported.<sup>24</sup>

### **Phase Behavior Measurements-Salinity Scans**

Phase behavior measurements were conducted on selected chemical systems to evaluate and quantify their respective oil/water solubilization capacities. The effects of several experimental factors on the phase behavior of the overall chemical/hydrocarbon systems were evaluated. From these experiments, the oil/water solubilization capacities of these systems were determined. These tests were conducted using chemical solutions that were made up at a fixed water-to-oil ratio ( $\text{volume}_{\text{water}} : \text{volume}_{\text{oil}} = 1$ ). These solutions were prepared in 10-mL glass pipets that were sealed and equilibrated in approved safety ovens at the desired temperature levels. The relative volumes of the different phases were read and recorded at set time intervals until constant readings were obtained. These constant phase volume readings were then used to calculate the solubilization parameters of the oil ( $\sigma_o = V_o/V_s$ ) and the brine ( $\sigma_w = V_w/V_s$ ). Unusual phase behavior such as the formation of gels, liquid crystalline phases, and precipitation was also observed and recorded. Details regarding these calculations have been reported.<sup>27</sup>

### **Interfacial Tension Measurements**

The interfacial tension (IFT) of the different chemical systems tested was measured using a Model 300 Spinning Drop Interfacial Tensiometer, manufactured at University of Texas at Austin. These measurements were conducted using several equilibrated and nonequilibrated systems and different hydrocarbons at selected conditions. These measurements were taken after sufficient equilibration time had been allowed at the temperature conditions desired. Several measurements were taken until reproducible IFT values were obtained. Other parameters needed in the calculation of the corresponding IFT, such as densities and refractive indices, were also measured. The procedure for measuring IFT and other experimental parameters have also been reported.<sup>12</sup>

## **RESULTS AND DISCUSSION**

### ***Mixed Surfactant Screening***

Experimental studies were conducted on selected series of ethoxylated nonionic surfactants in combination with a primary anionic surfactant system. The objective of these studies was to evaluate and identify combinations of these surfactants, both anionic-nonionic and nonionic-

nonionic mixtures, that may exhibit improved phase behavior and oil/water solubilization capacity, in comparison to that of the primary anionic formulation. Results from earlier studies have shown that these ethoxylated surfactants can be used in extending the range of application of the primary sulfonate system.<sup>13-14</sup> These nonionic surfactants were used in the study to evaluate the combinations of chemical systems that may exhibit favorable and improved overall solution behavior.

The primary anionic surfactant system used in this study was the TRS 10-410/IBA system. This surfactant system has been fairly well evaluated.<sup>14,17-18</sup> As previously mentioned, the results of prior screening tests showed that the addition of ethoxylated secondary surfactants can enhance the salinity tolerance of the overall system.<sup>13-14</sup> This work was conducted to extend the experimental evaluation performed in the earlier work to much elevated temperatures and in combinations with various n-alkanes. Much of the earlier work concentrated on using n-decane, with selected tests conducted using n-octane, with emphasis on operating at about 50° C. The current experimental work encompassed a temperature range up to 70° C and included various n-alkanes such as n-heptane, n-octane, n-nonane, n-decane, n-dodecane, and n-tetradecane. These experiments were designed to help evaluate and determine the phase behavior of the overall surfactant solution as a function of the amount and type of secondary surfactants added. Particular emphasis was given to determining the effect of the nonionic surfactant component's hydrophilic-lipophilic balance (HLB) values on overall solution behavior. Several experimental methods were employed in determining optimum conditions for the surfactant systems. These methods included the PIT method, salinity scans, and IFT measurements at various conditions.

### **Screening by Phase Inversion Temperature Method**

The PIT method was utilized as a means of screening these surfactant combinations for the range of applicable salinity levels. This relatively fast screening method was needed to effectively evaluate an exhaustive number of different combinations of nonionic-nonionic and anionic-nonionic surfactant systems. The purpose of these tests was to determine the range of optimal salinity of several chemical systems based on the HLB parameter of the nonionic component. These experiments were conducted to find systems where a favorable balance between salinity tolerance and oil solubilization can be maintained. These studies included a series of nonionic surfactants of different HLBs as well as combinations of these surfactants yielding intermediate HLB values. Several nonionic surfactants were tested using the above-mentioned method including a series of Genapol and Igepal surfactants of a wide range of HLB values. The surfactant systems studied are listed in Table 3. These surfactants were tested in combination with TRS 10-410/IBA [1:1] surfactant system at a fixed proportion of 1:1, at a total surfactant

concentration of 2 wt%. The chemical proportions used in the present study were similar to those used in the earlier study.<sup>14</sup>

Example results of the surfactant screening utilizing the PIT method are presented in Figs. 1 through 18. The remainder of the results from the study are presented in appendix A. Utilizing the PIT method, approximate optimal salinity conditions for these surfactant systems were identified and correlated with various experimental parameters such as HLB, n-alkane and temperature. Attempts to provide correlations for the observed optimal salinity behavior will be discussed in a later section. The results of these PIT studies were also used as means of determining the range of conditions where conventional salinity scans can be conducted. Using the PIT results as guides, a series of salinity scans were conducted on selected chemical systems. These salinity scans in turn provided information on the oil/water solubilization capacity of each of the systems tested. The results from the PIT studies were compared to the results of salinity scan studies. These comparisons are discussed in the next section.

Figures 1 through 4 are example summary plots of the optimum salinity ( $S^*$ ) of the different mixtures versus the HLB of the nonionic components using different alkanes at 50° C.

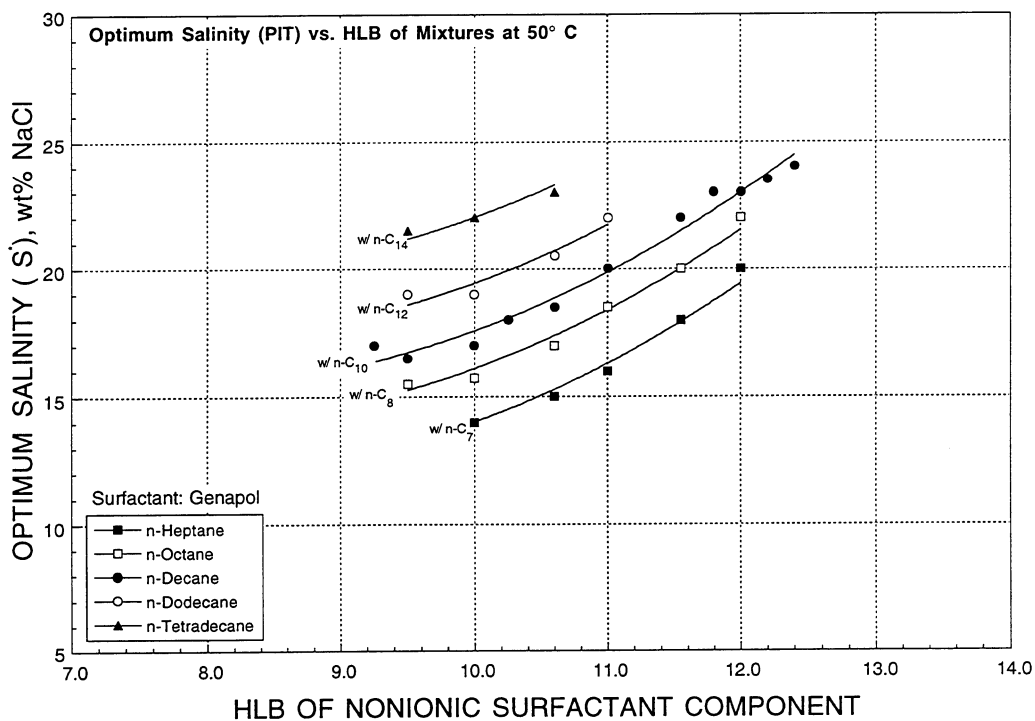


FIGURE 1. - Optimal salinity (PIT-method) vs. HLB of nonionic surfactant component using Genapol mixtures at 50° C with different alkanes.

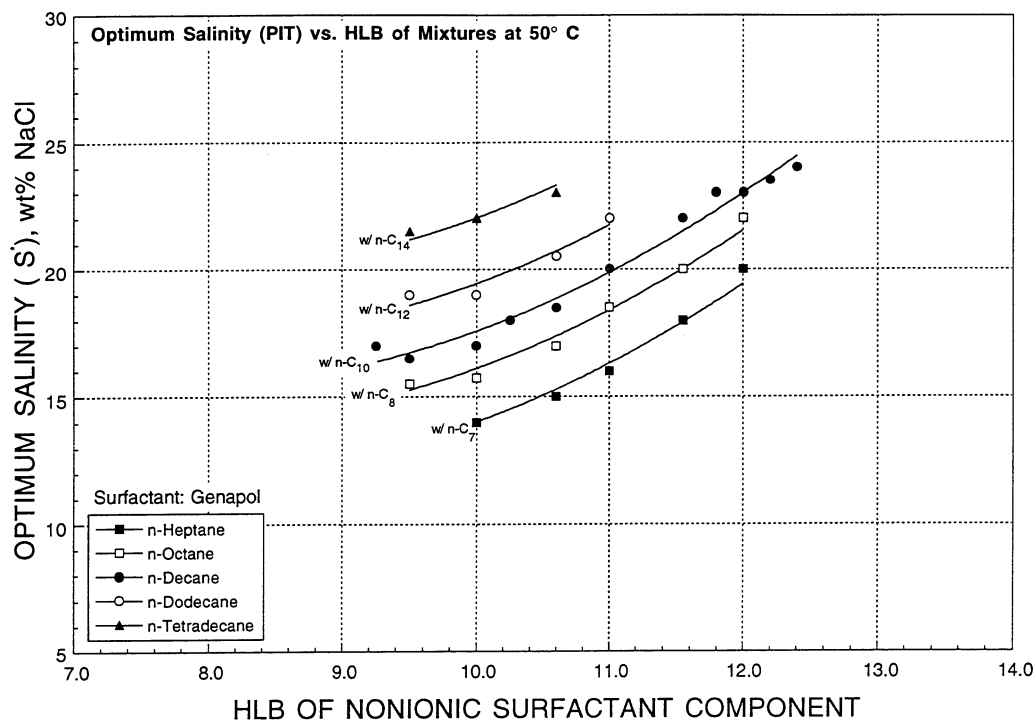


FIGURE 2. - Optimal salinity (PIT-method) vs. HLB of nonionic surfactant component using Igepal mixtures at 50° C with different alkanes.

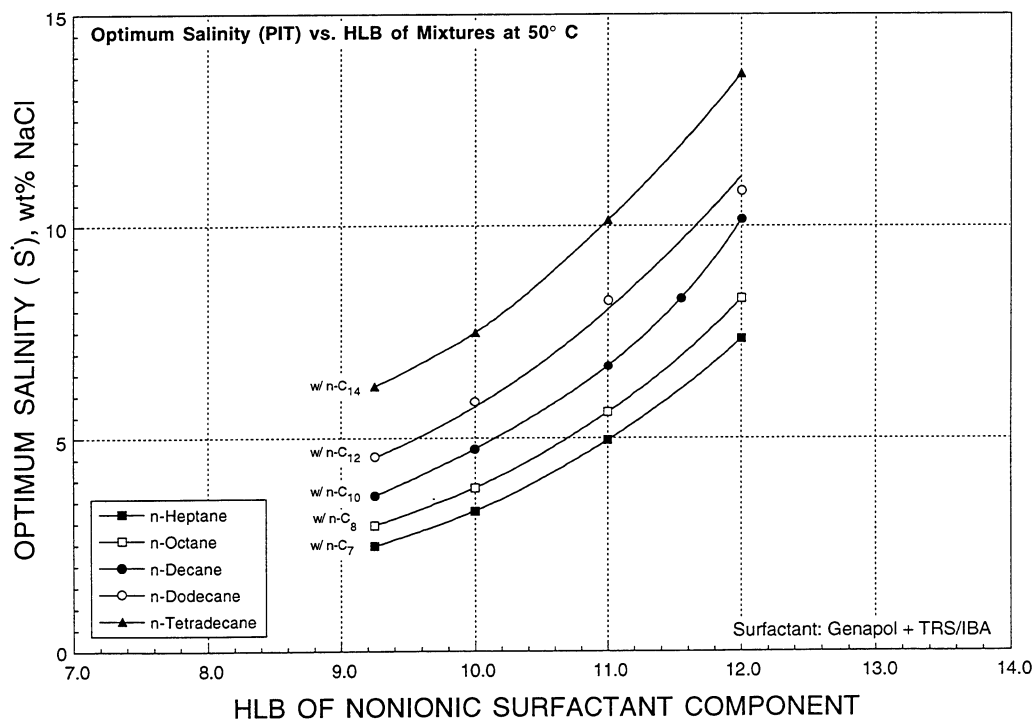


FIGURE 3. - Optimal salinity (PIT-method) vs. HLB of nonionic surfactant component using Genapol mixtures with TRS 10-410/IBA [1:1] at 50° C with different alkanes.

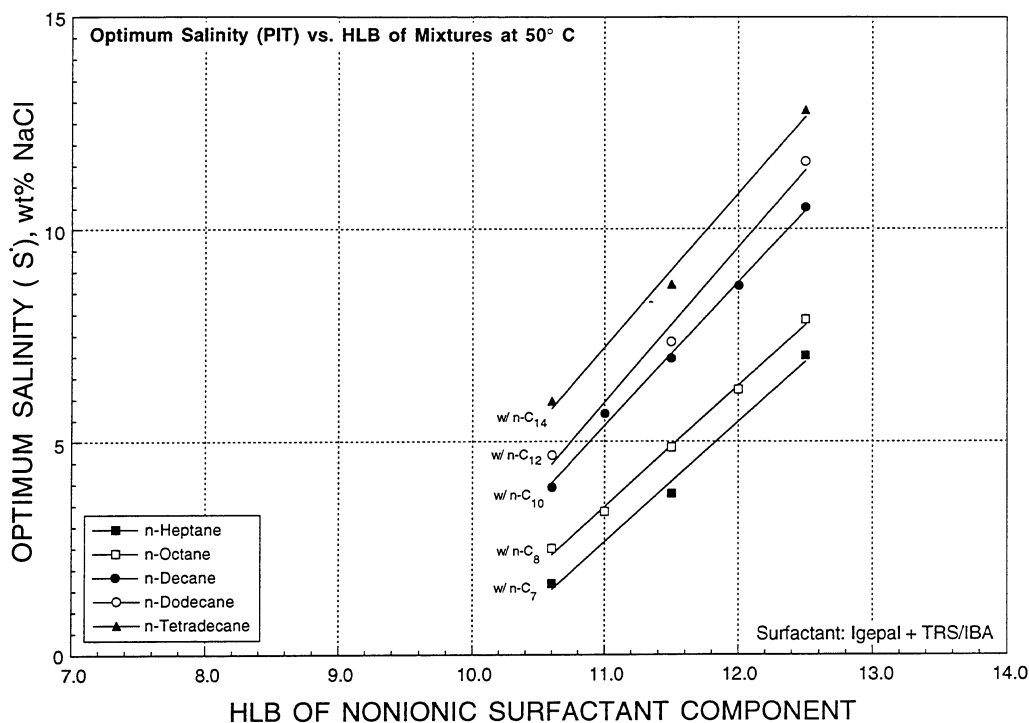


FIGURE 4. - Optimal salinity (PIT-method) vs. HLB of nonionic surfactant component using Genapol mixtures with TRS 10-410/IBA [1:1] at 50° C with different alkanes.

The results from these studies support the previous observations made in the earlier study<sup>14</sup> that the Genapol series of linear alkyl alcohol ethoxylates exhibited a very distinct behavior from the Igepal series of dialkyl phenol surfactants, at similar HLB levels. The mixtures of Igepal surfactants exhibited a more significant dependence on the HLB value than those of the Genapols. The contrast in the behavior of these two types of surfactants was more pronounced at lower HLB values and decreased at higher HLB values. The difference in overall behavior was also observed with the mixtures containing the TRS 10-410/IBA surfactant system. The mixtures containing the Genapol surfactants yielded much higher optimal salinity ranges compared to those of the mixtures containing the Igepal surfactants, at comparable HLB values. The trends in the dependence of the optimal salinity on HLB of the anionic-nonionic mixtures were similar to those exhibited by the nonionic-nonionic systems. The difference lies in the overall level of optimal salinity ranges for these different mixtures. The nonionic-nonionic mixtures generally exhibited considerably higher optimal salinity levels compared to those of the mixtures containing the anionic component alone.<sup>14</sup> The mixtures containing the anionic-nonionic components also exhibited considerably higher overall optimal salinity values than that exhibited by the base case anionic system.<sup>14</sup> The addition of the anionic component to the nonionic system contributed to a marked difference in the range of

applicable optimal salinity. The added nonionic component facilitated the shift in salinity tolerance of the overall mixtures.

Other observations provided some information on combinations of formulations and conditions that may be applicable for certain reservoirs. Decreasing the carbon chain length of the oil, from n-tetradecane to n-heptane, resulted in a reduction of the effective salinity range at a specific calculated HLB value and temperature. The reduction in salinity was necessary to rebalance the overall system due to the shift in the oil affinity of the system. Figures 5 and 6 show sample plots of the log of the optimal salinity for selected systems as a function of alkane carbon number at different HLB values. These plots better illustrate the dependence of optimal salinity on the carbon chain length of the oil at a specific HLB value and temperature. The optimal salinity increased proportionately with the increase in HLB of the surfactant system. The overall chemical system was rendered more hydrophilic at the higher HLB values. This increased hydrophilicity was offset by the need for higher salinity to shift the surfactant tendency to be more lipophilic. The dependence of optimal salinity versus HLB for surfactant systems is well documented. Similar observations were made for earlier studies.<sup>14</sup> The data scatter observed in these plots can be attributed to the difficulty in determining the approximate PIT for these colloidal systems, particularly for those that exhibited solution conductivity inversions that were not very significant.

Earlier attempts to evaluate the behavior of these surfactants showed that the logarithmic term for the optimal salinity provided more flexibility as a means to correlate the behavior of both nonionic-nonionic and anionic-nonionic mixtures.<sup>14</sup> Figures 7 through 10 are example plots of the log of the optimal salinity for each of the chemical systems presented in Figs. 1 through 4. Correlation with respect to the log of the optimal salinity was possible for most of the cases tested. A discussion on the correlation efforts is presented in the Modeling the Behavior of Mixed Surfactant section of this report.

The dependence of the solution behavior on temperature is better illustrated in Figs. 11 and 12. These figures show the plots of the log of the optimal salinity versus temperature at different HLB levels using a specific alkane, in this case dodecane. Several observations can be made from these figures. At a fixed temperature, the optimal salinity increased with the HLB. This was the same trend discussed in an earlier section of the report. The increased optimal salinity requirement balanced the higher hydrophilic tendency (higher HLB) of the overall chemical system. At a fixed HLB level, the results also indicated that higher optimal salinities were necessary for much lower operating temperature levels. The aqueous phase solubility and the lipophilic tendency of the surfactant were drastically affected by changes in the salinity (electrolyte concentration) of the overall solution. As reported earlier, the increase in salinity rendered the chemical system more lipophilic. A reduction in temperature was needed to maintain a new balance between the oil and

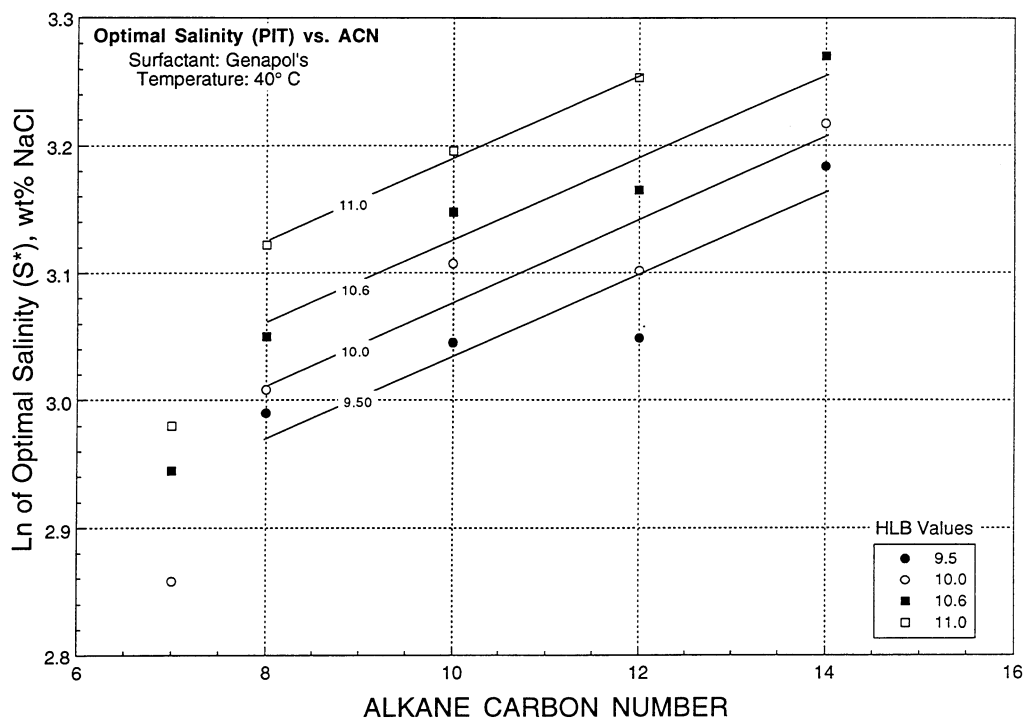


FIGURE 5. - Log of optimal salinity (PIT-method) vs. alkane carbon number of oil with different HLB of nonionic surfactant component using Genapol mixtures at 40° C.

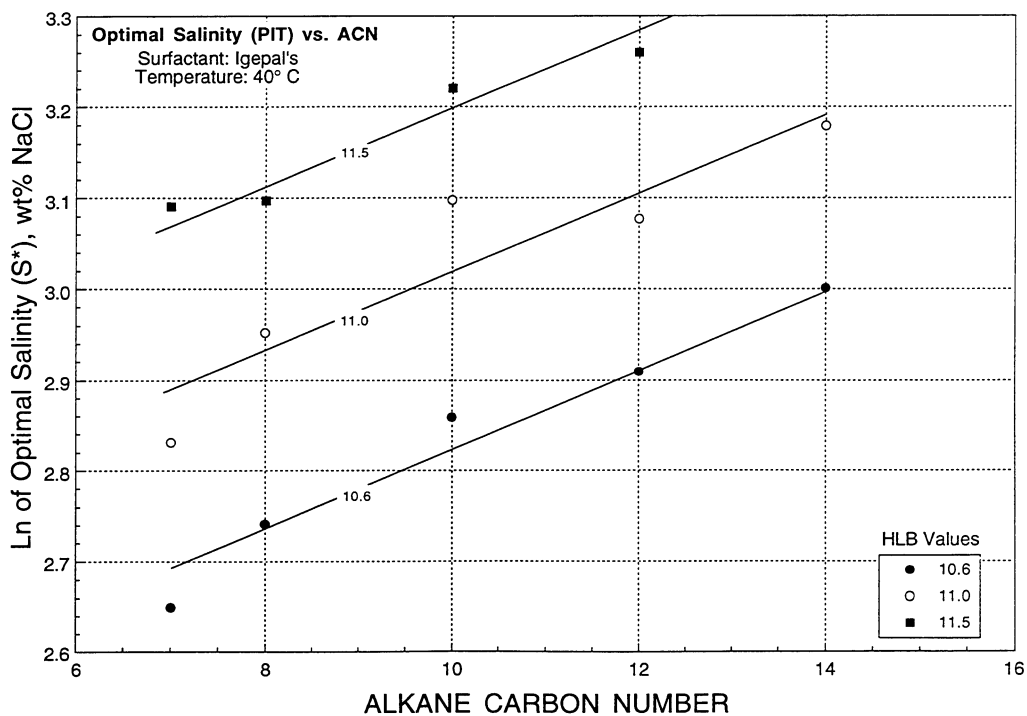


FIGURE 6. - Log of optimal salinity (PIT-method) vs. alkane carbon number of oil with different HLB of nonionic surfactant component using Igepal mixtures at 40° C.

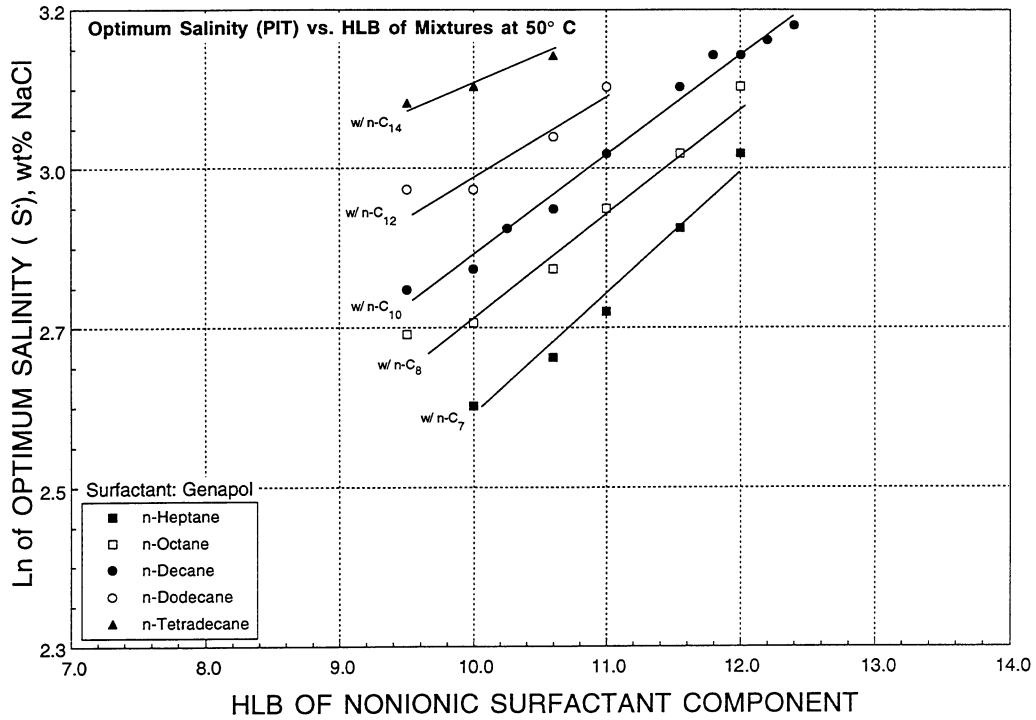


FIGURE 7. - Log of optimal salinity (PIT-method) vs. HLB of nonionic surfactant component using Genapol mixtures at 50° C with different alkanes.

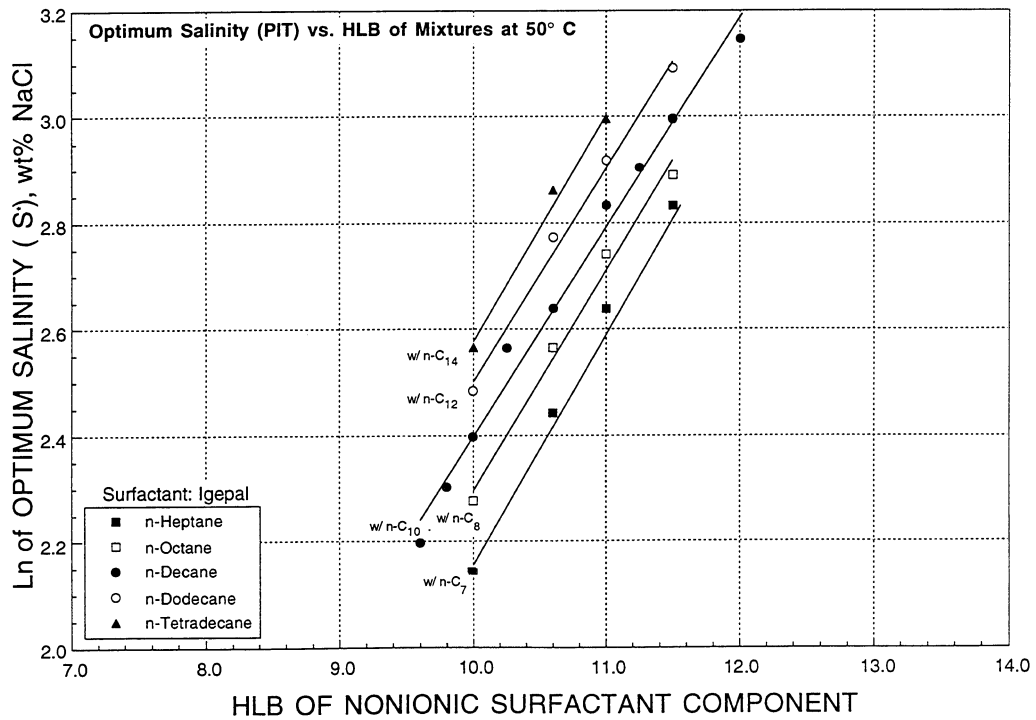


FIGURE 8. - Log of optimal salinity (PIT-method) vs. HLB of nonionic surfactant component using Igepal mixtures at 50° C with different alkanes.

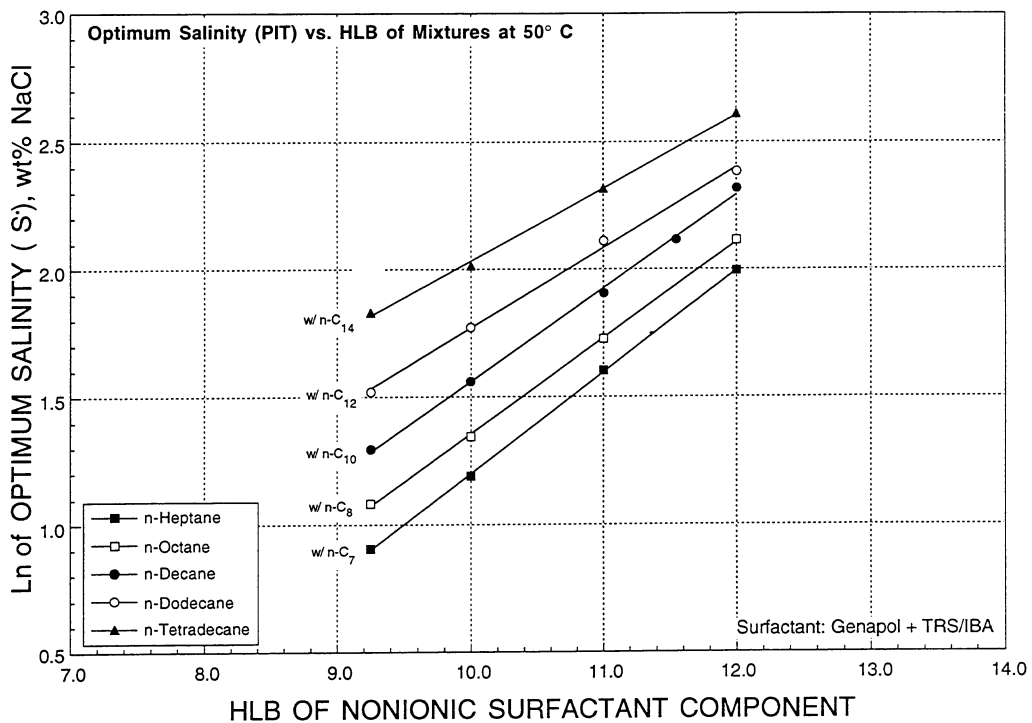


FIGURE 9. - Log of optimal salinity (PIT-method) vs. HLB of nonionic surfactant component using Genapol mixtures with TRS 10-410/IBA [1:1] at 50° C with different alkanes.

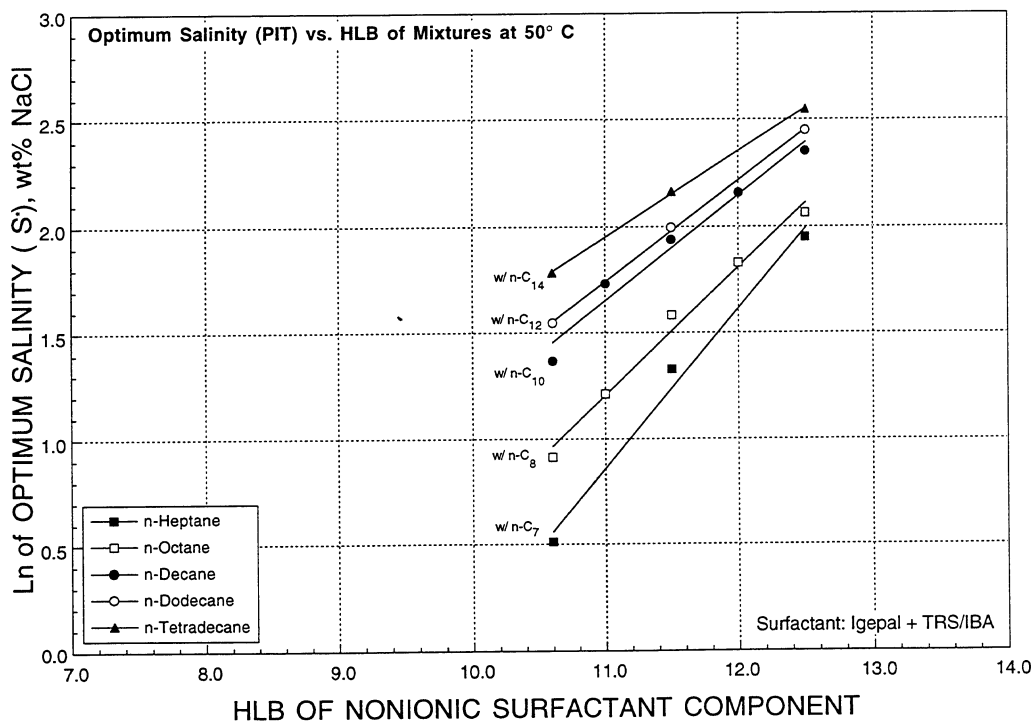


FIGURE 10. - Log of optimal salinity (PIT-method) vs. HLB of nonionic surfactant component using Genapol mixtures with TRS 10-410/IBA [1:1] at 50° C with different alkanes.

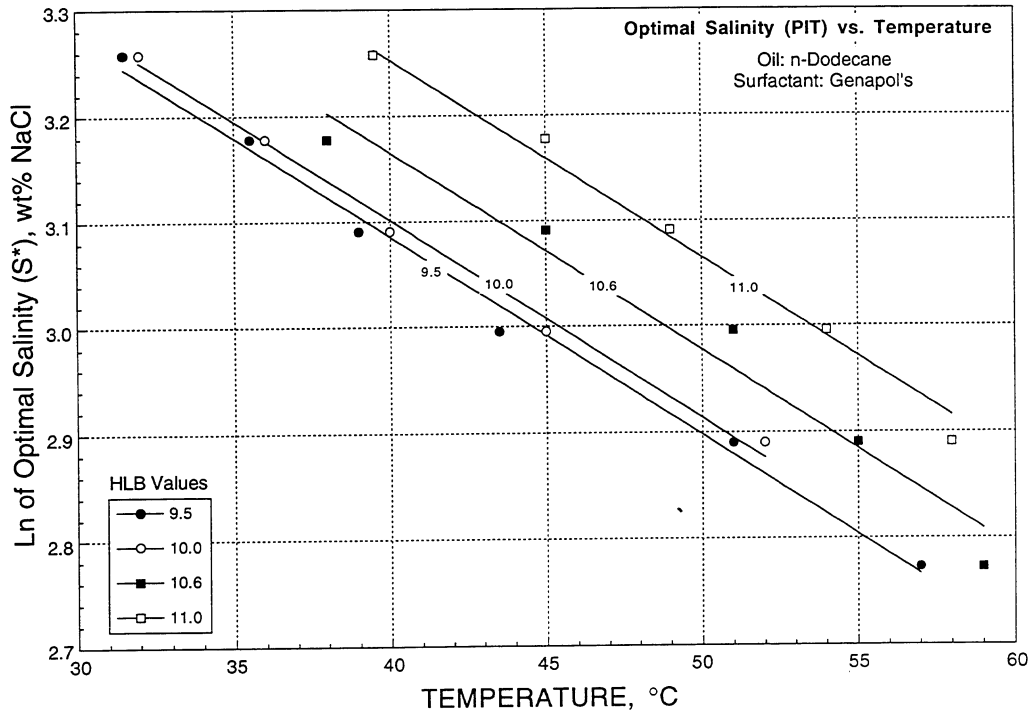


FIGURE 11. - Log of optimal salinity (PIT-method) vs. temperature with different HLB of nonionic surfactant component using Genapol mixtures with n-dodecane.

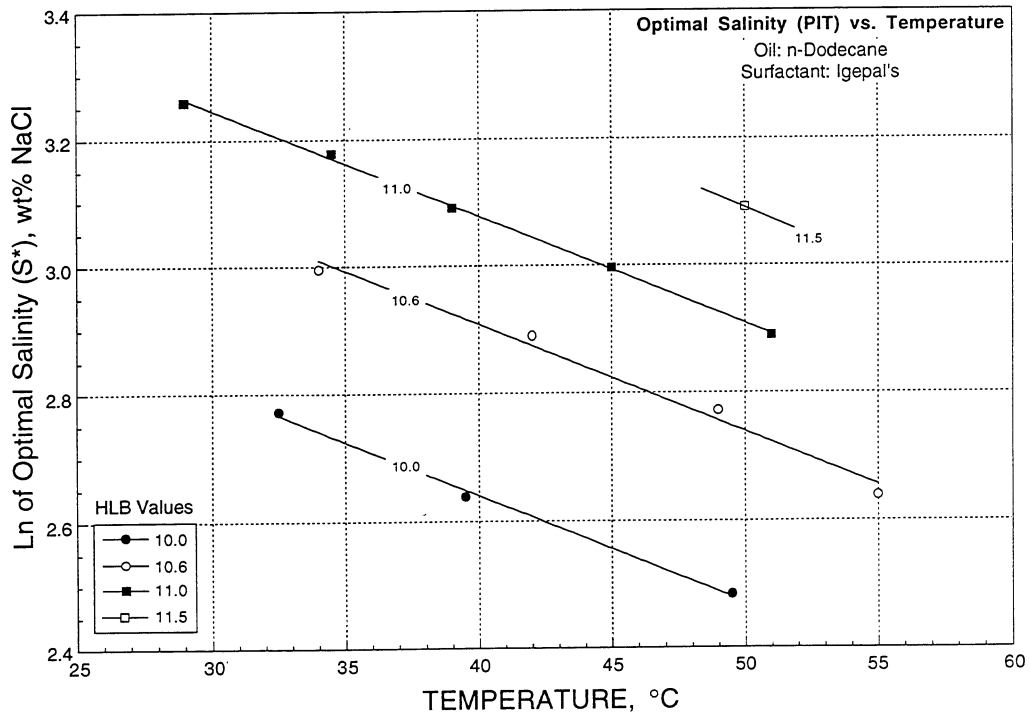


FIGURE 12. - Log of optimal salinity (PIT-method) vs. temperature with different HLB of nonionic surfactant component using Igepal mixtures with n-dodecane.

water affinity of the surfactant system. The system was rendered more hydrophilic as the temperature decreased. This in turn offset the system's increased lipophilic tendency due to the salinity increase. An increase in temperature effectively shifted the relative affinity of the surfactant for the oil (increased affinity) and the water (decreased affinity).<sup>28-29</sup> These results were similar to those previously reported by other researchers.

Figures 13 and 14 show similar plots of the log of the optimal salinity versus temperature at different HLB levels using n-dodecane in mixture containing the anionic surfactant system. As indicated in Figs. 11 and 12, much lower salinity ranges were also observed as the temperature of the system increased, at a fixed HLB value. The increase in temperature effectively increased the relative affinity of the surfactant for the oil while decreasing the relative water affinity. Much lower optimal salinity levels were then necessary to rebalance the overall system. The distinct difference in trend between the systems containing the two types of nonionic surfactants also seemed to decrease with the rise in temperature level. As reported earlier,<sup>14</sup> at HLB levels greater than 11, the pattern of behavior of the two types of nonionics was observed to be similar, with and without the presence of the primary anionic surfactant system. The difference in behavior was very much evident at lower HLB values, but the difference seemed to be suppressed in the presence of the anionic surfactant system. This difference in behavior in the presence of the anionic surfactant may be attributed to the relative effect of temperature variation of the individual anionic and nonionic surfactant components in the overall chemical system. The effect of temperature on nonionic and anionic surfactants, in terms of affinity for oil and water phases, are very different. Nonionic surfactants have a tendency to be more lipophilic at higher temperatures; while the opposite has been observed for anionic systems.<sup>14,28-29</sup> The additions of the primary anionic surfactant system may have suppressed some of the dominant temperature effects on the overall anionic-nonionic mixed system.

Preliminary experiments with other combinations of primary anionic and nonionic surfactants were also conducted. The primary anionic surfactant used in the later studies was the alpha olefin sulfonate (AOS). The purpose of replacing the TRS/IBA system with the AOS surfactant was aimed at determining and confirming the distinct behavior exhibited by the systems containing the Genapol and Igepal surfactants. The use of the AOS surfactant providing a means to determine the effect of each on the nonionic surfactants in improving solution behavior. These nonionics were also utilized as substitutes for the relatively high short-chain alcohol requirements of the AOS surfactant.<sup>30-31</sup>

The alpha olefin sulfonates (AOS) have been studied by earlier researchers as potential candidates for application in chemical flooding.<sup>30-31</sup> These systems have relatively good salt tolerance and yield favorable oil/water solubilization parameters and IFT's with selected oils. However, substantial amounts of alcohol and elevated temperatures were found to be necessary to

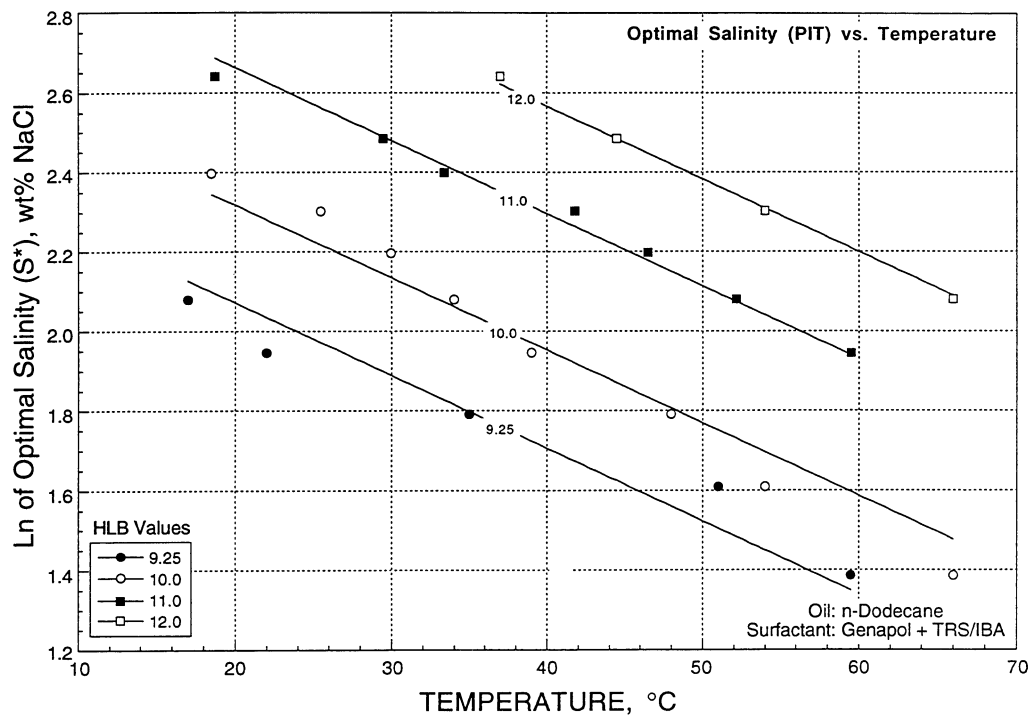


FIGURE 13. - Log of optimal salinity (PIT-method) vs. temperature with different HLB of nonionic surfactant component using Genapol + TRS/IBA mixtures with n-dodecane.

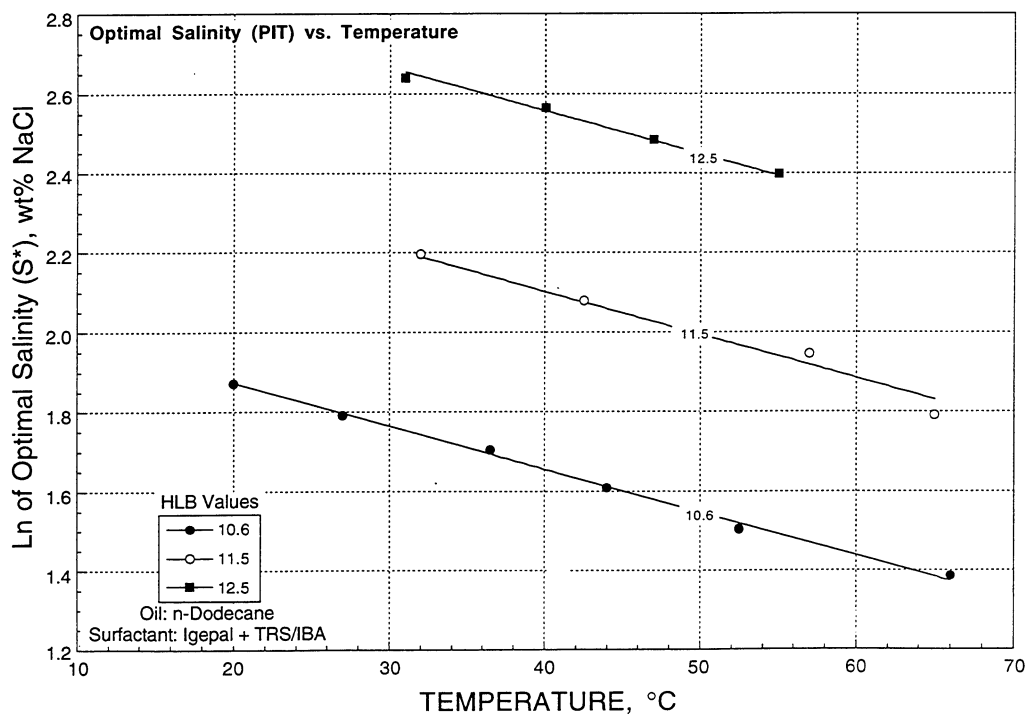


FIGURE 14. - Log of optimal salinity (PIT-method) vs. temperature with different HLB of nonionic surfactant component using Igepal + TRS/IBA mixtures with n-dodecane.

maintain favorable solubility in high salinity brines. Phase behavior studies as well as IFT measurements were conducted on selected samples of these anionic surfactants.

Initial experimental efforts included establishing base information on the degree of oil/water solubilization, IFT, and optimal salinity values for several commercial surfactants, i.e. C<sub>14-16</sub> AOS and C<sub>16-18</sub> AOS. Results of the screening study indicated relatively good agreement with results presented in the literature for a similar class of surfactants with different alkane chain structure.<sup>31</sup> Figures 15 and 16 show plots of the solubilization parameters determined for selected systems tested.

PIT experiments were then conducted on selected samples of these AOS systems, C<sub>14-16</sub> AOS and C<sub>16-18</sub> AOS, in combinations with Genapol and Igepal series of surfactants. The PIT studies with the primary anionic surfactant system alone did not indicate any trend in solution behavior of these systems over a selected range of salinities. However, tests with combinations of these AOS surfactants with selected nonionic surfactants at a fixed component proportion (50%:50% by weight) indicated some trends in solution conductivity changes that can be attributed to relative proximity of optimal conditions for these anionic-nonionic mixtures. Additional tests with these combinations indicated though that the trends with these mixtures were not as distinct compared to earlier results with the mixtures of TRS/IBA and the different nonionic components. Compared to earlier studies, the AOS-containing systems did not exhibit similar orders of magnitude change in solution conductivity upon reaching their respective phase inversion temperatures, unlike the TRS 10-410/IBA-containing systems. These results indicated that the AOS surfactant's solution behavior dominated the solution behavior of the overall mixture. Additional salinity scans and PIT tests were also conducted with mixtures containing higher nonionic component proportions (e.g. greater than 50% nonionic component). The results using systems with the higher nonionic component indicated very distinct phase inversion trends. These systems exhibited a degree of change in solution conductivity that was comparable to earlier studies with the TRS 10-410/IBA system. One drawback of utilizing more of the nonionics (e.g. greater than 50% nonionic surfactant) was that the nonionic's solution behavior appeared to almost completely dominate the overall solution behavior. No distinction in PIT behavior could be detected among the different samples tested when the proportion of the nonionic component in these systems was greater than 55%. The solubilization capacities and optimal salinity determined from these studies were also comparable to those from the studies using the nonionics alone. Additional investigation will be needed to provide a definitive evaluation of this anionic-nonionic surfactant combination. Preliminary results seem to indicate that the prospects for utilizing these combinations are limited.

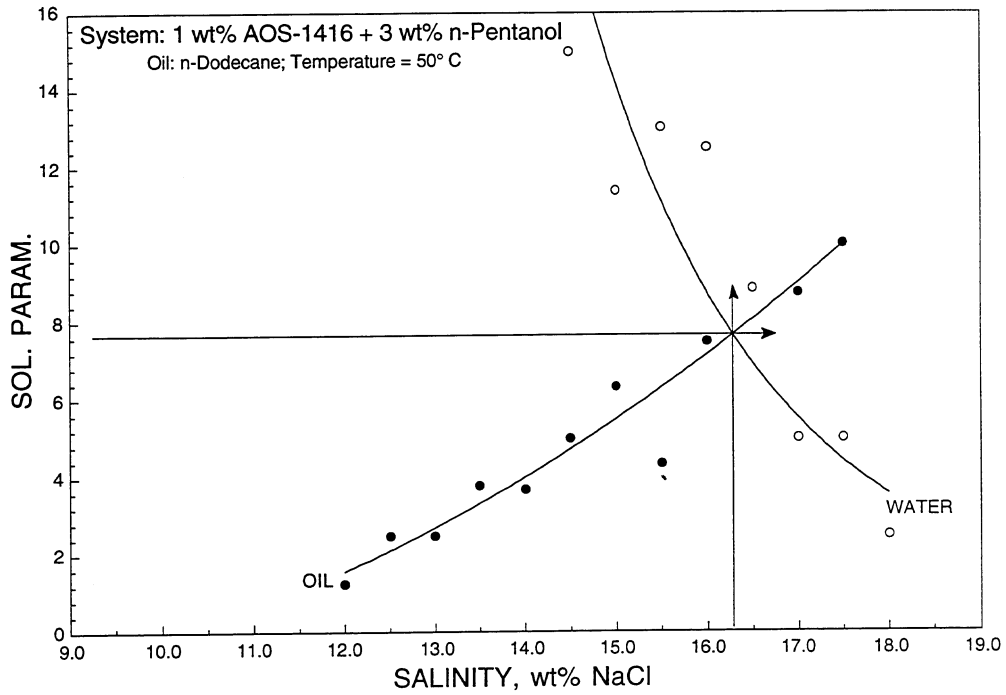


FIGURE 15. - Solubilization parameter vs. salinity using AOS-1416 + n-pentanol with n-dodecane at 50° C.

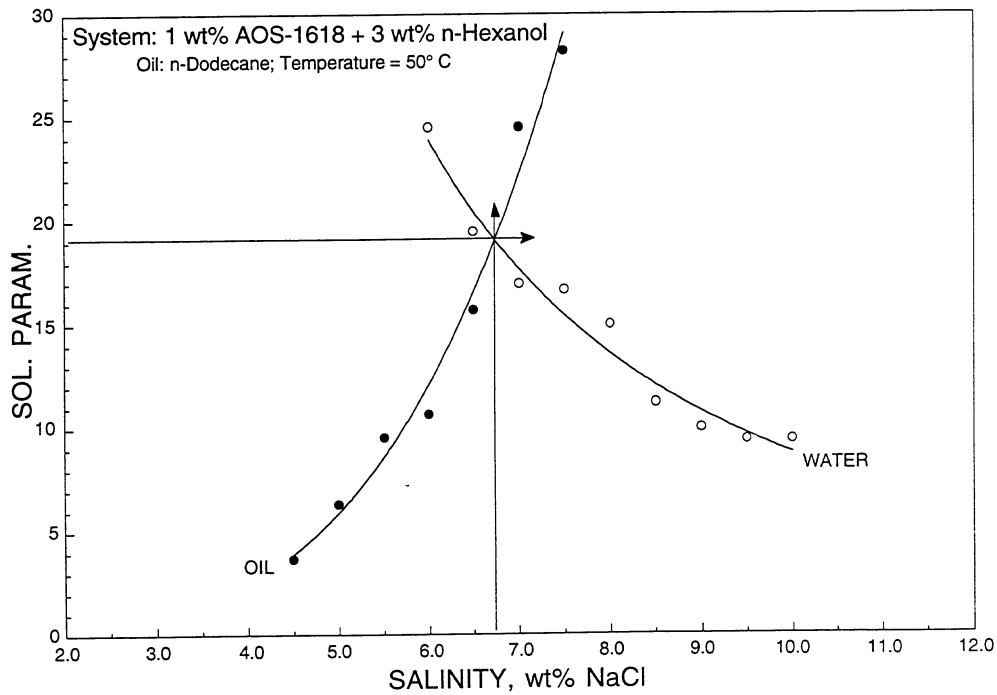


FIGURE 16. - Solubilization parameter vs. salinity using AOS-1618 + n-hexanol with n-dodecane at 50° C.

## Comparison of Methods of Surfactant Systems Screening

The PIT method has been shown to be a relatively fast screening method for determining the relative proximity of optimal conditions for selected surfactant systems. Although the method was primarily used for nonionic surfactants screening,<sup>25-26</sup> earlier studies have shown that this method can also be used for identifying possible combinations of anionic-nonionic mixtures. Utilizing the PIT method, it was possible to evaluate an exhaustive number of combinations of different surfactants within a relatively short time period. As mentioned in an earlier report, one drawback of this method is the lack of information in terms of the oil/water solubilization capacity of each of the chemical formulations.<sup>14</sup> The PIT method only provided information on the range of optimal salinity and temperature where selected chemical systems can be utilized. There is still the need to perform the more time-consuming phase behavior evaluation by means of salinity scans in order to quantify the solubilization parameters for these systems. The PIT method was useful in providing a narrower range of salinity conditions to be tested. Once these ranges were identified, salinity scans were conducted on selected systems. Earlier comparisons made from the results of both PIT and salinity scans showed fairly good agreement in the range of optimal salinities determined from both methods.<sup>14</sup> Similar comparisons are being made in this study. The results of the present comparisons also showed fairly good agreement between the salinity regions determined using both methods. These results support the need to utilize the PIT method, whenever applicable, for initially identifying the salinity regions of interest, to be followed by additional studies including salinity scans, IFT measurements, and oil displacement experiments to determine oil-recovery potential.

The limited number of measurements made by the phase volume method (salinity scan) gave an overall average difference from the PIT method of only 0.54%. This value is expressed as the overall average of the percentage difference between the measurements using the phase volume method and the PIT method divided by the value from the PIT measurement. This relatively low percentage value disguises the scatter in average difference with respect to temperature, as shown in Table 4. This again reflects the sensitivity of measurements on colloidal systems.

Table 5 shows the results of the salinity scans conducted on a select group of surfactant

TABLE 4. - Average difference in results due to temperature effects

Temperature, ° C	Average difference, %
40	-6.95
50	+2.87
60	+4.88

mixtures. The table also shows a comparison of the results from both methods. As mentioned earlier, these comparisons show very good agreement, within  $\pm 1.5$  wt% NaCl of each other.

From the list in Table 5, only two of the systems tested reached solubilization capacity exceeding the value of  $10 \text{ cm}^3/\text{cm}^3$ , namely plain Genapol with n-octane and plain Igepal with n-decane. Table 6 is a summary of the results presented in Table 5. Figures 17 and 18 show plots of the comparison of the solubilization parameters vs. HLB. The higher solubilization values occurred at lower values of HLB 9, but there was no systematic trend with respect to HLB that was indicated. On the other hand, there was a strong downward trend indicated with increasing temperature and increasing ACN. Adding the TRS/IBA system generally had an adverse effect on solubilization. Igepal was slightly superior to Genapol on the average, although this effect is strikingly reversed in Figs. 17 and 18.

TABLE 5.- Comparison of results from PIT method and salinity scans

Sys. No.	HLB	Temp.	S* (PIT) w/ C <sub>8</sub>	S* (PT) w/ C <sub>8</sub>	$\sigma^*$ w/ C <sub>8</sub>	S* (PIT) w/ C <sub>10</sub>	S* (PT) w/ C <sub>10</sub>	$\sigma^*$ w/ C <sub>10</sub>	S* (PIT) w/ C <sub>12</sub>	S* (PT) w/ C <sub>12</sub>	$\sigma^*$ w/ C <sub>12</sub>
Genapol at 40° C											
57	9.50	40.0	19.79	18.29	35.13	20.49				20.14	9.47
60	10.00	40.0	20.25	20.27	23.16	22.20	21.19	3.82	22.31	23.08	2.37
67	10.60	40.0	21.01	20.37	12.37	22.87	21.73	6.18	23.69	23.28	4.08
62	11.00	40.0	22.04	21.64	8.55	24.17	22.52	6.05	26.05	24.35	3.42
65	11.55	40.0	24.85	22.87	6.84	27.10	24.20	9.74		25.94	3.42
Genapol + TRS/IBA at 40° C											
50	9.50	40.0		3.37	3.55		4.52	4.87		5.51	3.68
51	10.00	40.0	4.71	4.48	5.66	6.17	5.75	4.21	7.03	7.08	2.63
52	10.60	40.0		5.37	5.92		6.82	3.55		8.33	3.29
53	11.00	40.0	7.02	6.44	5.00	8.85	8.87	3.95	9.87	8.87	3.95
54	11.55	40.0		7.90	4.21		10.19	3.29		10.42	3.82
Igepal at 40° C											
59	10.00	40.0	9.78	8.67	6.58	14.15	12.23	10.92	14.00	12.60	5.82
68	10.60	40.0	15.56	12.97	9.34	17.46	15.35	9.08	18.17	17.23	7.37
61	11.00	40.0	19.20	16.37	9.87	22.20	20.23	9.47	21.54	20.11	6.18
66	11.50	40.0	22.20	20.62	9.47	25.15	23.01	6.84	26.31	23.67	5.26
Igepal + TRS/IBA at 40° C											
3	10.60	40.0	2.89	2.60	7.37	3.96	3.53	5.53	5.21	5.00	4.43
45	11.00	40.0	3.88	3.50	7.89		4.61	5.92		5.87	5.13
46	11.50	40.0	5.70	5.05	7.76	7.03	6.82	7.63	8.21	8.19	4.60
47	12.00	40.0	7.21	6.58	9.08		8.65	6.32		9.58	4.47
Genapol at 50° C											
57	9.50	50.0	15.61	16.67	2.76	16.78	18.00	5.00		18.78	1.97
60	10.00	50.0	15.88	17.00	1.53	17.81	18.67	2.26	18.49	18.93	1.08
67	10.60	50.0	16.53	17.83	1.18	18.45	19.04	2.07	19.65	21.00	1.53
62	11.00	50.0	17.37	18.13	2.18	19.43	20.98	1.53	21.54	21.93	2.47
65	11.55	50.0	19.51	19.76	4.47	21.54	21.01	1.83		22.62	1.84

TABLE 5.- Comparison of results from PIT method and salinity scans - continued

Sys. No.	HLB	Temp.	S* (PIT) w/ C <sub>8</sub>	S* (PT) w/ C <sub>8</sub>	σ* w/ C <sub>8</sub>	S* (PIT) w/ C <sub>10</sub>	S* (PT) w/ C <sub>10</sub>	σ* w/ C <sub>10</sub>	S* (PIT) w/ C <sub>12</sub>	S* (PT) w/ C <sub>12</sub>	σ* w/ C <sub>12</sub>
Genapol + TRS/IBA at 50° C											
50	9.50	50.0		2.77	2.07		3.67	3.19		5.00	2.50
51	10.00	50.0	3.74	4.00	3.67	4.93	5.00	2.17	5.81	6.21	2.73
52	10.60	50.0		4.56	3.56		6.56	2.64		7.96	3.73
53	11.00	50.0	5.64	5.70	4.13	7.03	7.25	4.25	8.33	8.33	2.05
54	11.55	50.0		6.20	3.87		8.00	2.50		9.32	2.09
Igepal at 50° C											
59	10.00	50.0		7.08	3.82	11.36	10.00	3.42	11.76	12.47	4.22
68	10.60	50.0	12.49	12.00	4.04	13.94	14.00	4.32	15.49	17.00	2.18
61	11.00	50.0	15.41	16.00	3.75	17.81	18.71	4.48	18.27	19.36	2.88
66	11.50	50.0	17.81	19.05	3.08	20.09	20.00	3.75	22.00	21.03	2.33
Igepal + TRS/IBA at 50° C											
3	10.60	50.0	2.46	2.44	5.05	3.46	3.24	3.89	4.69	4.66	3.23
45	11.00	50.0	3.34	3.83	4.57		4.80	3.80		6.16	3.80
46	11.50	50.0	4.85	5.00	3.80	6.14	6.50	4.38	7.35	7.24	3.45
47	12.00	50.0	6.23	6.16	4.74		8.33	4.52		8.74	3.69
Genapol at 60° C											
57	9.50	60.0	12.30			13.46					
60	10.00	60.0	12.55			14.37			15.36		
67	10.60	60.0	13.07			14.78			16.28		
62	11.00	60.0	13.74			15.60			17.90		
65	11.55	60.0	15.39	17.45	1.00	17.29	18.00	1.53		19.12	1.89
Genapol + TRS/IBA at 60° C											
50	9.50	60.0		2.52	4.15		3.00	1.85		4.66	1.43
51	10.00	60.0	2.97	2.68	4.08	3.90	4.27	2.49	4.90	5.00	2.50
52	10.60	60.0		4.36	3.32		5.00	1.88		6.20	2.92
53	11.00	60.0	4.48	4.81	3.38	5.70	6.35	1.61	6.89	7.00	1.90
54	11.55	60.0		5.51	2.20		7.66	1.87		8.79	1.17
Igepal at 60° C											
59	10.00	60.0		6.78	1.61		8.65	1.37		10.75	1.54
68	10.60	60.0	10.12	10.67	2.07	11.25	11.56	1.56	13.13	12.98	1.96
61	11.00	60.0	12.49			14.22			15.56		
66	11.50	60.0	14.15	15.73	2.27	16.12	17.28	2.18	18.45	18.00	0.62
Igepal + TRS/IBA at 60° C											
3	10.60	60.0	2.14	2.17	3.27	3.00	3.00	2.47	4.24		
45	11.00	60.0	2.89	3.00	3.09		4.50	3.09		5.67	1.43
46	11.50	60.0	4.20	4.62	2.77	5.34	6.00	1.25	6.59	6.75	2.00
47	12.00	60.0	5.34	5.87	2.77		7.08	2.95		8.00	1.55

TABLE 6. - Summary for salinity scan results at 40° and 50° C

Average of Data at Conditions	Value of Solubilization Parameter
T= 40° C	6.95
T= 50° C	3.15
Using n-octane	6.67
Using n-decane	4.77
Using n-dodecane	3.64
HLB = 11.0	4.68
HLB = 14.0	4.99
Without TRS/IBA	5.78
With TRS/IBA	4.29
Using Genapol	4.66
Using Igepal	5.60

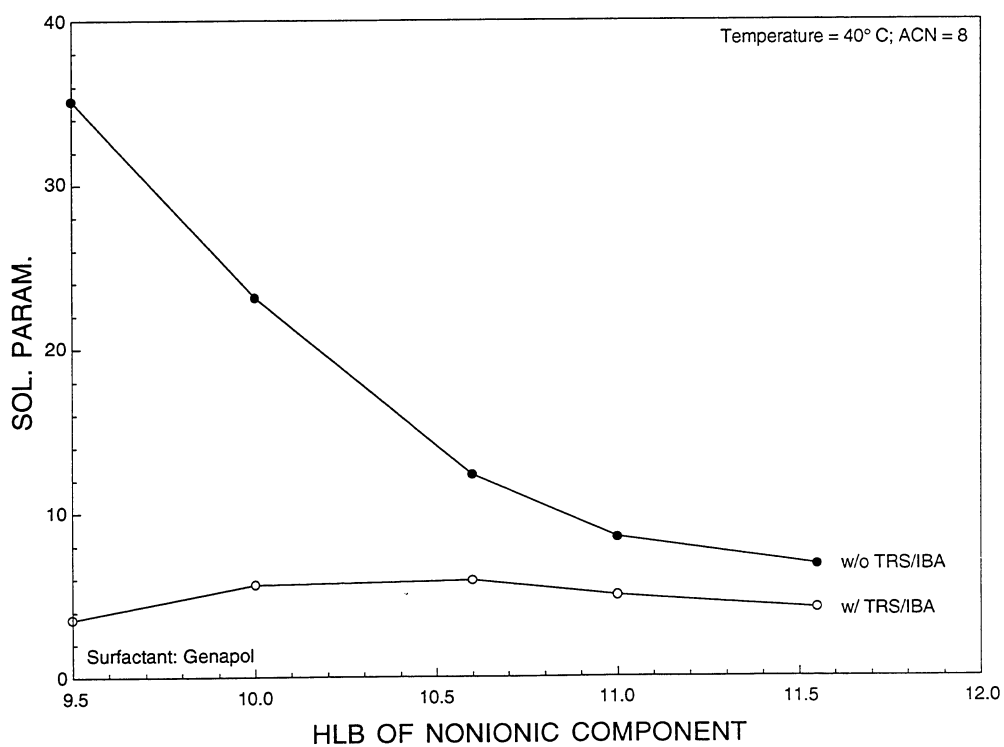


FIGURE 17. - Solubilization parameter at optimal salinity vs. HLB of nonionic component using Genapol with and without TRS/IBA with n-octane at 40° C.

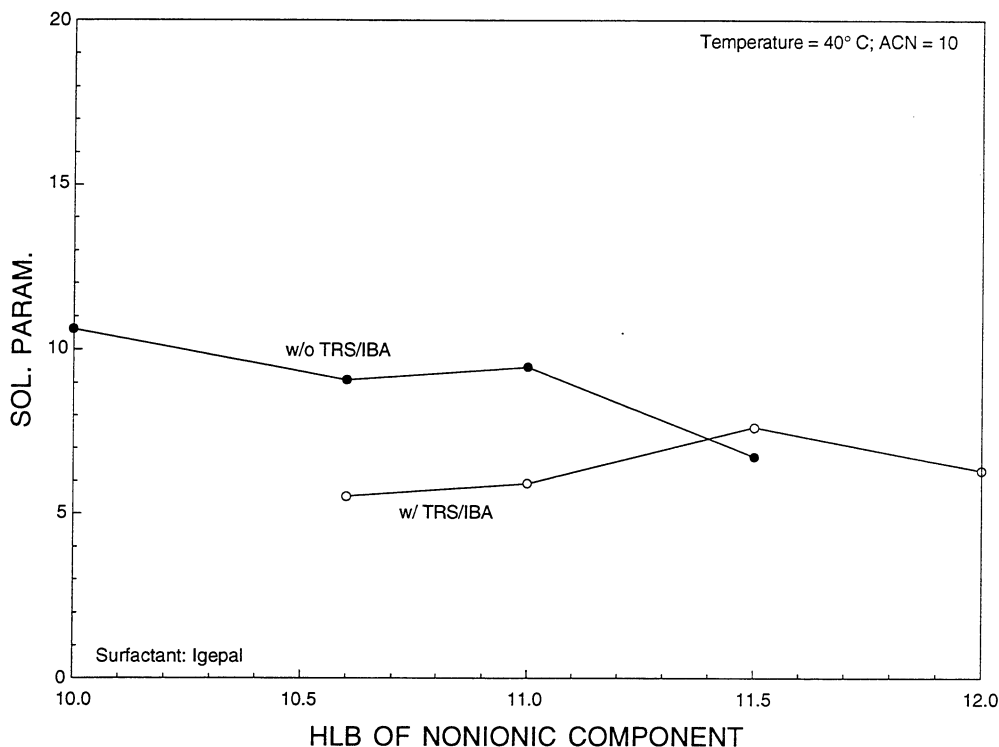


FIGURE 18. - Solubilization parameter at optimal salinity vs. HLB of nonionic component using Igepal with and without TRS/IBA with n-decane at 40° C.

### Modeling the Behavior of Mixed Surfactants

As shown in Figs. 5 through 14, the data show clear trends with respect to selected experimental parameters. It is the purpose of the present section to develop models that represent the trends for all parameters in a comprehensive manner. The models are used to compare the different surfactant systems and develop guidelines for design with variations in salinity, oil and temperature. Because of the scatter in the data – to be expected for colloidal systems – no model will be a precise predictor of behavior. Trends that are displayed by a majority of the data are assumed to be real, and the scatter is smoothed in the models. Smoothing is linear in most cases, but the trends that are consistently curved are modeled using quadratic expressions.

As previously cited<sup>14</sup> the University of Texas models<sup>29,32</sup> were presented as logarithmic in salinity for anionic surfactants, and linear for nonionic surfactants. To make comparisons easier, the logarithmic term of the salinity was used for all systems. For both types of surfactants,  $\ln S$  either gave a better correlation or there was little choice.

The linear plots of  $\ln S$  vs.  $T$ , presented in Figs. 11 through 14, were a convenient starting place for the correlation attempt, because it was observed that the slopes of these plots were invariant with respect to  $HLB$ . However, the slopes showed a trend with the alkane carbon

number (*ACN*) of the oil. This is presented for the four series of surfactants in Figs. 19 through 22. For three of the series, neither a linear nor a quadratic correlation is satisfactory. Two smoothing strategies were explored:

1. A bilinear correlation is more faithful to the data.
2. A linear correlation excluding results with n-heptane is more satisfactory for developing comparisons among the surfactants tested, for both temperature and oil-species effects.

After "standard" slopes had been established by either strategy, two approaches were employed to obtain "standard" intercepts ( $\ln S$  at  $T=0^\circ\text{C}$ ):

1. Create a model for intercept values (adjusted to fit the  $\ln S$  vs.  $T$  data best with the prescribed slope) as a function of *HLB*. The parameters of this model then exhibit trends with respect to *ACN* that are modeled.
2. Reverse the roles of *HLB* and *ACN*.

The first approach was more satisfactory in three of the four series, and was later used for the other system (Genapol) for uniformity of application. Table 7 gives details of the correlation, and the steps in deriving the parameters are illustrated in Figs. 23 through 31.

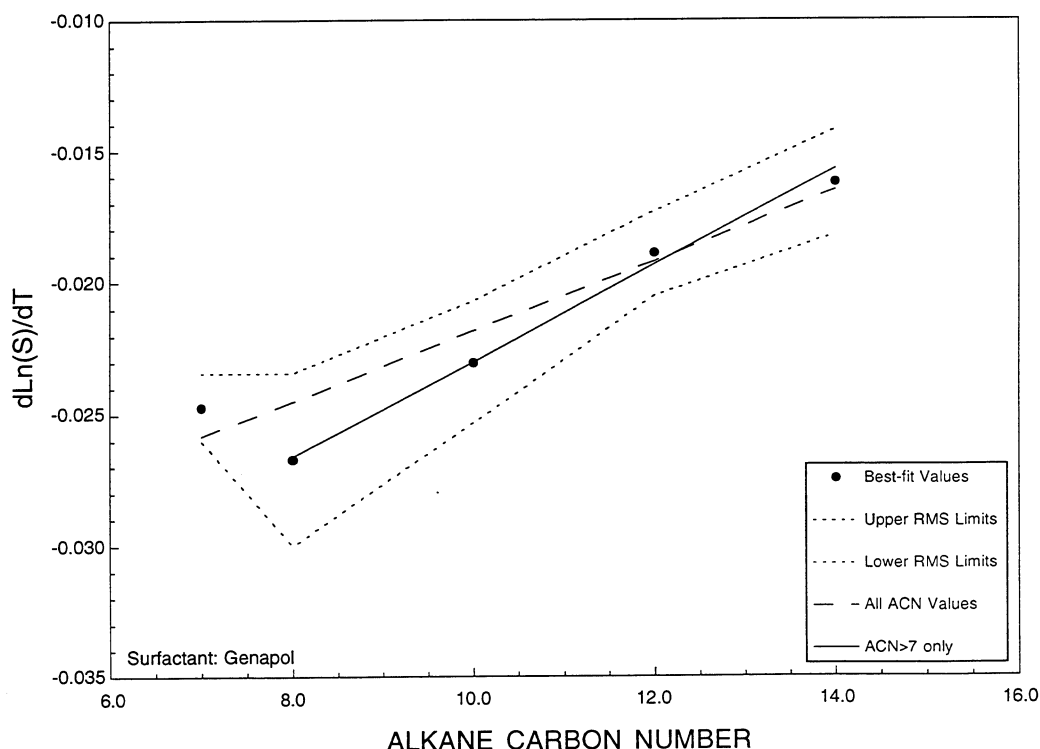


FIGURE 19. - Plot of  $d\ln S/dT$  vs. alkane carbon number using Genapol.

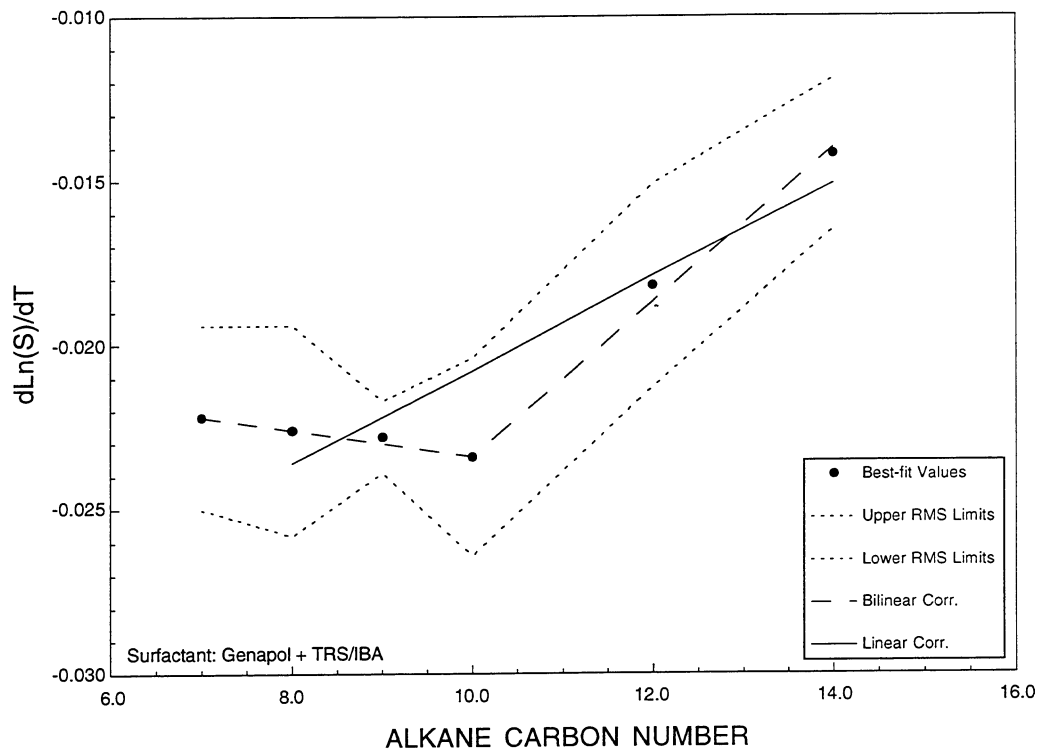


FIGURE 20. - Plot of  $d\ln S/dT$  vs. alkane carbon number using Genapol + TRS/IBA.

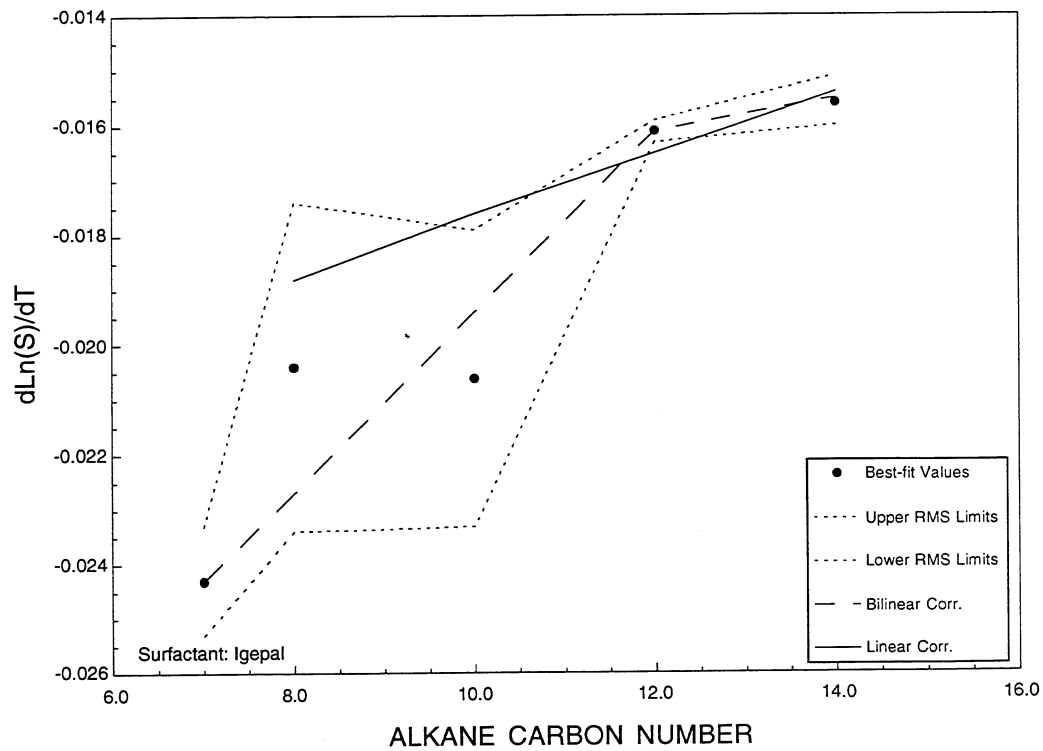


FIGURE 21. - Plot of  $d\ln S/dT$  vs. alkane carbon number using Igepal.

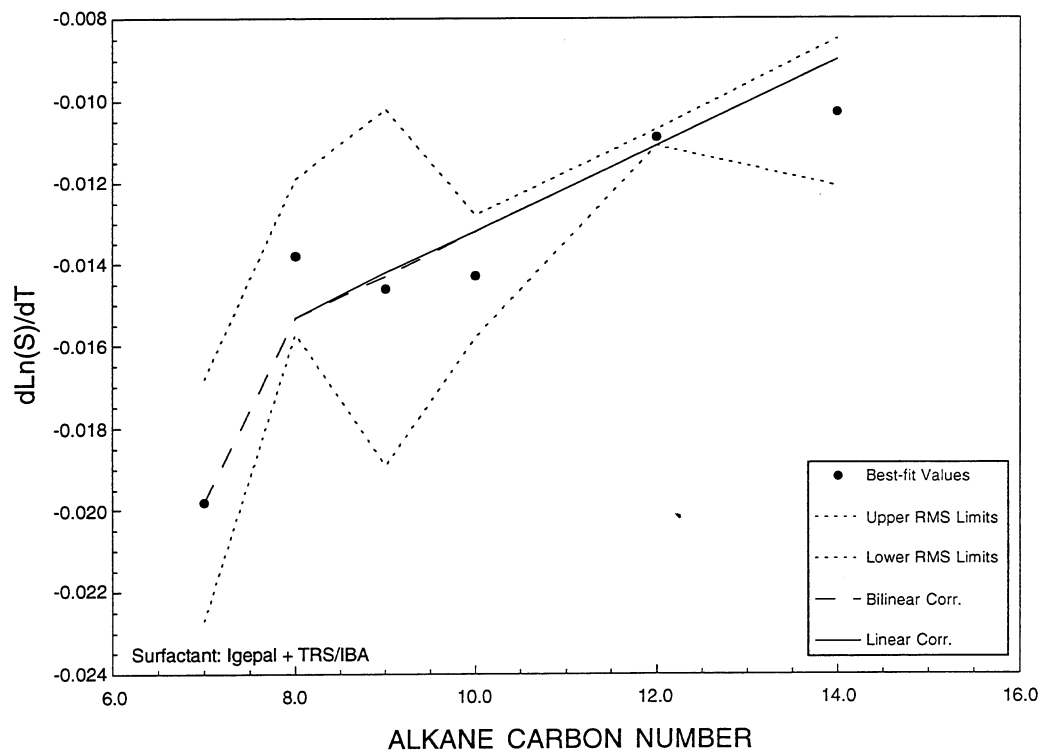


FIGURE 22. - Plot of  $d\ln S/dT$  vs. alkane carbon number using Igepal + TRS/IBA .

These operations lead to the development of three models:

Genapol without TRS/IBA:

$$\ln(S) = a_0 + a_1[ACN] + b_0[HLB] + b_1[ACN][HLB] + c_0[HLB]^2 + c_1[ACN][HLB]^2 + d_0T + d_1[ACN]T \quad (1)$$

Genapol with TRS/IBA:

$$\ln(S) = a_{00} + a_{01} + a_{10}[HLB] + a_{11}[ACN][HLB] + b_{01}T + b_{11}[ACN]T \quad (2)$$

Igepal with/ and without TRS/IBA:

$$\ln(S) = a + b[HLB] + c[HLB]^2 + d_{00}T + d_{01}[ACN]T \quad (3)$$

Values of the coefficients for these equations are listed in Table 8.

TABLE 7. - Method of obtaining model values for intercepts

Surfactant system	HLB functionality	Convexity	Figure No.	ACN smoothing	Figure No.
Genapol	quadratic	down	23	graphical all parameters	24
Genapol + TRS	linear		25	graphical both parameters	26
Igepal	quadratic	up	27	none needed	
Igepal + TRS	quadratic	up	28	quadratic one parameter	29,30,31

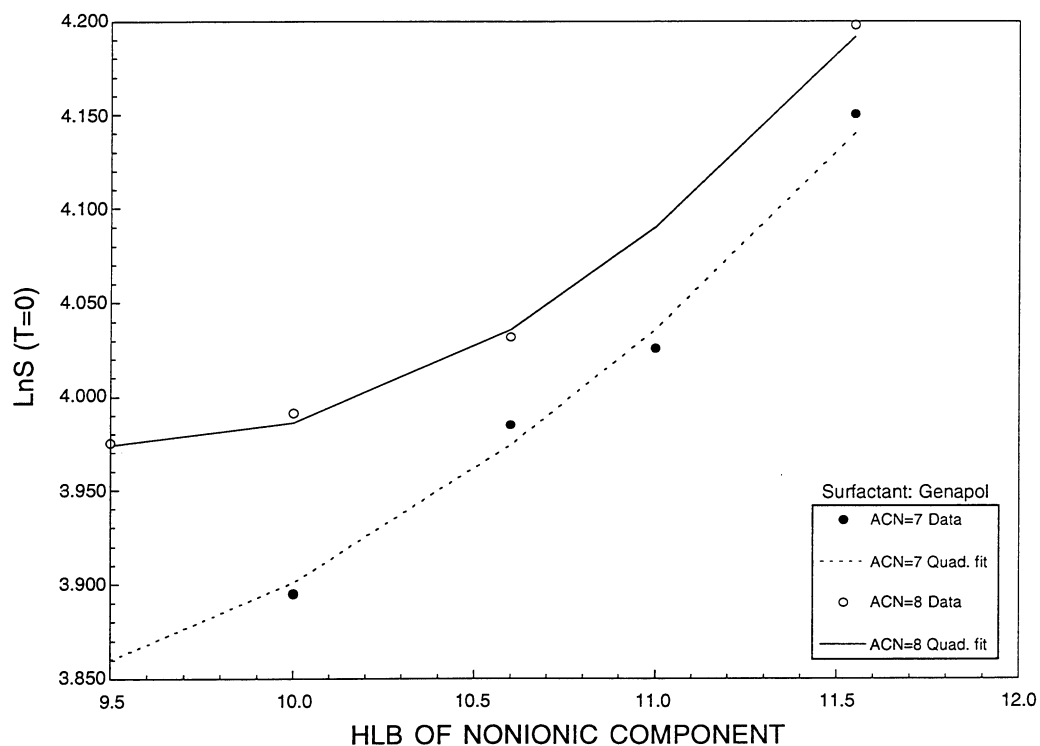


FIGURE 23a. - Plot of intercepts of log of salinity at T=0° C vs. HLB of nonionic component using Genapol. (ACN: 7 and 8).

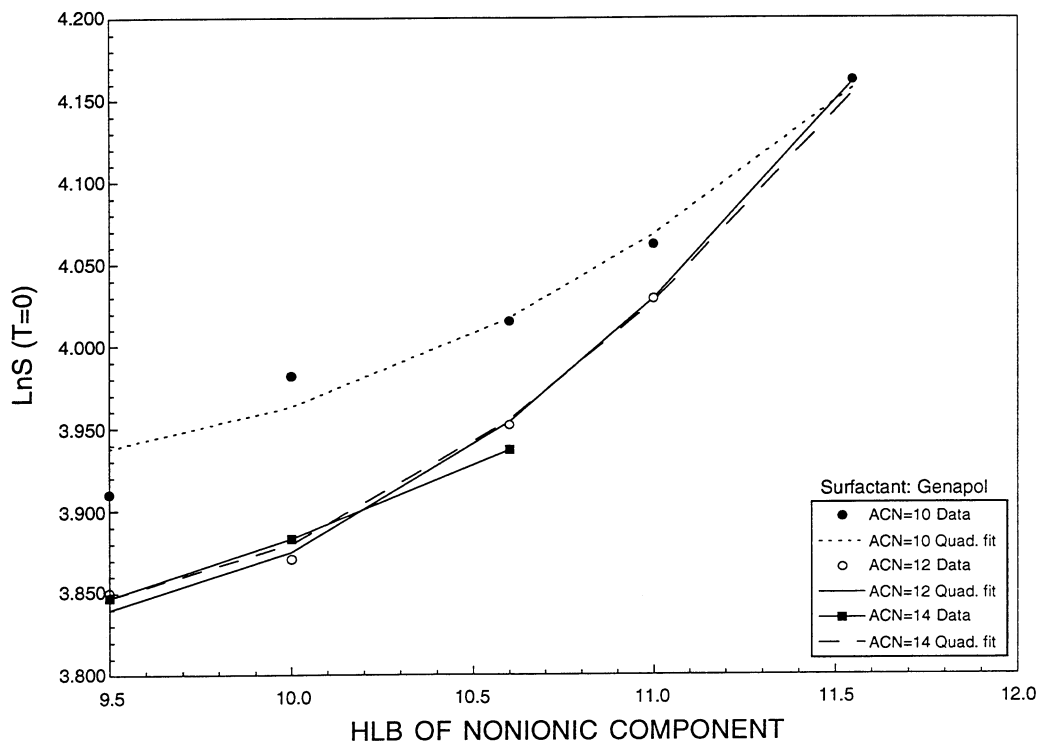


FIGURE 23b. - Plot of intercepts of log of salinity at T=0° C vs. HLB of nonionic component using Genapol. (ACN: 10, 12 and 14).

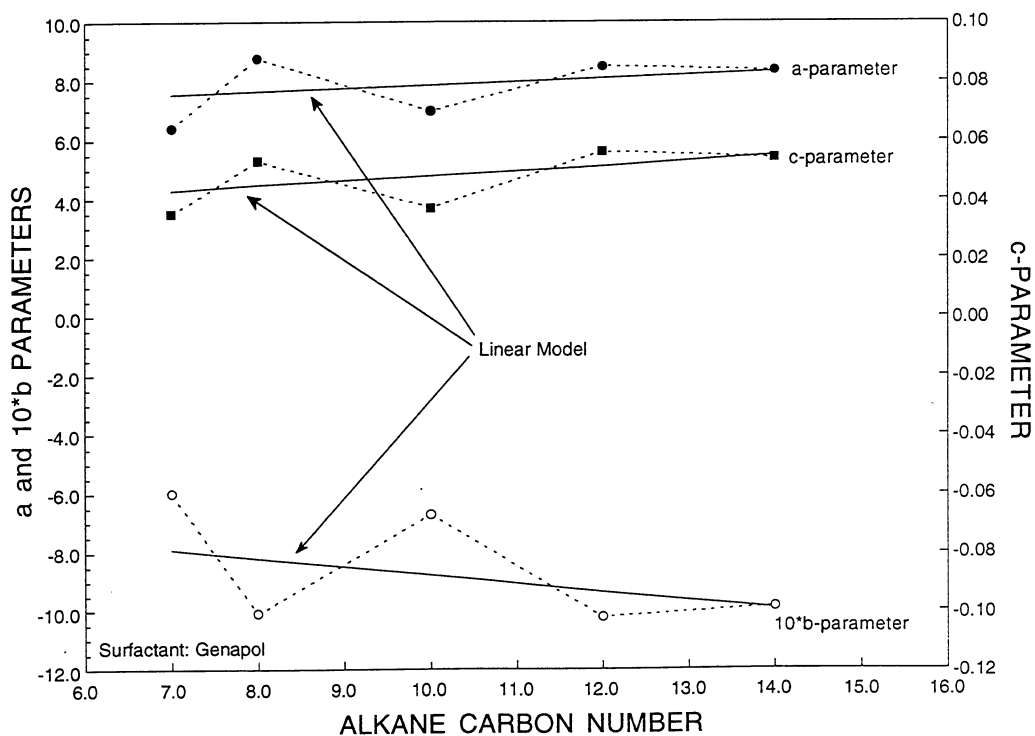


FIGURE 24. - Plot of quadratic parameters vs. alkane carbon number using Genapol. For intercept  $= a + b[HLB] + c[HLB]^2$ .

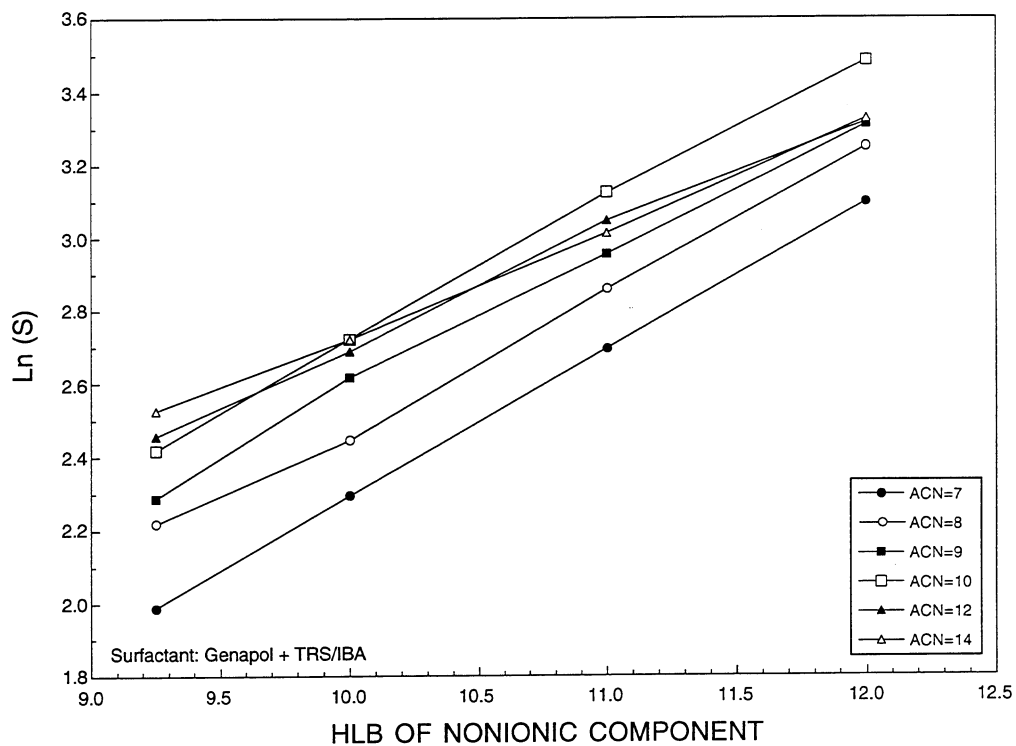


FIGURE 25. - Plot of intercepts of log of salinity vs. HLB of nonionic component using Genapol + TRS/IBA with different n-alkanes.

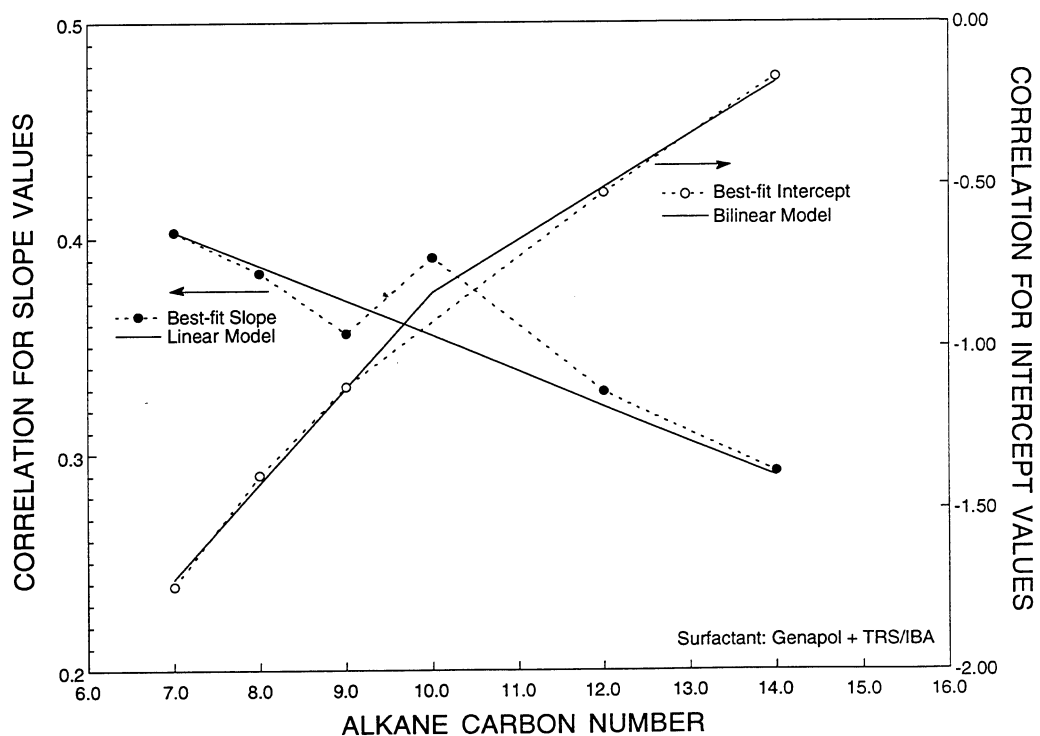


FIGURE 26. - Plot of correlation of slope and intercept values vs. alkane carbon number using Genapol + TRS/IBA .

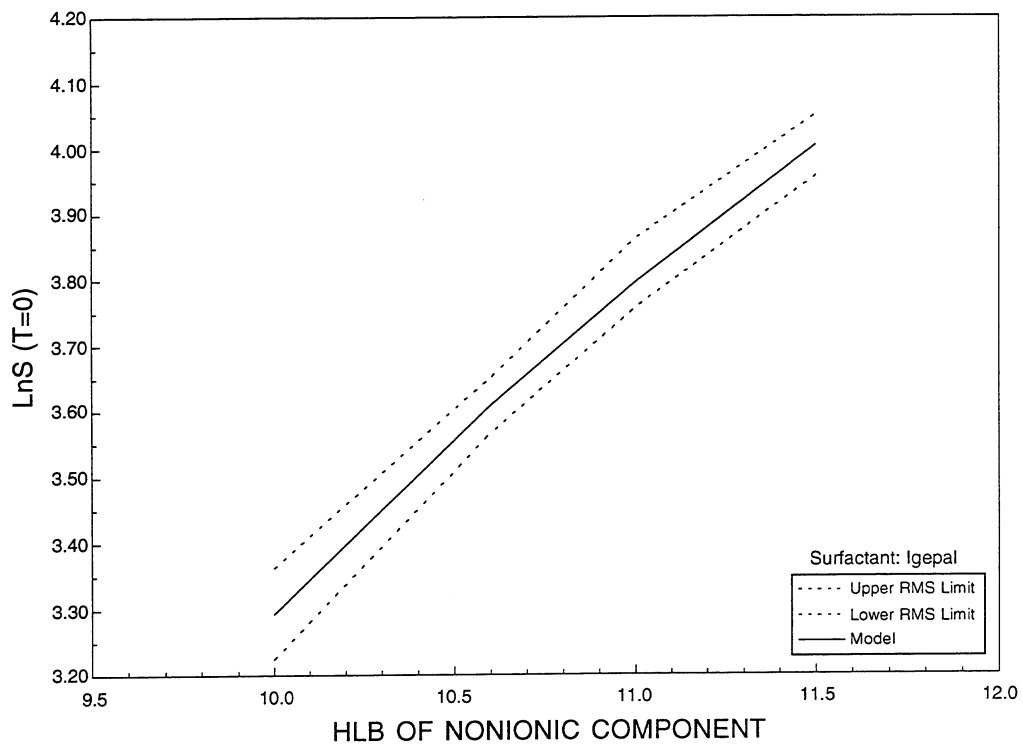


FIGURE 27. - Plot of intercepts of log of salinity at T=0° C vs. HLB of nonionic component using Igepal.

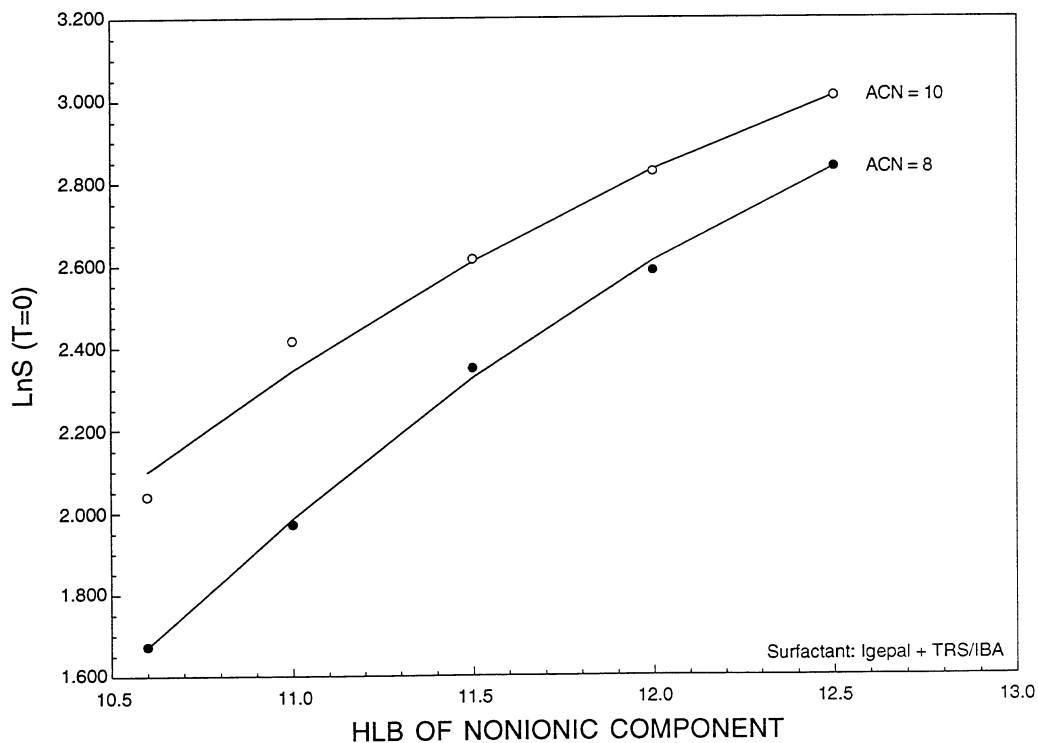


FIGURE 28. - Plot of intercepts of log of salinity at T=0° C vs. HLB of nonionic component using Igepal + TRS/IBA. (ACN: 8 and 10).

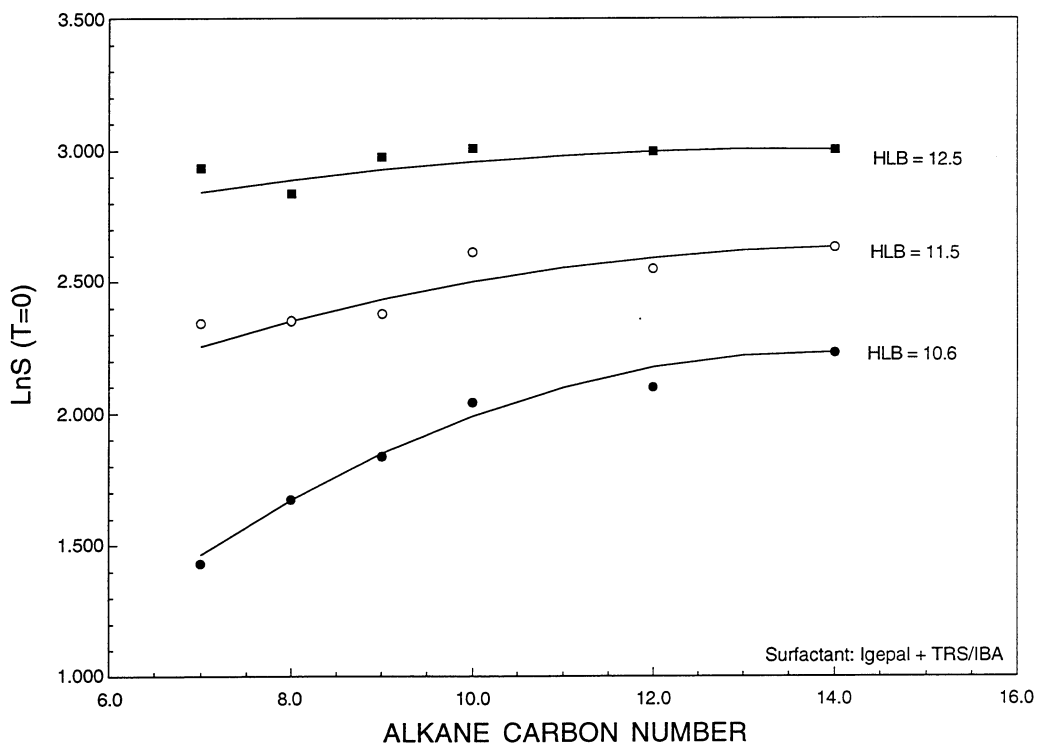


FIGURE 29. - Plot of intercepts of log of salinity at  $T=0^{\circ}\text{C}$  vs. alkane carbon number using Igepal + TRS/IBA with different HLB values.

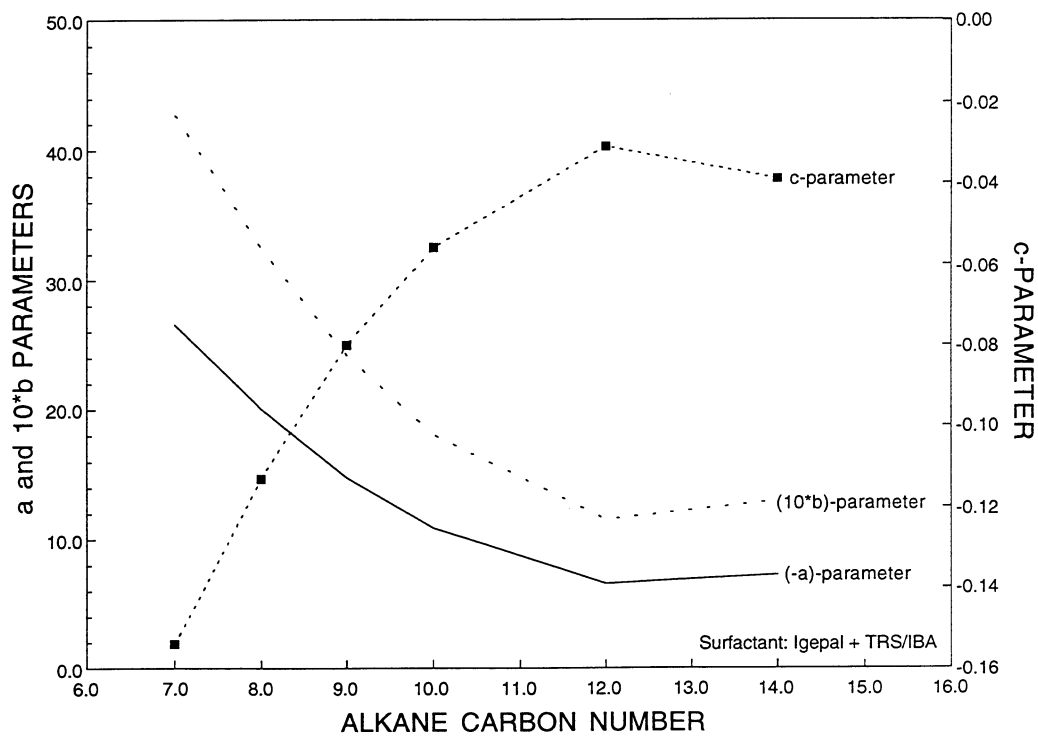


FIGURE 30. - Plot of quadratic parameters vs. alkane carbon number using Igepal + TRS/IBA. For intercept =  $a + b[\text{HLB}] + c[\text{HLB}]^2$ .

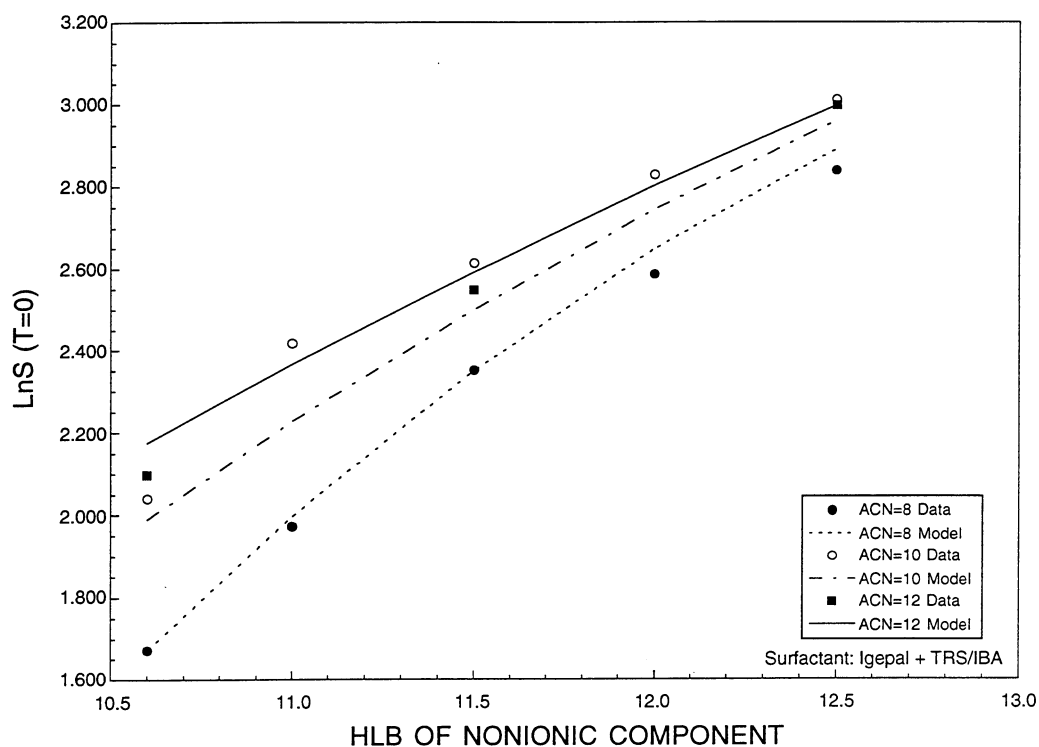


FIGURE 31. - Plot of intercepts of log of salinity at T=0° C vs. HLB of nonionic component using Igepal + TRS/IBA with different alkanes.

TABLE 8. - Values of coefficients in the models

<u>Genapol System</u>						
$a_0$	$a_1$	$b_0$	$b_1$	$c_0$	$c_1$	
6.774	0.1100	-0.586	-0.0291	0.0318	0.00163	
			All ACN	$d_0$	$d_1$	
			ACN>7 only	-0.0351	0.00133	
				-0.0413	0.00183	
<u>Genapol + TRS/IBA System</u>						
	$a_{00}$	$a_{01}$	$a_{10}$	$a_{11}$	$b_{01}$	$b_{11}$
<u>Bilinear</u>						
ACN (7-10)	-3.784	0.295	0.516	-0.0161	-0.0194	-0.00040
ACN (10-14)	-2.456	0.162	0.516	-0.0161	-0.0469	0.00235
<u>Linear</u>						
ACN (8-14)					0.0349	0.001414

TABLE 8. - Values of coefficients in the models – continued

<u>Igepal System</u>					
	a	b	c	d <sub>0</sub>	d <sub>1</sub>
	8.041	1.709	-0.057		
<u>Bilinear</u>					
ACN (7-12)				-0.0358	0.00164
ACN (12-14)				-0.0197	0.00030
<u>Linear</u>					
ACN (8-14)				-0.0233	0.000567
<u>Igepal + TRS/IBA System</u>					
	a	b	c	d <sub>0</sub>	d <sub>1</sub>
<u>ACN</u>					
7	-26.58	4.274	-0.154		
8	-20.06	3.246	-0.113		
9	-14.76	2.416	-0.080		
10	-10.86	1.807	-0.056		
12	-6.54	1.153	-0.031		
14	-7.18	1.299	-0.039		
<u>Bilinear</u>					
ACN (7-8)				-0.0513	0.0045
ACN (8-14)				-0.0237	0.00105
<u>Linear</u>					
ACN (8-14)				-0.0237	0.00105

Table 9 shows the conformance of the models to the data. *Deviation of slope* means the discrepancy between the  $d\ln(S)/dT$  for the model and the best-fit straight line (as in figures 11-14). *Deviation of position* means the discrepancy between the  $\ln S$  for the model and the straight line at the mid point of the data range, as a percent of the total range of  $\ln S$ . *RMS scatter* is a measure of the deviations of the individual data points from the best-fit straight line, as a percentage of the total range. The averages of the absolute values of the *deviation of slope* and *deviation of position* are about the same as the scatter about the basic plot of  $\ln S$  vs  $T$ , but the smaller averages of algebraic values show that the results are not skewed.

TABLE 9. - Conformance of the models to the data Percent Deviation

	Genapol	Genapol + TRS	Igepal	Igepal + TRS
Average value of deviation of slope	0.6	-0.3	4.9	-0.3
Average value of absolute value of deviation of slope	9.4	9.2	9.1	12.1
Average value of deviation of position	0.8	0.7	-3.0	3.4
Average value of absolute value of deviation of position	6.1	2.9	10.5	10.2
Average value of RMS scatter	4.5	2.4	5.6	3.3

Table 10 compares the conformance of the model to phase volume and PIT data on the same systems. The agreement is reasonably gratifying. The phase volume results are close to the model for the Igepal + TRS/IBA system, which is the worst case (shown in Fig. 31).

TABLE 10. - Conformance of the models to selected data at 50° C Percent RMS Deviation from the Model

Surfactant System	ACN	PIT Data <sup>1</sup>	Phase volume data <sup>2</sup>
Genapol	8	2.3	2.1
	10	0.6	1.6
	12	0.1	1.7
Genapol + TRS	8	2	4.7
	10	2.4	4.4
	12	1.9	2.9
Igepal	8	2.3	4.9
	10	2.8	2.1
	12	2.2	2.9
Igepal + TRS	8	4.9	5.4
	10	6.9	5.2
	12	2.8	3.6
Averages		2.6	3.5

<sup>1</sup>Salinity values from best-fit lines of ln(S) vs. T of PIT experiments.

<sup>2</sup> Salinity values from Phase Volume data.

The work done by the University of Texas<sup>32</sup> was on Igepal systems. Their model was linear in *EON*, which is proportional to  $[HLB]/(1-[HLB])$ , and did not have the cross term in  $[ACN]T$ . Using representative values at 40° C with n-decane and the HLB value of 10, the five terms in Eq. 3 have the following values:

$$a = -8; \quad b[HLB] = 17; \quad c[HLB]^2 = -6; \quad d_{00}T = -1; \quad d_{01}[ACN]T = 0.2$$

such that the temperature effect on the coefficient for  $[ACN]$  is unimportant, but the nonlinearity of  $\ln S$  in *HLB* is significant.

The Texas group placed emphasis on the linear relation between *EON* and *ACN*. Figures 32 through 37 show the relations predicted from our models. The relations are not rigidly linear, but any linearity is empirical, not theoretical. In at least some cases (compare Figs. 32 and 37) the *EON* vs *ACN* plot is more linear than *HLB* vs. *ACN*. The average slope of *EON* vs *ACN* is invariant in the Texas results. We observed the same thing for Genapol systems (Figs. 32 and 37) but this was not true for Igepal systems. Numerical values for the slopes obtained from Figs. 32 through 37 are presented in Table 11. The values of these slopes do not appear to be significantly affected by temperature.

TABLE 11. - Numerical values of slopes of *EON* vs. *ACN*

System	Temp., ° C	$\ln S$	$d[EON]/d[ACN]$
Genapol	50	3.1	-0.32
Genapol + TRS/IBA	50	1.8	-0.35
Igepal	50	1.6	-0.10
Igepal + TRS/IBA	50	1.6	-0.19
Igepal + TRS/IBA	50	3.1	-0.28
Texas results <sup>29</sup>	28	3.1	-0.15
Genapol	40	3.1	-0.29

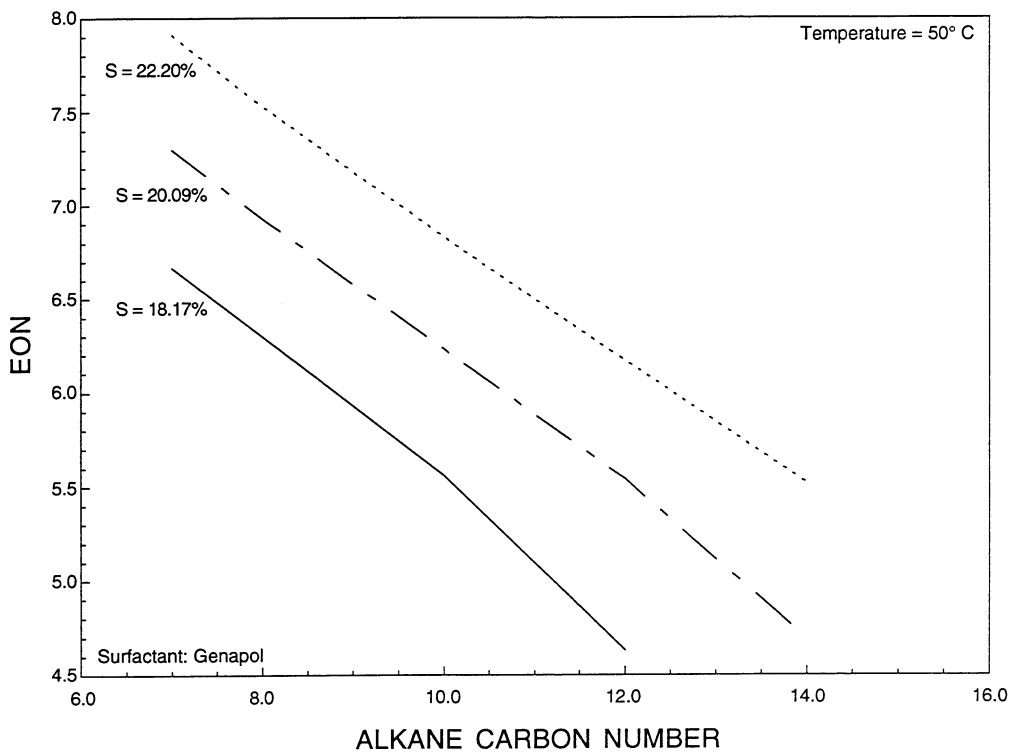


FIGURE 32. - Plot of EON vs. alkane carbon number using Genapol at different salinities and 50° C.

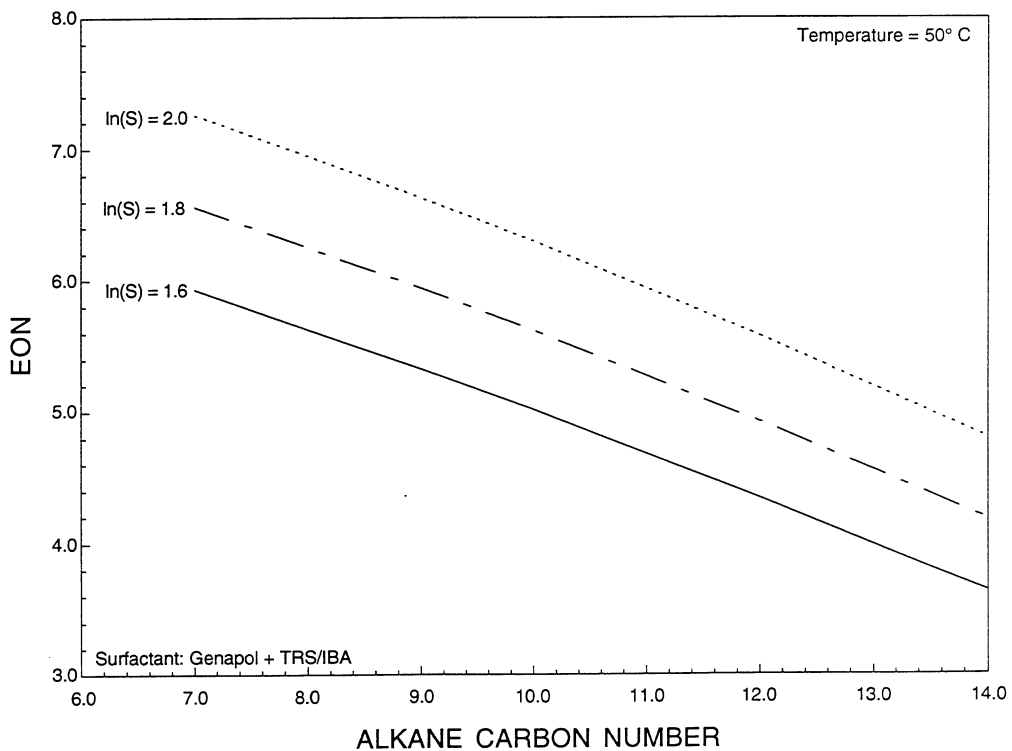


FIGURE 33. - Plot of EON vs. alkane carbon number using Genapol + TRS/IBA at different salinities and 50° C.

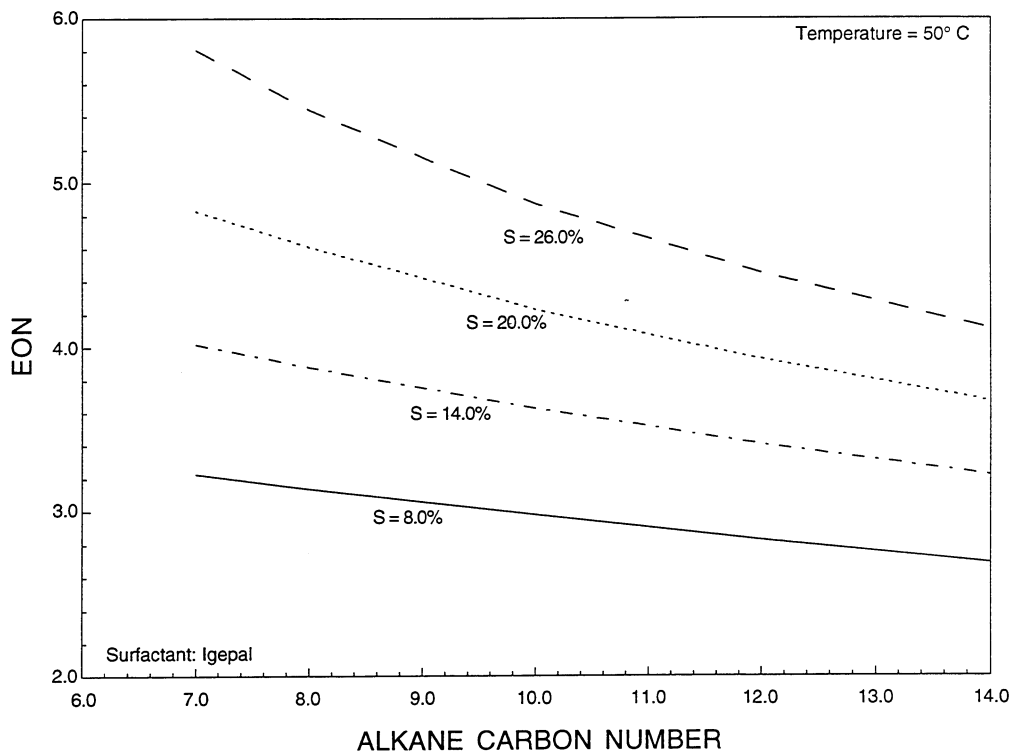


FIGURE 34. - Plot of EON vs. alkane carbon number using Igepal at different salinities and 50° C.

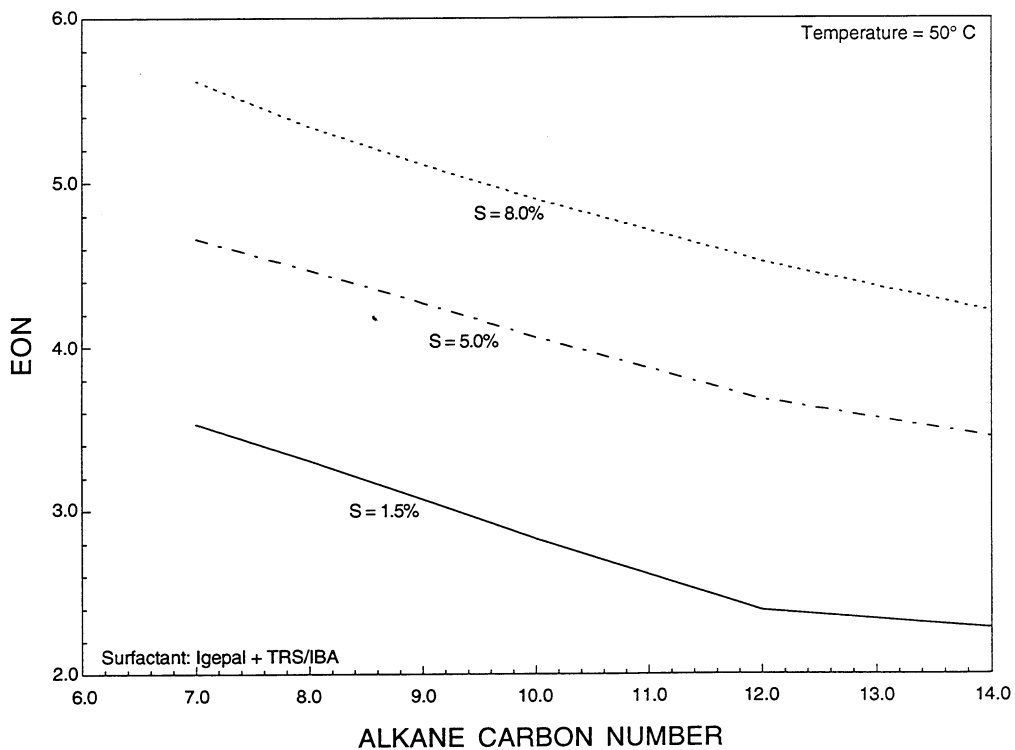


FIGURE 35. - Plot of EON vs. alkane carbon number using Igepal + TRS/IBA at different salinities and 50° C.

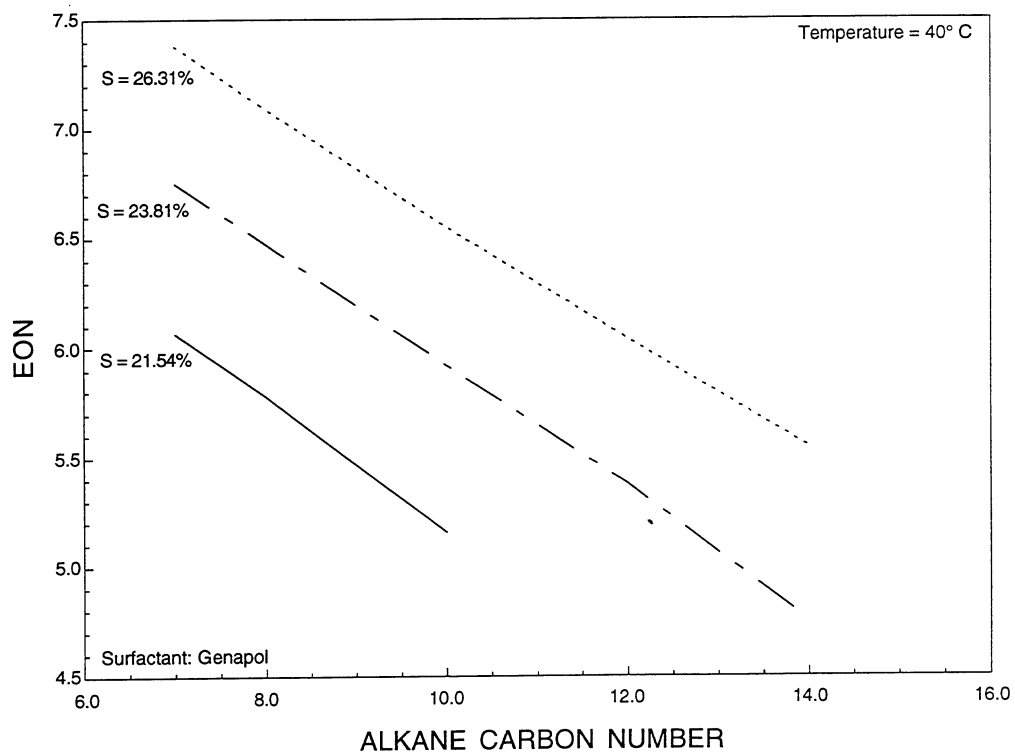


FIGURE 36. - Plot of EON vs. alkane carbon number using Genapol at different salinities and 40° C.

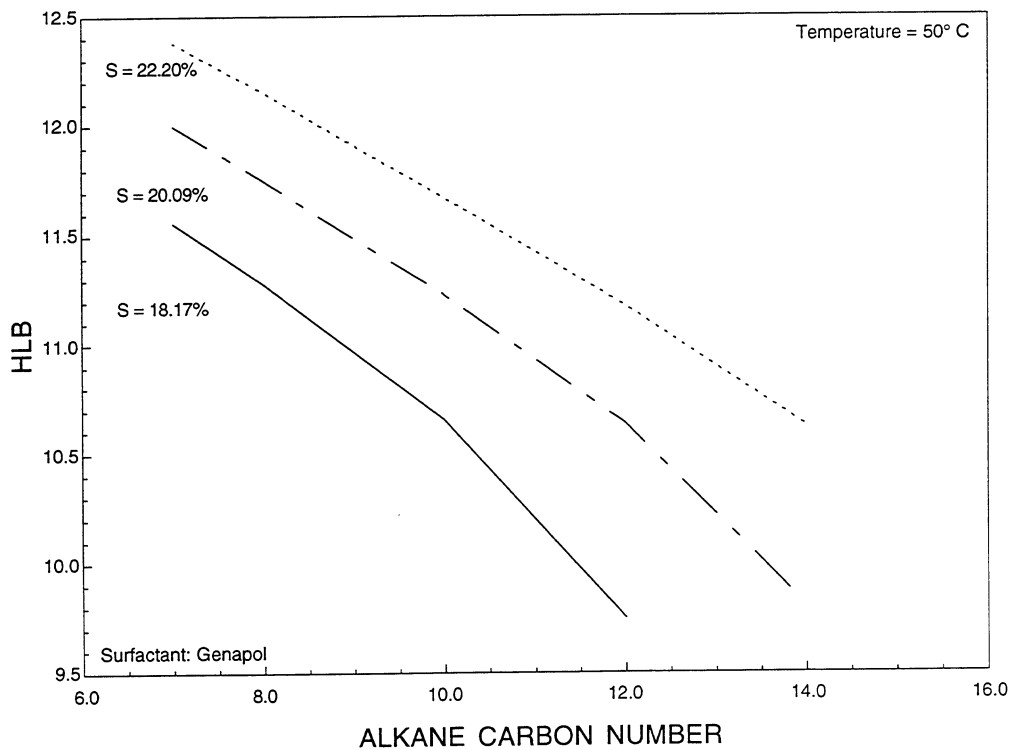


FIGURE 37. - Plot of calculated HLB vs. alkane carbon number using Genapol at different salinities and 50° C.

## Application of the Models

Tables 12 and 13 show the predicted qualitative effects of the various parameters on the properties of the different chemical systems. These are illustrated in Figs. 38 through 45. Figures 38 and 39 show the bilinear models for the temperature coefficients, which are closest to the data. However, we used the linear models that represent results fairly well for n-octane to n-tetradecane, and provide a more straight-forward comparison of the four surfactant systems with respect to their temperature sensitivity and the effect of ACN.

The relative effect of the different parameters on the model is presented as: +, -, 0, <1, and >1. The plus, minus and zero representation indicates either an increase, a decrease, or a little or no effect on the predicted model values as a function of the different parameters. The greater than and less than representation corresponds to the ratio of the values obtained for the Genapol-containing systems compared to those obtained for the systems using Igepal.

Table 14 shows the temperature effects quantitatively. Figure 42 is a plot of the ACN coefficient for the Genapol systems. This coefficient for the Igepal systems depends on temperature only ( $=d_{01}T$ ). At 50° C, it is 0.0283 for plain Igepal and 0.0525 for Igepal + TRS/IBA.

TABLE 12.- Effect of parameters on coefficients

Parameter	$ d\ln S/dT $	$d\ln S/d[ACN]$	$d\ln S/d[HLB]$
T	0	+	0
ACN	-	0	+ (Gen); 0 (Ig)
HLB	0	+	+ (Gen); - (Ig)
Genapol/Igepal	>1	>1	<1

TABLE 13. - Effect of parameters on ratio (with/without TRS/IBA)

Parameters	Opt. salinity	$ d\ln S/dT $	$d\ln S/d[ACN]$	$d\ln S/d[HLB]$
TRS Effect	-	-	+	+ for low ACN > higher
T	0	0	+ (small)	0
ACN	+	-	0	-
HLB	+	0	-	-
Genapol/Igepal	>1	>1	>1 at low HLB <1 at high HLB	variable

+ increase

-decrease

0 little or no effects

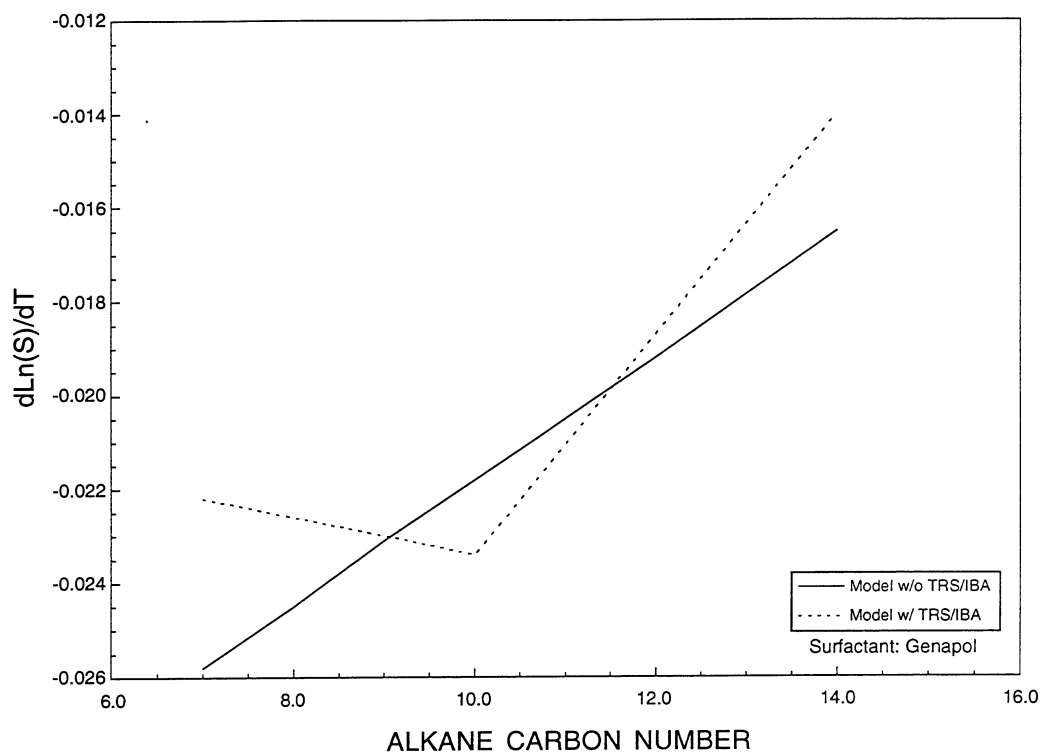


FIGURE 38. - Plot of  $d\ln S/dT$  vs. alkane carbon number using Genapol with and without TRS/IBA.

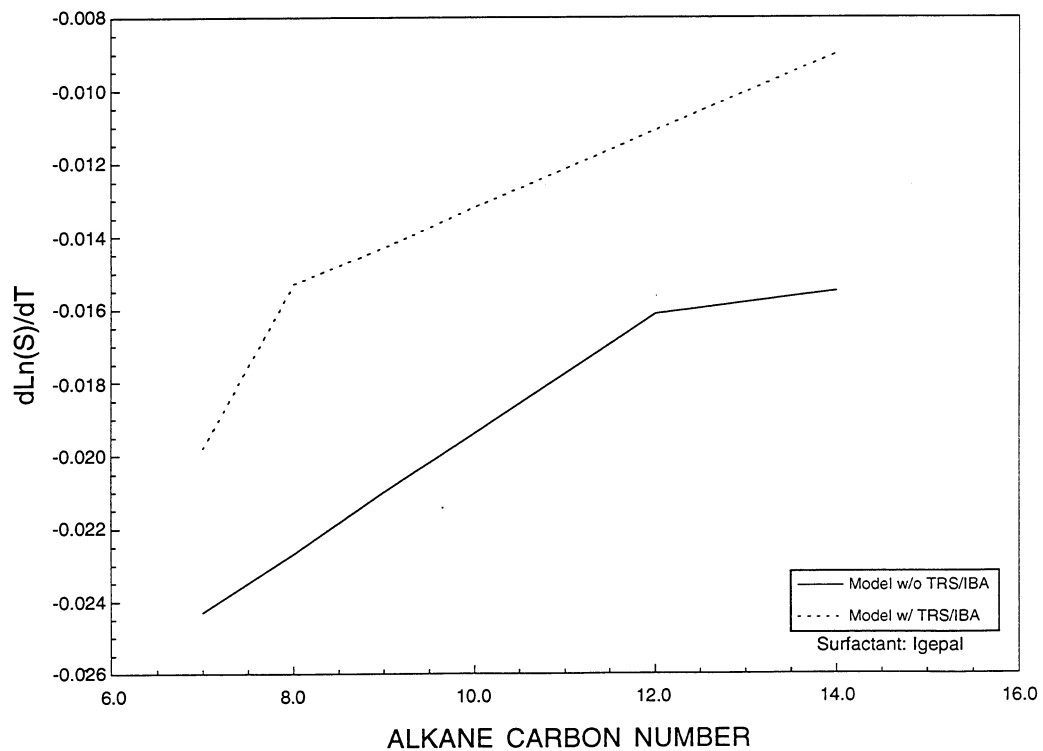


FIGURE 39. - Plot of  $d\ln S/dT$  vs. alkane carbon number using Igepal with and without TRS/IBA.

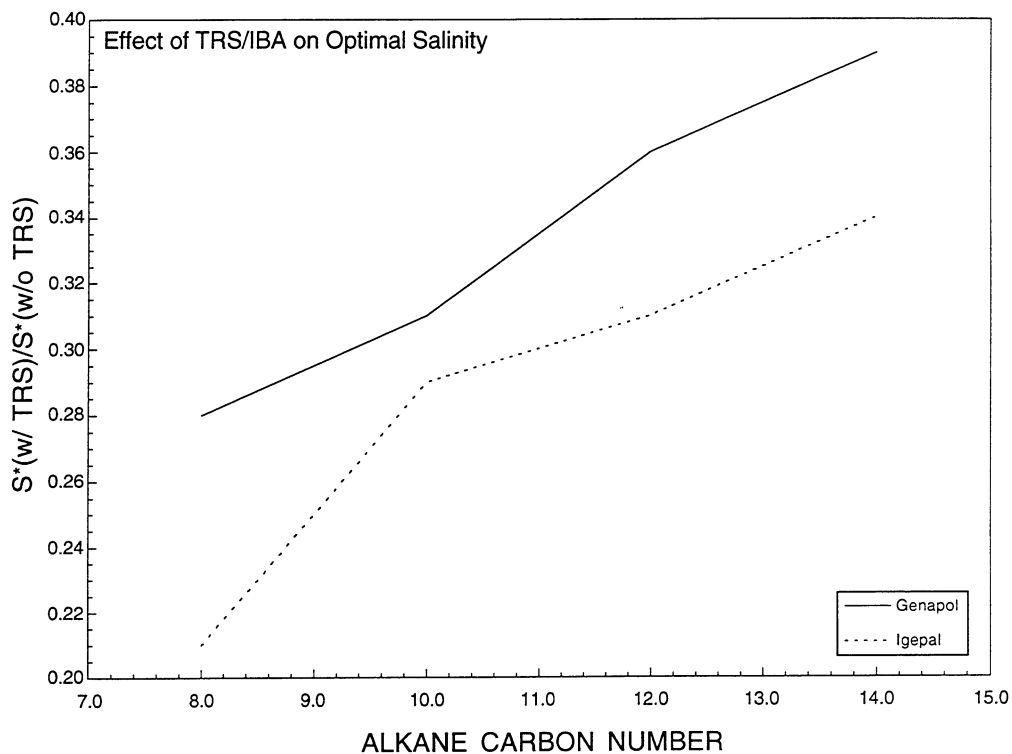


FIGURE 40. - Plot of ratio of optimal salinities ( $S^*_{w/ TRS} / S^*_{w/o TRS}$ ) vs. alkane carbon number using Genapol and Igepal with and without TRS/IBA.

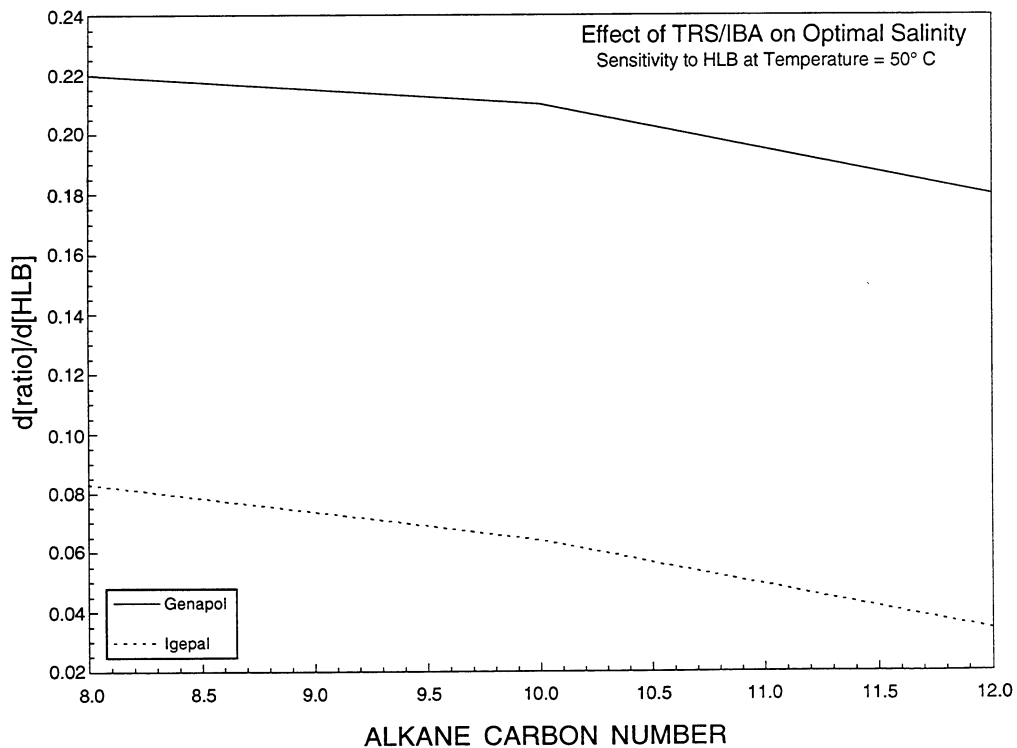


FIGURE 41. - Plot of  $d[\text{optimal salinity ratio}]/d[\text{HLB}]$  vs. alkane carbon number using Genapol and Igepal with and without TRS/IBA at 50° C.

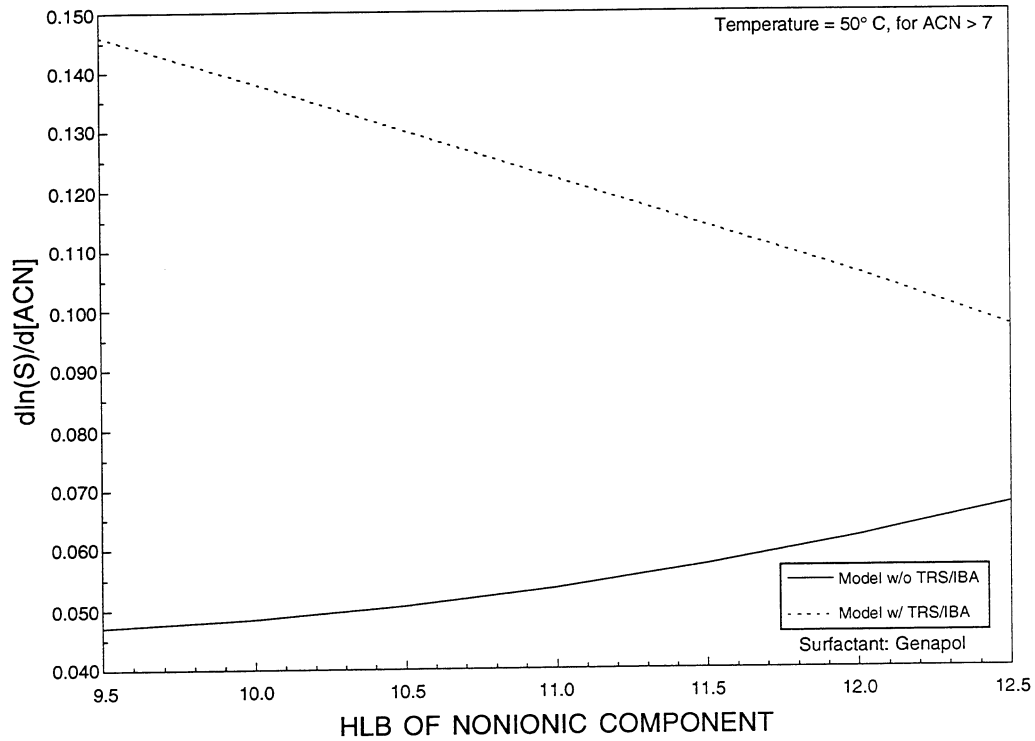


FIGURE 42. - Plot of  $d\ln(S)/d[ACN]$  vs. HLB of nonionic component using Genapol with and without TRS/IBA at 50° C. (ACN > 7)

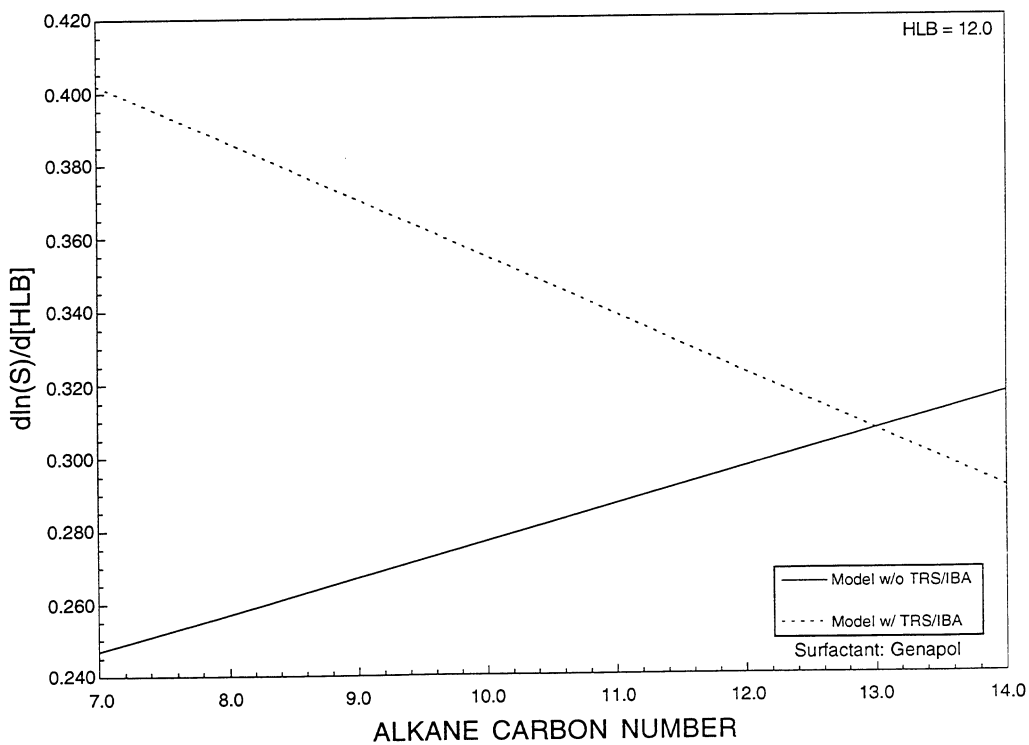


FIGURE 43. - Plot of  $d\ln(S)/d[HLB]$  vs. alkane carbon number using Genapol with and without TRS/IBA.

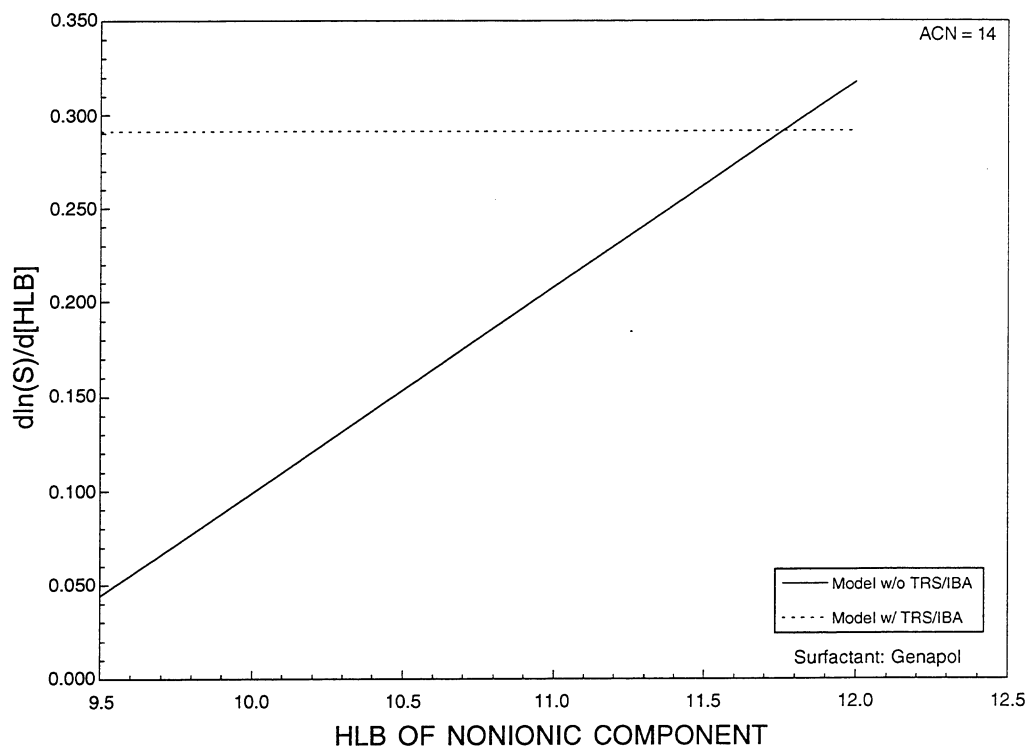


FIGURE 44. - Plot of  $d\ln(S)/d[HLB]$  vs. HLB of nonionic component using Genapol with and without TRS/IBA. (ACN=14)

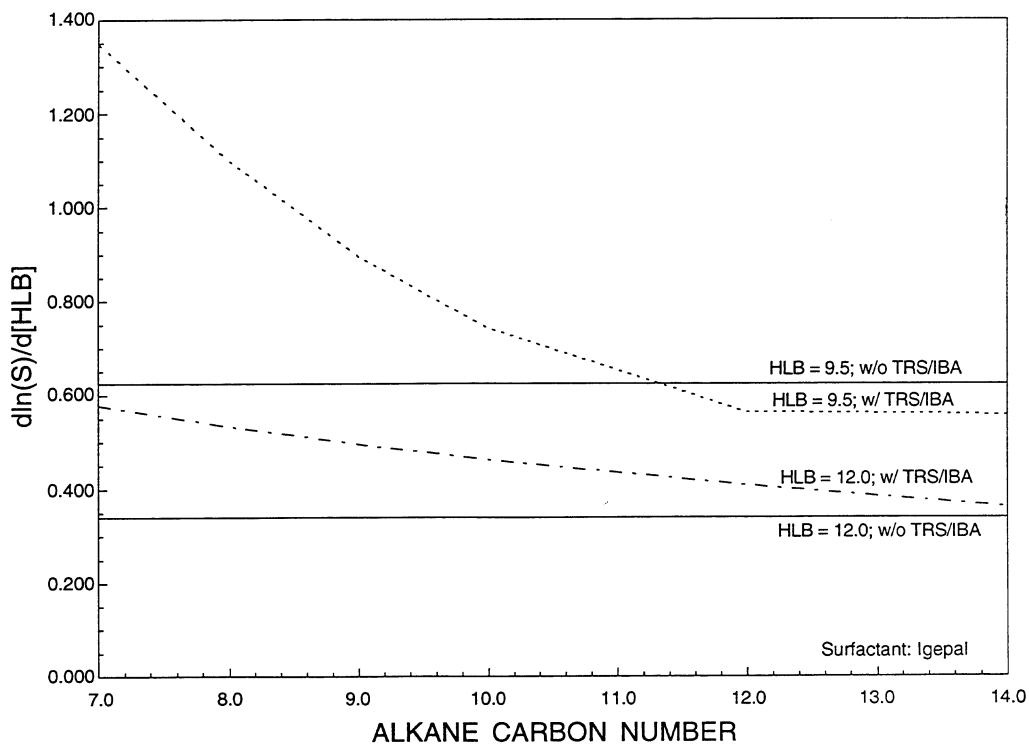


FIGURE 45. - Plot of  $d\ln(S)/d[HLB]$  vs. alkane carbon number using Igepal with and without TRS/IBA at different HLB values.

TABLE 14. - Effect of addition of TRS/IBA on temperature coefficients

Linear model values of  $\ln(S)/dT$  from ACN = 8 to 14

Surfactant system	ACN 8	ACN 10	ACN 12	ACN 14
Genapol	-0.0266	-0.0230	-0.0193	-0.0157
Genapol + TRS	-0.0236	-0.0208	-0.0179	-0.0151
Igepal	-0.0188	-0.0176	-0.0165	-0.0154
Igepal + TRS	0.0153	-0.0132	-0.0111	-0.0090

Ratio of Temperature Coefficients with/without TRS/IBA Added

Surfactant system	ACN 8	ACN 10	ACN 12	ACN 14
Genapol	0.964	0.951	0.936	0.915
Igepal	0.815	0.749	0.673	0.586

Some conclusions from this study are as follows:

1. The reduction in optimal salinity by TRS/IBA is smaller at high *ACN* and high *HLB*. The reduction is larger (and more sensitive to *HLB*) for Genapol than for Igepal. Since only Genapol at low *ACN* and low *HLB* achieved solubilization high enough to be of interest, this is an example of how the most effective systems are the most sensitive to changes in the conditions.

2. It is well known that the nonionics are more temperature sensitive. In our results, the temperature sensitivity is in the order:

$$\text{Genapol} > \text{Igepal} > \text{TRS/IBA}$$

3. The sensitivity to oil type is in the order:

$$\text{TRS/IBA} > \text{Genapol} > \text{Igepal}$$

A Genapol or TRS/IBA system developed for a particular oil would require more re-tailoring than Igepal when applied to another oil.

4. For most systems within the range of our experiments, the sensitivity to *HLB* is much higher when TRS/IBA is added. Conversely, a nonionic-rich blend should

be less dependent on accurate adjustments of *HLB* to be effective than a nonionic-lean blend. However, the difference decreases as either *ACN* or *HLB* gets larger, and changes sign at high values.

### *Summary and Conclusions of Mixed Surfactant System Studies*

Selected surfactant systems containing a series of ethoxylated nonionic surfactants in combination with an anionic surfactant system have been studied to evaluate and identify mixtures of these surfactants, both anionic-nonionic and nonionic-nonionic, that may exhibit improved phase behavior and oil/water solubilization capacity, in comparison to that of the anionic formulation. The effects of different parameters including (a) salinity, (b) temperature, (c) alkane carbon number, (c) *HLB* of nonionic component, and (d) type of surfactant on the behavior of the overall chemical system were evaluated. Several anionic surfactant systems were used in this study, namely; the TRS 10-410/IBA and two varieties of an alpha olefin sulfonate (AOS). Both surfactant types have been fairly well evaluated. Most of the experimental work, PIT and phase volume measurements, was conducted using the TRS 10-410/IBA system. The current experimental work encompassed a temperature range up to 70° C and included various n-alkanes such as n-heptane, n-octane, n-nonane, n-decane, n-dodecane, and n-tetradecane.

The results from the present study provided significant support to the observations made in the earlier study that the Genapol series of linear alkyl alcohol ethoxylates exhibited a very distinct behavior from that of the Igepal series of dialkyl phenol surfactants, at similar *HLB* levels. The Igepal surfactants exhibited a more significant dependence on the *HLB* value than the linear alcohol ethoxylates. The difference in the behavior of these types of systems was observed to be more pronounced at lower *HLB* values, with and without the addition of the anionic component. In general, the mixtures containing the Genapols exhibited considerably higher salinities compared to those containing the Igepals, at similar *HLBs*. The dependence of the optimal salinity on *HLB* was similar for both anionic-nonionic and nonionic-nonionic mixtures. The nonionic-nonionic mixtures generally yielded considerably higher optimal salinity levels compared to those of the anionic-nonionic and anionic systems. The anionic-nonionic mixtures also exhibited relatively higher salinity values than the anionic system alone. Mixing the nonionic surfactant with the anionic component contributed to a significant improvement in the overall solutions' range of applicable optimal salinities.

The effect of the oil on overall solution behavior was also significant. Systematically decreasing the alkane carbon number of the oil used in the experiments, from n-tetradecane to n-heptane, resulted in a reduction of the effective salinity range, at fixed *HLB* and temperature conditions. Replacing the oil phase with different alkanes resulted in a shift in the oil affinity of the

chemical system. A reduced salinity requirement was necessary to offset this shift. Increasing the HLB of the surfactant system, rendering the system more hydrophilic, also resulted in an increase in optimal salinity. The higher salinity requirement was needed to shift the surfactant tendency to be more lipophilic. Changes in operating temperature also had a significant effect on solution behavior. Optimal salinity values were observed to be inversely proportional to temperature variations. At a fixed HLB level, higher optimal salinities were needed for much lower operating temperatures. The aqueous phase solubility and the lipophilic tendency of the surfactant were drastically affected varying the salinity of the overall solution. Increasing the salinity rendered the chemical system more lipophilic, such that a much lower temperature was needed to maintain a new balance between the system's oil and water affinities. Lowering the temperature rendered the system more hydrophilic, which in turn balanced the increased lipophilic tendency due to the salinity increase.

It was also observed that the temperature had an effect on diminishing the difference in behavior between the two nonionic surfactant systems, in the presence of the anionic component. The distinct difference in trend between these systems seemed to decrease with increasing temperature. As previously reported,<sup>14</sup> at HLB levels greater than 11, the pattern of behavior of these nonionics was observed to converge, with and without the anionic surfactant component. The contrast in behavior was very much evident at lower HLB values, but the difference seemed to be suppressed in the presence of the anionic system. This difference in behavior when the anionic surfactant was added may be attributed to the relative effect of temperature on each of the chemical components in the mixture. Temperature has different effect on the oil/water affinity of nonionic and anionic surfactants. The nonionic surfactants are more lipophilic at higher temperatures; while the opposite effect has been exhibited by anionic systems. The presence of the anionic surfactant may have suppressed some of the dominant temperature effects exhibited of the nonionic component in the mixed system.

Experiments with other combinations of anionic-nonionic surfactants were also conducted. The anionic surfactant used in these studies was the alpha olefin sulfonate (AOS). The replacement of the TRS/IBA system with the AOS component was aimed at confirming the different trends observed with the systems containing the Genapols and Igepals. These nonionics were also evaluated as possible substitutes for the relatively high short-chain alcohol requirements of the anionic surfactant. Phase volume and IFT measurements were conducted on selected samples of these anionic surfactants. Experimental information on the oil/water solubilization capacities, IFT, and optimal salinity values for several commercial AOS surfactants were obtained. Relatively good agreement was obtained from these results compared to results presented in the literature. PIT experiments were also conducted on selected samples of these anionics, in combinations with the nonionic surfactants. Tests with the anionic-nonionic systems indicated some trends in their

solution conductivity changes that can be attributed to the relative proximity of optimal conditions. Further tests showed that much higher nonionic component proportions were necessary in order to obtain distinct trends in solution conductivity changes. These results indicated that the AOS surfactant's solution behavior dominated the solution behavior of the overall mixture, at proportions containing less than 50 wt% nonionic. The results using systems with the higher nonionic component indicated very distinct phase inversion trends. These systems exhibited a degree of change in solution conductivity that was comparable to earlier studies with the TRS 10-410/IBA system. One drawback of utilizing more of the nonionics was that the nonionic's solution behavior appeared to almost completely dominate the overall solution behavior. No distinction in behavior could be detected between the samples containing greater than 55 wt% nonionics. The solubilization parameters and optimal salinities determined from these studies were similar to those when using the nonionics alone. The preliminary results from the study of these anionic-nonionic systems seem to indicate limited prospects for application.

The PIT method has been used in this study as a relatively fast screening method for determining the relative proximity of optimal conditions for selected surfactant systems. Utilizing this method, it was possible to evaluate an exhaustive number of surfactant systems in a timely manner. The results from the PIT screening were useful in providing a narrower range of salinity conditions to be tested using the more time-consuming phase volume measurements. Comparisons of results of the two experimental methods are very favorable. The results of the present comparisons showed fairly good agreement between the salinity regions determined using both methods. These results support the need to utilize the PIT method, whenever applicable, for initially identifying the salinity regions of interest. This procedure then is followed by additional studies including salinity scans, IFT measurements, and oil displacement experiments to determine oil-recovery potential. As mentioned earlier, these comparisons show very good agreement, with an average difference of 0.3%. From the phase volume measurement studies, only two of the systems tested reached solubilization capacity exceeding the value of  $10 \text{ cm}^3/\text{cm}^3$ . These systems were Genapol with n-octane and Igepal with n-decane, both without the anionic component added. The higher solubilization values occurred at relatively lower values of HLB. Although there was no systematic trend with respect to HLB observed from the results, there was a strong downward trend indicated with respect to increasing temperature and increasing ACN. The addition of the anionic system was observed to have had an adverse effect on solubilization capacity. The development of a mathematical model for values of the solubilization parameters was not attempted because there was no striking pattern observed from the experimental results.

Efforts to correlate the behavior of these anionic-nonionic and nonionic-nonionic systems have led to the formulation of several models for each of the systems tested. The models were used to compare the different surfactant systems and provide some guidelines for designing them

to account for variations in salinity, oil and temperature. A linear smoothing function was applicable in most cases tested, but the trends that were consistently curved were modeled using quadratic expressions. Earlier references to the model developed by the University of Texas group<sup>14,29,32</sup> were presented as logarithmic in salinity for anionic surfactants, and linear for nonionic surfactants. To make comparisons easier, the logarithmic term of the salinity was used for all systems tested. Several smoothing strategies were employed. Both linear and bilinear correlations were evaluated, and corresponding parameter coefficients were obtained. An evaluation of the model was then made to determine conformance with the results from both PIT and phase volume measurements. The model provided good agreement with the results from both experimental studies.

Several observations were also made with regards to the results from the modeling effort and the experimental work. It was observed that the effect of the addition of anionic component on reduction in overall solution optimal salinity diminished with increasing ACN and HLB levels. The salinity reduction was larger and more sensitive to HLB for the Genapol systems than for the Igepals. For most systems tested, the sensitivity to HLB was much higher when the anionic component was added. Conversely, a nonionic-rich blend would then be less dependent on accurate adjustments of HLB to be effective than a nonionic-lean blend. However, the difference in dependence decreased with increasing ACN or HLB values. As mentioned earlier, temperature had a significant effect on nonionic surfactants. The nonionics tended to be more temperature sensitive than the anionic surfactants did. In our results, the observed temperature sensitivity was in the order: Genapol > Igepal > TRS/IBA. The sensitivity of the chemical system to oil type was observed to be of the following order: TRS/IBA > Genapol > Igepal. Based on this oil sensitivity order, chemical systems of Genapol or TRS/IBA that have been formulated for a particular oil would tend to require more "re-tailoring"/"re-formulation" effort than the Igepals would in order to be optimized for application with another target oil.

## II. CT-IMAGING OF CHEMICAL EOR COREFLOODING EXPERIMENTS

### *Materials and Experimental Procedures*

#### **CT-imaging Techniques**

The CT equipment and general operating procedures at NIPER have been developed and described previously.<sup>19,22</sup> The use of the equipment and techniques for surfactant enhanced oil recovery experiments have also been described.<sup>16,23</sup> Figure 46 shows a representation of a core that has been scanned using the CT equipment. The saturations within the core are calculated and slices are combined using programs written by the NIPER Imaging Group.<sup>22</sup> A commercial software package, trademark SPYGLASS, developed by the National Center for Supercomputer Applications, University of Illinois, is then used for data display and analysis. Any 3D object can be rotated and sliced for viewing along any of the XY, XZ, and YZ planes through the object. Figure 46 shows a vertical view down the length of the core and four of the individual slices that were combined to form the reconstructed image. This image represents initial stages of a chemical flood. Injection of the surfactant is nonuniform even within a few centimeters of the core face.

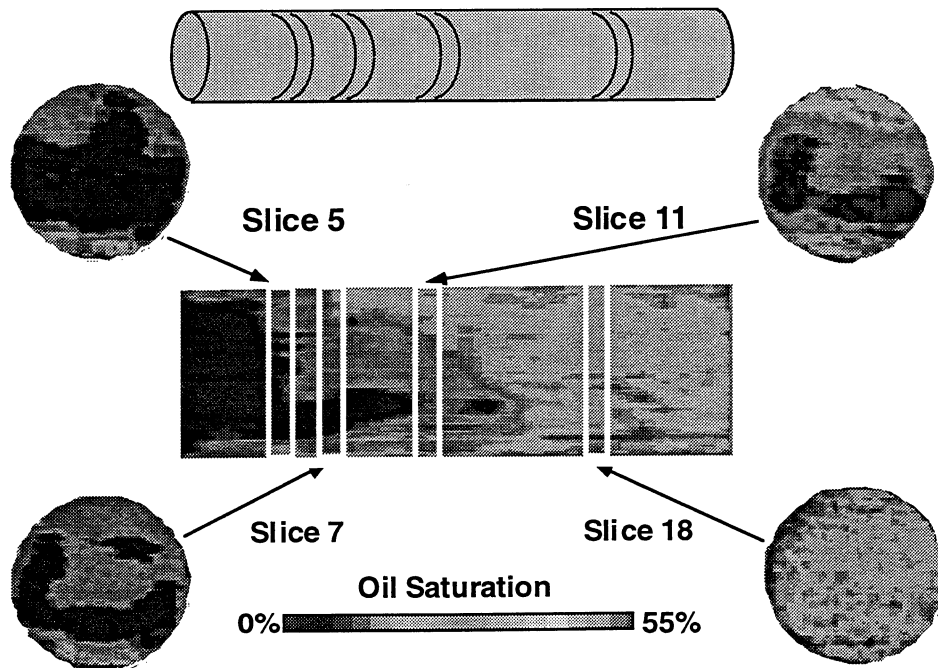


FIGURE 46.-

Composite CT image of surfactant-enhanced chemical coreflood after injection of the surfactant slug. X-ray images are obtained along the core length. The slices are then merged into one data file, and cross sections of fluid distribution along any axis can be reconstructed.

## Materials

Commercial chemicals used in this study are identified in Table 15.

Two oils, both from Class 1 reservoirs, have been used for CT-coreflooding experiments. Their properties differed significantly from each other, as shown in Table 16; however, to visualize oil saturation using the CT, the oils were tagged with 16 to 20% iododecane. Addition of iododecane reduced the viscosity of Hepler oil to approximately 35 to 40cP but did not affect the viscosity of NBU oil. All viscosity values reported were measured at ambient temperature.

Cores were initially saturated with either the brine used to make surfactant solutions or with simulated reservoir brine for Hepler or North Burbank fields. The composition of simulated Hepler brine is 1.02% NaCl, 0.39% CaCl<sub>2</sub>, and 0.33% MgCl<sub>2</sub>, and the composition of NBU brine is 6.65% NaCl, 1.54% CaCl<sub>2</sub>, and 0.24% MgCl<sub>2</sub>. (Concentrations are reported as weight to weight.)

## Coreflooding

Coreflooding procedures used for these tests have been described previously.<sup>13,16</sup> A general outline of the steps involved in conducting coreflood experiments with CT imaging is provided in appendix B.

TABLE 15. - Commercial chemicals used for CT-monitored corefloods

Chemical type	Company	Tradename	Activity, wt%
Mixed anionic surfactant	Stepan	B-105	51.4
alkyl aryl sulfonate	Stepan	B-110	48.3
petroleum sulfonate	Witco	TRS 10-410	62.0
Xanthan gum, biopolymer	Pfizer	4800C	13 to 16

TABLE 16. - Oils used in CT-monitored corefloods

Field (oil name)	State	Gravity, °API	Viscosity, cP 23° C	Viscosity of tagged oil, cP
Hepler	Kansas	26.1	76	38
N. Burbank Unit	Oklahoma	39.5	8.6	8

## RESULTS AND DISCUSSION

### *Effect of Surfactant Slug Size on Oil Production*

CT-imaging of oil saturation distributions was used to monitor oil movement and recovery for a low-concentration alkaline surfactant polymer system that has been studied extensively with Hepler oil.<sup>13,16,23,33</sup> Table 17 shows a summary of fluid compositions and core permeabilities for the CT tests discussed in this report. All corefloods except NBU-2 were conducted in Berea sandstone core at ambient temperature. Test NBU-2 was conducted at 50° C.

### **Oil Production**

Reducing the amount of surfactant injected during low-concentration alkaline-surfactant-polymer flooding resulted in lower oil production and higher remaining oil saturations for tests CT-CF 7, 8, and 9, as compared to CT-CF 1 and 3, which injected approximately 0.8 PV of low-concentration surfactant. The amount of oil recovered, however, was not directly proportional to the amount of injected surfactant. Other factors appear to influence the amount of oil produced in addition to reduction in the amount of surfactant injected. These factors include mobility control polymer concentration and high permeability streaks in the core.

Figures 47 through 49 show the oil production curves for tests CT-CF 1, 7, and 8. In each test, the amount of injected surfactant has been reduced by approximately 50%. Less oil was produced as the amount of injected surfactant was reduced. However, the test using the least amount of surfactant (CT-CF 8) was more successful than the test using an intermediate volume of surfactant (CT-CF 7). Several problems encountered while conducting CT-CF 7 may account for the reduced oil production. The alkaline preflush for this test had been flushed from the core before surfactant was injected. An alkaline preflush is effective in reducing surfactant loss caused by adsorption and precipitation in the core. Previous studies<sup>34</sup> with high-permeability Berea sandstone cores showed that oil recovery with this chemical system was reduced to approximately 75-80 % OOIP from approximately 95% OOIP when no preflush was used. Total oil production for CT-CT 7 was in this range.

In addition, the polymer used for mobility control was initially injected at a lower concentration level (500 ppm rather than 3500 ppm), resulting in an unfavorable mobility ratio with the oil. The problem was corrected, and the viscosity of the mobility slug was increased. The effect this had on oil production, however, is difficult to assess. Previous studies have shown that reduction of polymer concentration significantly reduced oil recovery efficiency for this system.<sup>13,33</sup> Figure 50 shows the oil production curves for test CT-CF 3 which used a lower

TABLE 17. - Summary of fluid compositions and core permeabilities for the CT-monitored corefloods

Coreflood name	Oil	Surfactant No. 1	Surfactant No. 2	Ratio, % of total conc	Total conc,		Surfactant volume injected, PV	Brine for chemical slug	Biopolymer conc, ppm	Core liquid permeability, mD
					wt %	Cosurfactant				
CT-CF 1	Hepler	B-110	B-105	62.5/37.5	0.4	2% 2-butanol	0.79	1% NaCl + 0.95N NaHCO <sub>3</sub> and Na <sub>2</sub> CO <sub>3</sub>	3,500	560
CT-CF 3	Hepler	B-110	B-105	62.5/37.5	0.4	2% 2-butanol	0.77	1% NaCl + 0.95N NaHCO <sub>3</sub> and Na <sub>2</sub> CO <sub>3</sub>	1,000	440
CT-CF 7	Hepler	B-110	B-105	62.5/37.5	0.4	2% 2-butanol	0.43	1% NaCl + 0.95N NaHCO <sub>3</sub> and Na <sub>2</sub> CO <sub>3</sub>	560 and 3400	600
CT-CF 8	Hepler	B-110	B-105	62.5/37.5	0.4	2% 2-butanol	0.20	1% NaCl + 0.95N NaHCO <sub>3</sub> and Na <sub>2</sub> CO <sub>3</sub>	3,400	530
CT-CF 9	Hepler	B-110	B-105	62.5/37.5	0.4	2% 2-butanol	0.43	1% NaCl + 0.95N NaHCO <sub>3</sub> and Na <sub>2</sub> CO <sub>3</sub>	3,400	720
CT-CF 4	NBU	TRS 10-410		100	5.0	3% 2-butanol	0.11	0.9% NaCl	1,500	290
CT-CF 5	NBU	TRS 10-410		100	5.0	3% 2-butanol	0.21	0.9% NaCl	500	740
CT-CF 10	NBU	TRS 10-410		100	5.0	3% 2-butanol	0.11	0.5% NaCl + 0.02% CaCl <sub>2</sub>	1,500	480
NBU-1	NBU	B-110	B-105	12.5/87.5	1.0	none	0.3	6.6% NaCl + 1.5% CaCl <sub>2</sub> + 0.24% MgCl <sub>2</sub>	1,200	50
NBU-2	NBU							6.6% NaCl + 1.5% CaCl <sub>2</sub> + 0.24% MgCl <sub>2</sub>		50

concentration polymer slug after surfactant injection. Significantly less oil was produced when lower viscosity polymer was used.

An additional coreflood (CT-CF 9) was conducted to repeat the conditions of CT-CF 7. Oil production curves of CT-CF 9 are shown in Fig. 51. Although the final oil saturation after the chemical flood was lower than that for CT-CF 7 (11% versus 18%), oil production was delayed relative to any of the other tests. Oil production did not start until after injection of more than 2 PV of chemical injection. In most cases with this chemical system, major oil production started after approximately 1 pore volume (PV) of chemicals had been injected. Oil produced before injection of at least 1 pore volume occurred only for cores with oil saturations greater than 30% after the waterflood.<sup>13,34</sup> Delayed production, as seen for CT-CF 9, has not been observed in previous tests.

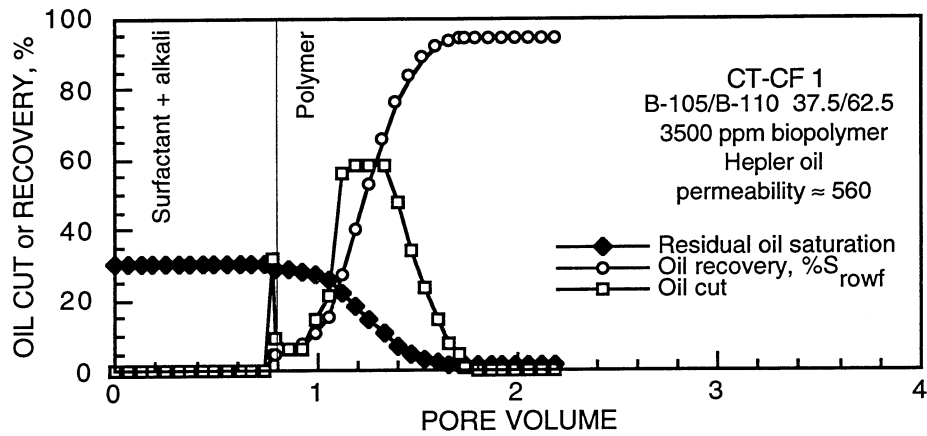


FIGURE 47.- Oil recovery, oil cut, and residual oil saturation for CT-CF 1. Injection of 0.77 PV of low-concentration alkaline/surfactant chemical system produced most of the oil from the core.

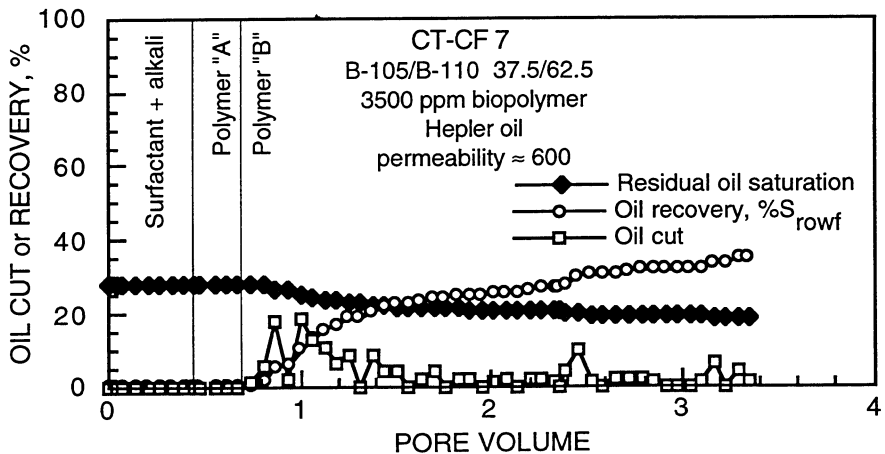


FIGURE 48.- Oil recovery, oil cut, and residual oil saturation for CT-CF 7. Alkaline/surfactant chemical slug size was reduced to 0.43 PV.

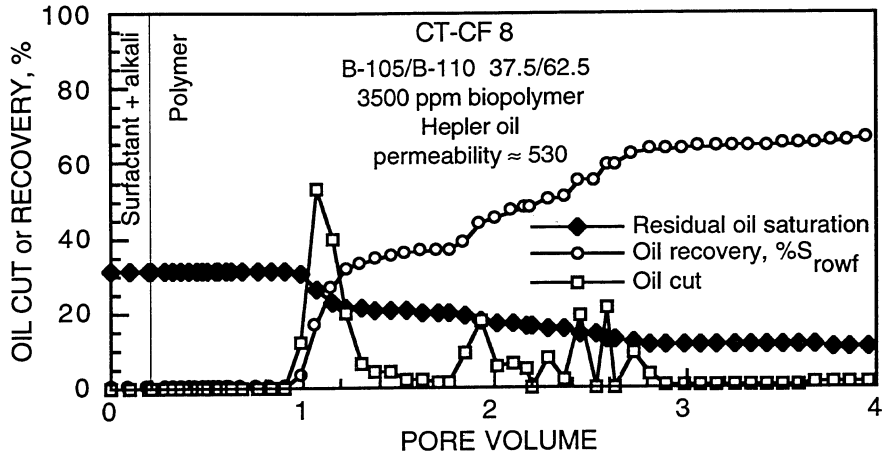


FIGURE 49.- Oil recovery, oil cut, and residual oil saturation for CT-CF 8. Alkaline/surfactant chemical slug size was reduced to 0.2 PV.

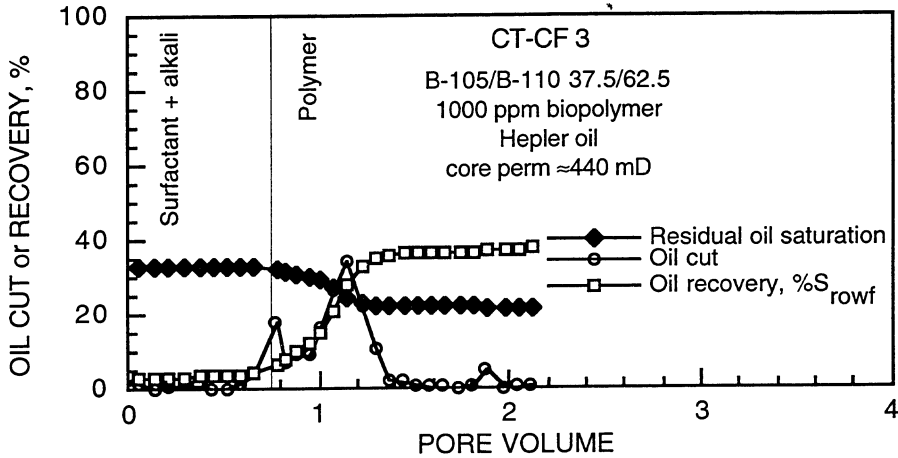


FIGURE 50.- Oil recovery, oil cut, and residual oil saturation for CT-CF 3. Alkaline/surfactant chemical slug size was the same as CT-CF 1. Mobility control polymer concentration was reduced, however. Oil recovery was reduced.

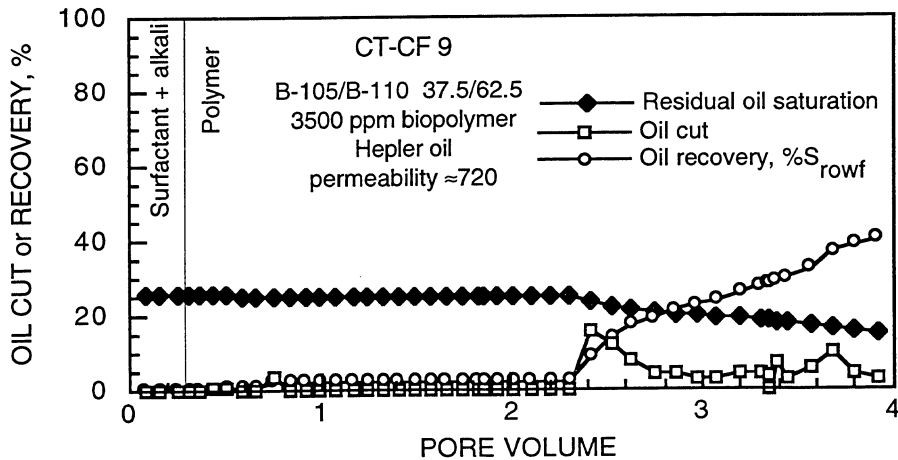


FIGURE 51.- Oil recovery, oil cut, and residual oil saturation for CT-CF 9. This was a repeat of CT-CF 7. Oil production after injected more than 2 PV of chemicals suggest channeling of fluids and slow propagation of the oil through the core.

Examination of CT images of CT-CF 9 suggest that the oil saturation distribution after the waterflood was not uniform. The outer edge of the core was, on the average, at least 10% lower in saturation than other areas of the core. Waterflood oil production after water breakthrough continued in small amounts for each increment in water injection. Figure 52 shows one CT slice in the middle of the core that shows the ring of lower oil saturation around the core edge (image a). Previous CT-monitored corefloods have not exhibited this type of saturation distribution after waterflooding. After injection of 1.8 PV of chemicals, the same slice (Fig. 52, image b) shows the edges even lower in oil saturation and an increase in saturation in the middle of the core. These pictures suggest that only a fraction of the injected fluids passed through the main section of the core and that a greater proportion of the chemicals have bypassed the oil. Continued injection of polymer results in slower movement of oil through the central part of the core. An additional injection of 2 PV of polymer results in a relatively low oil saturation throughout the core. Oil production, however, is inefficient under these conditions.

Table 18 summarizes average oil saturations after waterflood and after chemical flood from volumetric measurements. Production declined as the amount of surfactant injected declined, in agreement with previous studies using Hepler oil and low-concentration alkaline-surfactant systems.<sup>11</sup> Production also declined with a reduction in polymer concentration. Reducing the amount of surfactant, however, was less detrimental to overall production than reducing polymer

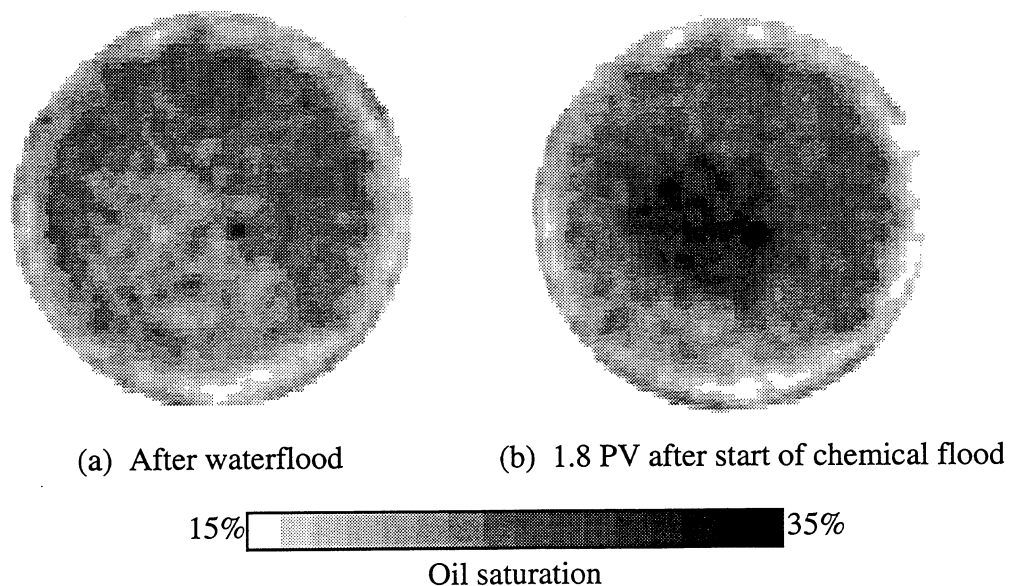


FIGURE 52.- CT image of a slice from CT-CF 9 16.5 cm from the core inlet. The outer edges of the core are very well swept of oil. A higher proportion of injected fluids may have flowed through this area. Higher saturation in the middle of the core after 1.8 PV injected indicates that oil is propagating slowly through the entire core, however.

TABLE 18.— Residual oil saturations after waterflood and chemical flood for CT-monitored chemical flooding experiments

Coreflood identification	$S_{rowf}$ , %PV	$S_{rocf}$ , %PV	Comment
CT-CF 1	36	6	0.79 PV surfactant and good mobility control.
CT-CF 3	35	22	0.77 PV surfactant and poor mobility control.
CT-CF 7	28	18	0.43 PV surfactant, no preflush and ? mobility control problems.
CT-CF 8	32	11	0.2 PV surfactant.
CT-CF 9	28	13	0.43 PV surfactant and chemical bypass of oil.

effectiveness. From these studies, cost savings by reducing surfactant use may be a reasonable strategy. However, mobility control design may be critical to determining the cost effectiveness of the chemical EOR project. These studies were conducted in high permeability rock. Loss of surfactant from precipitation or adsorption would modify these conclusions.

### Oil Saturation Distribution

Composite CT images of each core during various stages of the EOR experiment are compiled in Appendix C. The views represent oil saturation distributions in a vertical plane transecting the middle of the core from inlet to outlet. For CT-CF 7, because of the length of the core, approximately 5 cm at the core exit was not scanned. For CT-CF 8, the core inlet was shielded for the first several centimeters, which blocked the view of the initial oil bank formation. All other tests showed oil saturations for the entire core length.

Average oil saturations for each 8 mm core section were calculated, and results for tests CT-CF 7-9 are plotted in figures 53 through 55. Plots of this type for CT-CF 1 and 3 can be found in reference 8. Comparison of these figures illustrate once again that movement and production of oil does not depend directly on the amount of surfactant injected. With the larger injected pore volume (0.77 PV, CT-CF 1), more oil is produced with less total fluid injected. With less surfactant injected, oil appeared to move more slowly through the core. Oil banks did form with oil saturations 10-15 % greater than oil saturations after waterflood. They appeared to spread out, however, as the chemical front advanced. Oil was then produced via a stripping action.

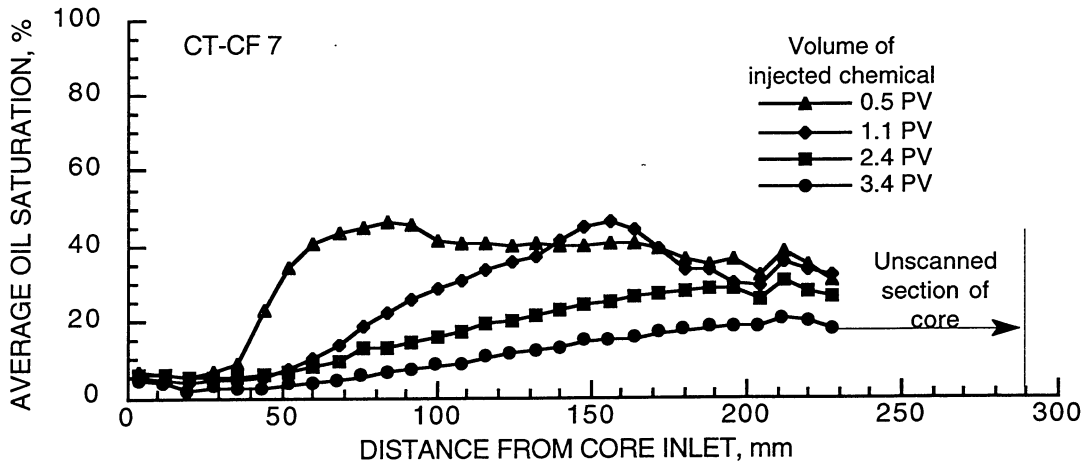


FIGURE 53.- Average oil saturations along the length of the core as a function of injected pore volume for CT-CF 7. Each point represents an average distance of 8 mm. The core was longer than the CT scanned length.

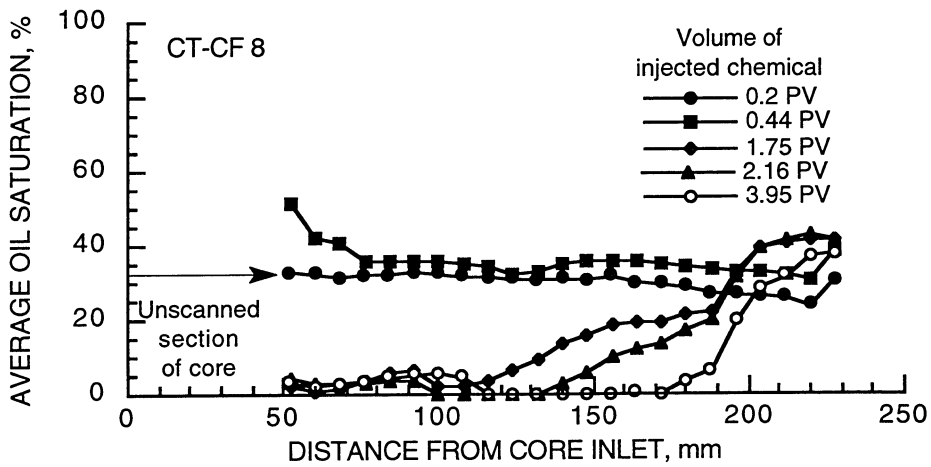


FIGURE 54.- Average oil saturations along the length of the core as a function of injected pore volume for CT-CF 8. The inlet section of the core was not scanned. It appears, however, that saturations in this area should be very low after the oil front had move through. The oil front can be seen after 0.44 PV injected.

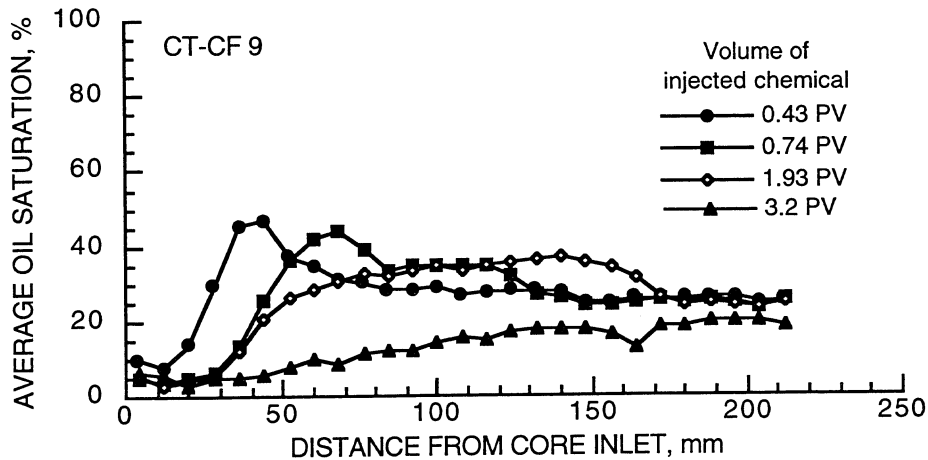


FIGURE 55.— Average oil saturations along the length of the core as a function of injected pore volume for CT-CF 9. The 0.43 PV curve compares with CT-CF 7, but movement of oil appears to be retarded as injection continues. After 1.93 PV, the oil saturations have not been reduced very far into the core compared to both CT-CF 7 and 8.

These observations suggest that instead of decreasing surfactant slug size, increasing the volume of low-concentration surfactant might help oil production and reduce the required amount of polymer to maximize production potential. Depending on relative surfactant and polymer costs, the economics of the chemical flood might not be greatly affected by this strategy.

In summary, a reduction in surfactant slug size for an alkaline/surfactant/polymer chemical system reduced overall oil production and extended the required time to reduce the oil saturation. CT imaging techniques were especially helpful in keeping track of the chemical flood progress and determining if further injection of chemicals would continue to produce additional increments of oil. CT imaging also helped to point out well swept areas of the core (CT-CF 9) after the waterflood that probably influenced the rate of oil movement through the core. Reducing low-concentration surfactant slug size may not be the best method to reduce chemical costs. Savings achieved by reducing the amount of surfactant will be offset by increased requirements for mobility control polymer injection.

### *Oil Movement in the Core Under Shut In Conditions*

Laboratory chemical EOR coreflood tests are time-consuming. Fluids may have to stay in the core under static conditions while waiting for available equipment such as a CT scanner. Therefore, an experiment was conducted to determine if static conditions had an effect on oil saturation distributions during intermediate stages of the coreflood.

Coreflood CT-CF 5 was conducted using NBU oil and a chemical system designed for an optimal salinity of approximately 1 % NaCl at ambient temperature. Table 17 summarizes the conditions of the coreflood. CT images of the core were taken immediately after injection of the surfactant. The core was shut in for 1 week and then rescanned. Figure 56 shows a comparison

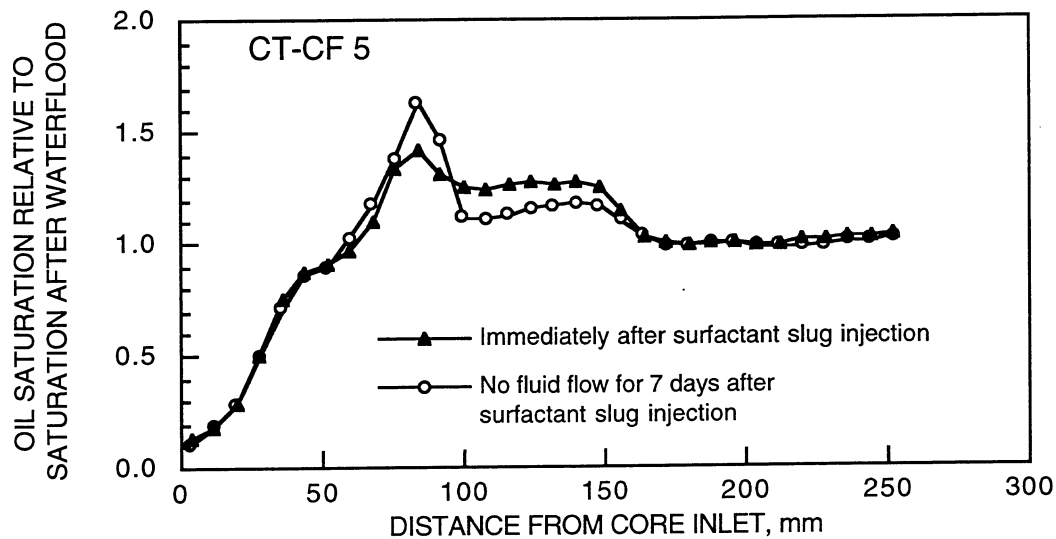


FIGURE 56.— Average oil saturation along the core length for CT-CF 5 after surfactant injection and after shut in for 1 week. Redistribution of oil in the region of the oil front can be observed.

of the average oil saturations along the core length for the two cases. A comparison of the CT composite images is shown in Fig. 57.

The oil front sharpened during the 1-week shut in. The change in saturation, however, only occurred in areas of increased saturation caused by the surfactant injection. Oil saturations did not change around the inlet where oil saturation has been greatly reduced or in the core not yet contacted by the chemical flood.

Changes in oil saturation within the core can occur during periods of static flow. The effect this phenomenon may have on oil propagation and production has not been fully evaluated, however. Further investigations including observations of the dynamics of oil movement under gravitational or other forces can be monitored using CT-imaging techniques.

### *CT-imaging of Oil Production for Different IFT Conditions*

Surfactants have the potential of producing significant amounts of incremental oil because they reduce the interfacial forces between oil and water and allow the fluids to overcome capillary forces trapping oil in the rock pore spaces. Reconnection of isolated oil droplets (formation of an oil bank) also helps to sweep oil from injector to producer. Maximum oil recovery is usually obtained for the lowest IFT systems.

An experiment was conducted to determine oil production and saturation distributions from CT-imaging as the IFT of the surfactant system changed. Experiments (CT-CF 4 and CT-CF 5) conducted up to this time using the petroleum sulfonate chemical system (TRS 10-410 and IBA) were optimized with NBU oil to obtain a very low IFT ( $<.001$  mN/m). Changing the salinity of

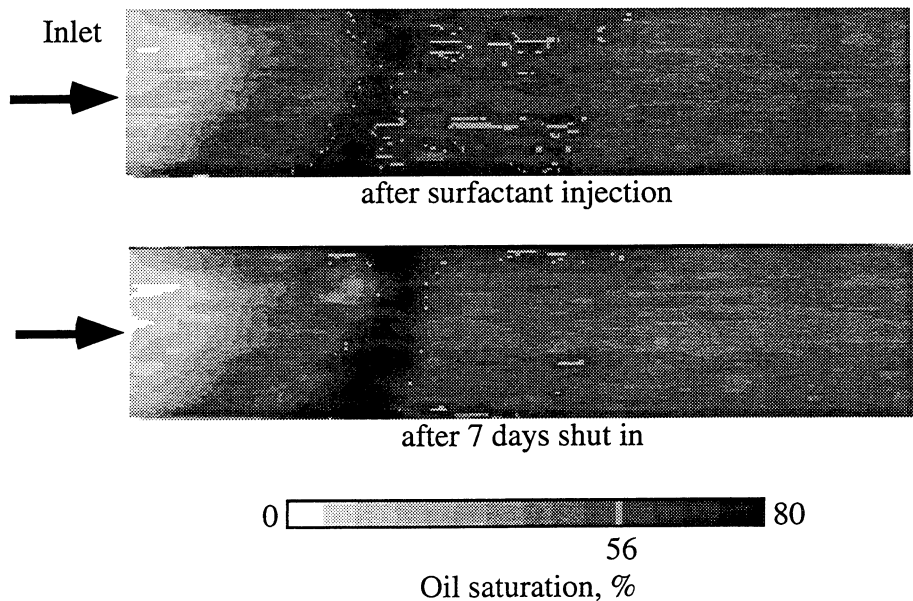


FIGURE 57.— Composite CT images of CT-CF 5 after surfactant injection showing the change in oil saturation distribution before and after 1 week of shut in time.

the brine and chemical slug would change the interfacial tension between the oil and aqueous phases. For this experiment (CT-CF 10), the aqueous phase composition was 0.5% NaCl and 0.02% CaCl<sub>2</sub>. The IFT for this under optimum surfactant system was 0.02 mN/m. Coreflood details are given in Table 17.

Changing the IFT of the injected fluids with NBU oil, in this experiment, however, had little effect on oil production, propagation, and average saturation distributions for tests CT-CF 4 and CT-CF 10. Figure 58 shows the oil production curves for the two tests.

After completion of the chemical flood, final oil saturation for CT-CF 10 was only slightly higher than for CT-CF 4, 0.9% and 0.6%, respectively. Figures 59 and 60 show average oil saturations along the core length after injection of 0.15 to 0.2 PV chemicals (immediately after injection of surfactant) and after completion of the tests. Average saturations are very similar in both cases.

Therefore, for these tests, the change in IFT was insufficient to greatly affect oil mobilization. Additional studies are suggested where either greater capillary forces must be overcome (lower permeability core) or fluids are used that have IFT values of greater contrast to those investigated in this study.

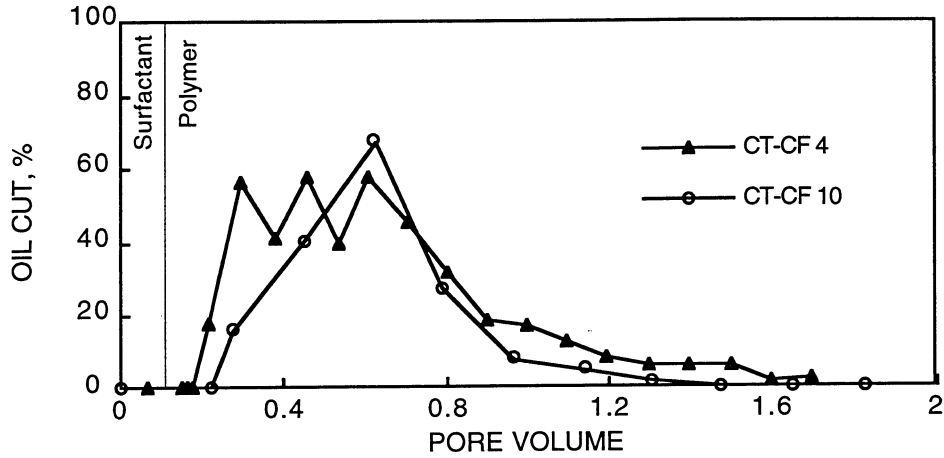


FIGURE 58.— Oil cut production of tests CT-CF 4 and CT-CF 10. The IFT between oil and surfactant for CT-CF 4 was 0.001 mN/m and 0.02 mN/m for CT-CF 10.

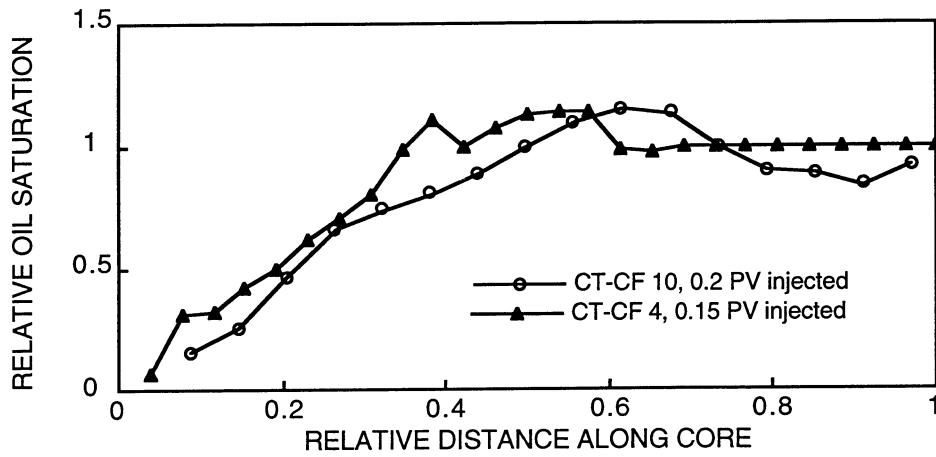


FIGURE 59.— Average oil saturations from CT measurements after injection of surfactant slug for tests CT-CF 4 and 10. Distance along the core is normalized to take into account different core lengths.

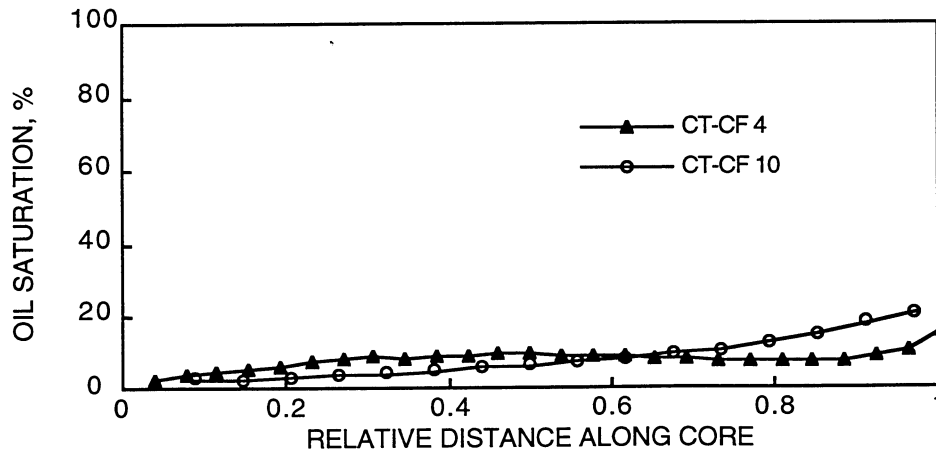


FIGURE 60.— Average oil saturations from CT measurements after completion of chemical flood for tests CT-CF 4 and 10. Distance along the core is normalized to take into account different core lengths.

## *CT-Imaging of Corefloods in Reservoir Rock*

CT-imaging of corefloods conducted in reservoir rock samples is particularly helpful in interpreting oil movement and production efficiency for chemical EOR studies. Reservoir core may contain permeability streaks that can have a significant effect on oil recovery when small core samples are used to evaluate a chemical system oil recovery efficiency.

Reservoir core from North Burbank Unit (NBU), Osage County, Oklahoma was characterized using CT tracer tests and minipermeameter measurements prior to use in coreflooding experiments. The NBU reservoir is a Class 1 reservoir that is oil-wet because of a coating of chamosite, an iron-rich mineral, on the pore surfaces.<sup>18</sup> Tracer tests (tracer=10% NaI) were conducted on two cores, designated NBU-1 and NBU-2. Each core shows a significant variation in permeability within the 1.5-in diameter core that extends through the core sample. Figure 61 shows a tracer profile of the two tests. NBU-1 shows a higher permeability area in the lower half of the core. Very little tracer passes through the upper section of the core. For NBU-2, a lower permeability area extends through the middle of the core in a slightly rising plane from inlet to outlet of the core.

Prior to conducting the tracer test, NBU-2 was cleaned with toluene and methanol. After cleaning, dark colored stains appeared on a portion of the previously unmarked core surface. A permeability distribution was obtained on the core faces using a minipermeameter, which measures

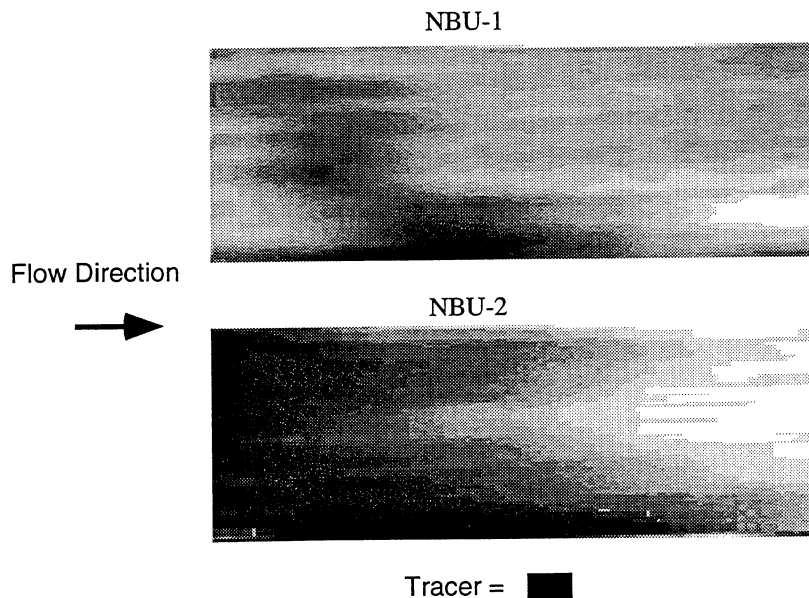


FIGURE 61.— CT composite images of tracer injection in two core samples from North Burbank Reservoir, Osage County, Oklahoma. The dark color is tracer (10% NaI). A larger slug size was injected for NBU-2 than for NBU-1.

permeability to  $N_2$  gas for a small area of the core surface. The minipermeameter indicated that the stained areas were lower in permeability than the adjacent areas of the core. Figure 62 shows the permeability variation observed along the core faces. The low permeability area extends through the core, affecting the flow of fluids as shown by the tracer test in Fig. 61.

An oil recovery experiment was conducted using NBU-1. The coreflood was conducted at reservoir temperature ( $50\text{ }^\circ\text{C}$ ) using simulated reservoir water (6.65% NaCl, 1.54%  $\text{CaCl}_2$ , and 0.24%  $\text{MgCl}_2$ ) and NBU oil that was tagged with 18% iododecane to provide greater CT density contrast between the aqueous and hydrocarbon fluids in the core. The surfactant system was used previously with NBU oil at this temperature and salinity for oil recovery experiments in water-wet Berea sandstone cores.<sup>13,16</sup> The surfactants were Stepan B-105, a mixed anionic surfactant (alkyl aryl sulfonate and ethoxylated sulfate), and Stepan B-110 (alkyl aryl sulfonate) in a 7 to 1 ratio. Total surfactant injected was 0.3 PV of a 1% active weight solution. Mobility control was provided by 1500 ppm Xanthan polymer solution. All injected chemicals were prepared in simulated NBU water. No alkaline chemicals ( $\text{NaHCO}_3$  and  $\text{Na}_2\text{CO}_3$ ) were used during this flood because high calcium ion concentration in NBU brine would react with the carbonates and form precipitates.

Volumetric measurements of oil recovery indicated that approximately 80% of the residual oil after waterflood was produced by this chemical system. This compares with approximately 40% of  $S_{\text{rowf}}$  produced from a water-wet core (all other conditions remaining the same). This may represent optimistic recovery conditions, however, because the initial oil saturation was lower for the oil-wet core than for the water-wet core. Injection of oil under higher pressure conditions may be required to increase the initial oil saturation in the oil-wet core. If higher saturations could be achieved, the incremental oil may or may not be produced as easily by the chemical system. CT

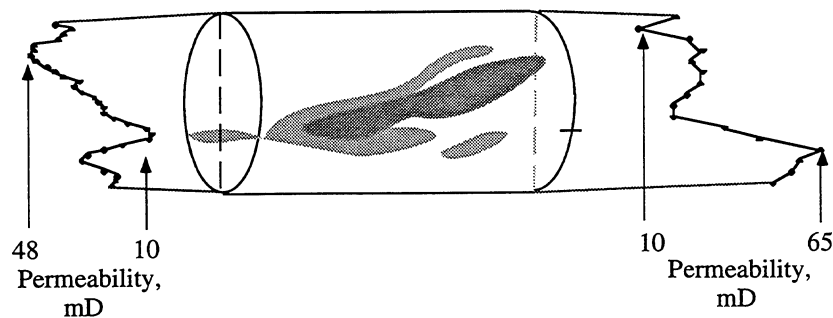


FIGURE 62.— Drawing of core NBU-2 showing discolored areas that could be seen after cleaning. The minipermeameter values for measurements taken along the core face indicated that a 4- to 6-fold change in permeability existed across the discoloration. Figure 61 shows the effect on fluid flow through the core.

pictures showed that the higher permeability zones in the core were well swept by chemicals. A smaller fraction of both oil and chemicals contacted the rest of the core. Further corefloods are planned using reservoir rock to investigate the effects of rock structure on chemical flood efficiency.

### *Summary and Conclusions for CT-Monitored Corefloods*

Chemical EOR coreflood experiments were conducted in conjunction with CT-imaging techniques to investigate the effects on oil recovery of changing chemical injection size and chemical interfacial tension with oil. Reducing the amount of surfactant injected during low-concentration alkaline-surfactant-polymer flooding resulted in lower oil production and higher final oil saturations. The amount of oil recovered, however, was not directly proportional to the amount of injected surfactant. A number of factors appear to influence the amount of oil produced in addition to reduction in the amount of injected surfactant. These factors include mobility control, polymer concentration, and higher permeability streaks in the core.

Reducing the amount of surfactant was less detrimental to overall oil production than reducing polymer effectiveness. From these studies, cost savings by reducing surfactant use may be reasonable. However, mobility control design may be critical to determining the cost effectiveness of the chemical EOR project.

The CT-images, however, suggested that reduction in the amount of injected surfactant allowed the oil bank to spread out. Oil was then produced in smaller amounts or over a longer period of time, more like a stripping action rather than the advance of a well defined oil bank. This suggests that low-concentration surfactant should continue to be injected. This strategy may allow for a reduction in the amount of polymer required to produce the oil, providing cost savings in this area.

CT imaging techniques were especially helpful in keeping track of the chemical flood progress, and determining if further injection of chemicals would continue to produce additional increments of oil. CT imaging also helped to point out well swept areas of the core after the waterflood that probably influenced the rate of oil movement through the core.

Oil saturation within a core after surfactant injection could change under static flow conditions. The effect this phenomenon may have on oil propagation and production has not been fully evaluated, however. Further investigations including observations of the dynamics of oil movement under gravitational or other forces can be monitored using CT-imaging techniques.

Coreflood oil saturation distributions and production were compared for chemical systems at and below optimal salinity. For the system below optimal salinity, interfacial tension between oil and aqueous phases was approximately 20 times greater than for the optimized system. Little difference was observed, however, for both oil saturation distribution after surfactant injection and

at the completion of the experiment. Oil saturation after the chemical flood was similar, 6% for the optimized system and 9% for the under optimum system. The coreflood was conducted in a high permeability Berea sandstone core. The increase in IFT may not have been detrimental to oil mobilization in this case. Experiments in lower permeability core are recommended.

Corefloods in reservoir rock from North Burbank Unit (a Class 1 reservoir) were initiated. The rock is oil-wet and contains significantly more permeability heterogeneities than the Berea sandstone used for previous CT-monitored corefloods. The core flow properties were characterized using CT tracer tests and minipermeameter measurements. Most of the oil saturating the core was produced by waterflood and chemical flood using a chemical system designed for the high salinity NBU brine. However, saturating conditions probably did not force oil into the smaller pores, and the introduced oil could be produced relatively easily. The use of CT imaging was helpful in interpretation of these results. Additional studies using reservoir rock are recommended.

CT-imaging is a valuable tool to aid in evaluation of laboratory chemical EOR coreflood experiments.

## REFERENCES

1. Tham, M. K., T. E. Burchfield, T. H. Chung, P. B. Lorenz, R. S. Bryant, P. Sarathi, M. M. Chang, S. Jackson, and L. Tomutsa. Research Needs to Maximize Economic Producibility of the Domestic Oil Resource. Part I - Literature Review and Areas of Recommended Research. Department of Energy Report No. NIPER-527, July 1991.
2. National Petroleum Council. Enhanced Oil Recovery. June 1984.
3. Nelson, R. C. Chemically Enhanced Oil Recovery: The State of the Art. Chemical Engineering Progress, Mar. 1989, pp. 50-57.
4. Thomas, S. and S. M. Farouq-Ali. Micellar-Polymer Flooding: Status and Recent Advances. Pres. at the 40th Annual Technical Meeting of the Petroleum Society of CIM in Banff, B.C. May 28-31, 1988. Paper 89-40-47.
5. Gall, B. L., F. M. Llave, and M. K. Tham. NIPER-DOE Chemical EOR Workshop. Department of Energy Report No. NIPER-698, Aug. 1993.
6. Combe, J., P. Corlay, E. Valentin, J. Bosio, H. J. De Haan, R. I. Hawes, G. Pusch, G. Sclocchi and F. Stockenhuber. EOR in Western Europe: Status and Outlook. Rev. de l'Inst. Franc. du Petrole, Jan.-Feb. 1990, pp. 5-37.
7. Moritis, G. Annual Production Report. Oil & Gas J., Apr. 23, 1990, pp. 49-82.
8. U. S. Department of Energy. Opportunities to Improve Oil Productivity in Unstructured Deltaic Reservoirs - Technical Summary and Proceedings of the Technical Symposium. Department of Energy Report No. DOE/BC-91/6/SP, July 1991.
9. Moritis, G. Annual Production Report. Oil & Gas J., Apr. 20, 1992.
10. Lorenz, P. B. Correlation of Laboratory Design Procedures with Field Performance in Surfactant-Polymer Flooding. Department of Energy Report No. NIPER-408, Feb. 1989.
11. Lowry, P. H., H. H. Ferrell, and D. L. Dauben. A Review and Statistical Analysis of Micellar-Polymer Field Test Data. Department of Energy Report No. DOE/BC/10830-4, November 1986, 27 pp.
12. Llave, F. M., B. L. Gall, and L. A. Noll. Mixed Surfactant Systems for Enhanced Oil Recovery. Department of Energy Report No. NIPER-497, Dec. 1990.
13. Llave, F. M., B. L. Gall, T. R. French, L. A. Noll and S. A. Munden. Phase Behavior and Oil Recovery Investigations Using Mixed and Alkaline-Enhanced Surfactant Systems. Department of Energy Report No. NIPER-567, Mar. 1992.
14. Llave, F. M., T. R. French, and P. B. Lorenz. Evaluation of Mixed Surfactants for Improved Chemical Flooding. Department of Energy Report No. NIPER-631, Nov. 1992.
15. Tomatsu, L., D. Doughty, S. Mahmood, A. Brinkmeyer, and M. Madden. Imaging Techniques Applied to Fluid Saturation. Department of Energy Report No. NIPER 485, Aug. 1990.
16. Gall, B. L. CT Imaging of Surfactant Enhanced Oil Recovery Experiments. Department of Energy Report No. NIPER 661, July 1992.
17. Glinsmann, G. R. Aqueous Surfactant Systems for InSitu Multiphase Microemulsion Formation. U.S. Patent No. 4,125,156. Nov. 14, 1978.
18. Boneau, D. F. and R. L. Clampitt. A Surfactant System for the Oil-Wet Sandstone of the North Burbank Unit. J. Pet. Technol., May 1977. pp. 501-506.

19. Tomutsa, L., D. Doughty, S. Mahmood, A. Brinkmeyer, and M. Madden. Imaging Techniques Applied to the Study of Fluids in Porous Media. Dept. of Energy Report No. NIPER-485, Aug., 1990.
20. Morgan, C. L. *Principles of Computed Tomography*. University Park Press, Baltimore, MD, 1983.
21. Wellington, S. L., and H. J. Vinegar. X-ray Computerized Tomography. *J. Pet. Technol.*, Aug. 1987, pp. 885-898.
22. Tomutsa, L., D. Doughty, A. Brinkmeyer, and S. Mahmood. Imaging Techniques Applied to the Study of Fluids in Porous Media. Department of Energy Report No. NIPER-582, Feb. 1992.
23. Gall, B. L. CT Imaging of Surfactant Enhanced Oil Recovery Experiments. Pres. at the 205th Mtg. of the ACS, Denver, CO., Mar. 28-Apr. 2, 1993.
24. Llave, F. M. and D. K. Olsen. Development of an Automated System for Phase Inversion Temperature Measurements. Department of Energy Report No. NIPER-318, June 1988.
25. Shinoda, K. and H. Arai. The Correlation Between Phase Inversion Temperature in Emulsion and Cloud Point in Solution of Nonionic Emulsifier. *J. Phys. Chem.*, v. 68, 1964, pp. 3485-3490.
26. Shinoda, K. and M. Kuneida. Conditions to Produce So-called Microemulsions: Factors to Increase the Mutual Solubility of Oil and Water by Solubilizer. *J. Coll. and Interface Sci.*, v. 42, 1973, p. 381.
27. Lorenz, P. B. and S. Brock. Surfactant and Cosurfactant Properties of Mixed and Polysulfonated Surfactant by Phase Volume Measurements. Department of Energy Report No. NIPER-256, Oct. 1987.
28. Marzall, L. HLB of Nonionic Surfactants: PIT and EIP Methods. *Nonionic Surfactants: Physical Chemistry*, ed. by M. J. Schick., Marcel Dekker, Inc. New York, 1987, pp. 493-547.
29. Bourrel, M., J. L. Salager, R. S. Schechter, and W. H. Wade. A Correlation for Phase Behavior of Nonionic Surfactants. *J. Coll. and Interface Sci.* v. 75 (2), June 1980.
30. Barakat, Y., L. N. Fortney, R. S. Schechter, W. H. Wade, and S. H. Yiv. Alpha-Olefin Sulfonates for Enhanced Oil Recovery. Pres. at 2nd European Symp. on EOR, Paris, France, Nov. 8-10, 1982.
31. Barakat, Y., L. N. Fortney, C. LaLanne-Cassou, R. S. Schechter, W. H. Wade, U. Weerasooriya, and S. Yiv. The Phase Behavior of Simple Salt-Tolerance Sulfonates. *SPEJ* v. 23(6), Dec. 1983, pp. 913-918.
32. Salager, J. L., J. Morgan, R. S. Schechter, W. H. Wade, and E. Vasquez. A Correlation for Phase Behavior of Nonionic Surfactants. *SPEJ* v. 19, 1978, pp 242.
33. French, T. R. Surfactant-Enhanced Alkaline Flooding Field Project. Department of Energy Report No. NIPER-569, Oct. 1991.
34. French, T. R., and C. B. Josephson. Alkaline Flooding Injection Strategy. Department of Energy Report No. NIPER-563, Sept. 1991.

## APPENDIX A – Graphic results of PIT data for nonionic and anionic surfactants

Appendix A shows plots of the results of the phase inversion temperature (PIT) measurements conducted on combinations of nonionic-nonionic and anionic-nonionic surfactants. The results for each surfactant combination, at a given set of conditions (i.e. salinity, temperature or HLB values) are presented as plots of: (1) log of optimal salinity vs. HLB of nonionic surfactant component with a specific hydrocarbon at different temperatures; (2) log of optimal salinity vs. temperature with a specific hydrocarbon at different HLB values; and (3) phase inversion temperature vs. HLB of nonionic surfactant component with a specific hydrocarbon at different salinities. The plots are arranged in the following order of surfactant series: (1) Genapol; (2) Igepal; (3) Genapol + TRS/IBA; and (4) Igepal + TRS/IBA. Each surfactant series is also presented in the following order of hydrocarbons tested: (1) n-heptane; (2) n-octane; (3) n-nonane<sup>1</sup>; (4) n-decane; (5) n-dodecane; and (6) n-tetradecane.

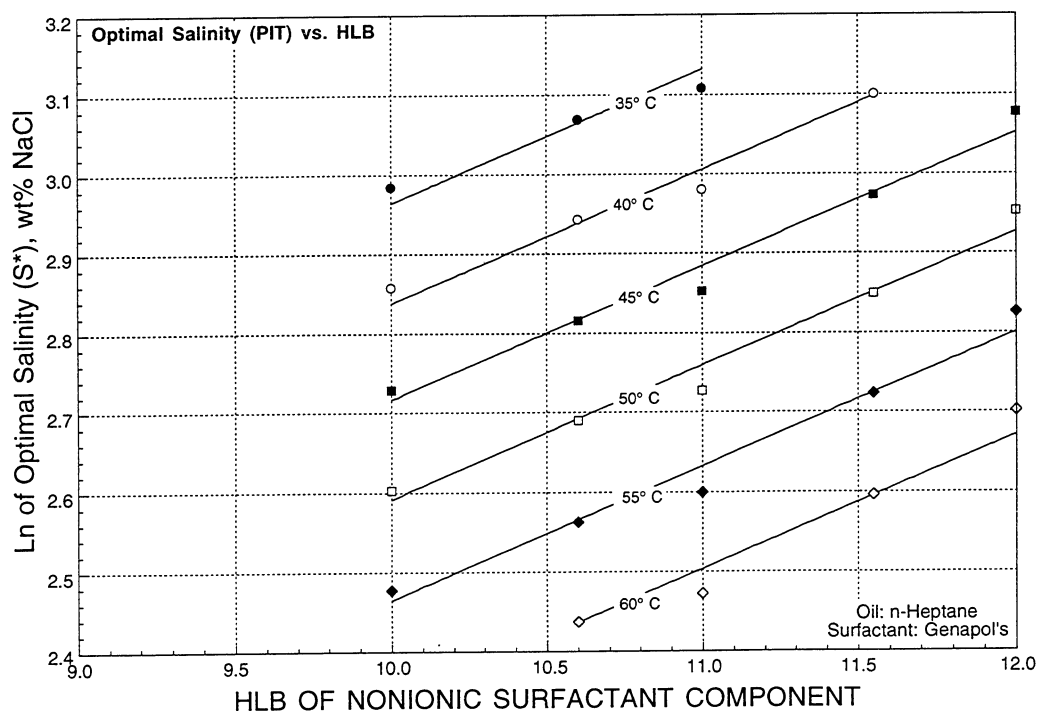


FIGURE A1. - Log of optimal salinity vs. HLB of nonionic surfactant component using Genapol with n-Heptane at different temperatures.

<sup>1</sup>only the mixtures with TRS/IBA were tested with n-nonane.

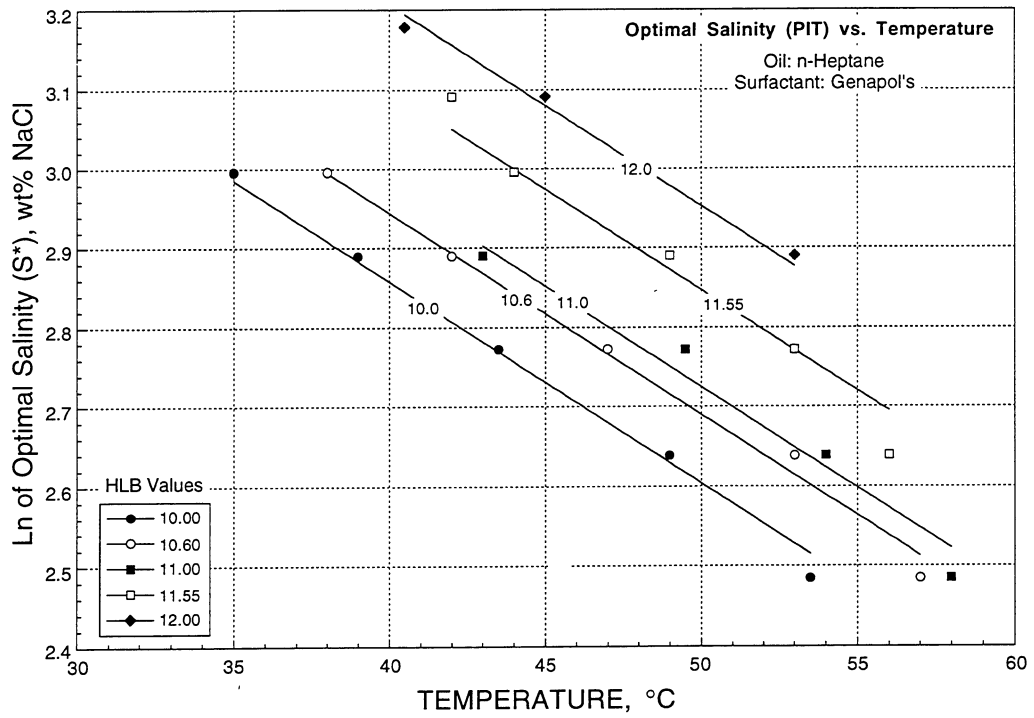


FIGURE A2. - Log of optimal salinity vs. temperature using Genapol with n-Heptane at different HLB values.

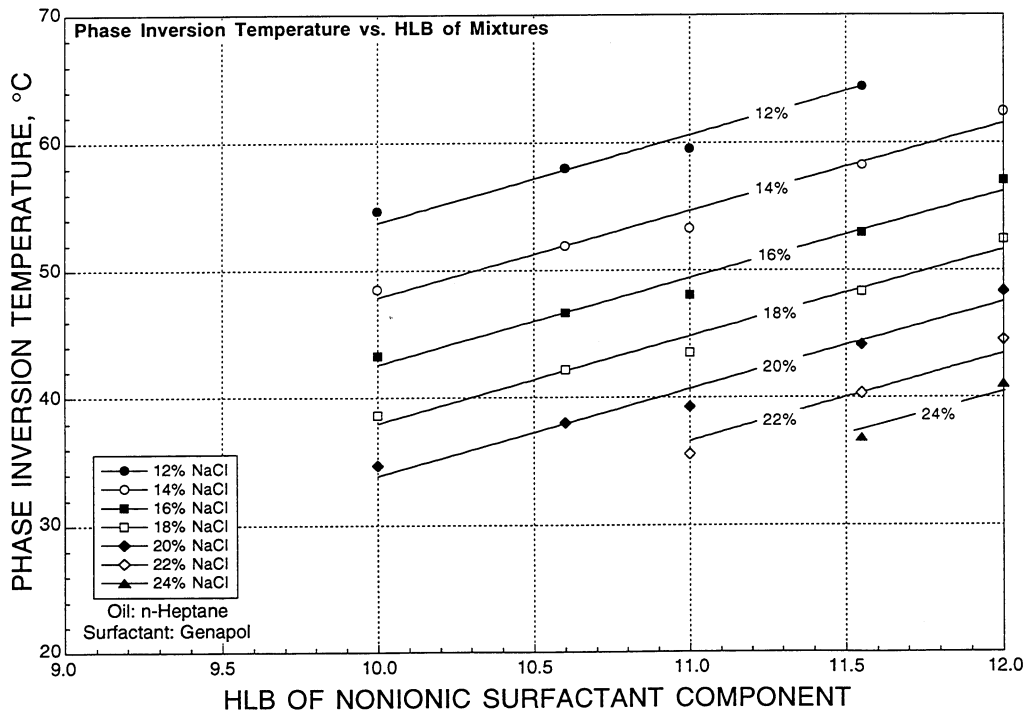


FIGURE A3. - Phase inversion temperature vs. HLB of nonionic surfactant component using Genapol with n-Heptane at different salinities.

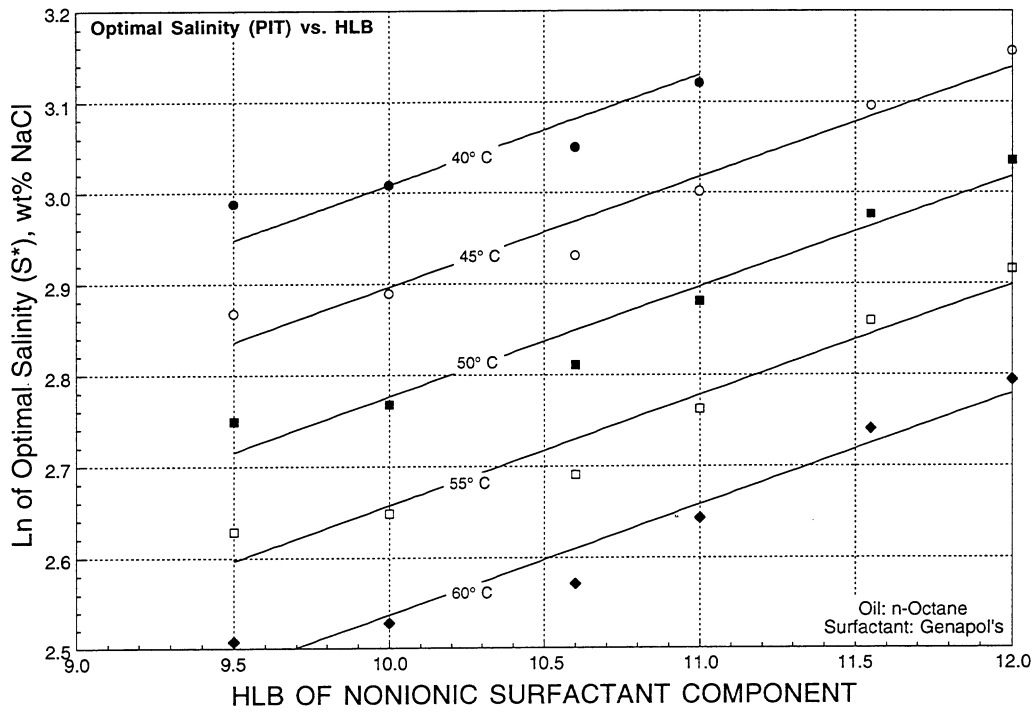


FIGURE A4. - Log of optimal salinity vs. HLB of nonionic surfactant component using Genapol with n-Octane at different temperatures.

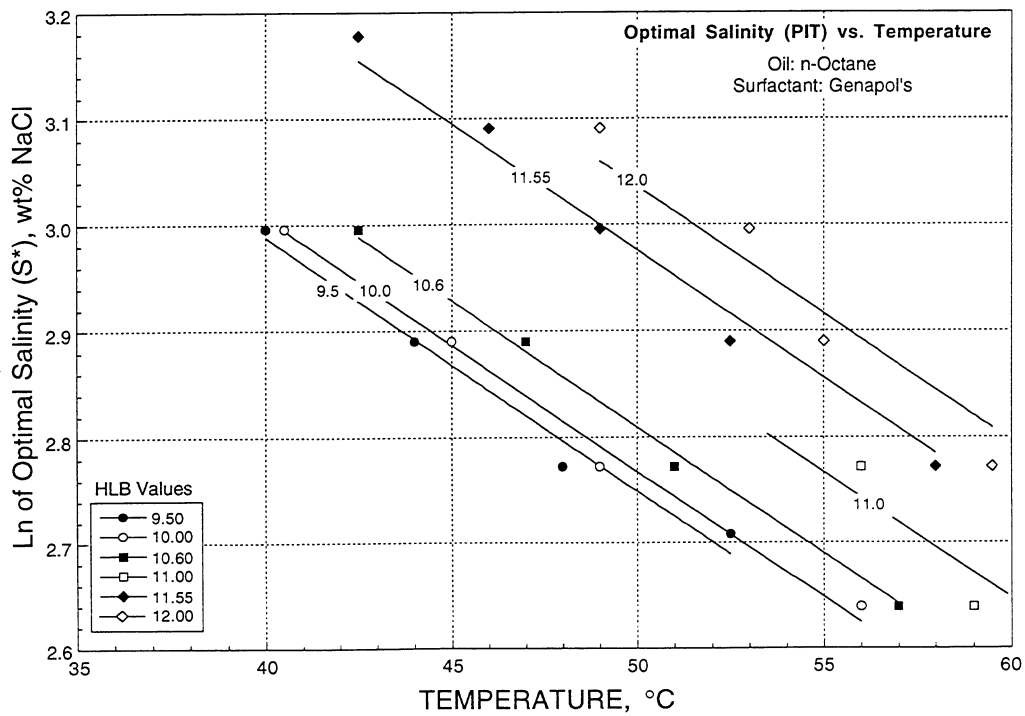


FIGURE A5. - Log of optimal salinity vs. temperature using Genapol with n-Octane at different HLB values.

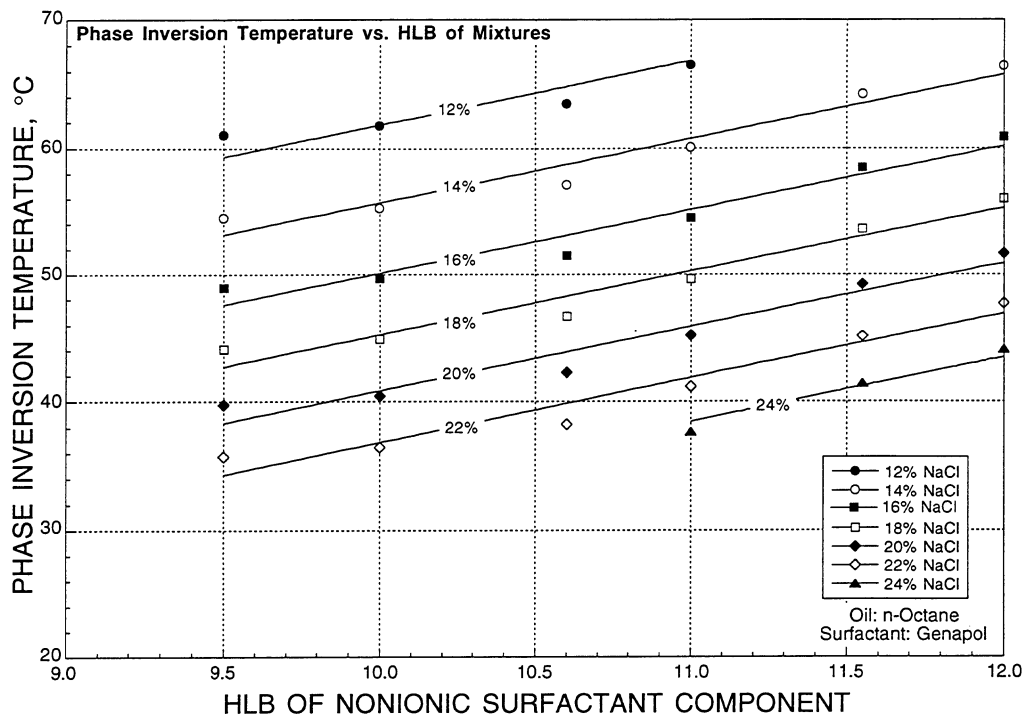


FIGURE A6. - Phase inversion temperature vs. HLB of nonionic surfactant component using Genapol with n-Octane at different salinities.

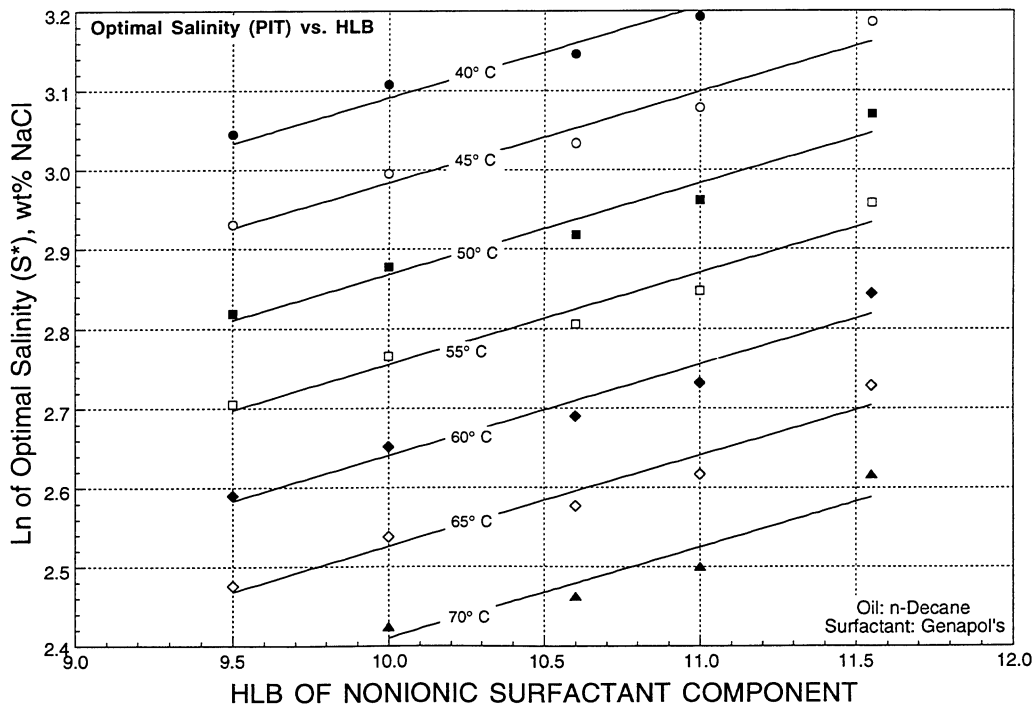


FIGURE A7. - Log of optimal salinity vs. HLB of nonionic surfactant component using Genapol with n-Decane at different temperatures.

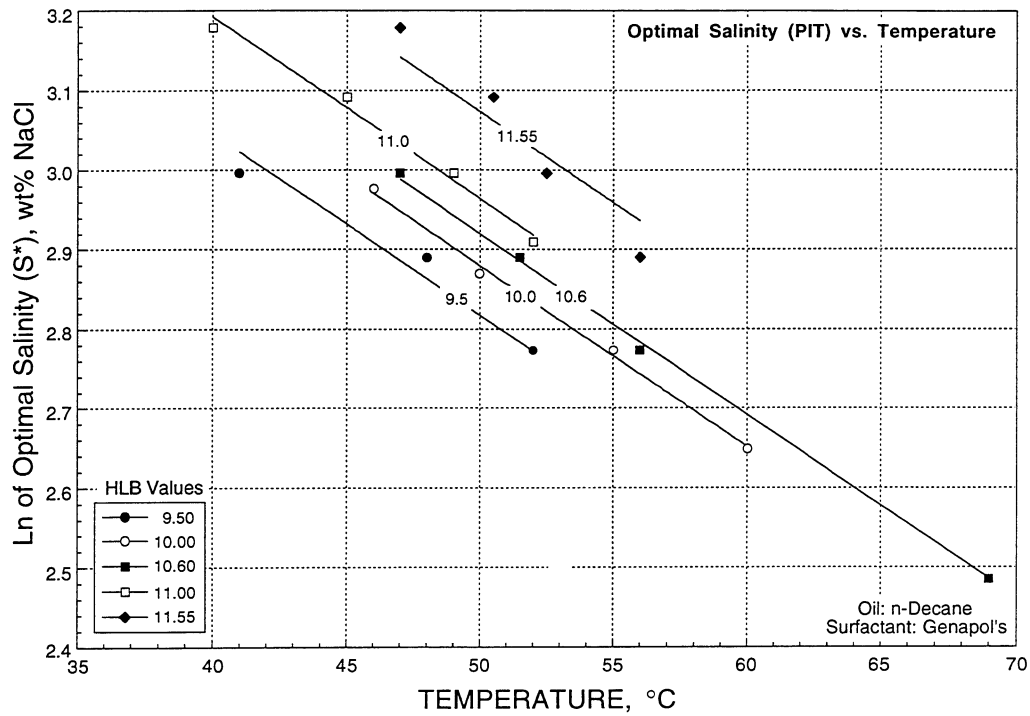


FIGURE A8. - Log of optimal salinity vs. temperature using Genapol with n-Decane at different HLB values.

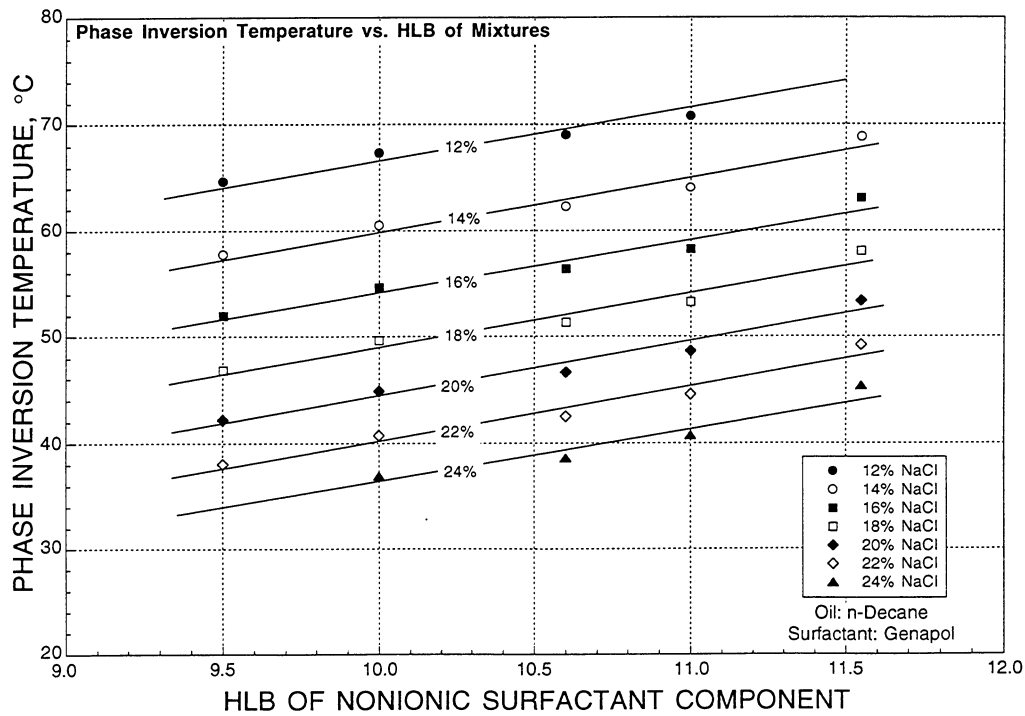


FIGURE A9. - Phase inversion temperature vs. HLB of nonionic surfactant component using Genapol with n-Decane at different salinities.

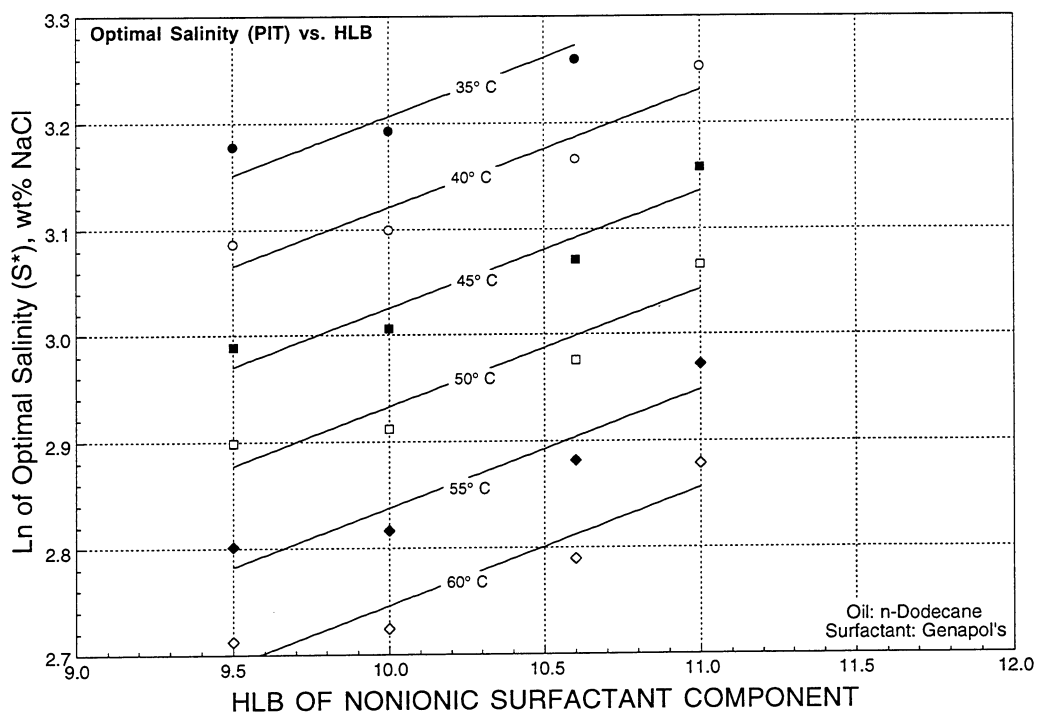


FIGURE A10. - Log of optimal salinity vs. HLB of nonionic surfactant component using Genapol with n-Dodecane at different temperatures.

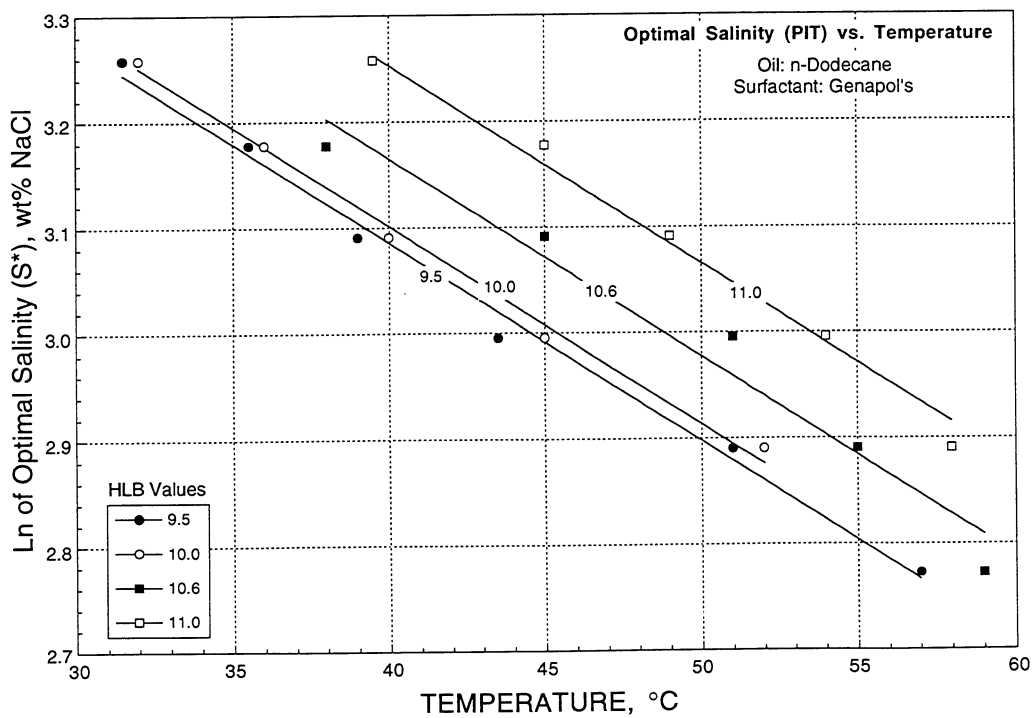


FIGURE A11. - Log of optimal salinity vs. temperature using Genapol with n-Dodecane at different HLB values.

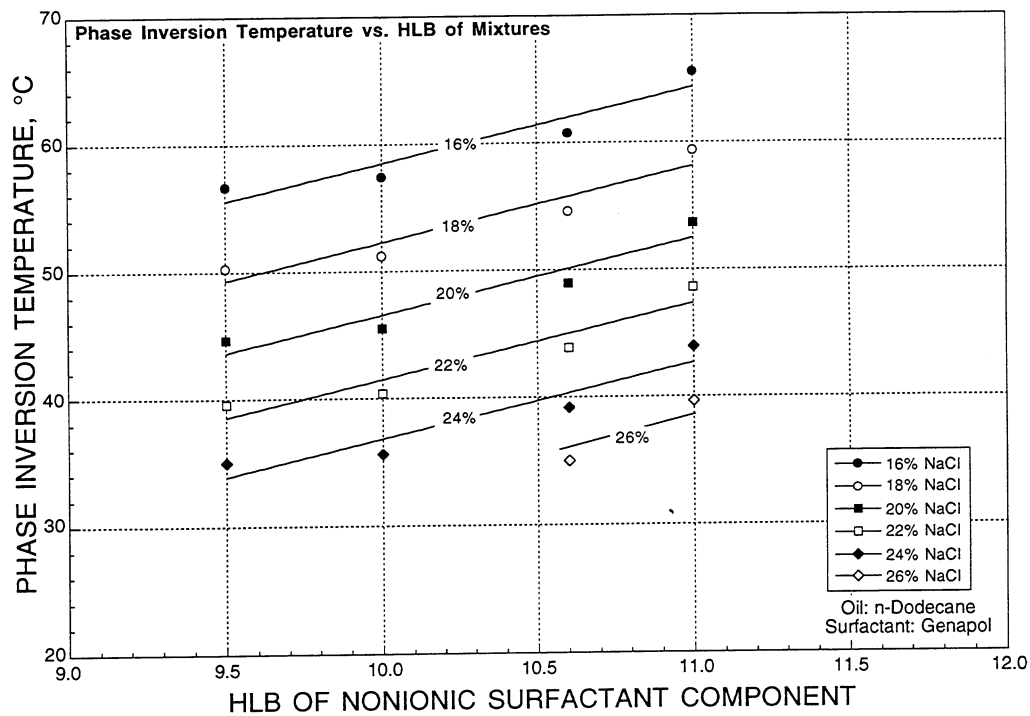


FIGURE A12. - Phase inversion temperature vs. HLB of nonionic surfactant component using Genapol with n-Dodecane at different salinities.

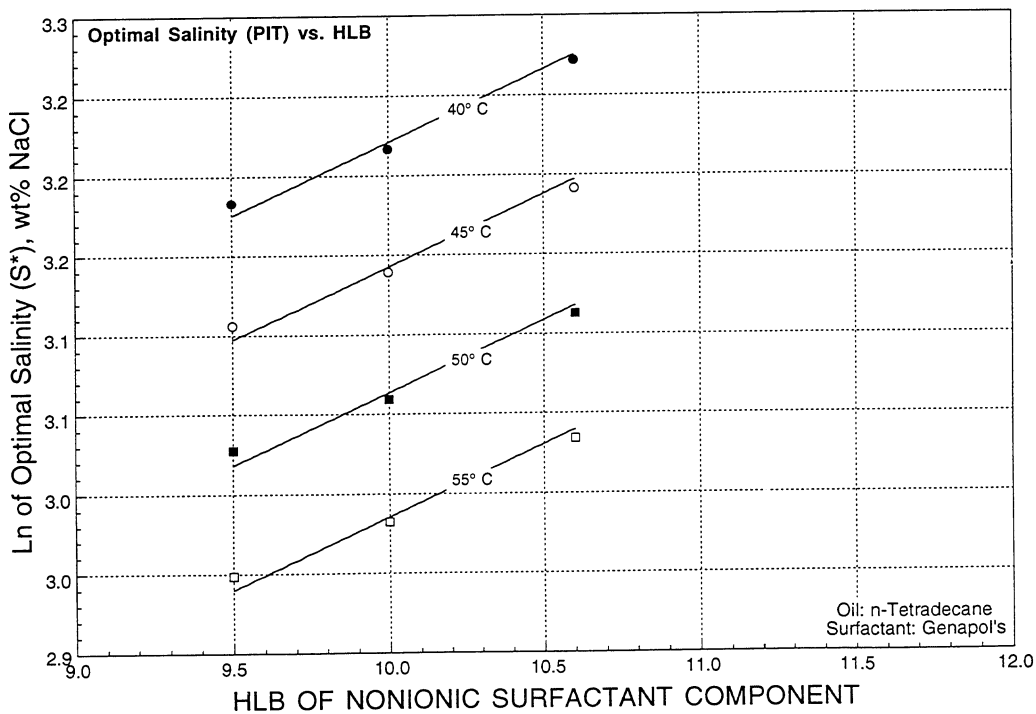


FIGURE A13. - Log of optimal salinity vs. HLB of nonionic surfactant component using Genapol with n-Tetradecane at different temperatures.

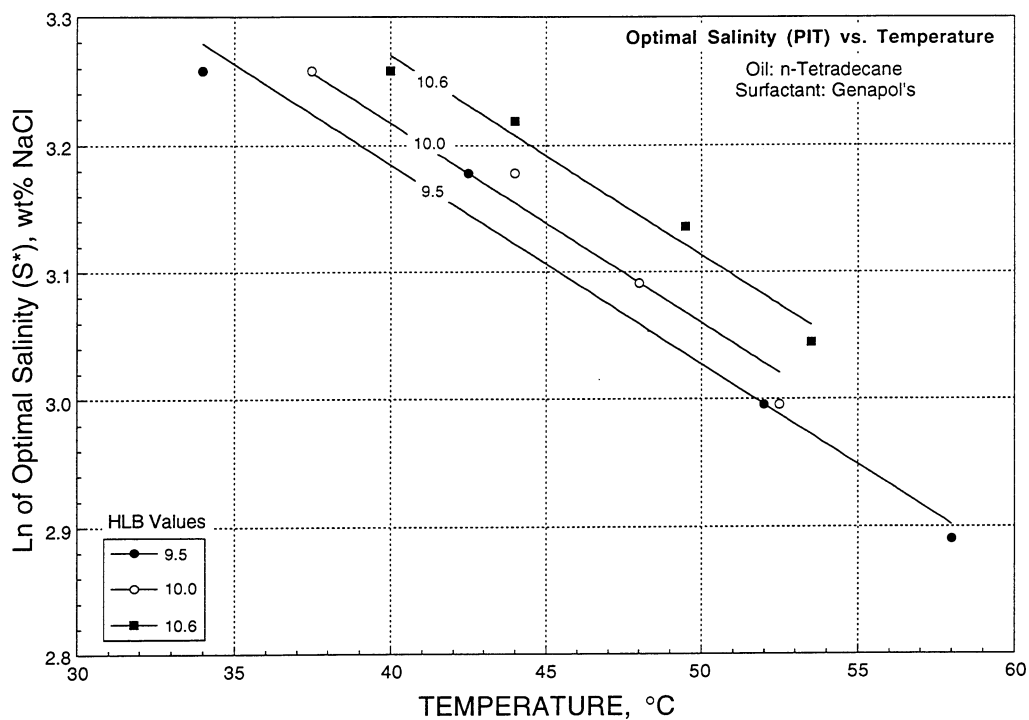


FIGURE A14. - Log of optimal salinity vs. temperature using Genapol with n-Tetradecane at different HLB values.

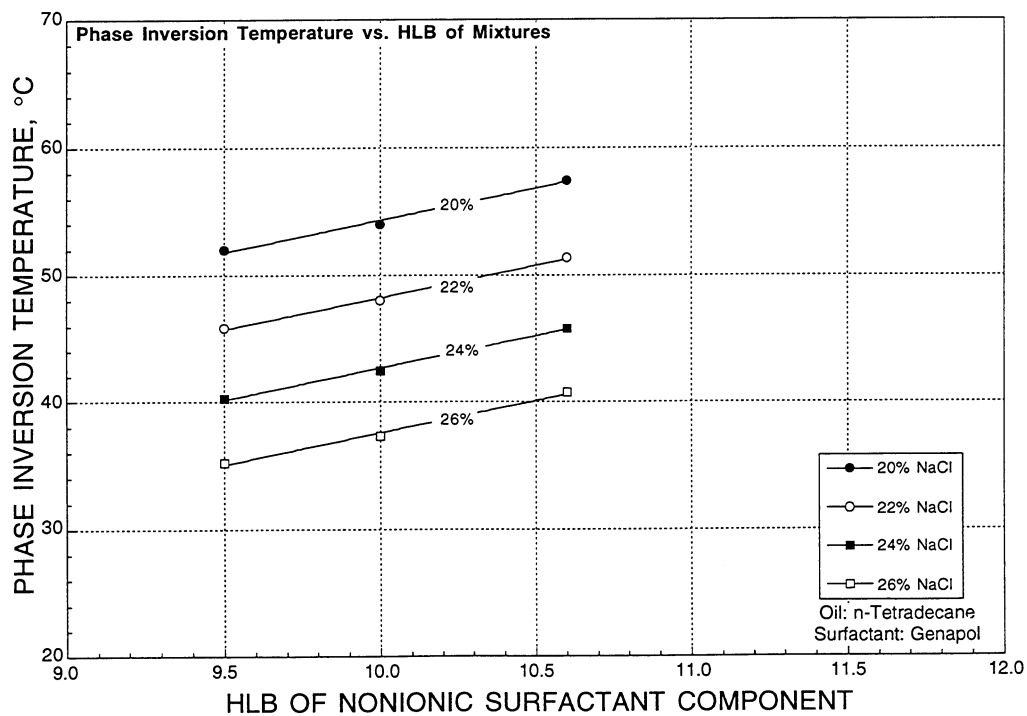


FIGURE A15. - Phase inversion temperature vs. HLB of nonionic surfactant component using Genapol with n-Tetradecane at different salinities.

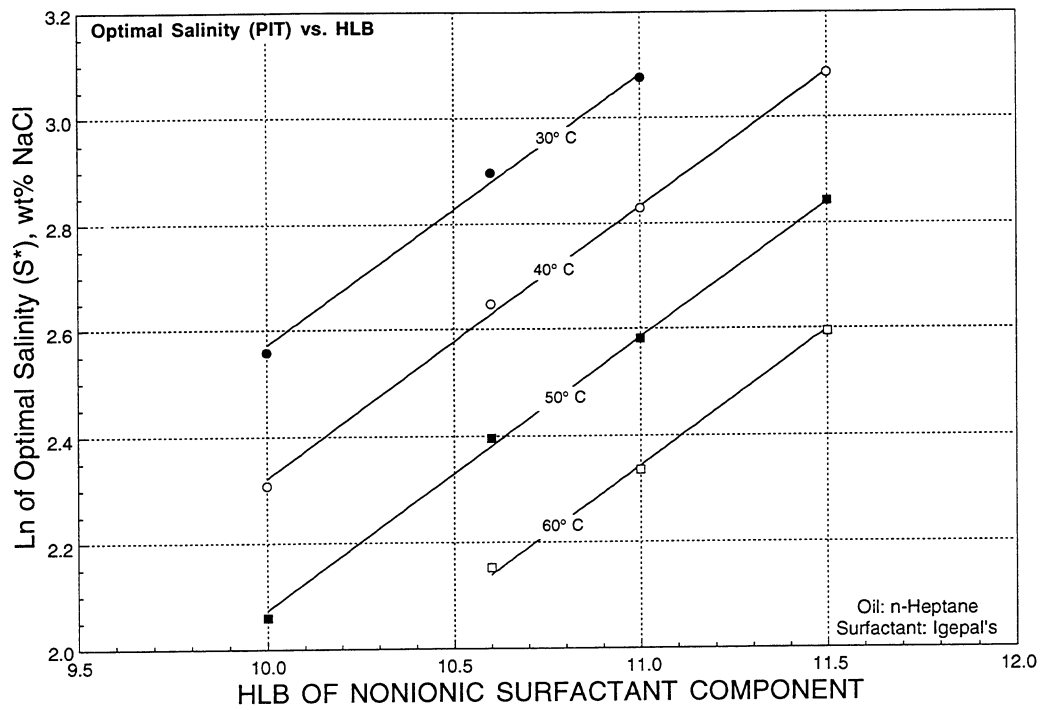


FIGURE A16. - Log of optimal salinity vs. HLB of nonionic surfactant component using Igepal with n-Heptane at different temperatures.

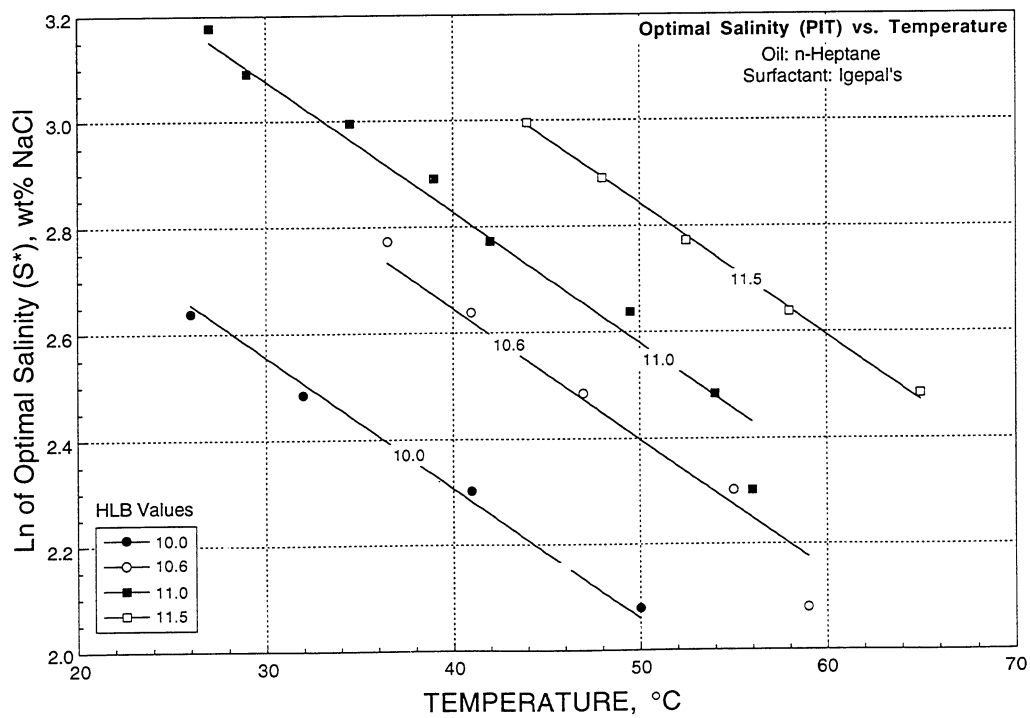


FIGURE A17. - Log of optimal salinity vs. temperature using Igepal with n-Heptane at different HLB values.

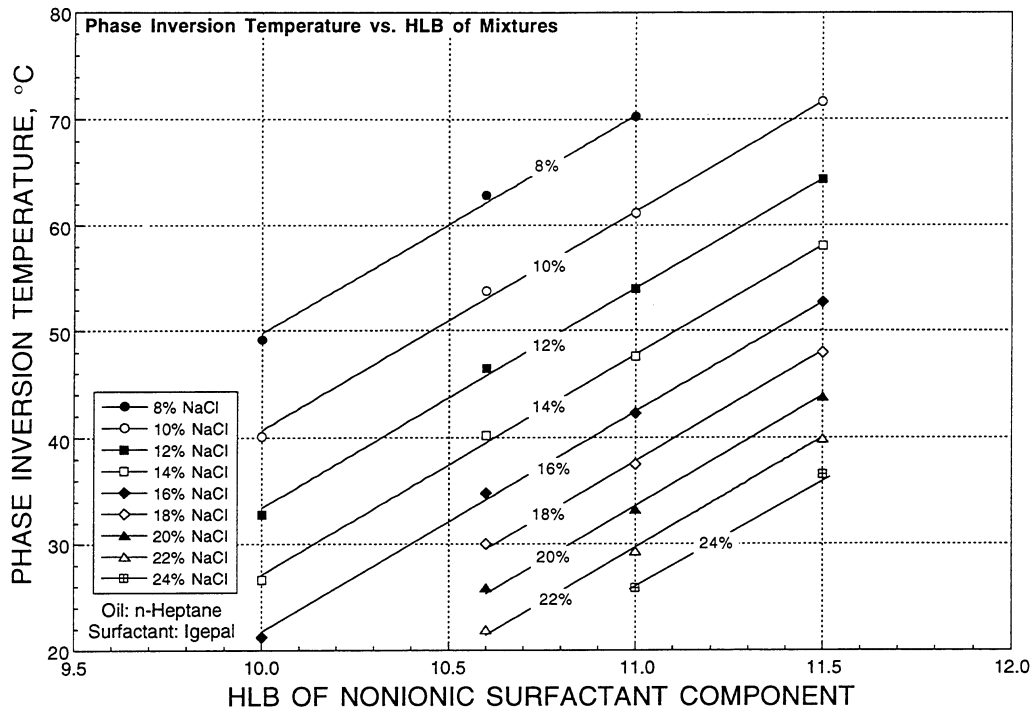


FIGURE A18. - Phase inversion temperature vs. HLB of nonionic surfactant component using Igepal with n-Heptane at different salinities.

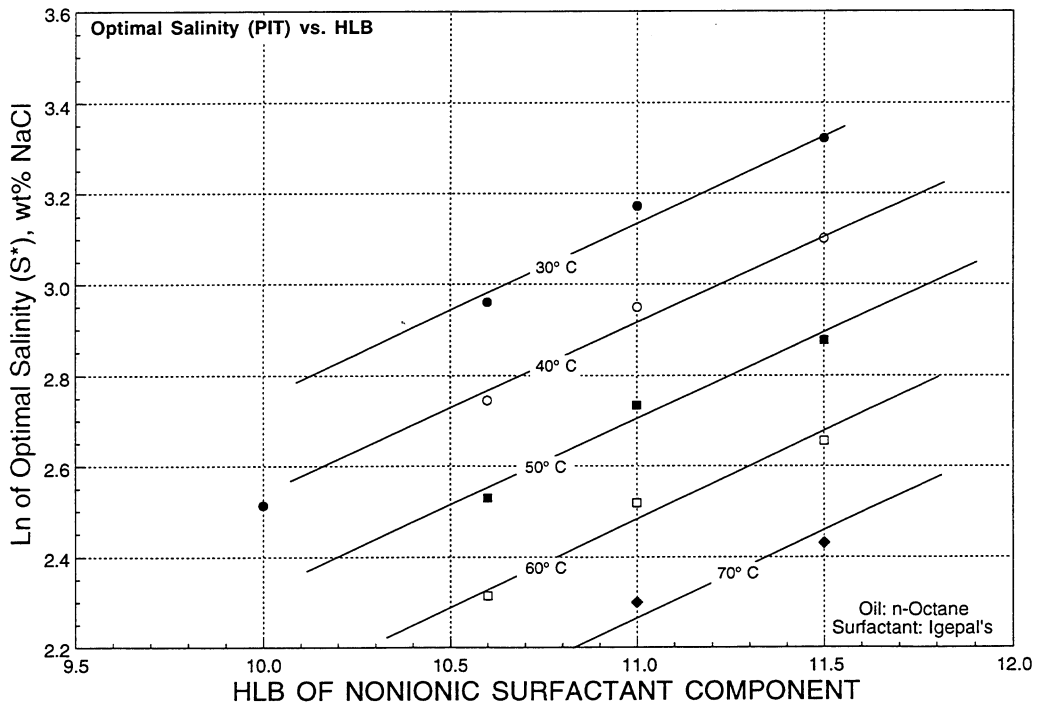


FIGURE A19. - Log of optimal salinity vs. HLB of nonionic surfactant component using Igepal with n-Octane at different temperatures.

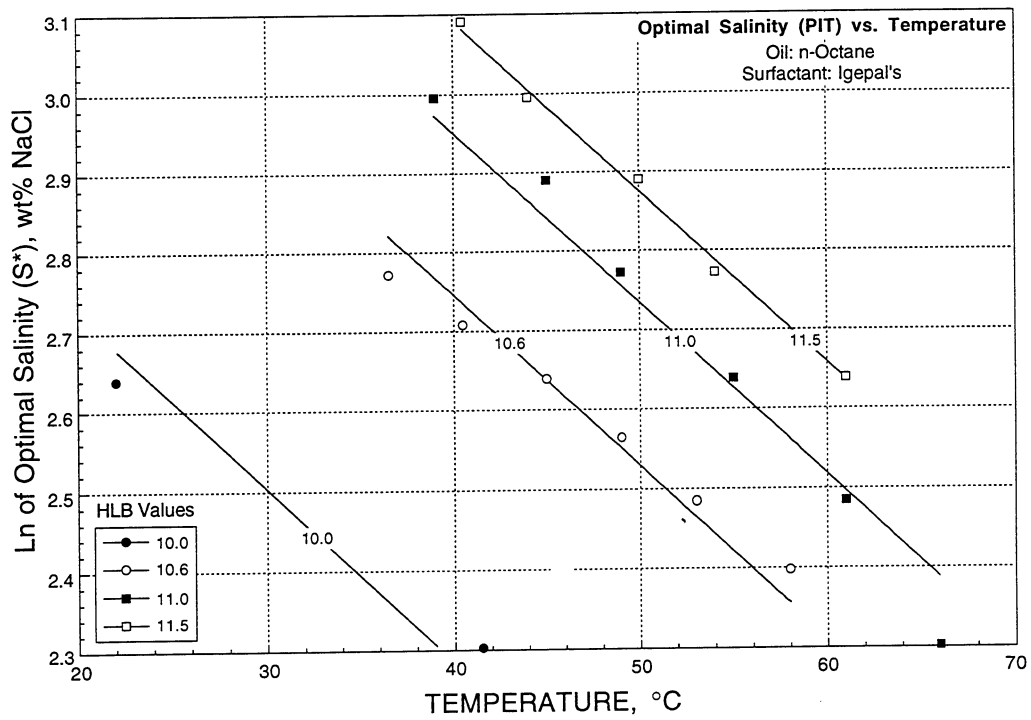


FIGURE A20. - Log of optimal salinity vs. temperature using Igepal with n-Octane at different HLB values.

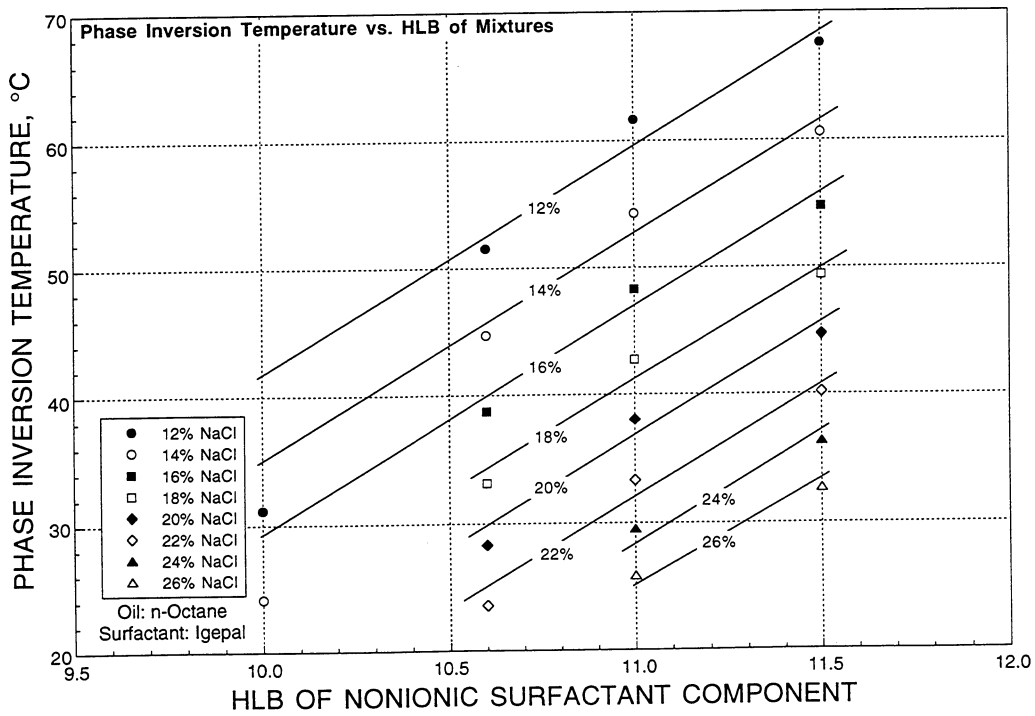


FIGURE A21. - Phase inversion temperature vs. HLB of nonionic surfactant component using Igepal with n-Octane at different salinities.

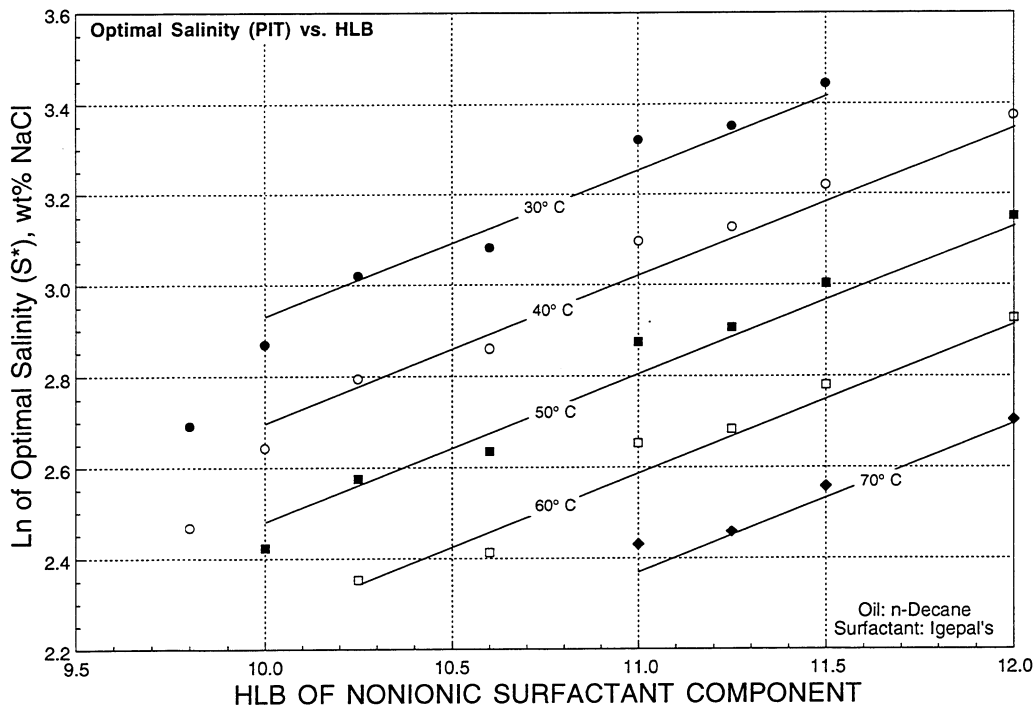


FIGURE A22. - Log of optimal salinity vs. HLB of nonionic surfactant component using Igepal with n-Decane at different temperatures.

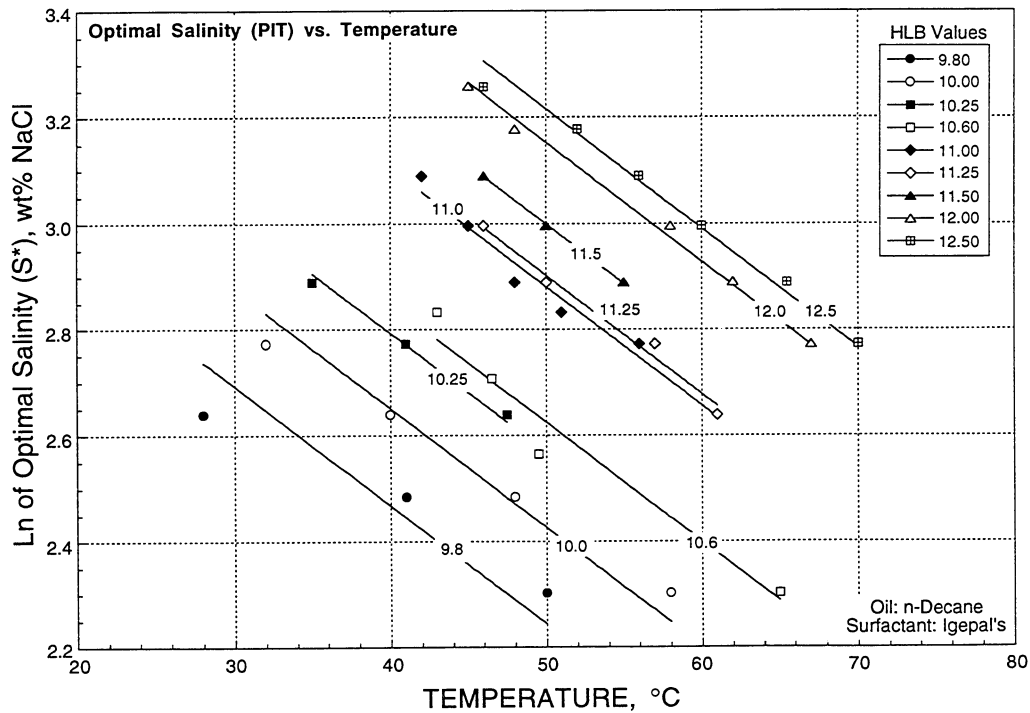


FIGURE A23. - Log of optimal salinity vs. temperature using Igepal with n-Decane at different HLB values.

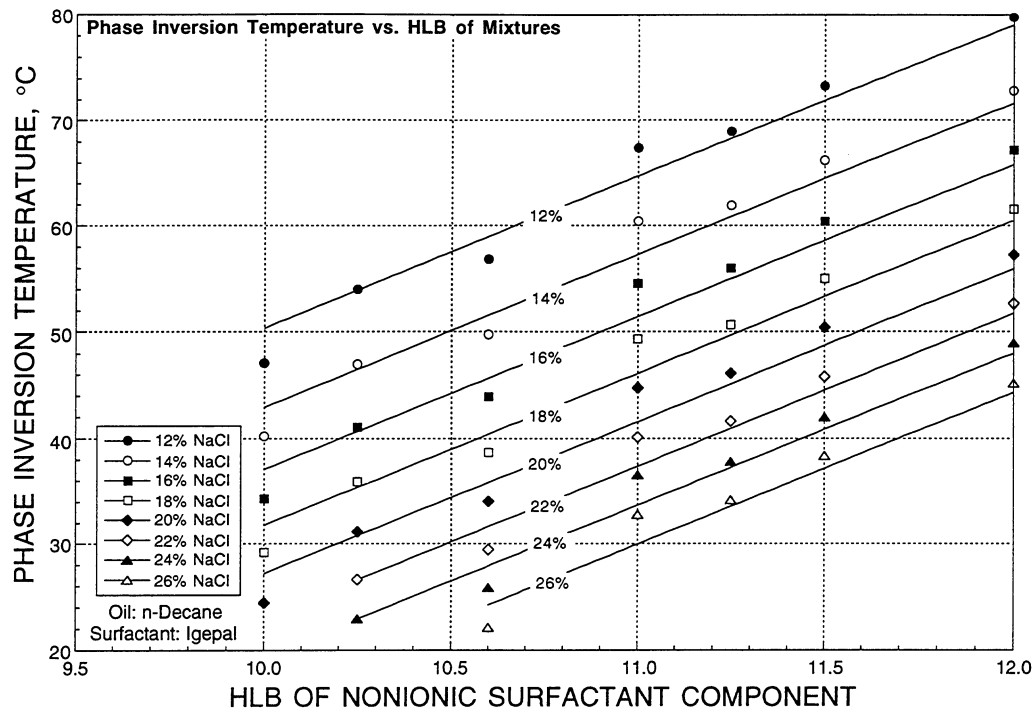


FIGURE A24. - Phase inversion temperature vs. HLB of nonionic surfactant component using Igepal with n-Decane at different salinities.

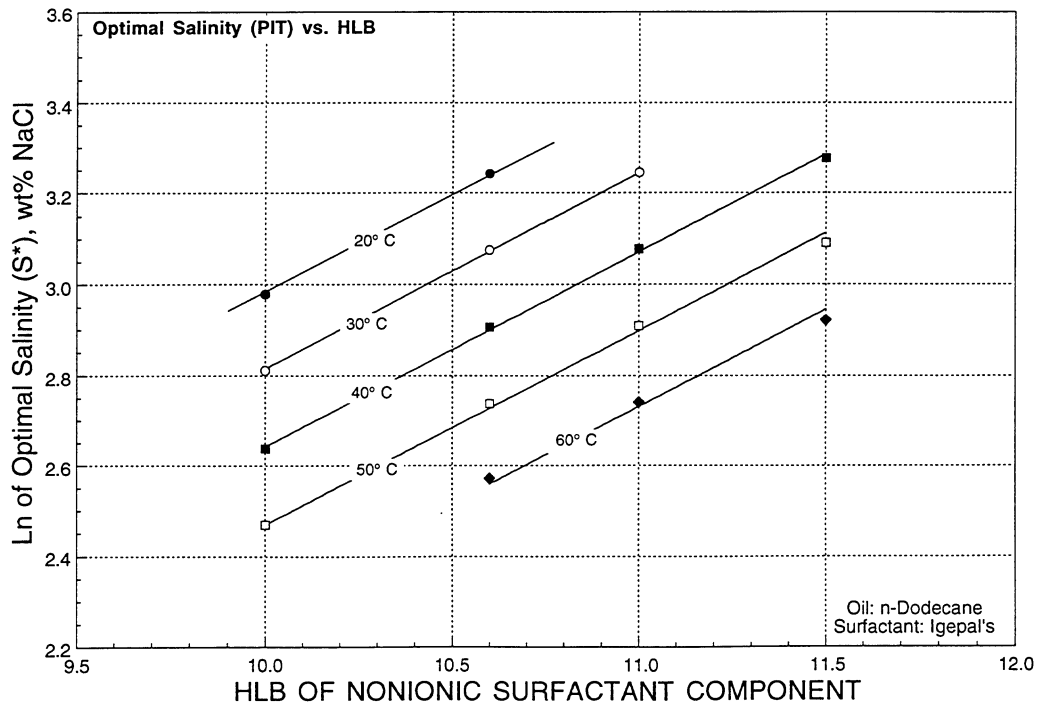


FIGURE A25. - Log of optimal salinity vs. HLB of nonionic surfactant component using Igepal with n-Dodecane at different temperatures.

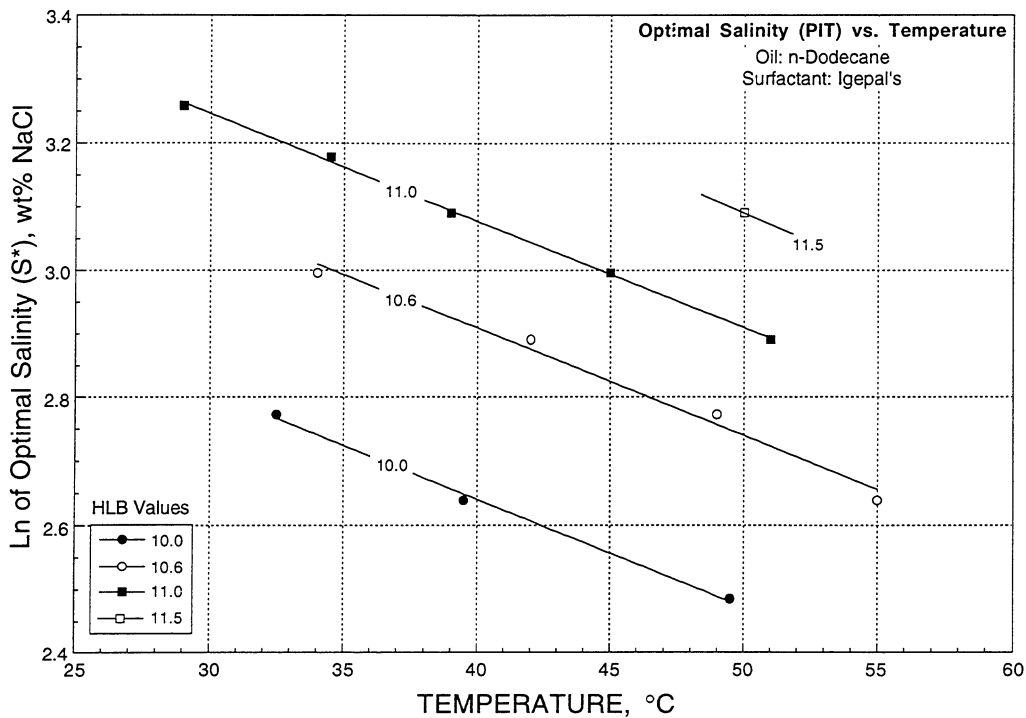


FIGURE A26. - Log of optimal salinity vs. temperature using Igepal with n-Dodecane at different HLB values.

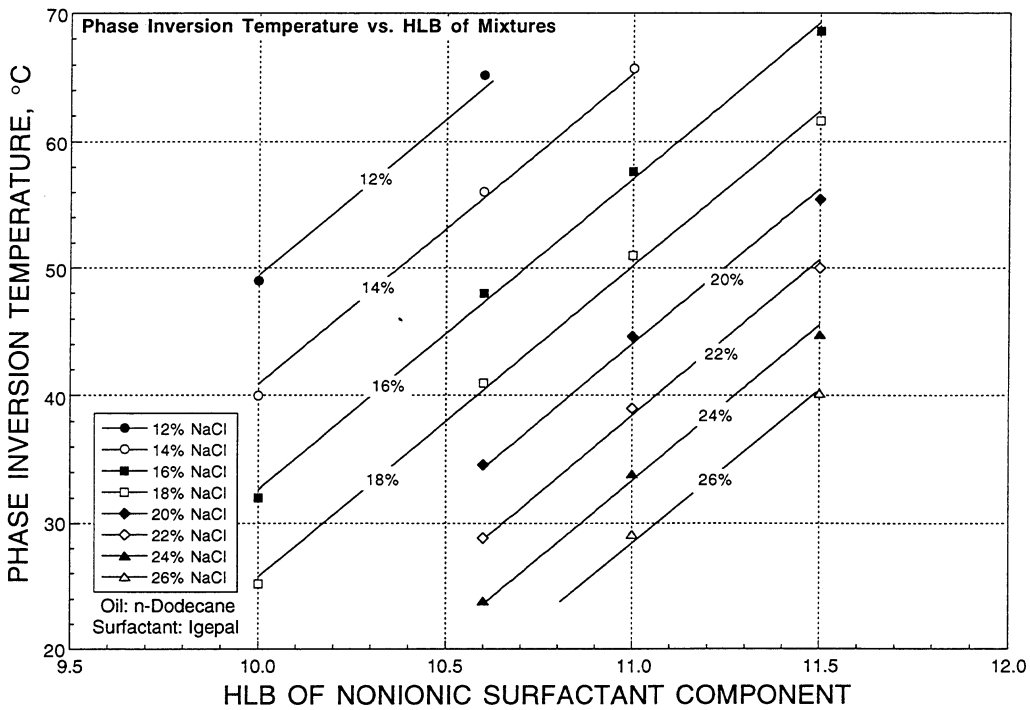


FIGURE A27. - Phase inversion temperature vs. HLB of nonionic surfactant component using Igepal with n-Dodecane at different salinities.

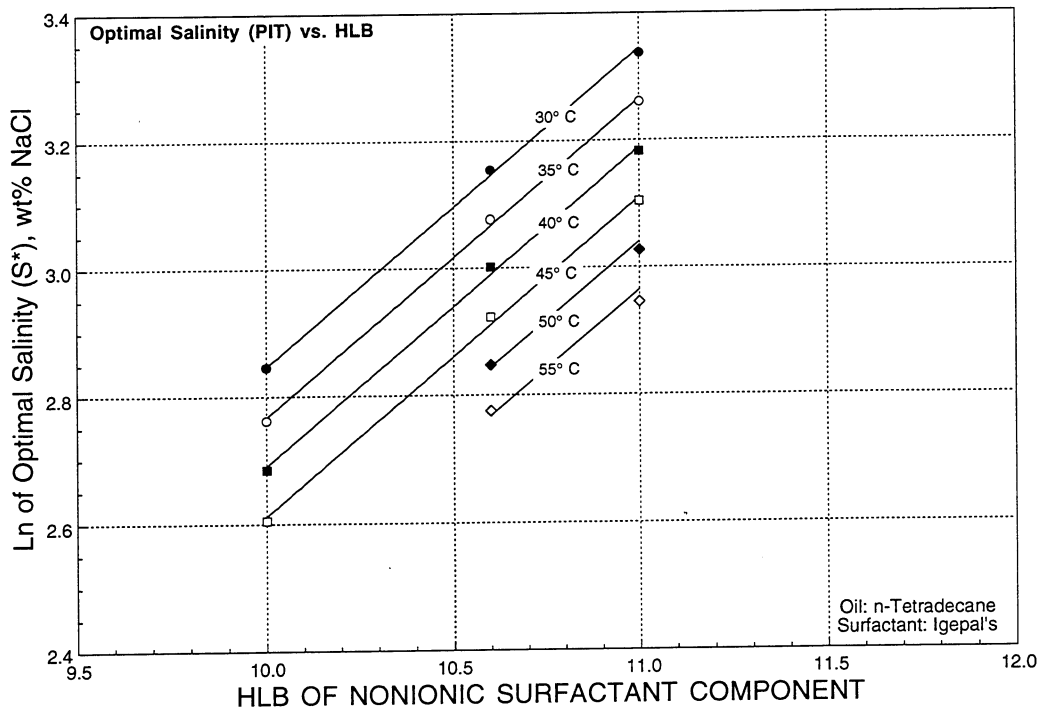


FIGURE A28. - Log of optimal salinity vs. HLB of nonionic surfactant component using Igepal with n-Tetradecane at different temperatures.

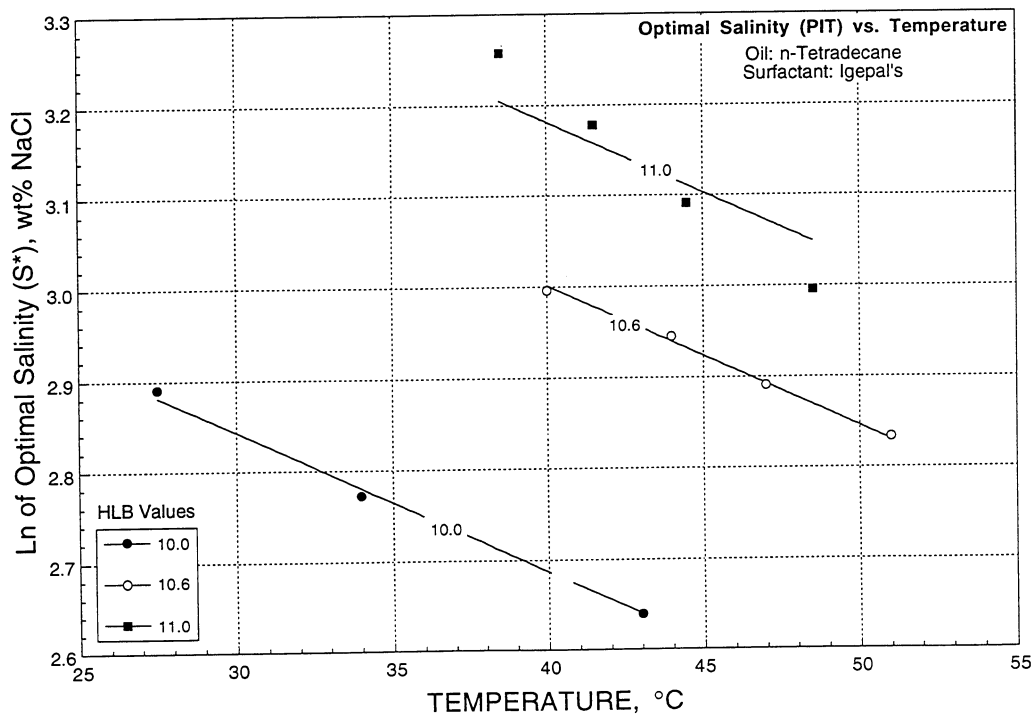


FIGURE A29. - Log of optimal salinity vs. temperature using Igepal with n-Tetradecane at different HLB values.

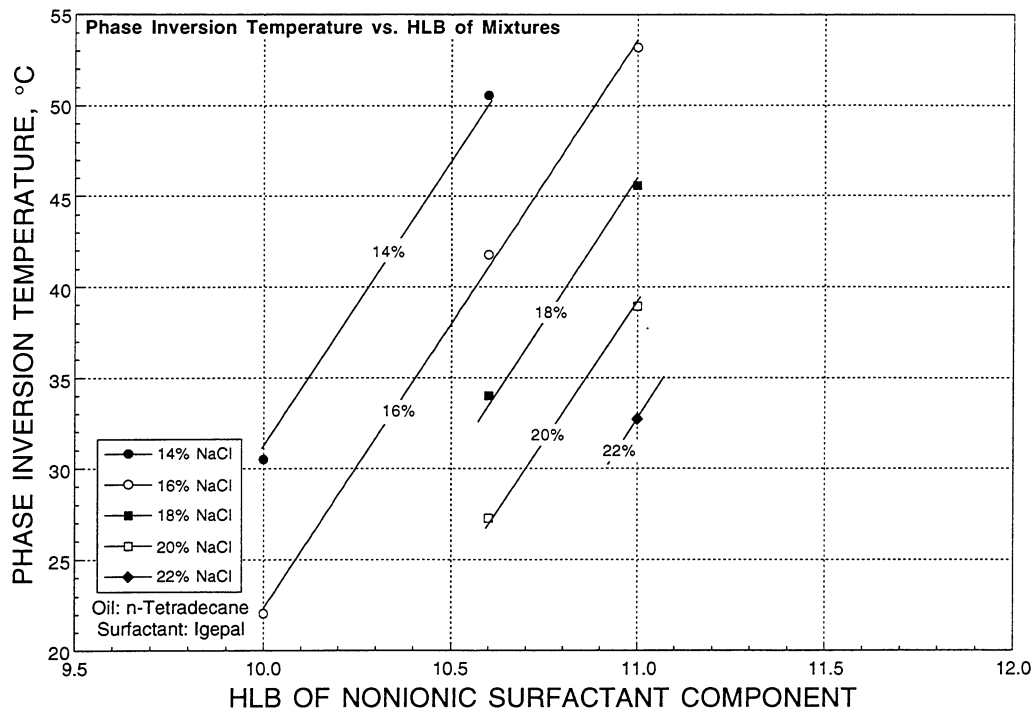


FIGURE A30. - Phase inversion temperature vs. HLB of nonionic surfactant component using Igepal with n-Tetradecane at different salinities.

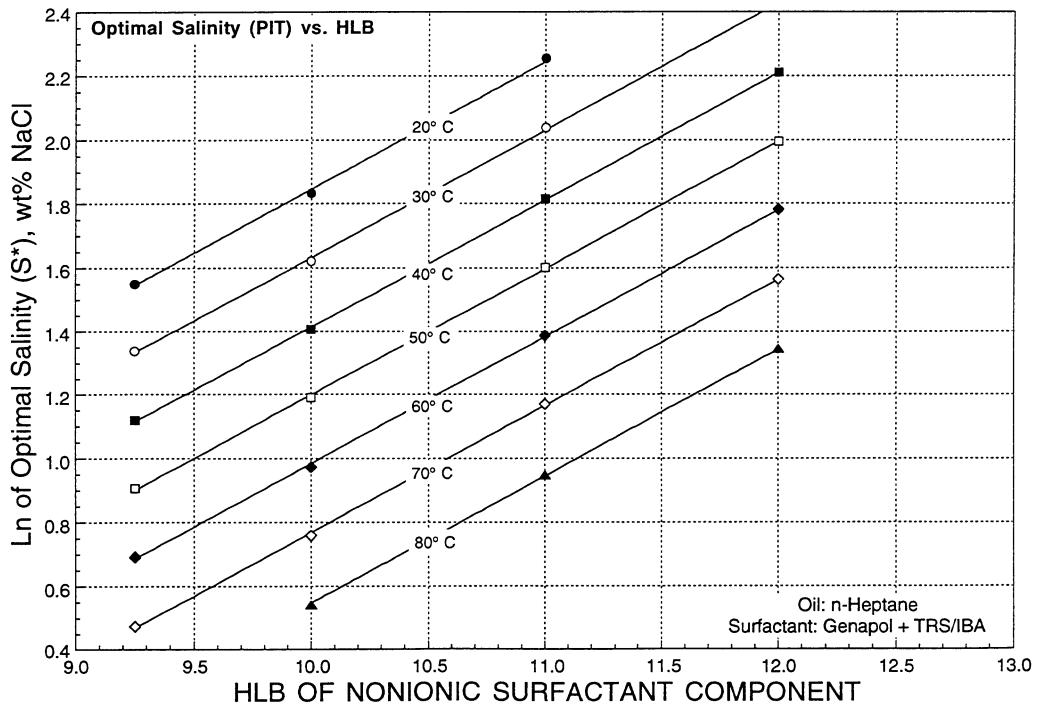


FIGURE A31. - Log of optimal salinity vs. HLB of nonionic surfactant component using Genapol + TRS/IBA with n-Heptane at different temperatures.

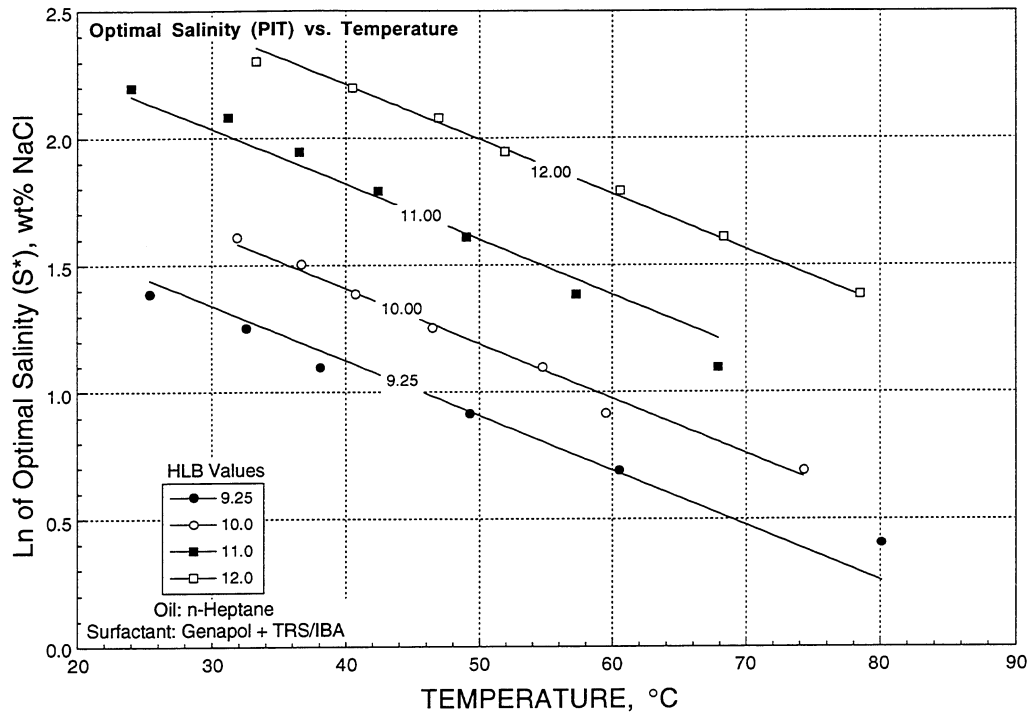


FIGURE A32. - Log of optimal salinity vs. temperature using Genapol + TRS/IBA with n-Heptane at different HLB values.

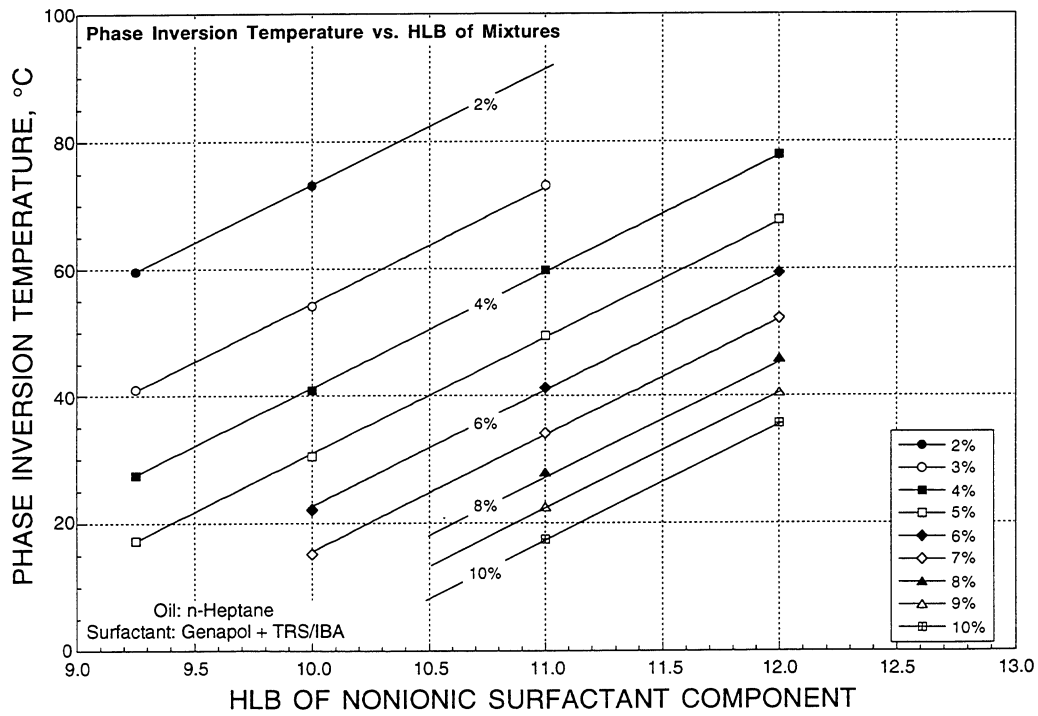


FIGURE A33. - Phase inversion temperature vs. HLB of nonionic surfactant component using Genapol + TRS/IBA with n-Heptane at different salinities.

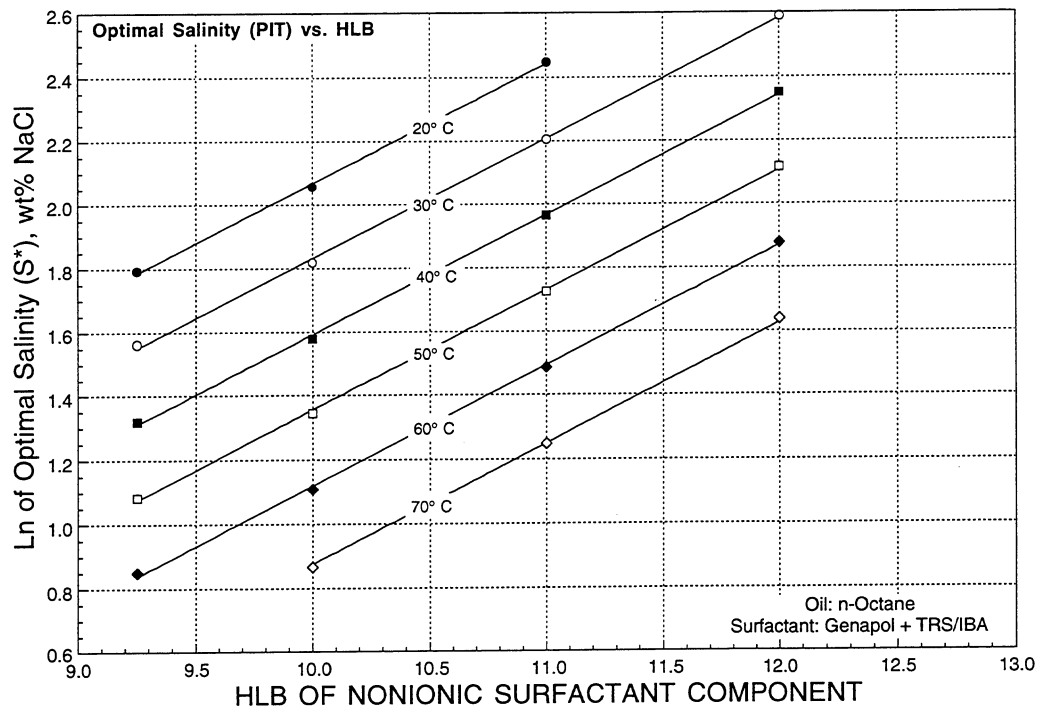


FIGURE A34. - Log of optimal salinity vs. HLB of nonionic surfactant component using Genapol + TRS/IBA with n-Octane at different temperatures.

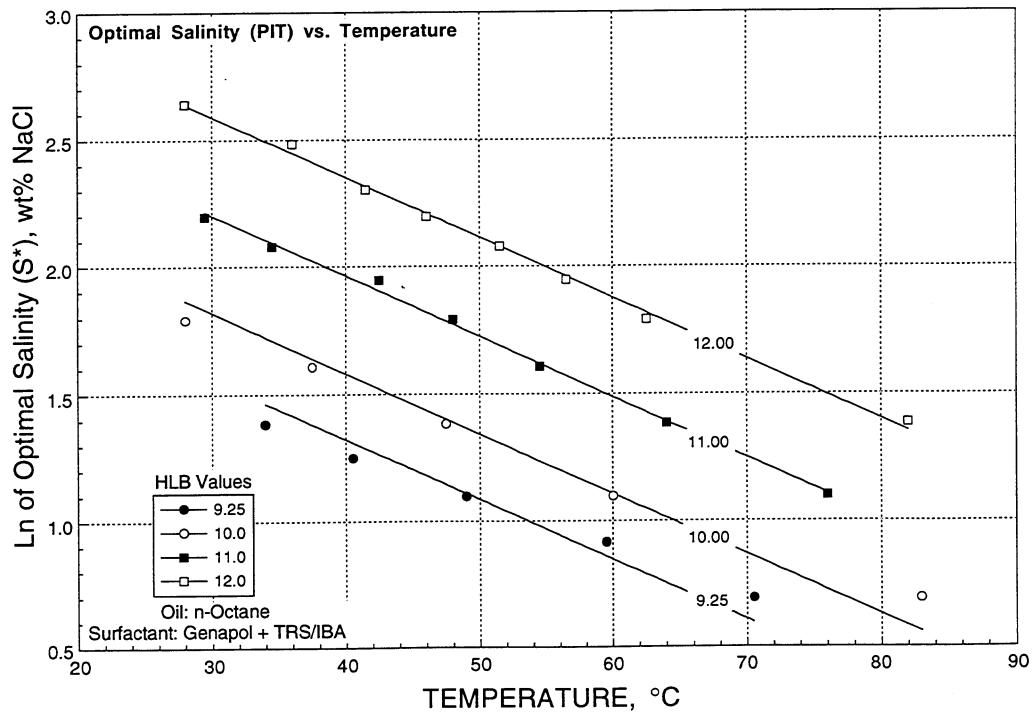


FIGURE A35. - Log of optimal salinity vs. temperature using Genapol + TRS/IBA with n-Octane at different HLB values.

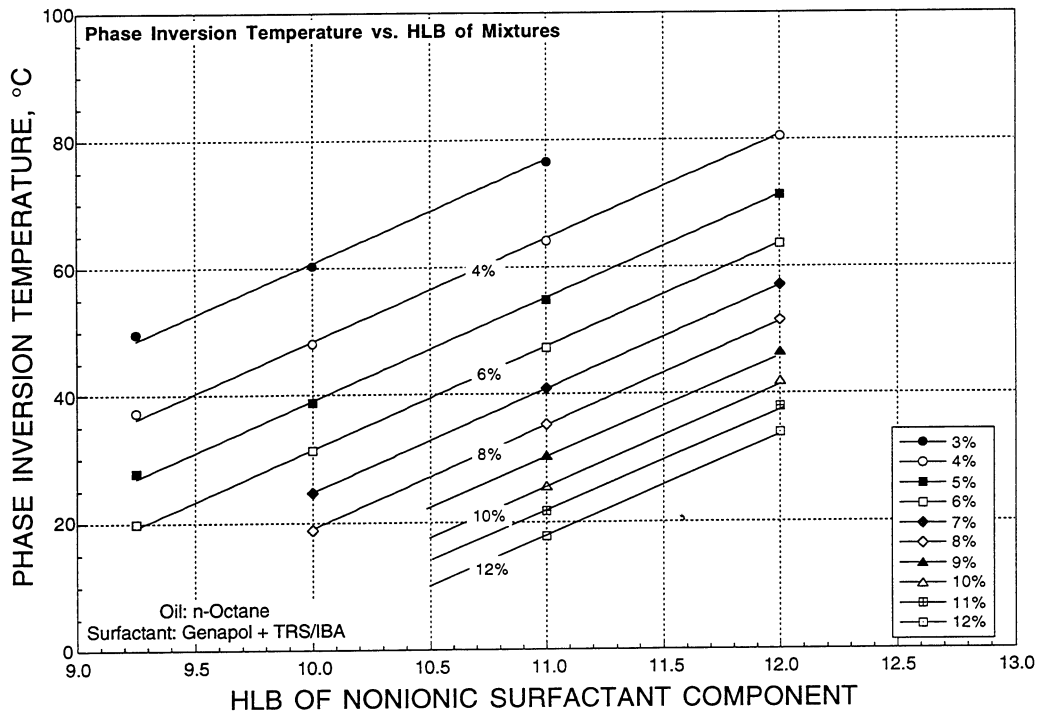


FIGURE A36. - Phase inversion temperature vs. HLB of nonionic surfactant component using Genapol + TRS/IBA with n-Octane at different salinities.

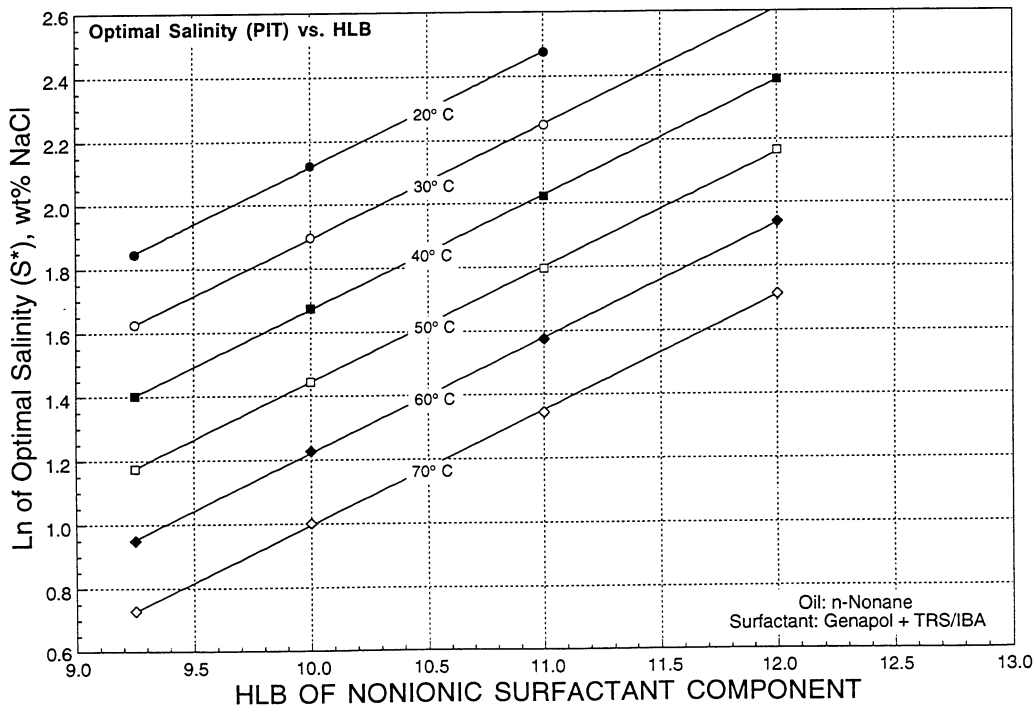


FIGURE A37. - Log of optimal salinity vs. HLB of nonionic surfactant component using Genapol + TRS/IBA with n-Nonane at different temperatures.

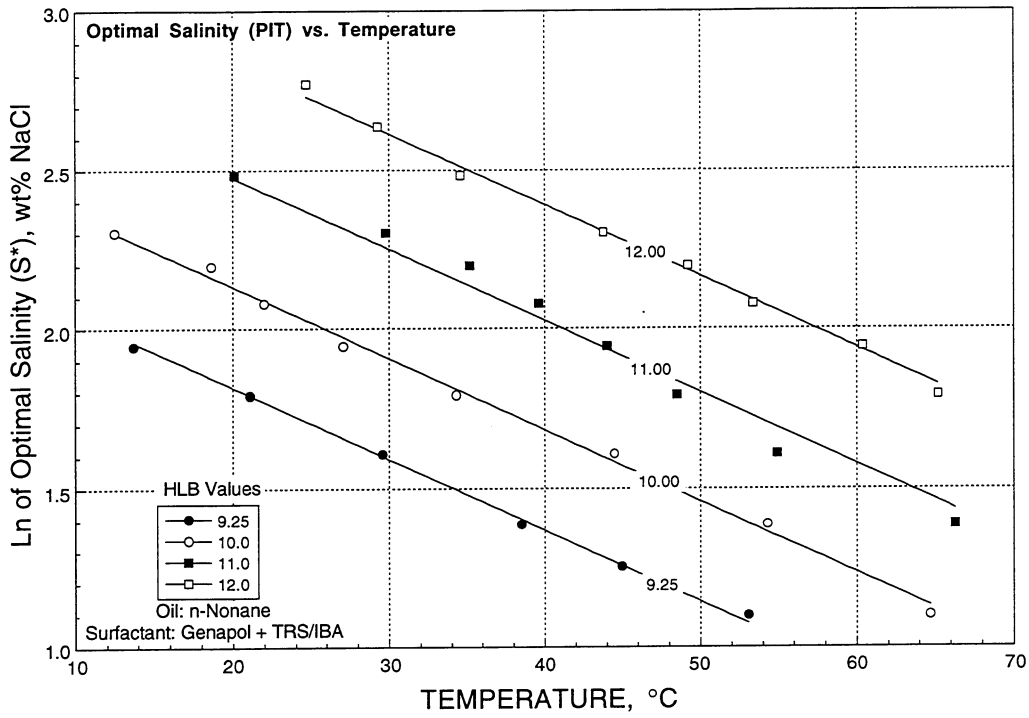


FIGURE A38. - Log of optimal salinity vs. temperature using Genapol + TRS/IBA with n-Nonane at different HLB values.

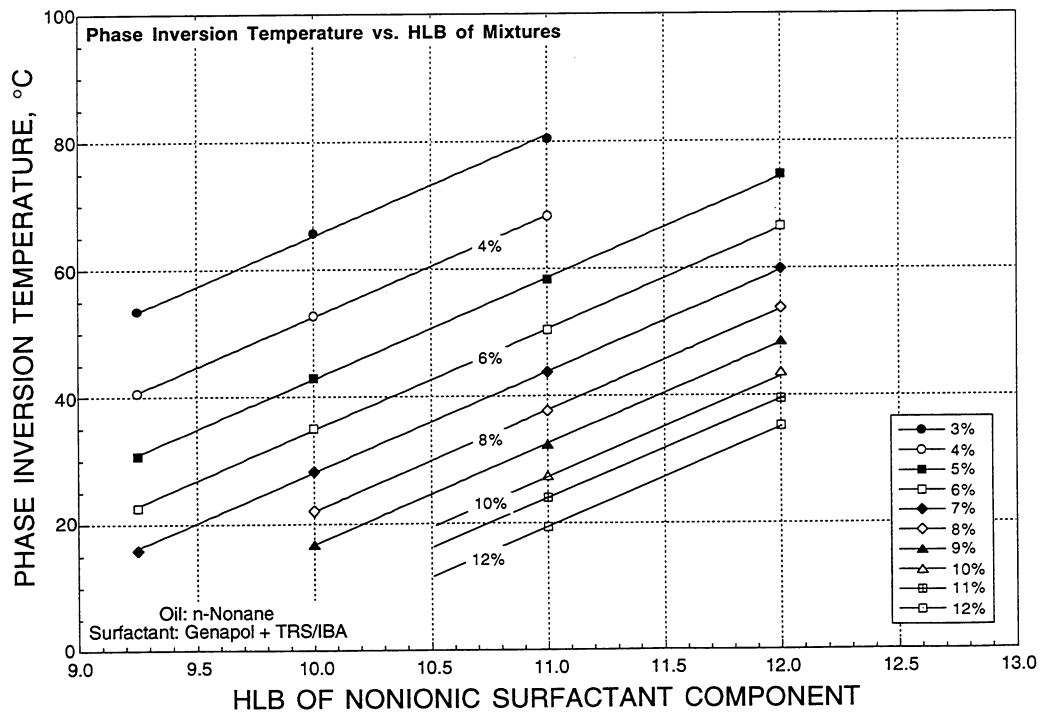


FIGURE A39. - Phase inversion temperature vs. HLB of nonionic surfactant component using Genapol + TRS/IBA with n-Nonane at different salinities.

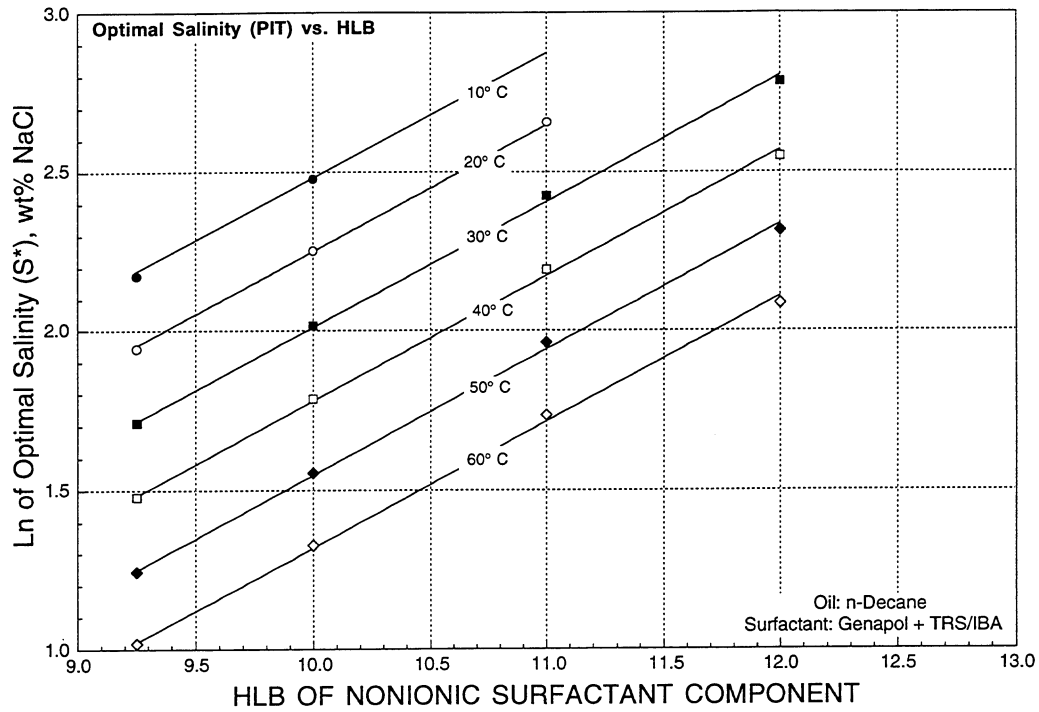


FIGURE A40. - Log of optimal salinity vs. HLB of nonionic surfactant component using Genapol + TRS/IBA with n-Decane at different temperatures.

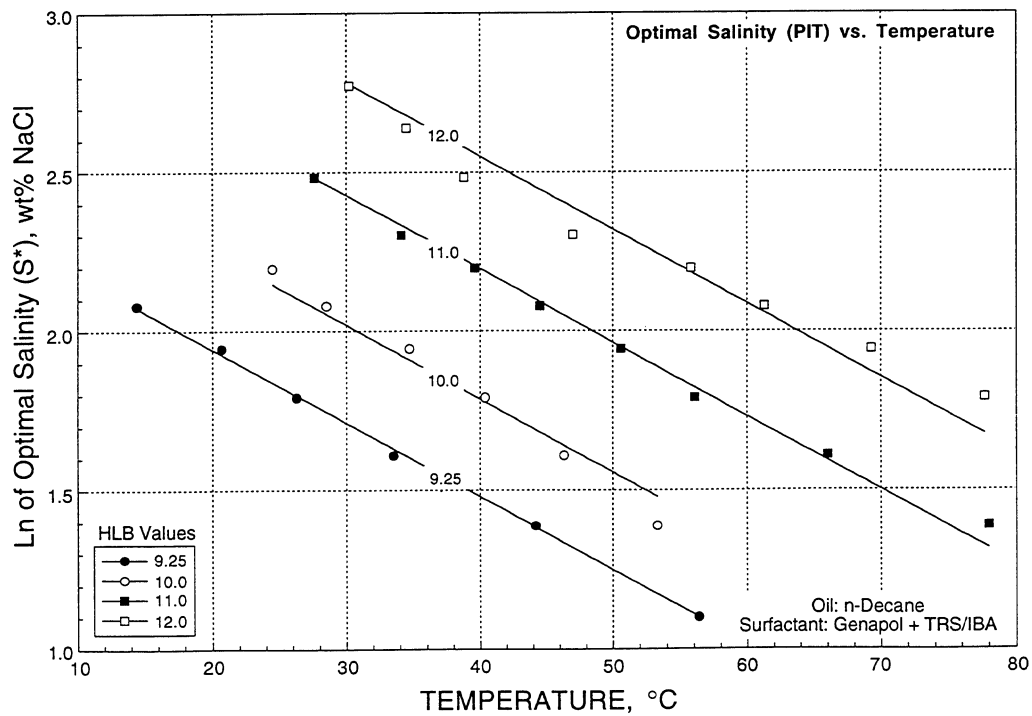


FIGURE A41. - Log of optimal salinity vs. temperature using Genapol + TRS/IBA with n-Decane at different HLB values.

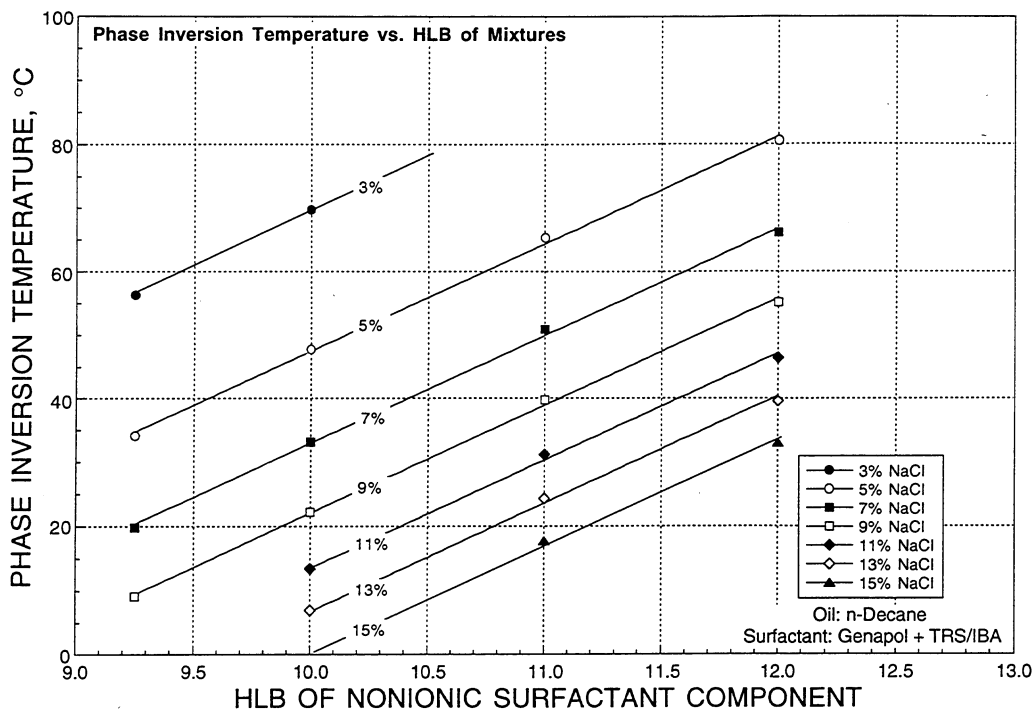


FIGURE A42. - Phase inversion temperature vs. HLB of nonionic surfactant component using Genapol + TRS/IBA with n-Decane at different salinities.

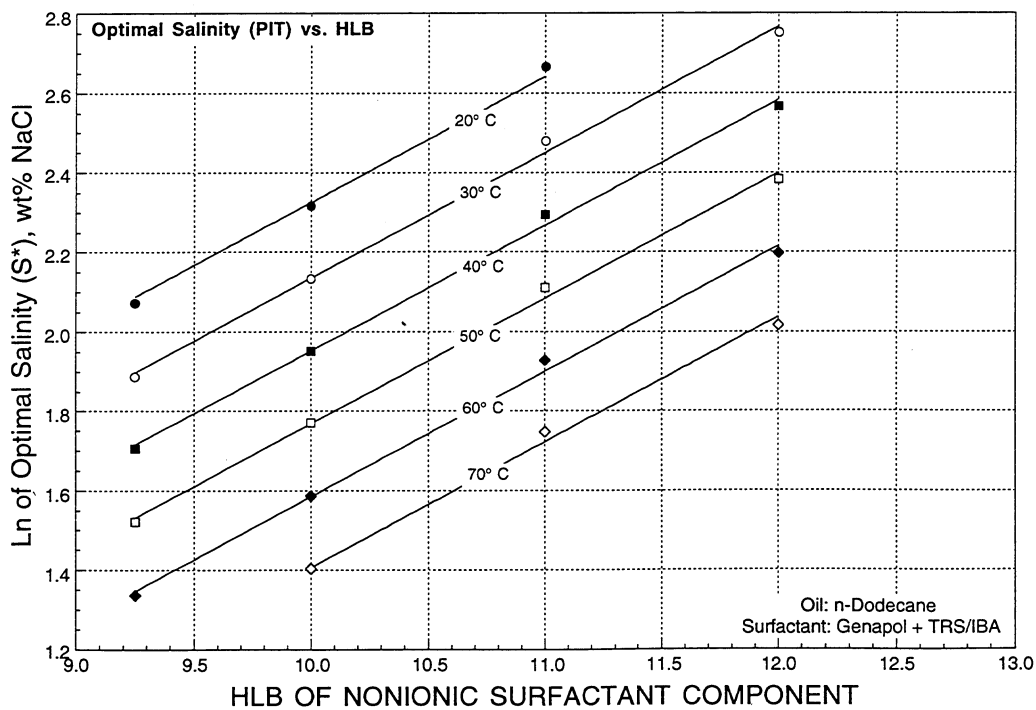


FIGURE A43. - Log of optimal salinity vs. HLB of nonionic surfactant component using Genapol + TRS/IBA with n-Dodecane at different temperatures.

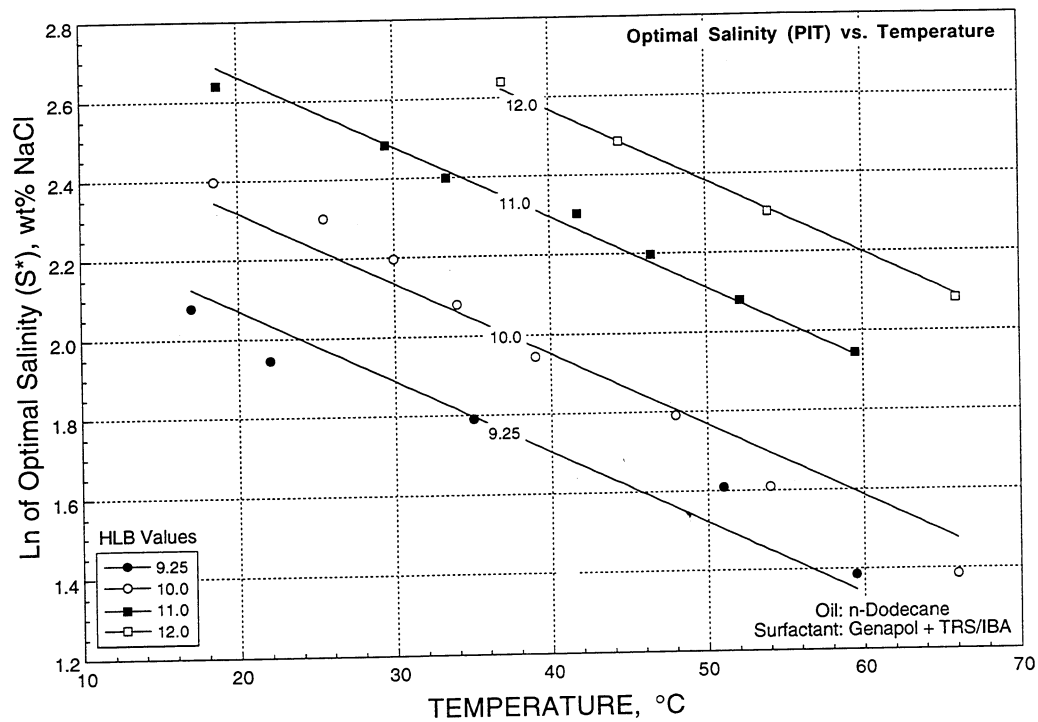


FIGURE A44. - Log of optimal salinity vs. temperature using Genapol + TRS/IBA with n-Dodecane at different HLB values.

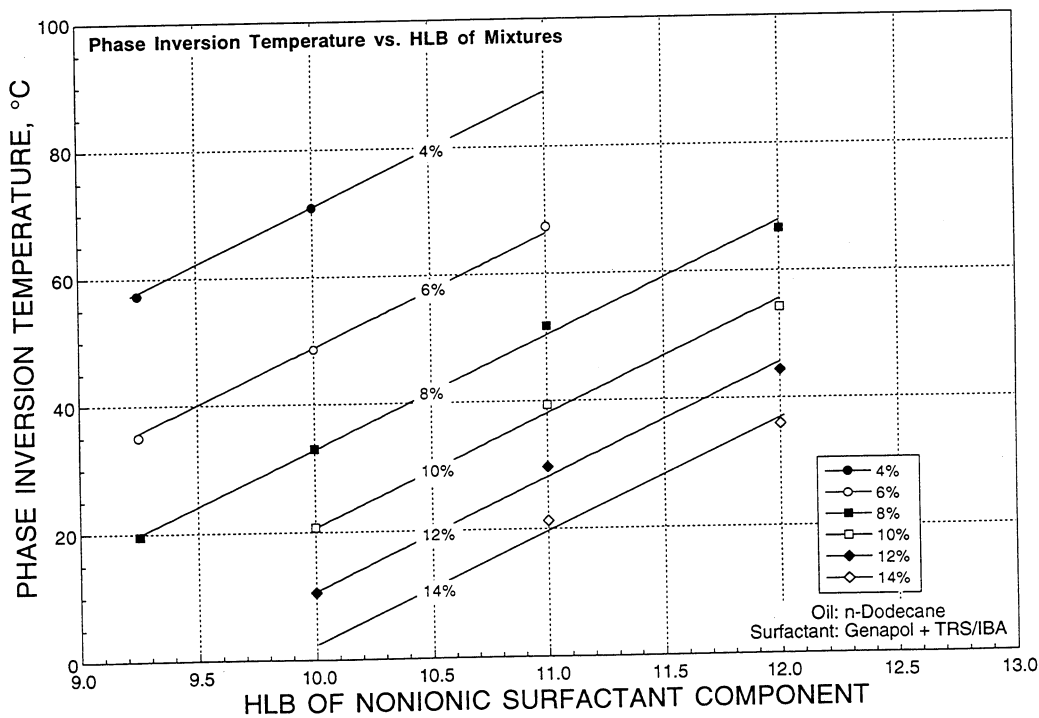


FIGURE A45. - Phase inversion temperature vs. HLB of nonionic surfactant component using Genapol + TRS/IBA with n-Dodecane at different salinities.

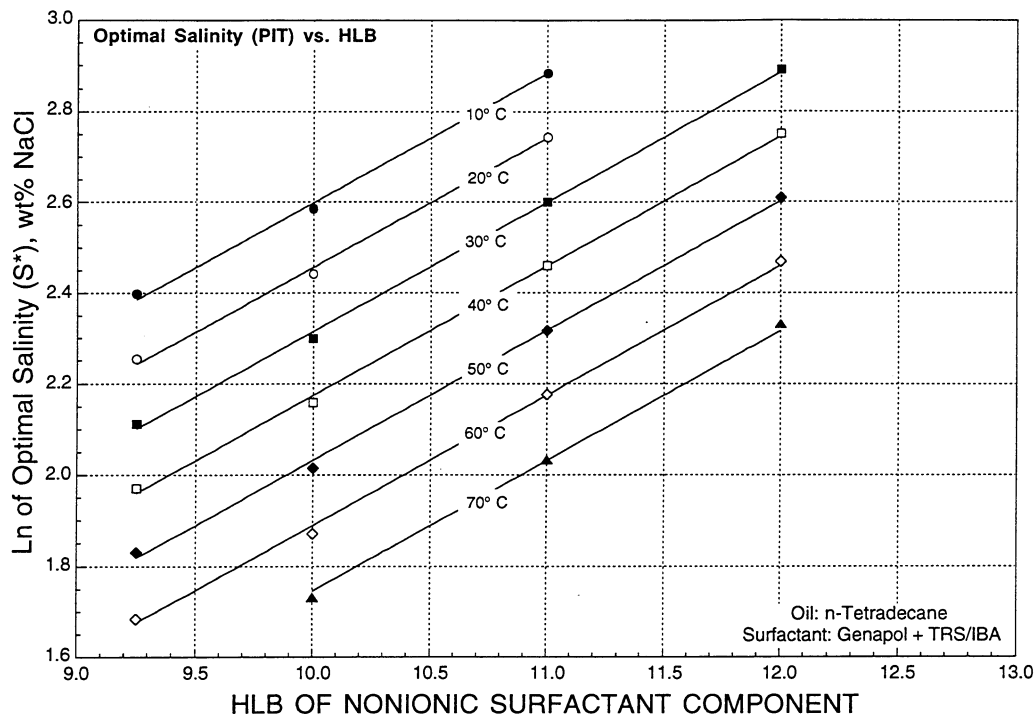


FIGURE A46. - Log of optimal salinity vs. HLB of nonionic surfactant component using Genapol + TRS/IBA with n-Tetradecane at different temperatures.

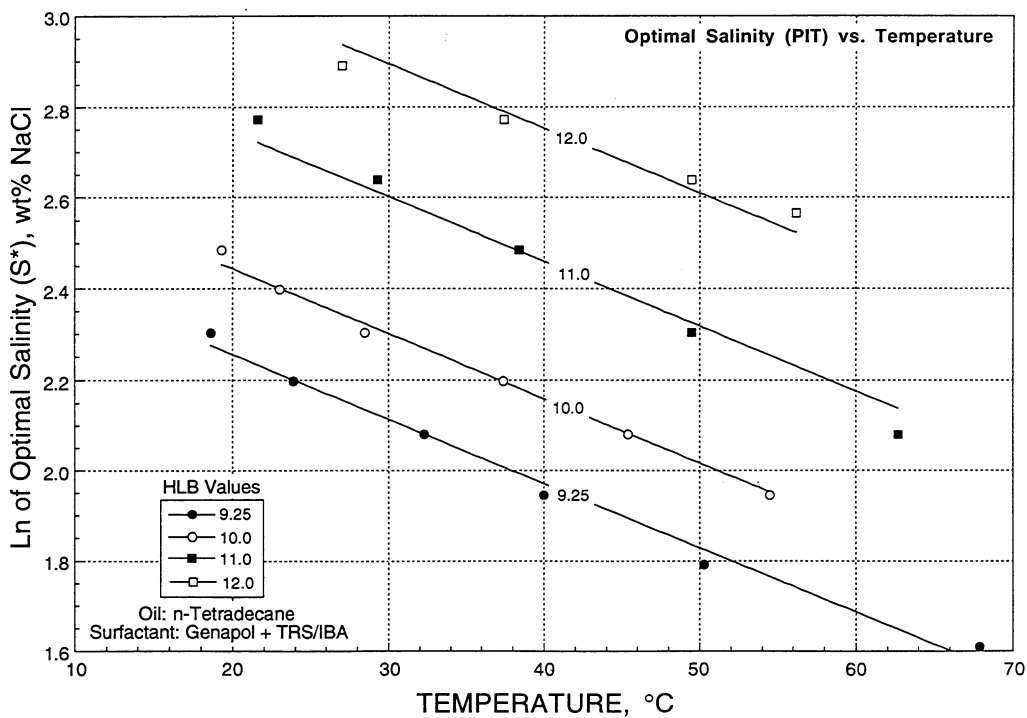


FIGURE A47. - Log of optimal salinity vs. temperature using Genapol + TRS/IBA with n-Tetradecane at different HLB values.

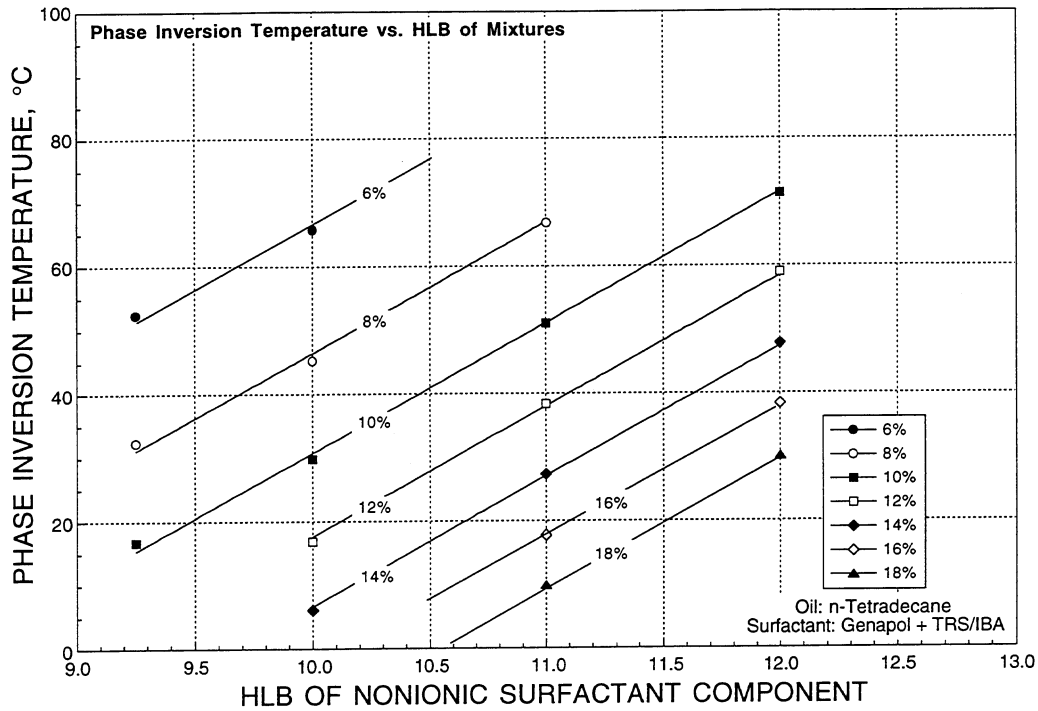


FIGURE A48. - Phase inversion temperature vs. HLB of nonionic surfactant component using Genapol + TRS/IBA with n-Tetradecane at different salinities.

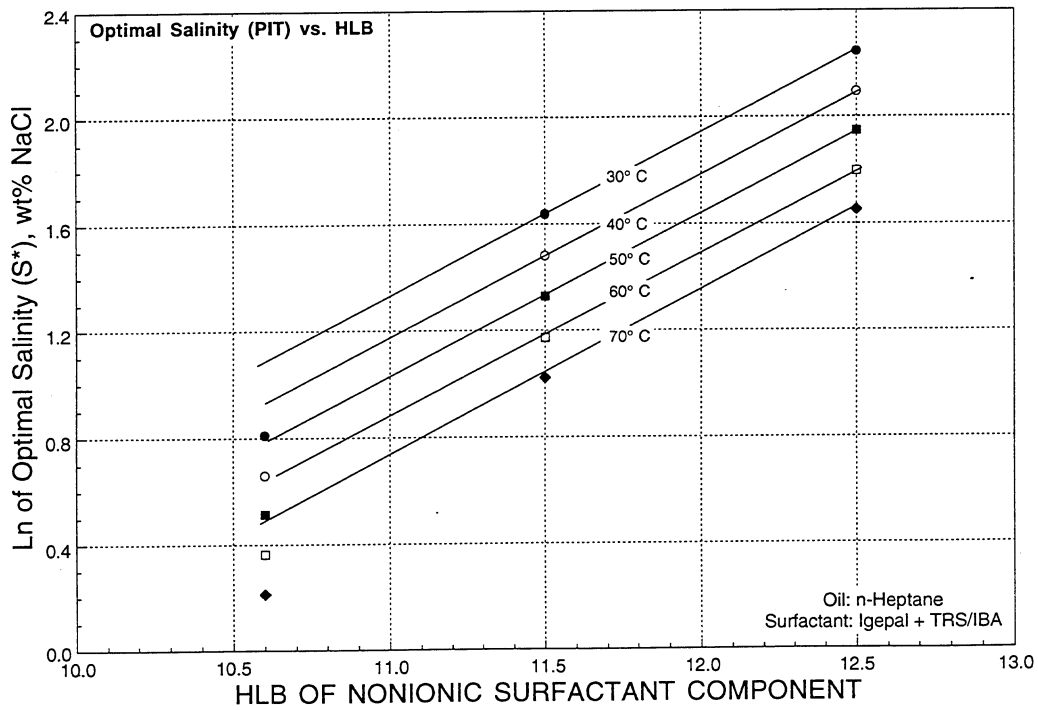


FIGURE A49. - Log of optimal salinity vs. HLB of nonionic surfactant component using Igepal + TRS/IBA with n-Heptane at different temperatures.

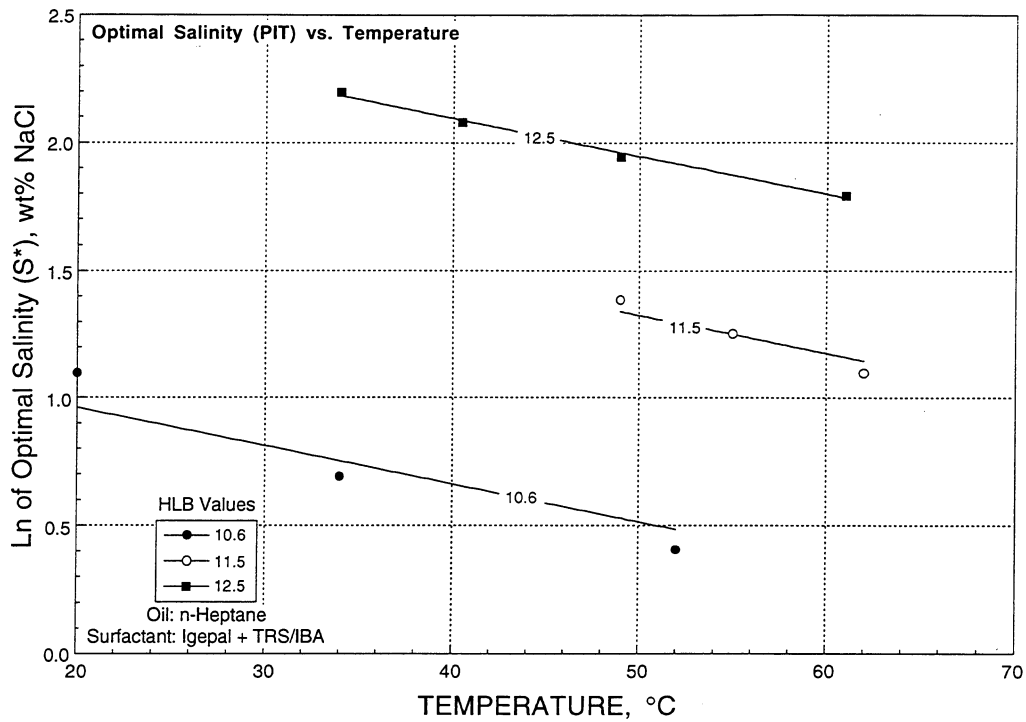


FIGURE A50. - Log of optimal salinity vs. temperature using Igepal + TRS/IBA with n-Heptane at different HLB values.

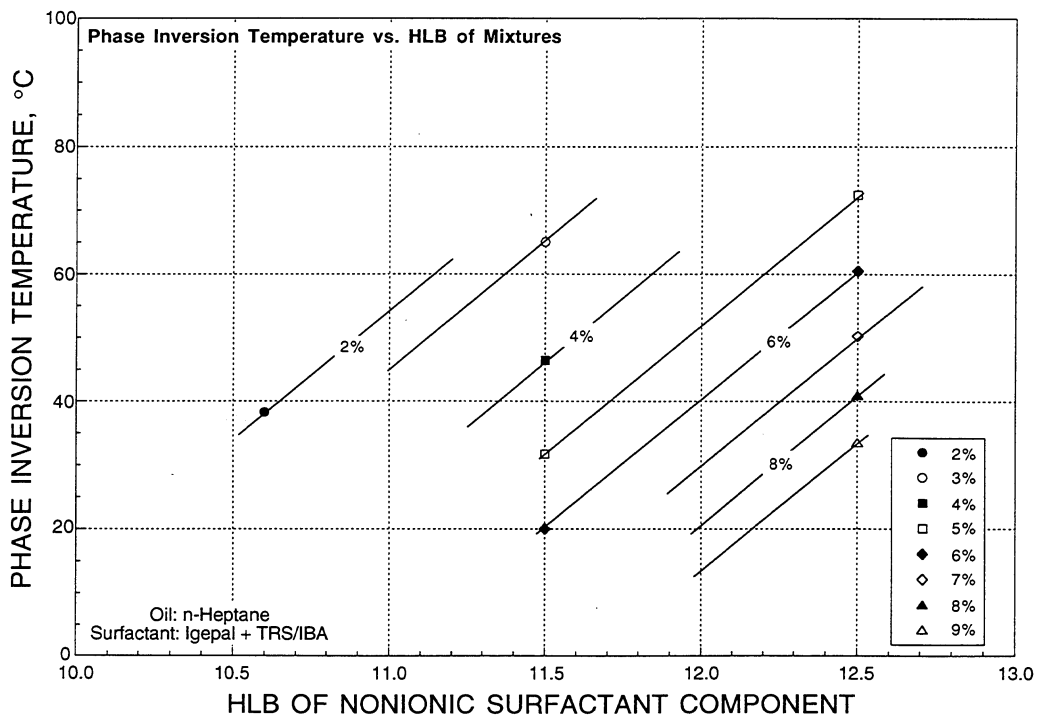


FIGURE A51. - Phase inversion temperature vs. HLB of nonionic surfactant component using Igepal + TRS/IBA with n-Heptane at different salinities.

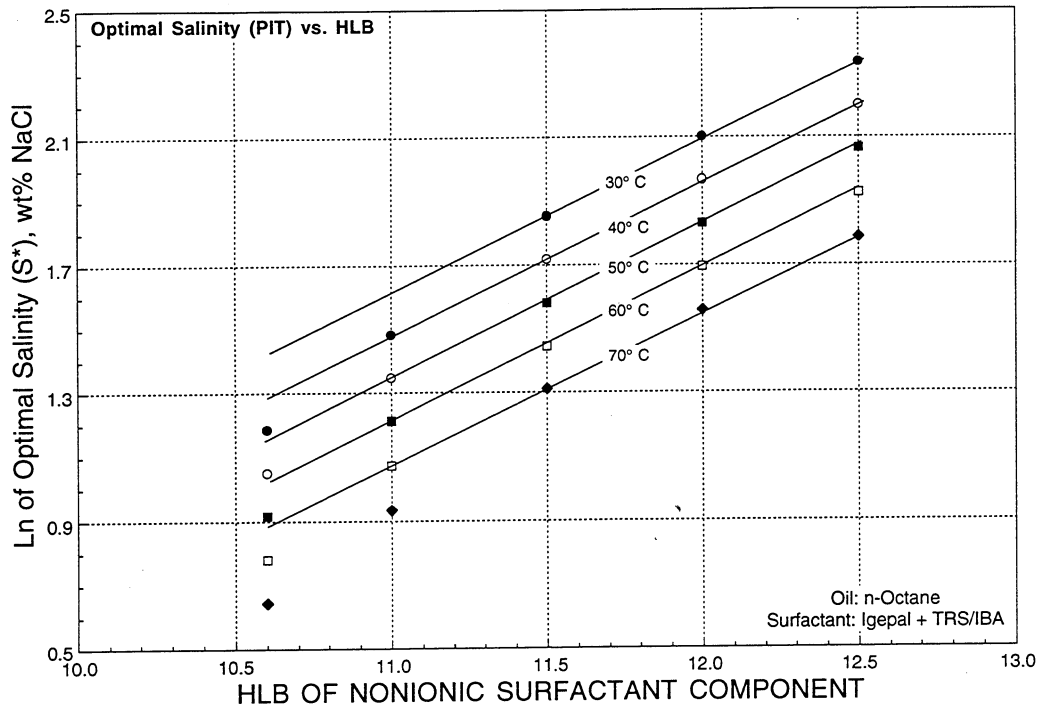


FIGURE A52. - Log of optimal salinity vs. HLB of nonionic surfactant component using Igepal + TRS/IBA with n-Octane at different temperatures.

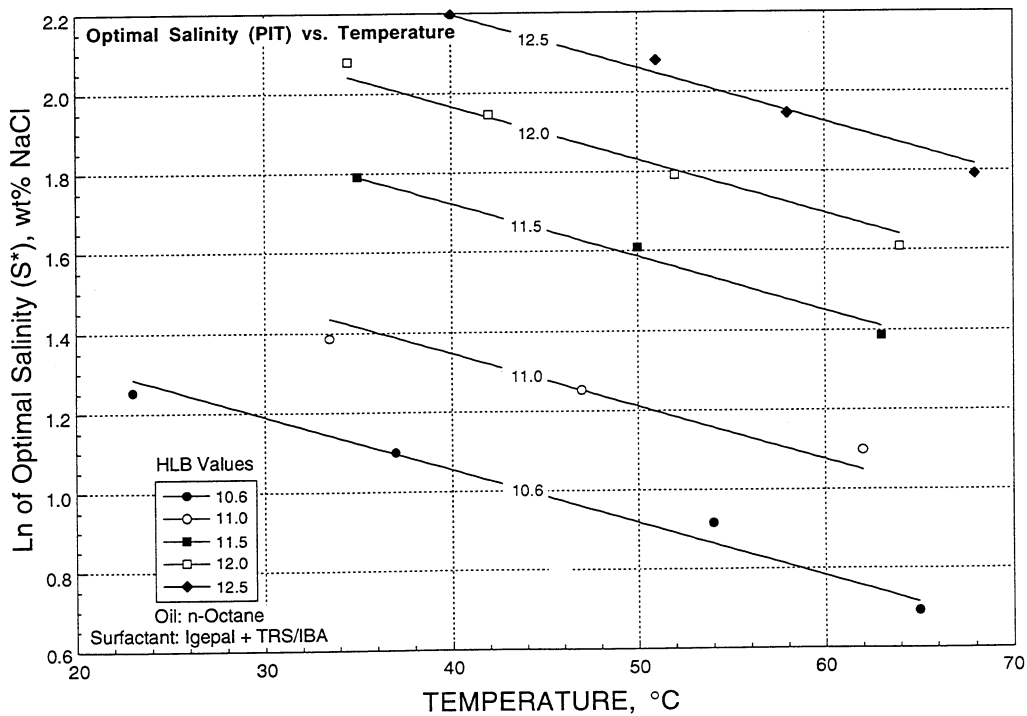


FIGURE A53. - Log of optimal salinity vs. temperature using Igepal + TRS/IBA with n-Octane at different HLB values.

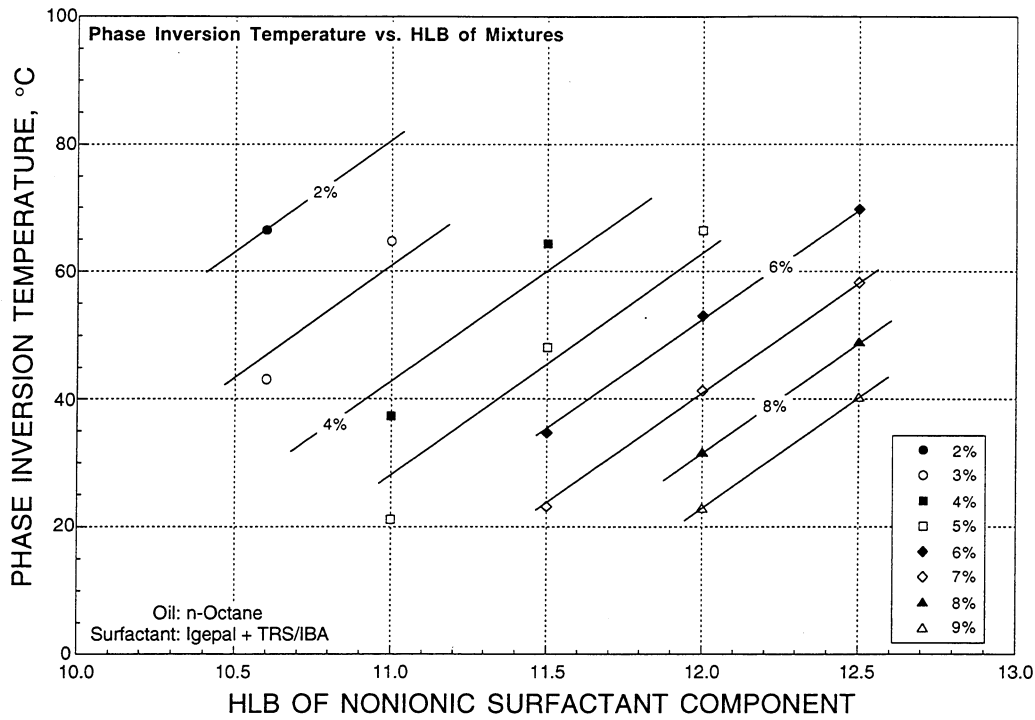


FIGURE A54. - Phase inversion temperature vs. HLB of nonionic surfactant component using Igepal + TRS/IBA with n-Octane at different salinities.

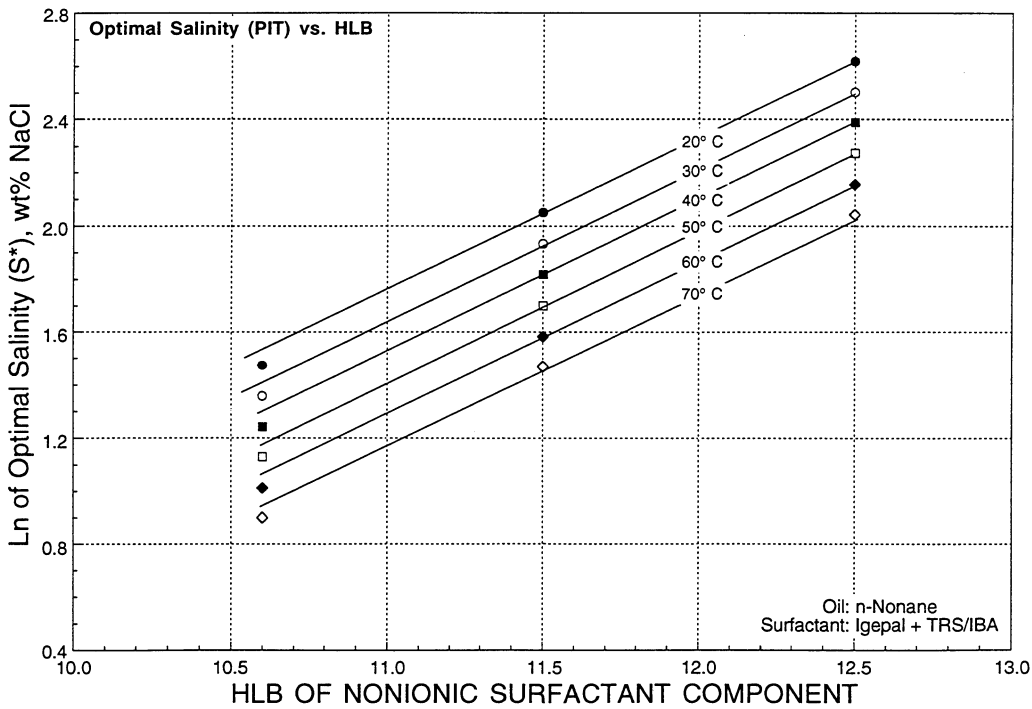


FIGURE A55. - Log of optimal salinity vs. HLB of nonionic surfactant component using Igepal + TRS/IBA with n-Nonane at different temperatures.

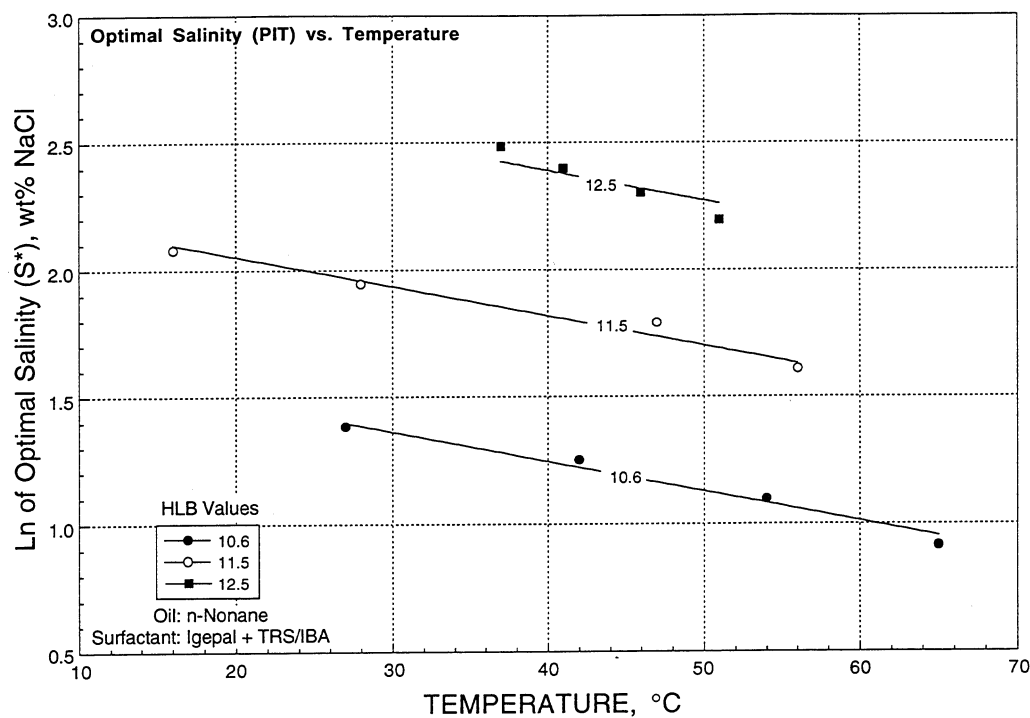


FIGURE A56. - Log of optimal salinity vs. temperature using Igepal + TRS/IBA with n-Nonane at different HLB values.

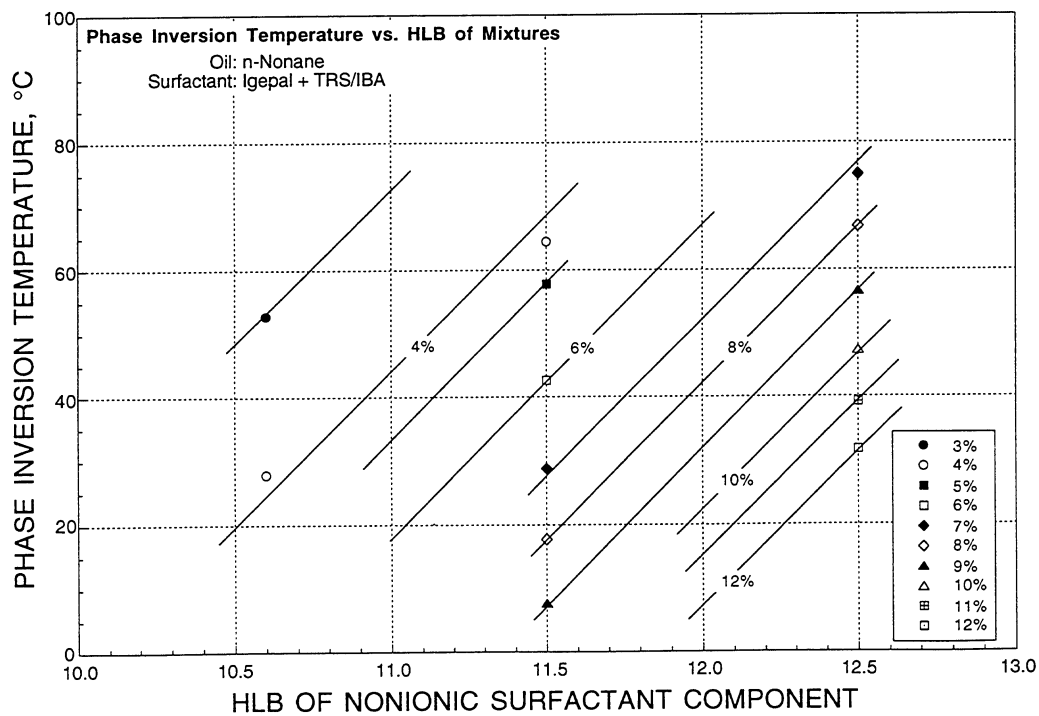


FIGURE A57. - Phase inversion temperature vs. HLB of nonionic surfactant component using Igepal + TRS/IBA with n-Nonane at different salinities.

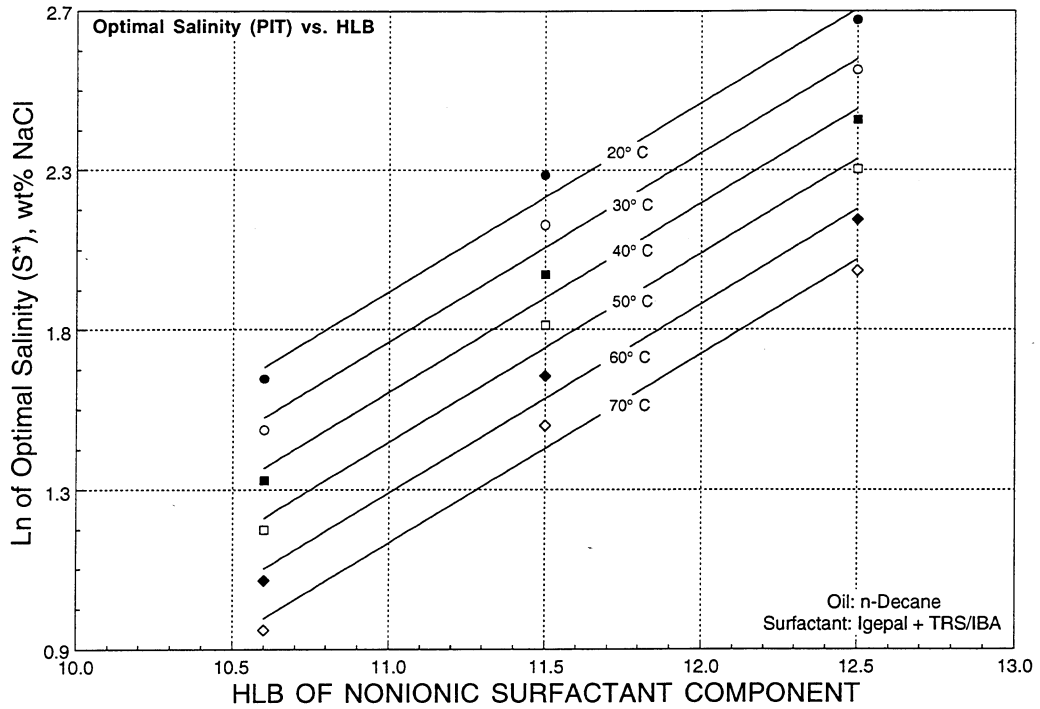


FIGURE A58. - Log of optimal salinity vs. HLB of nonionic surfactant component using Igepal + TRS/IBA with n-Decane at different temperatures.

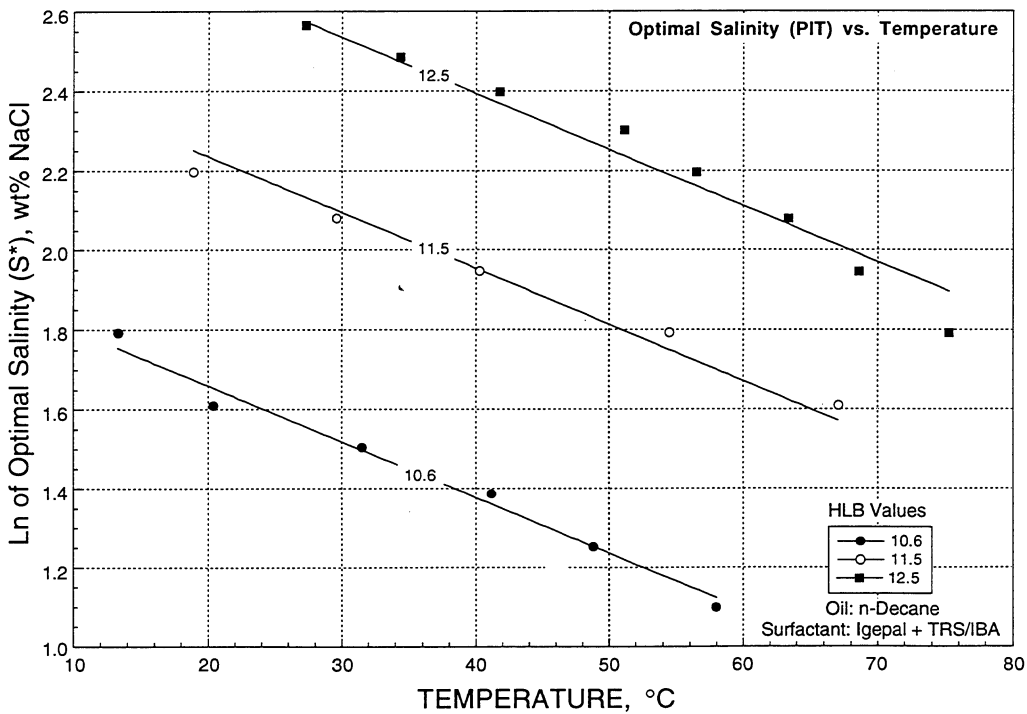


FIGURE A59. - Log of optimal salinity vs. temperature using Igepal + TRS/IBA with n-Decane at different HLB values.

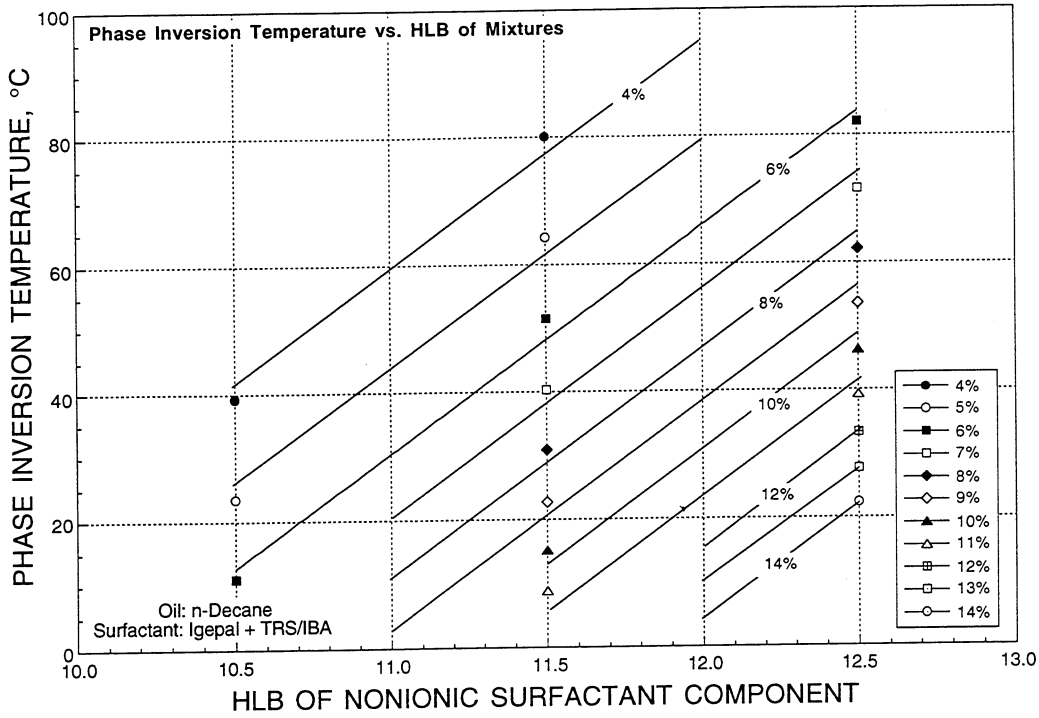


FIGURE A60. - Phase inversion temperature vs. HLB of nonionic surfactant component using Igepal + TRS/IBA with n-Decane at different salinities.

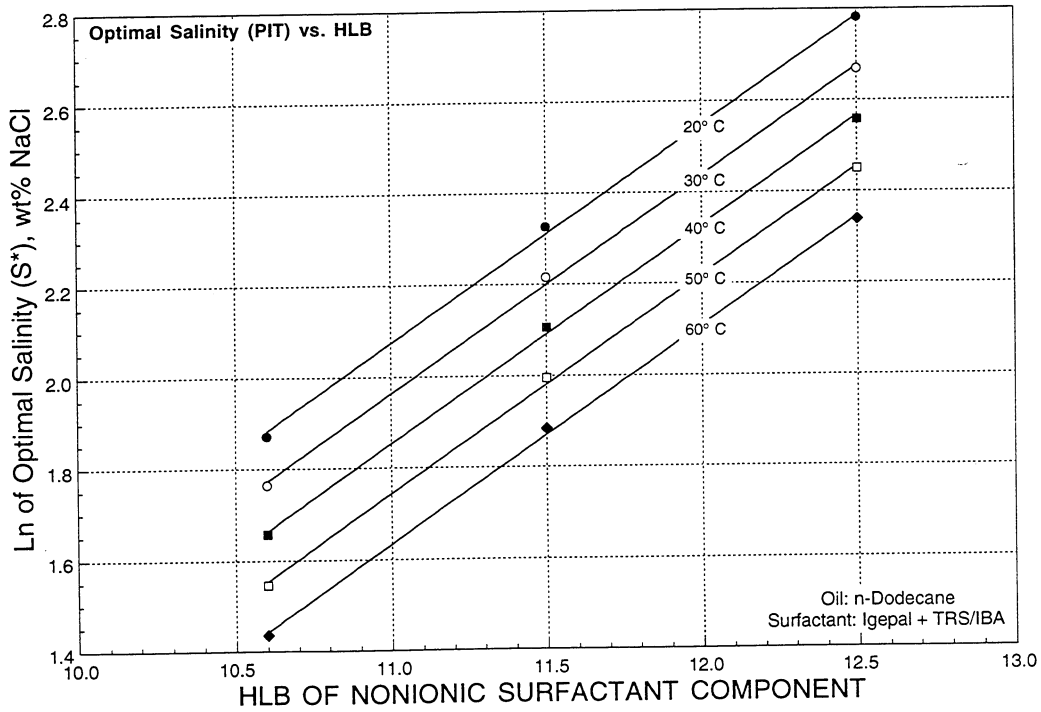


FIGURE A61. - Log of optimal salinity vs. HLB of nonionic surfactant component using Igepal + TRS/IBA with n-Dodecane at different temperatures.

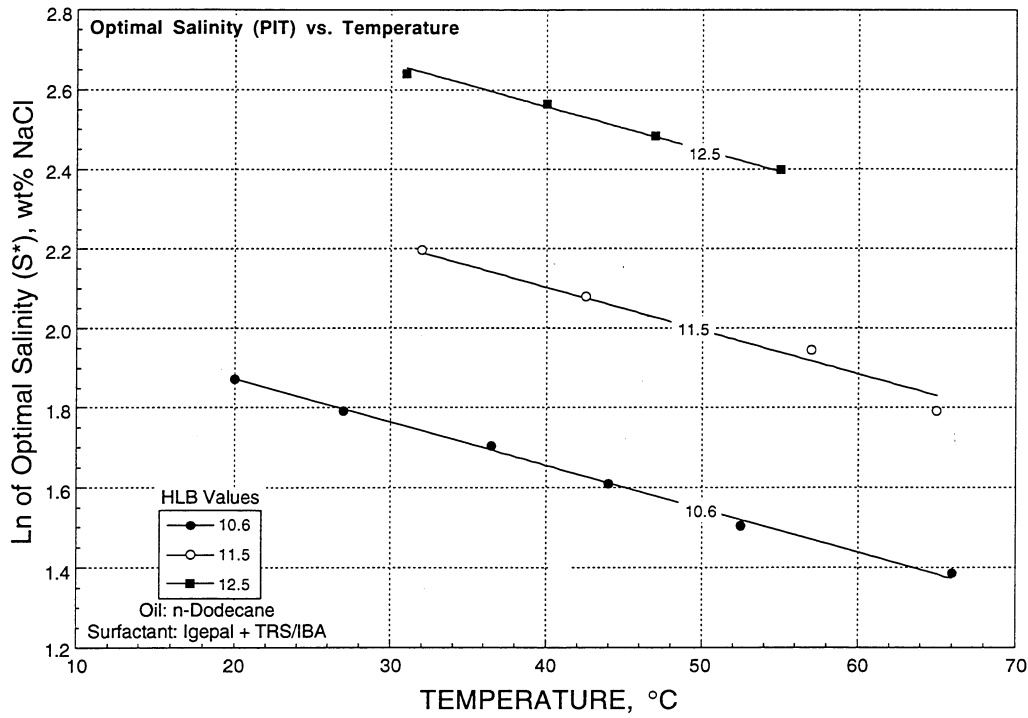


FIGURE A62. - Log of optimal salinity vs. temperature using Igepal + TRS/IBA with n-Dodecane at different HLB values.

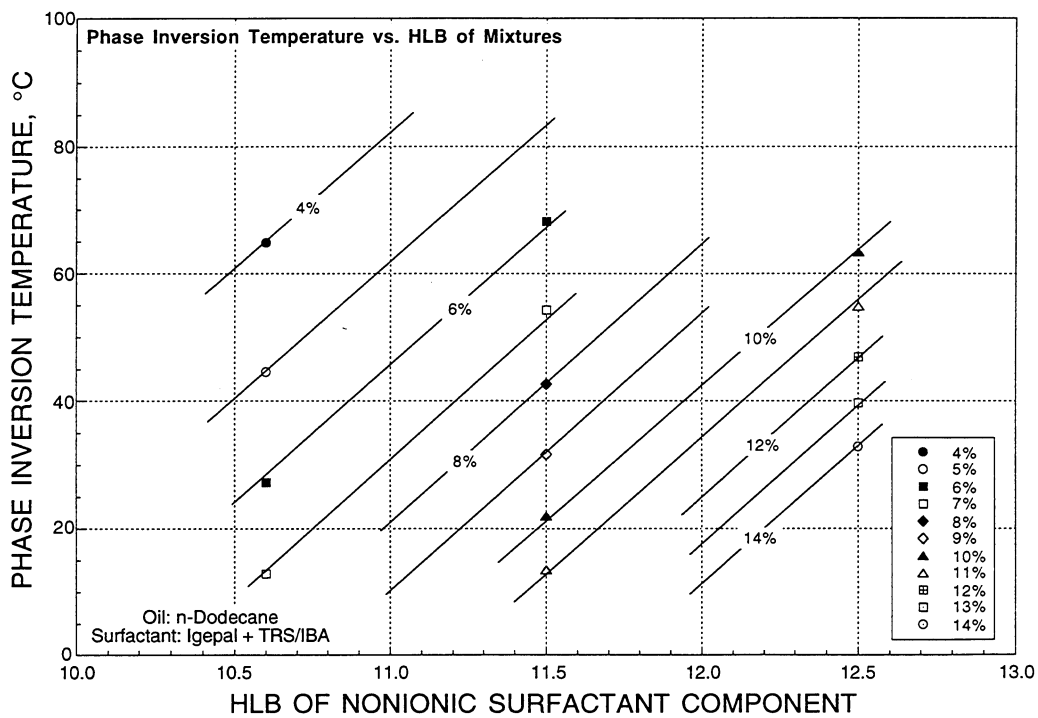


FIGURE A63. - Phase inversion temperature vs. HLB of nonionic surfactant component using Igepal + TRS/IBA with n-Dodecane at different salinities.

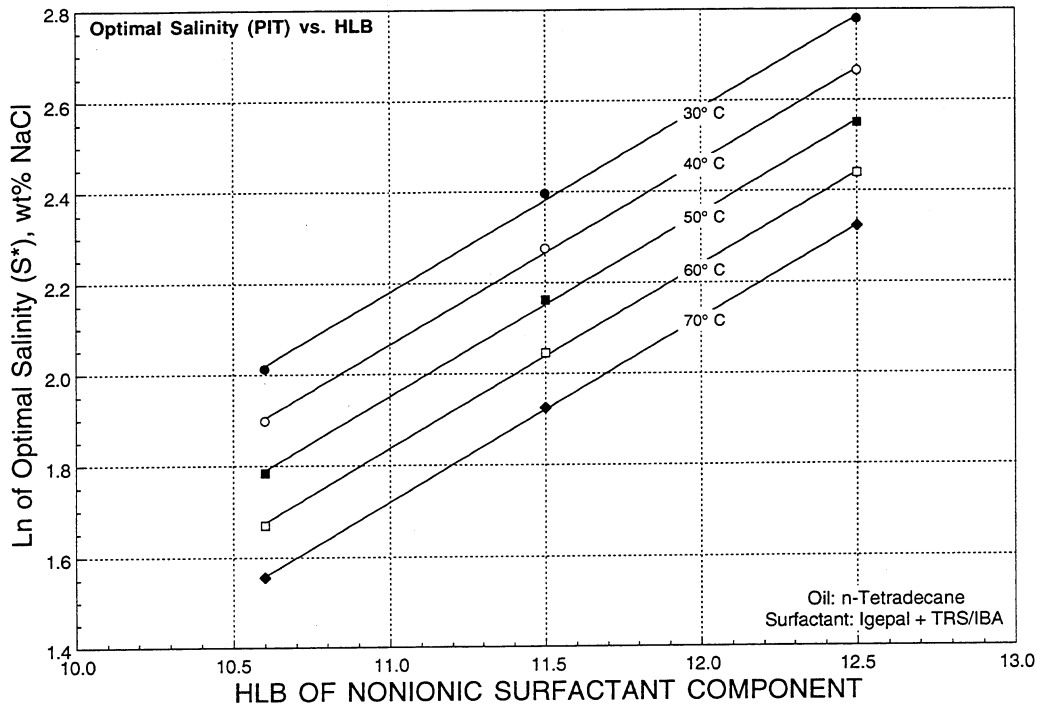


FIGURE A64. - Log of optimal salinity vs. HLB of nonionic surfactant component using Igepal + TRS/IBA with n-Tetradecane at different temperatures.

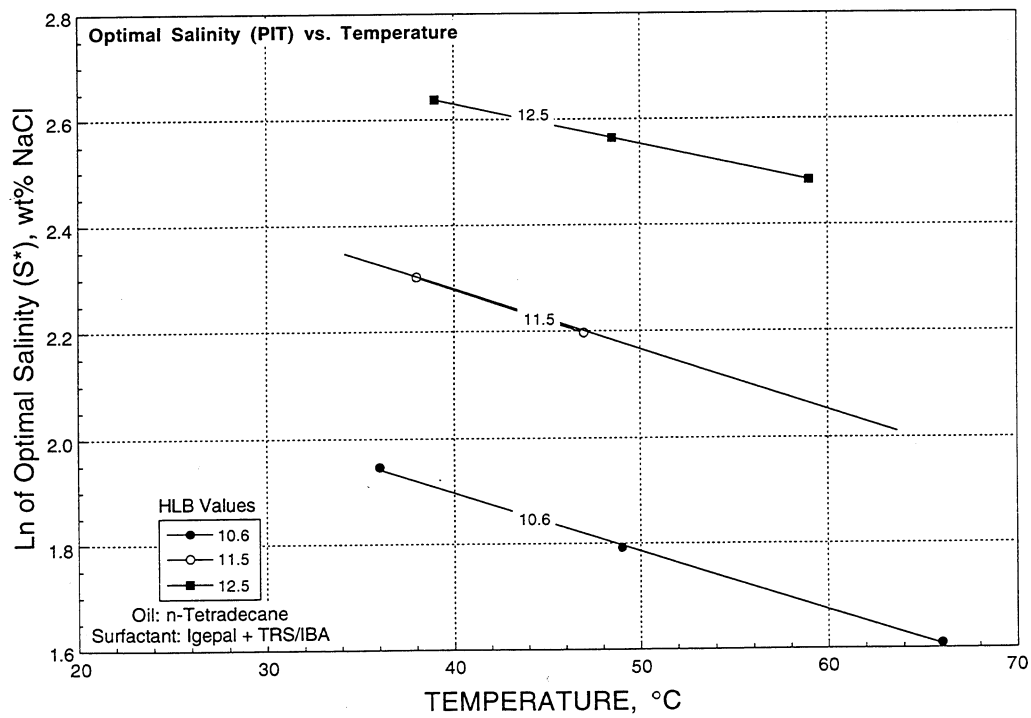


FIGURE A65. - Log of optimal salinity vs. temperature using Igepal + TRS/IBA with n-Tetradecane at different HLB values.

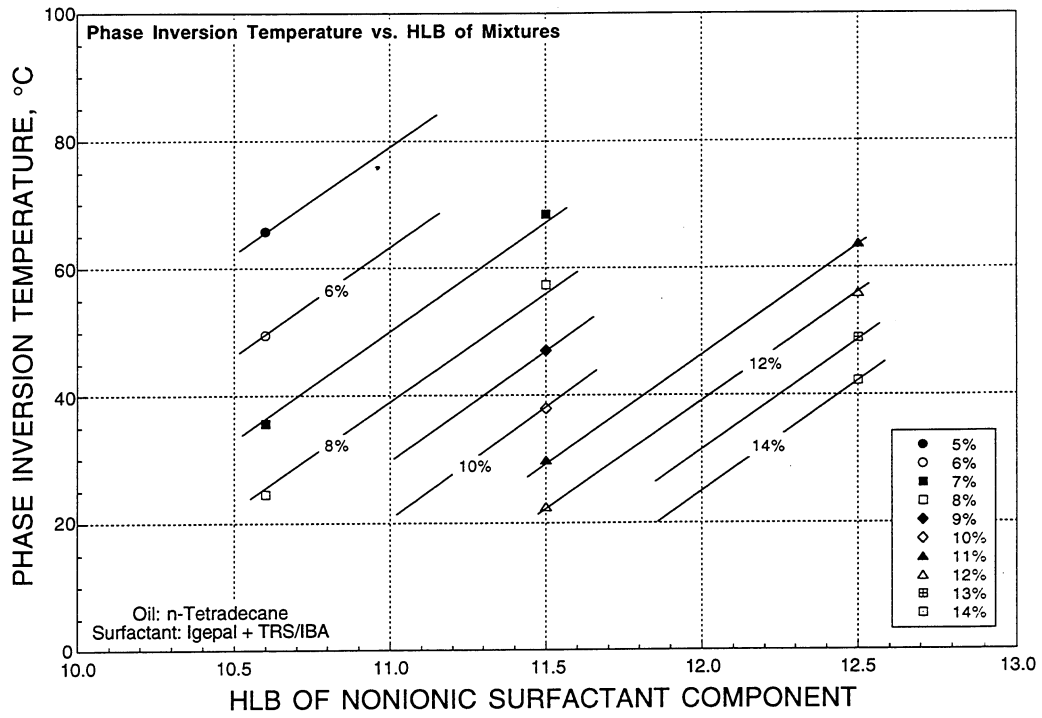


FIGURE A66. - Phase inversion temperature vs. HLB of nonionic surfactant component using Igepal + TRS/IBA with n-Tetradecane at different salinities.

## APPENDIX B

### Summary of CT coreflood operations

Experimental operation	Measurement	Calculation	CT scan
Select, trim, clean (as required) and dry core	Measure core dimensions Save trimmed ends, mark orientation and send pieces for thin section and/or XRD		
Encase core in epoxy with endpieces Pressurize with CO <sub>2</sub> and test for leaks (about 30 psi) or load in an aluminum coreholder	Measure dry weight		Scan dry core
Evacuate, saturate with CO <sub>2</sub> (2 cycles), saturate with degassed brine	Measure saturated weight	Calculate pore volume	Scan saturated core
Conduct tracer test with 10% NaI brine			Scan with time as tracer moves through core
Flow tagged oil to residual brine saturation	Measure brine out	Calculate oil saturation at residual water sat.	Scan oil saturated core
Waterflood to residual oil saturation	Measure oil out	Calculate residual oil saturation	Scan waterflooded core
Inject chemicals preflush surfactant polymer etc., as needed	Measure oil and brine production	Calculate: Pore volume, oil cut, changes in residual oil. accumulated oil production, etc.	Scan several times as needed to monitor oil advance
	Analytical measurements on effluent samples, as needed: viscosity, pH, surfactant concentration, etc.	Calculate values from measurements Calculate CT oil saturation distributions	

**APPENDIX C - Selected CT-composite images of chemical coreflooding experiments**

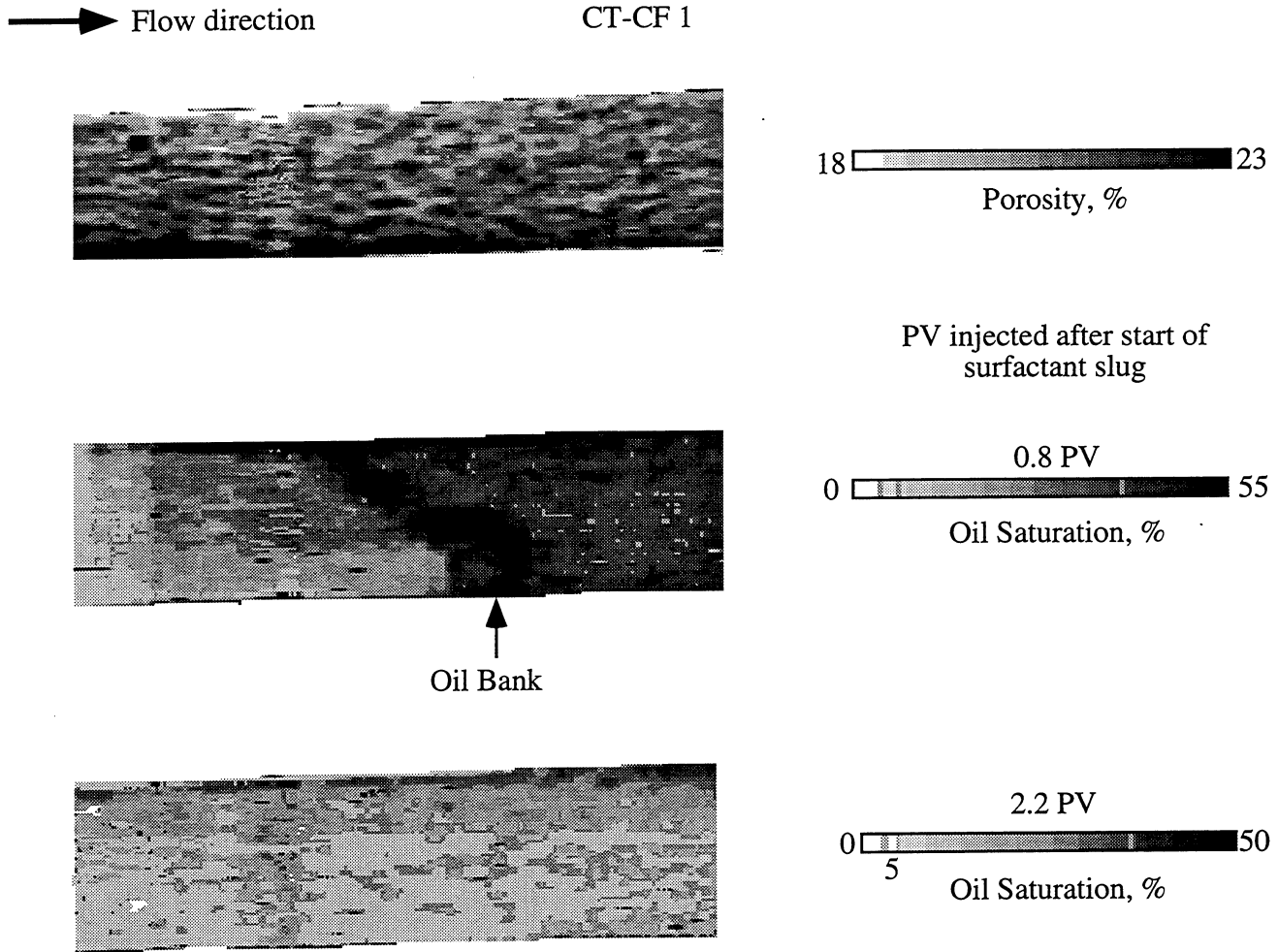


FIGURE C1 - Porosity and oil saturation distributions for CT-CF 1.  
Chemical formulations are given in Table 17.

→ Flow direction

CT-CF 3

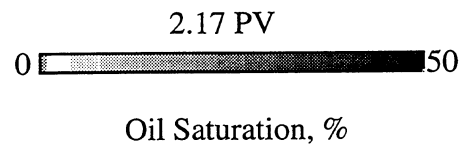
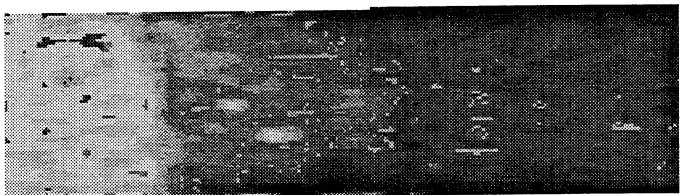
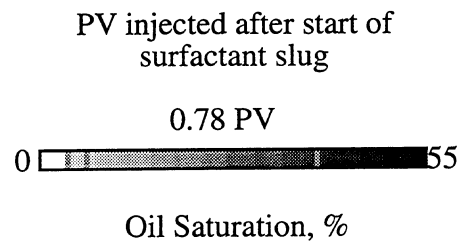
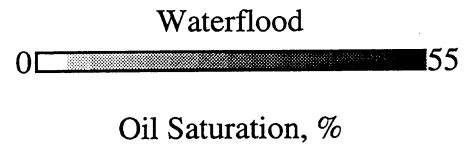
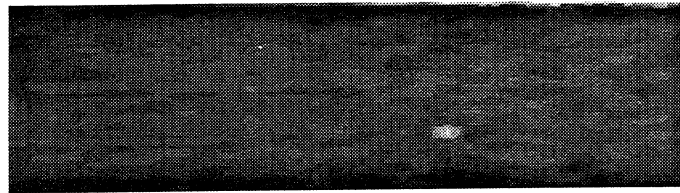
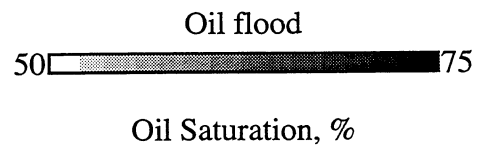
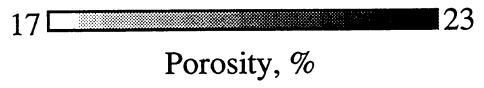


FIGURE C2 - Porosity and oil saturation distributions for CT-CF 3.  
Chemical formulations are given in Table 17.

→ Flow direction

CT-CF 4

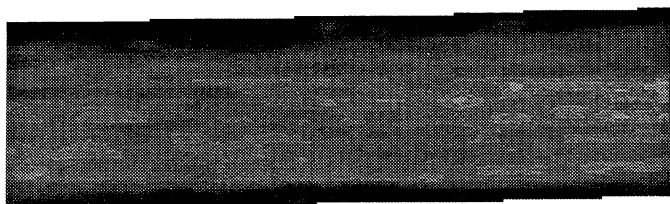


17 22

Porosity, %

Oil flood

Oil CT-density value was too high to see saturation differences



Waterflood

0 55

Oil Saturation, %

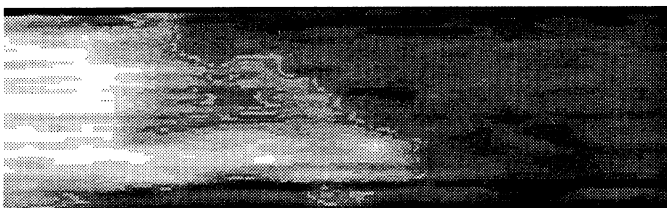
PV injected after start of surfactant slug



0.15 PV

0 55

Oil Saturation, %



0.3 PV

0 50

Oil Saturation, %



1.7 PV

0 50

Oil Saturation, %



Tracer =

FIGURE C3 - Porosity and oil saturation distributions for CT-CF 4. Chemical formulations are given in Table 17.

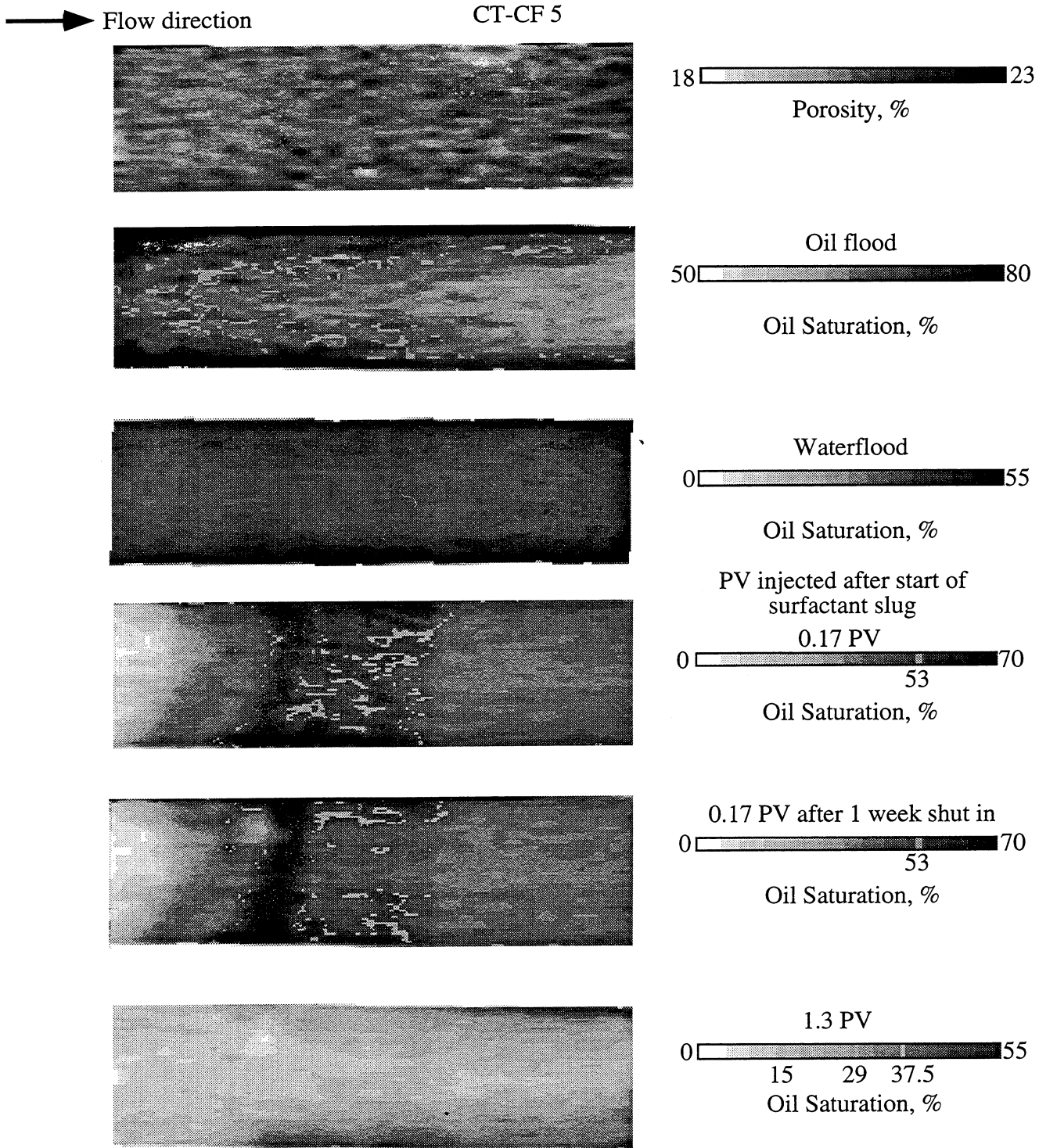


FIGURE C4 - Porosity and oil saturation distributions for CT-CF 5.  
 Chemical formulations are given in Table 17.

CT-CF 7

→ Flow direction

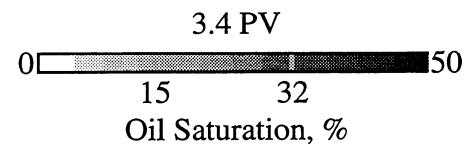
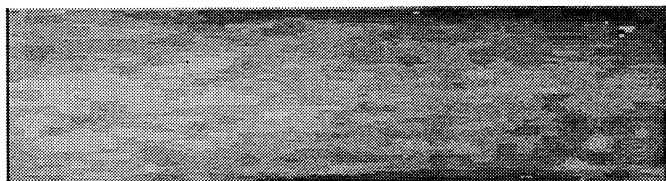
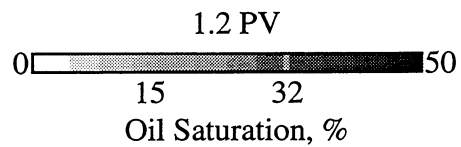
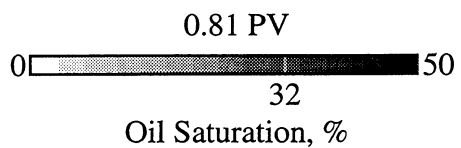
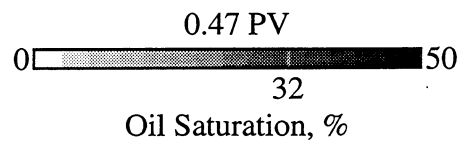
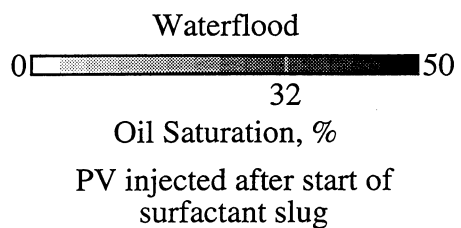
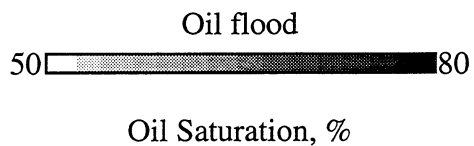
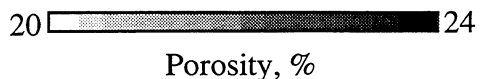


FIGURE C5 - Porosity and oil saturation distributions for CT-CF 7.  
Chemical formulations are given in Table 17.

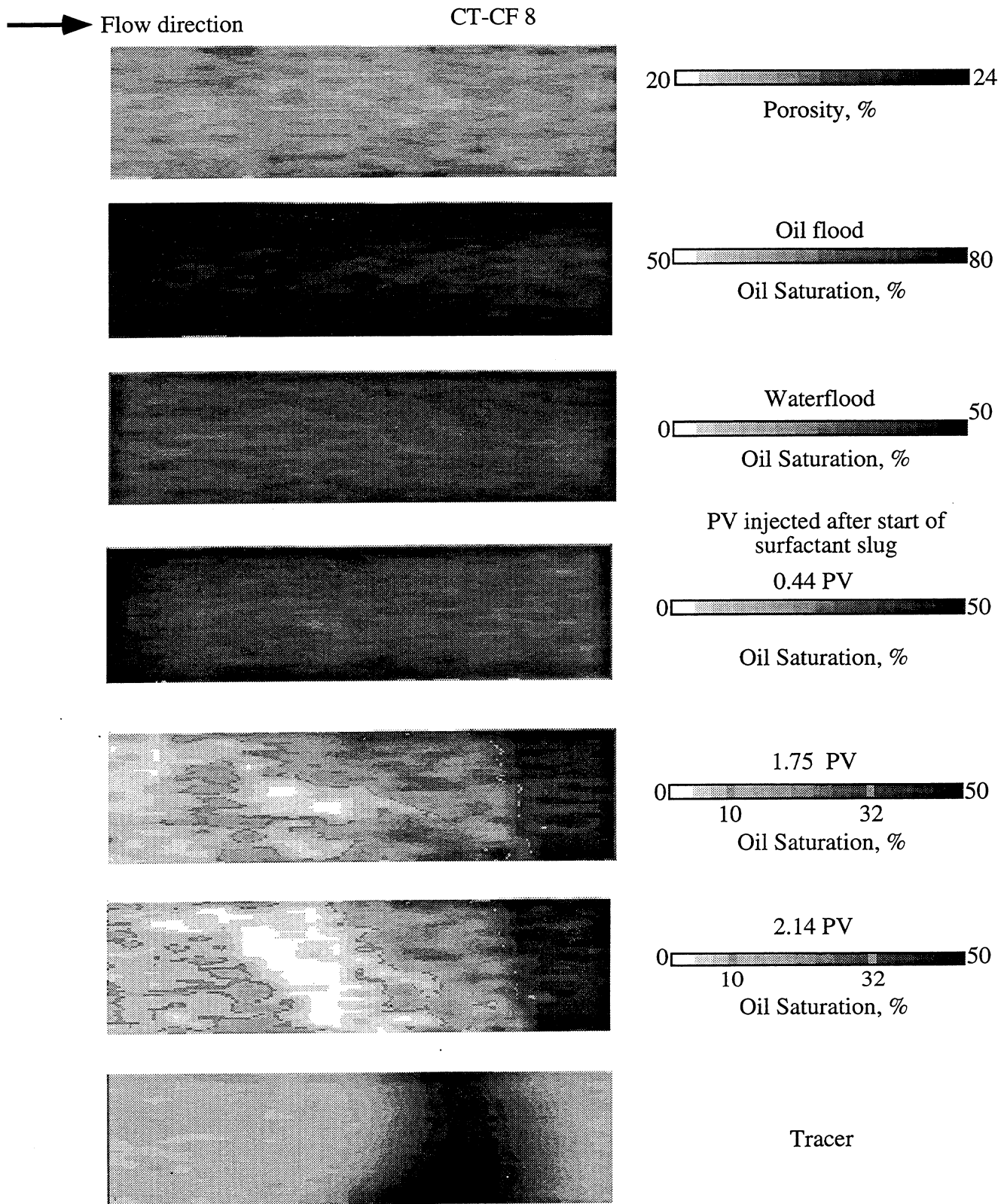


FIGURE C6 - Porosity and oil saturation distributions for CT-CF 8  
 Chemical formulations are given in Table 17.

→ Flow direction

CT-CF 9

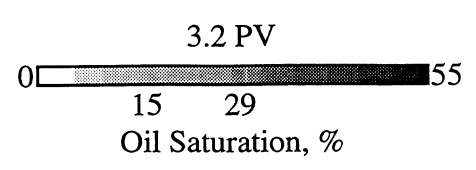
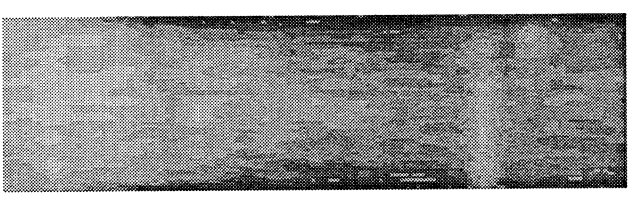
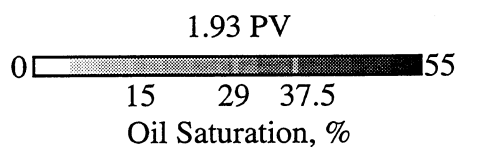
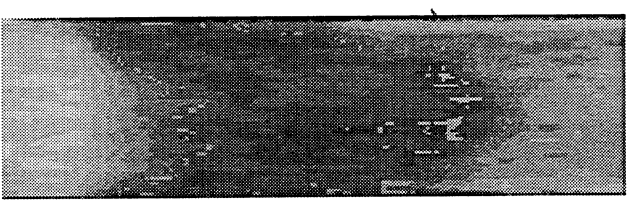
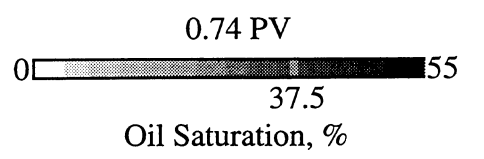
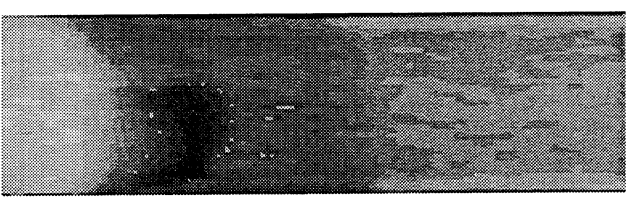
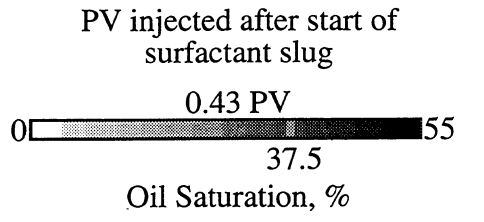
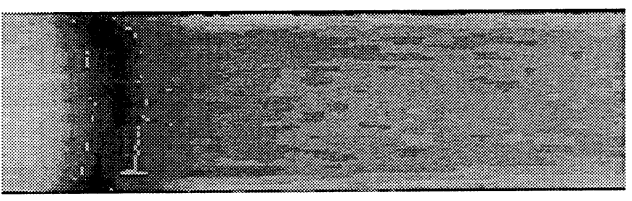
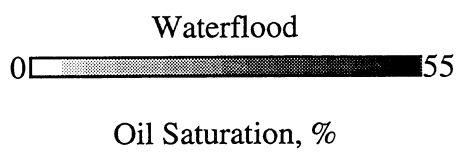
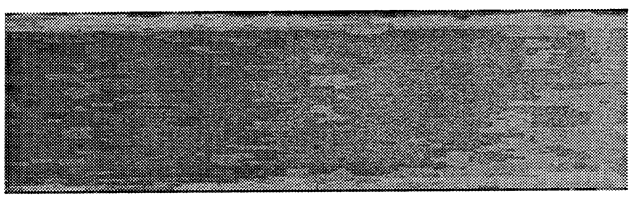
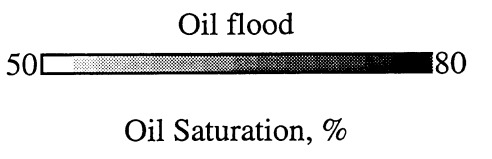
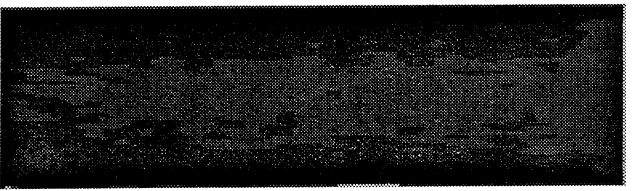
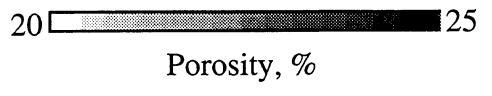
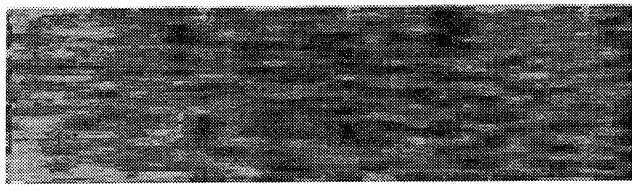


FIGURE C7 - Porosity and oil saturation distributions for CT-CF 9  
Chemical formulations are given in Table 17.

→ Flow direction

CT-CF 10

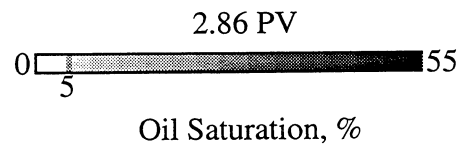
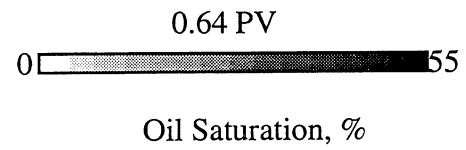
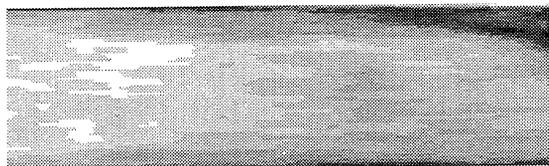
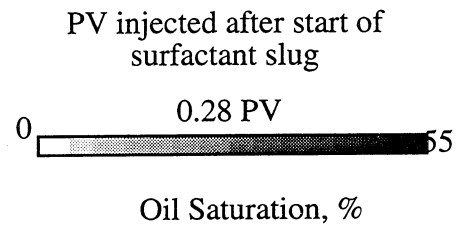
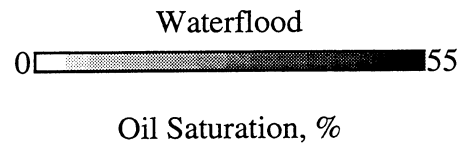
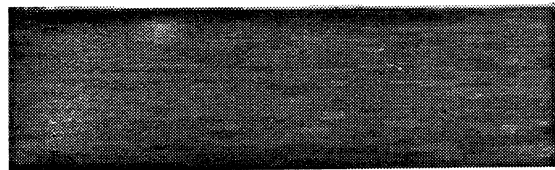
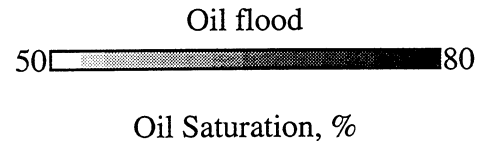
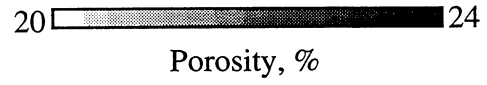
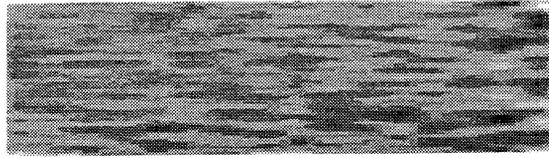


FIGURE C8 - Porosity and oil saturation distributions for CT-CF 10.  
Chemical formulations are given in Table 17.





